SYNTHESIS, MORPHOLOGIES AND APPLICATIONS OF POLYOXOMETALATE-CONTAINING DIBLOCK COPOLYMERS

A DISSERTATION IN
Chemistry
and
Pharmaceutical Sciences

Presented to the Faculty of the University
of Missouri-Kansas City in partial fulfillment of
the requirements for the degree

DOCTOR OF PHOLOSOPHY

by
SANJIBAN CHAKRABORTY

B.Sc. Calcutta University, 2000
B.Tech. Calcutta University, 2003

Kansas City, Missouri
2012

SYNTHESIS, MORPHOLOGIES AND APPLICATIONS OF

POLYOXOMETALATE-CONTAINING DIBLOCK COPOLYMERS

Sanjiban Chakraborty, Candidate for the Doctor of Philosophy Degree

University of Missouri-Kansas City, 2012

ABSTRACT

Block copolymers by virtue of their ability to self assemble and microphase-separation due to the contrast in chemical and physical properties of the covalently linked blocks constitute the essential building blocks towards various nano or micro sized architectures. Polyoxometalates (POM), on the other hand, being an interesting class of metal-oxygen nanometer-sized anionic clusters, are regarded highly due to their excellent electron accepting capability. Combining POM clusters with diblock copolymers can lead to a fascinating class of hybrid materials where the POM cluster not only affect the self-assembly process of various diblock copolymers but also brings its unique electronic properties into the hybrid system. Herein we report the detailed synthesis and characterizations of two hybrid coil-coil diblock copolymers along with two hybrid rod-coil diblock copolymers through polymerization-hybridization approach. The coil-coil diblocks were synthesized via atom transfer radial polymerization (ATRP) of styryl-type monomers and 4-vinylpyridine in sequence. For rod-coil diblock copolymers, the coil block was synthesized through ATRP, followed by the conversion of the terminal bromide to an azide. Ethynyl terminated poly (p-phenylenevinylene) (PPV) and poly (3-

hexylthiophene) (P3HT) were prepared separately as the rod blocks. The rod block and the coil block were connected through click chemistry to yield rod-coil diblock copolymers. After removing the phthalimide protecting groups to regenerate aryl amines, POM clusters were finally linked to the coil block of all diblock copolymers to yield the targeted hybrid diblock copolymers. The covalent cluster attachment was confirmed by UV-Vis spectroscopy, FTIR and cyclovoltammetry measurements. The structures, solution and film optical properties, self-assembled morphologies and solar cell performances of these hybrids have been studied. It has been found that solar cell devices based on hybrid P3HT exhibited rather poor performances. Fluorescence dynamic studies indicate that the photoinduced electron transfer process from the rod block to pendant POMs is quite inefficient which may account for the poor device performance. Though the self-assembly process of these hybrid diblock copolymers and the preliminary morphologies has been demonstrated, detailed and systematic study of morphological control requires further extensive research.

This abstract of 334 words is approved as to form and content.

APPROVAL PAGE

The faculty listed below, appointed by the Dean of the College of Arts and Sciences have examined a dissertation titled “Synthesis, Morphologies and Applications of Polyoxometalate-Containing Diblock Copolymers”, presented by Sanjiban Chakraborty, candidate for the Doctoral of Philosophy degree, and certify that in their opinion it is worthy of acceptance.

Supervisory Committee

Zhonghua Peng, Ph.D., Committee Chair
Department of Chemistry

James R. Durig, PhD.
Department of Chemistry

Nathan Oyler, PhD.
Department of Chemistry

Simon Friedman, PhD.
Department of Pharmaceutical Sciences

William G. Gutheil, PhD.
Department of Pharmaceutical Sciences

CONTENTS

ILLUSTRATIONS

Figure Page

ILLUSTRATIONS

Scheme Page

TABLES

ACKNOWLEDGEMENTS

I would like to express my heartiest and sincerest gratitude to my advisor and the chair of my committee Dr. Zhonghua Peng for providing me with the valuable opportunity to work under his supervision. It would have been impossible to reach thus far without his constant guidance and support not to mention motivation. Had he not been instrumental in aiding me identify my strengths and weaknesses, this long journey wouldn't have persisted. Acquiring knowledge and putting it into practical effect are two different aspect of education. Prior to joining his research group, I had no practical experience whatsoever in conducting any type of research work. It is he who guided me through with his unremitting constructive criticism to establish any concept by combining the acquired knowledge with thorough, systematic investigation.

I would also like to thank my dissertation committee members, Dr. James R. Durig, Dr. Nathan Oyler, Dr. Simon Friedman and Dr. William Gutheil for lending their time and valuable insights in reviewing my dissertation.

I must mention some names without whom my journey would not have been completed. I am really grateful to Dr. Andrew Keightley at the School of Biological Sciences, UMKC for MALDI-TOF mass measurement study. I wish to record my gratefulness to Dr. Da-Ming Zhu at the Physics Department for his assistance in obtaining the AFM images. It is my absolute pleasure to express my earnest gratitude and thanks to Dr. Xingzhong Yan and Dr. Yong Li at South Dakota State University for providing me with the invaluable information about lifetime fluorescence measurements

and solar cell device studies. I am also very much thankful to Michael Wulsar for his relentless effort in assisting me in my research endeavors. I would like to thank all the members of Dr. Peng's group, both past and present: Dr. Jeonghee Kang, Dr. Degang Wang, Dr. Mahuya Bagui, Mr. Tanmoy Dutta, Mr. Jeffrey Hsu, Mr. Chingen Chou, Mr. Shaohua Li, Ms. Jin Lu and Mr. Zhongkai Qu. I really cherish the nice moments I experienced working with them in the lab over the years. Great appreciation and thanks go to all the staff of the Department of Chemistry: Ms Josephine Maningat, Ms. Florence Middleton, Mr. Michael T. Sykora, Mr. John Whitchurch and Ms. Kathy A. Garrison.

Finally, I wish to acknowledge the people who have not only been supportive through thick and thin but also played a key role in shaping my career. I express my deepest love, gratitude and respect to my mom, Mrs. Lekha Chakraborty, and my dad, Mr. Swapan Chakraborty. I owe everything to them. Words are falling short to thank them for all their blessings. You have been the greatest pillar of strength to me for all these strenuous years. Last but not the least I want to thank Dr. Sourangsu Sarkar and Dr. Arindam Ganguly whose encouragement has provided me the strength to pursue my aspirations.

Dedicated to my beloved parents

CHAPTER 1

INTRODUCTION

1.1. Block Copolymers

Block copolymers by virtue of their ability to self-assemble [1] due to the immiscibility of the covalently linked blocks and the contrast in chemical and physical properties, constitute the essential building blocks of various nano- or micro- sized architectures. As the blocks are covalently linked to each other it is difficult for the individual domains to grow that much larger than a typical block length. Due to this molecular size constraint microphase separation and microdomain formation are natural phenomenon in block copolymers. [2] However the orientation of these domains is not always perfect. So controlling the self-assembly and orientation of block copolymers is an important research arena. Numerous experimental and theoretical studies have been devoted to the understanding of the phase separation of the simplest case of diblock copolymer i.e. fully flexible one or coil-coil diblock copolymer where the molecular shape closely matches Gaussian coil models. An unfavorable mixing enthalpy and small mixing entropy drives the self-assembly process. They can assume diverse microseparated phases like spheres, gyroids, hexagons, vesicles, cylinders, lamellae, etc. depending on the total degree of polymerization or N (entropy factor), the Flory-Huggins parameter or interaction enthalpy (χ) and the volume fractions of the constituent blocks.[3] The strength of microphase separation of two blocks is proportional to the segregation parameter (χN). Three separate regions are distinguished in the phase diagram depending on the value of χN: weak segregation limit (WSL) when $\chi N \leq 10$, intermediate

segregation region (ISR) when $10 < \chi N \leq 50$ and strong segregation limit (SSL) when $\chi N \rightarrow \infty$. Most of the work has been done in the SSL region. The phase boundaries are vertical lines and the different morphologies can be altered by changing the volume fraction of the blocks. [4] The ordered system is predicted to become disordered or pass through its order-disorder temperature (ODT) when $\chi N < 10$. Morphology can also be adjusted by changing the chemical structure of constituent blocks along with their conformational properties and composition. Figure 1a shows the typical predicted phase diagram for coil-coil diblock copolymer and 1b elucidates some phase separated geometries as function of relative block lengths.[5]

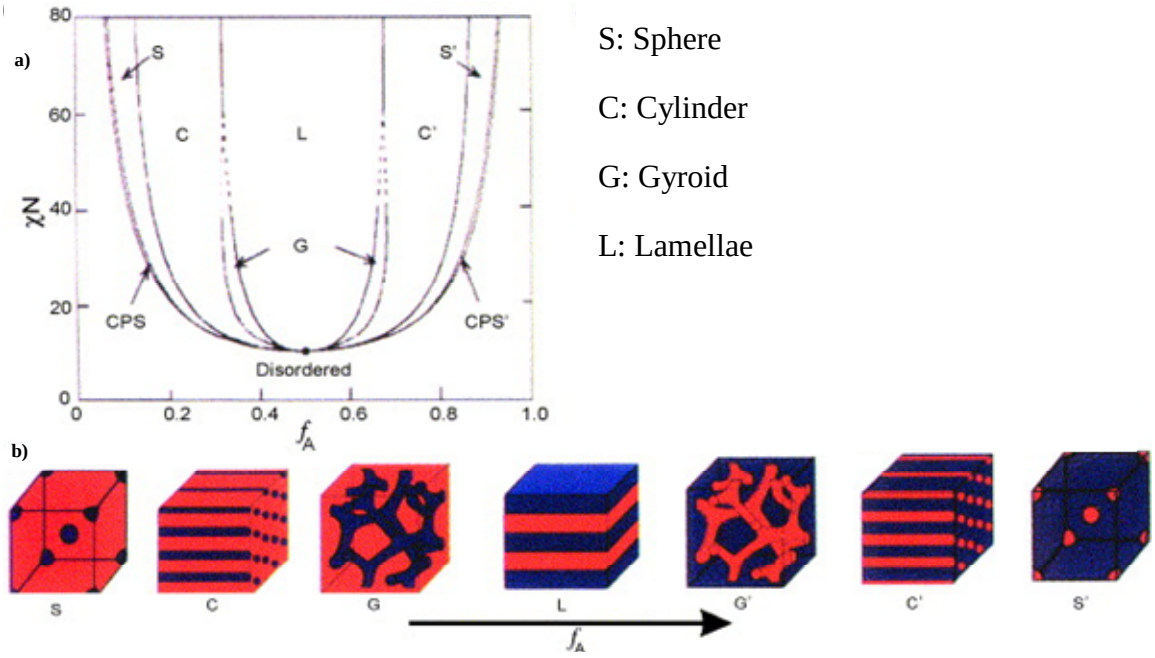

Figure 1. a) Predicted microphase separated self-assembled structure of coil-coil diblock copolymers. b) Different geometries as a function of block lengths.

Rod-coil diblock copolymers, on the other hand, are a fascinating class of block copolymers with hierarchical ordered structures at various length scales [6] where one of the block has a persistence length of the order of the end-to-end distance or greater corresponding to the number of monomer units. The long persistence length can be formed either by α-helices in case of polypeptides or by π-electron delocalization over multiple carbon atoms in the case of π-conjugated systems.[7] The self-assembly of rod-coil diblocks is fundamentally different from that of coil-coil due to the effect of chain topology on conformational entropy and molecular packing geometries. The rod block lacks the same conformational entropy as that of coil block which not only limits its ability to stretch to accommodate packing within self-assembled structure but also prevents to gaining conformational entropy when dissolved in solution.[8] The introduction of a rigid rod segment results in a disparity in stiffness between constituent blocks which in turn increases the χ value compared to the coil-coil diblock. Another phenomenon competing with the phase separation during self-assembly is the interactions between the anisotropic rod blocks. The rigid rod block serves as a liquid crystal forming mesogen, [9] which may coexist with the microdomains during microphase separation. In addition to the Flory-Huggins parameter and volume fraction of two blocks similar to coil-coil systems, two other parameters contribute to the phase behavior of rod-coil diblock copolymers. One is the Maier-Saupe parameter (ω) for liquid crystalline interactions or rod-rod steric repulsion while the other one is a geometric factor accounts for the

conformational asymmetry between the rod and the coil blocks.[10] The possible routes for self-assembly of a rod-coil type diblock from an isotropic melt or an isotropic solution is illustrated in Figure 2.[4]

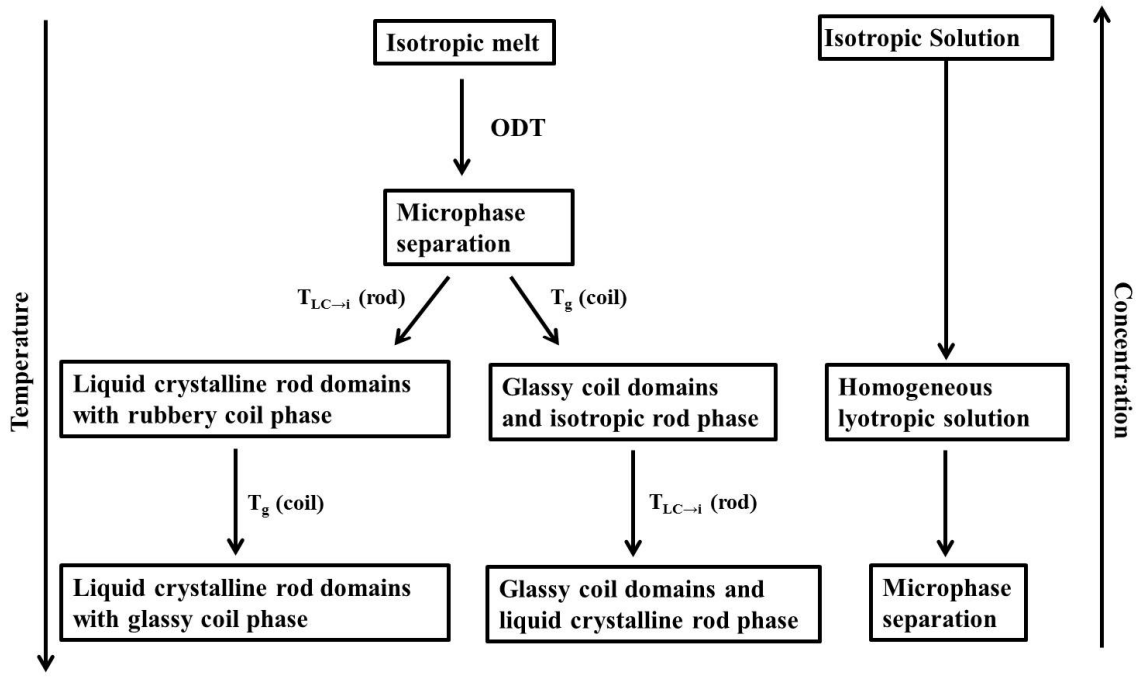

Figure 2. Probable routes for the self-assembly of rod-coil diblock copolymers.

Different scenarios evolved on cooling an isotropic melt depending on the glass transition temperature (T_g) of the coil block and the isotropization temperature ($T_{LC\rightarrow i}$) of the rod block. The interplay between liquid crystalline ordering with extended crystalline

phases or higher order smectics and microphase separation between geometrically mismatched rods and coils coupled with multiple parameters for phase characterizations render complexity to its phase diagram.[11] For instance, seven different lamellar phases (according to liquid crystal nomenclature, lamellar phase for rod-coil is known as smectic phase) namely monolayer smectic A (Sm_A), bilayer Sm_A, bilayer smectic C (Sm_C), smectic B, smectic E, smectic F and smectic O (Sm_O) have been reported for rod-coil DCP's as opposed to the simple lamellar morphology of the coil-coil one.[12] Nevertheless, unique morphologies exhibited on nanometer scale have been exploited to the design of diverse functional systems with tailored optical and photonic properties. One interesting kind of functional system is the use of conjugated polymers as the rod segment to create a new class of self assembling electroactive materials in which various diblock copolymer morphologies enables the one-, two-, or three dimensional confinement of electroactive regions.[13] These diblocks have emerged as efficient optoelectronic devices since last decade due to its flexibility towards attaching different functional units through chemical linkage at the same time allowing the fine tuning of the optoelectronic properties. Mutual interactions of the rod-like mesogens to form the ordered phases enhance the optoelectronic properties of these diblocks[14] containing a conjugated hole-transporting rod block and an electron transporting block. Donor-acceptor block copolymers which exhibit optimized orientation and ordering of the phase separated microdomains are potential efficient photovoltaic materials.[15] Control of the interfacial structure and morphology on the exciton diffusion length scale (10 nm) is critical for the optimization

of device performances. Rod-coil diblock copolymers have been extensively used for such applications.

1.2. Polyoxometalates (POM) and their Functionalization

The early transition metals like V, Nb, Ta, Mo, and W in their higher oxidation states are capable of forming metal-oxygen cluster anions which are commonly known as polyoxoanions or polyoxometalates (POM).[16-24] These are characterized by an intriguing variety of architectures and topologies with applications in catalysis, biology, medicine, magnetism, materials science, optics and nanoscience.[17] They are actually oligomeric aggregations of metal cations (mostly d^0 species) bridged by oxide anions formed by self-assembly precesses. [18]

POMs can be classified as two major categories: i) isopolyanions and ii) heteropolyanions. The isopolyanions contain the d^0 metal cations with oxide anions having the general formula of $[M_mO_o]^{-p}$. The heteropolyanions as the name suggests contain one or more heteroatoms in addition to the d^0 metal cations and oxide anions and have the general formula of $[X_xM_mO_o]^{-q}$. M is molybdenum or tungsten, less commonly vanadium, niobium and tantalum whereas X could be Si^V, P^{IV}, B^{III},V^V and others. Based on the shapes and symmetries, POMs can be classified into six major categories: Lindqvist, Keggin, Dawson, Anderson, Waugh and Silverton.[16a,19] Figure 3 shows the structures of some important isopolyanions[16d, 20]while some heteropolyanion structures are shown in Figure 4. [16d]

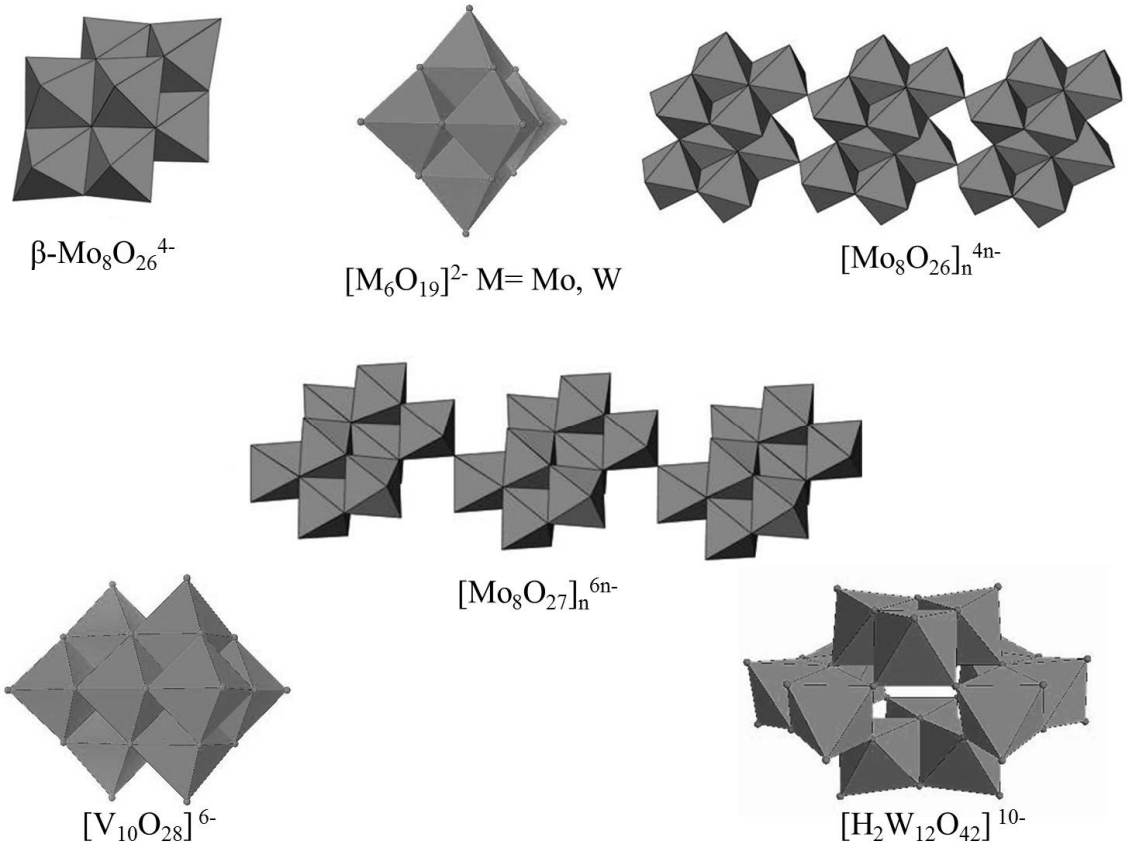

Figure 3. Some important isopolyanion structures.

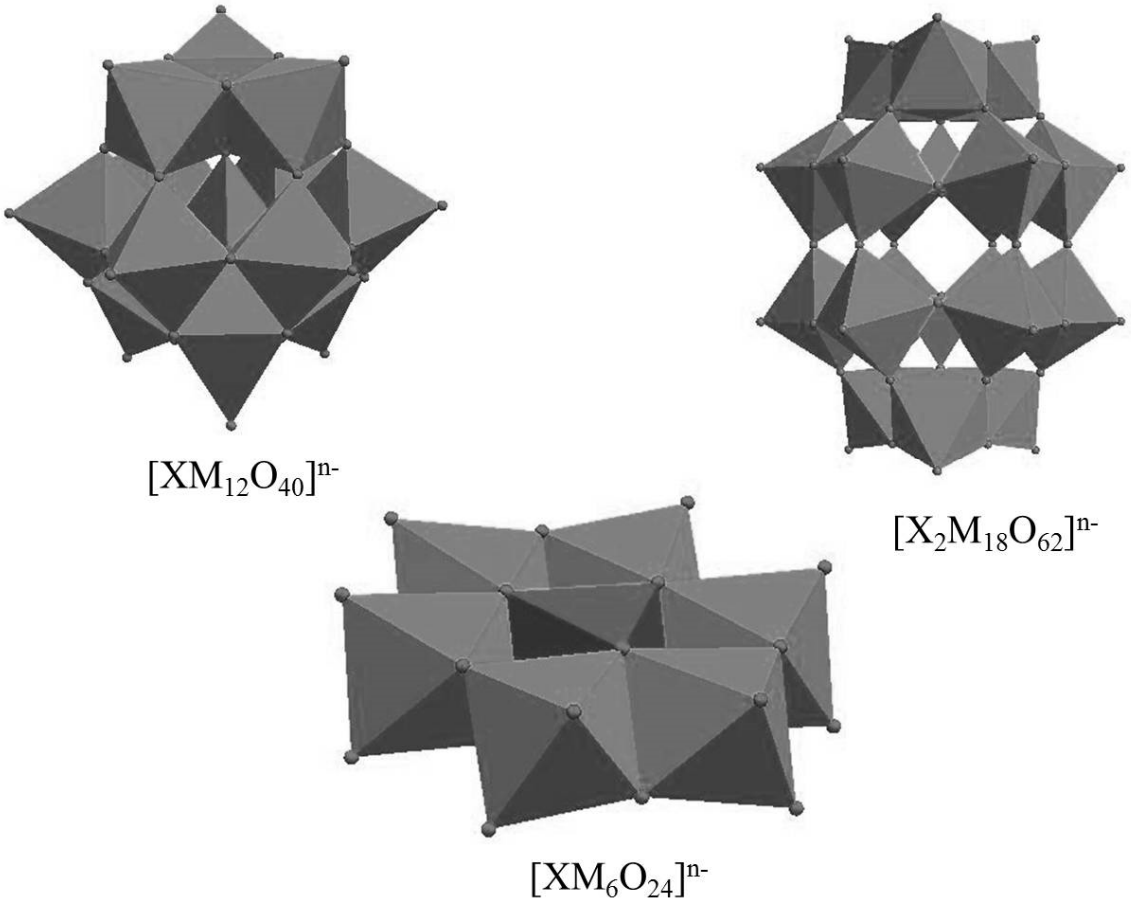

Figure 4. Some heteropolyanion structures.

The POM structures are formed by MO_6 octahedra that share points, edges or faces. Each octahedron represents a metal atom in the center of octahedron and each corner represents an oxygen atom in the structure. The oxygen atoms can serve as bridging ligands besides terminal ligands. Heteropolyanions have central heteroatoms which are tetrahedrally coordinated for Keggin and Dawson structures whereas for Anderson structures the central heteroatom is octahedrally coordinated. Considering the

possibility of different atoms that can be incorporated into POMs and the arrangements of those atoms, the number of POMs is very large. In general they are stable towards H_3O^+, and numerous crystalline heteropoly acids are known.

One interesting feature of POMs is their rapid and reversible redox processes which are easily achievable if each Mo_6 octahedron possesses only one terminal oxygen atom. As the added electron enters the non-bonding orbital of M, no change in bond length is observed. This is applied to Keggin ($XM_{12}O_{40}$), Dawson ($X_2M_{18}O_{62}$), hexametalate (M_6O_{19}), decatungstate ($W_{10}O_{32}$) and related structures. These are strong oxidizing agents which undergo multiple reversible one-two-electron reductions leading to intense colored (mostly blue) mixed-valence species known as heteropoly blues.[60d] Some of them can accommodate as many as 32 electrons without major structural changes. If the Mo_6 octahedron has two cis-terminal oxygen atoms as in the case of Anderson structure, XMo_6O_{24}, the extra electron enters the anti-bonding orbital resulting in large structural variation. These are either inactive or exhibit irreversible reduction in cyclic voltammetry (CV) spectra. This sharp contrast in reducibility can be rationalized on the basis of individual Mo_6 octahedron electronic structures, hinting that the bonding in POMs is not extensively delocalized compared to organic aromatic systems.[16d]

One of the prototype of the Lindqvist type metal-oxygen cluster is the hexametalates, [$(Mo_6O_{19})^{n-}$, when n = 2, M= Mo or W; when n = 8, M= Nb or Ta] along with variety of mixed-metal analogues. Because of their potential applications in electrochemistry, analytical chemistry, photocatalytic reactions and optoelectronic fields,

significant effort has been devoted in the experimental investigations of these isopoly oxometalates. The structure is shown in Figure 5. [21]

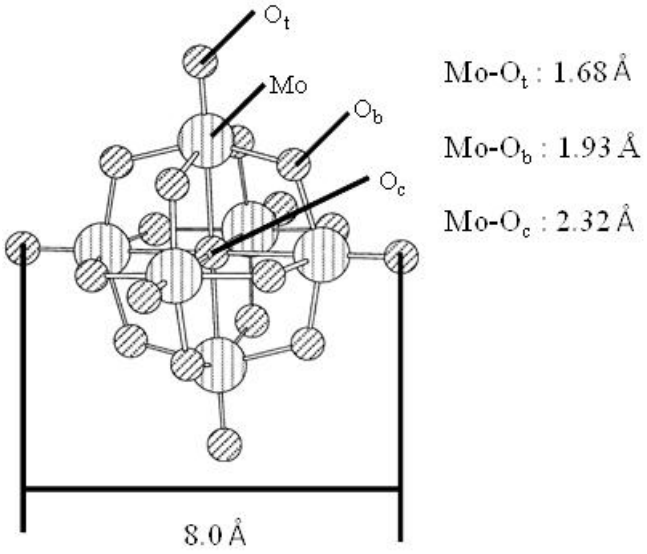

Figure 5. Structure of the hexamolybdate anion.

The structure consists of a central oxygen atom (O_c) around which six molybdenum atoms are arranged in an octahedral fashion. Each molybdenum atom carries one terminal oxygen atom (O_t) and shares additional four μ_2 –oxygen atoms (bridge oxygen, O_b) with adjacent molybdenum atoms. Overall symmetry of the system approaches approximately O_h. It can be assumed that the structure contains mutually perpendicular M_4 $(\mu\text{-}O)_4$ planar rings. The short M-O_t distances point to the possible

existence of (d-p) π conjugation effects.[22] The mean bond lengths are as follows: Mo-O_t 1.68 Å, Mo-O_b 1.93 Å and Mo-O_c 2.32 Å. The size of hexamolybdate is 8 Å comparable to fullerene C_{60} (7.1 Å).[23] In Pope's classification,[22] this is a type-I polyanion, i.e., each metal center only has one terminal oxo ligand. The bonding of the Mo_6 octahedron unit, consisting of one terminal triple bonds, four bridging single bonds and one weak internal single bond, is the basis of qualitative understanding of the electronic structures.[22]

Hexamolybdates undergo reversible one electron reduction ($E_{1/2}$ = -830 mV) without any loss of stability. [21] The very small changes of the bond distances before and after reduction ensure the similar stability even after reduction. Table 1 shows the Mo-O bond distances before and after reduction.[24]

Table 1. Mo-O bond distances (Å) of $[(Mo_6O_{19})^{2-}]$

	Molecule	Mo-O_c	Mo-O_b	Mo-O_t
Before reduction	$[(Mo_6O_{19})^{2-}]^a$	2.32	1.93	1.68
	$[(Mo_6O_{19})^{2-}]^b$	2.32	1.93	1.71
After reduction	$[(Mo_6O_{19})^{3-}]^b$	2.33	1.93	1.73

(a) experimental results (b) calculated results

Table 2 shows the calculated charge distribution of hexamolybdate anion before and after reduction which reveals that the negative charges and added electron in the reduction are distributed over all types of atoms.[24]

Table 2. Calculated charges of $[(Mo_6O_{19})^{2-}]$

	Molecule	Mo	O_t	O_b	O_c
Before reduction	$[(Mo_6O_{19})^{2-}]$	2.19	-0.66	-0.83	-1.19
After reduction	$[(Mo_6O_{19})^{3-}]$	2.11	-0.72	-0.85	-1.18

Polyoxometalates, among various metal-oxygen clusters, are attractive not only because of their structural versatility and rich optoelectronic properties but also because of their discrete molecular structures which allow surface functionalization in a controlled and rational way.[16] This nanometer sized, spherical anionic clusters are regarded highly due to their excellent electron accepting capability similar to fullerene but at a much lower cost. Their molecular identity is maintained both in solid state and in solutions. Over the years there has been increasing interest in the chemistry of organically derived POMs.[18b] Among the many organic derivatives, organoimido derivatives have attracted particular attention as the organic π-electrons can extend their conjugation into

the inorganic framework resulting in strong d-π interactions. In addition to that organoimido derivatives of POMs with a remote functional group can be used as building blocks to generate complicated POM-organic hybrids. [25]

In organoimido derivatives majority of the work has been centered on hexamolybdate ion, $(Mo_6O_{19})^{2-}$ where the terminal oxygen atoms can be replaced by various organic species or ligands like nitrosyl,[26] diazenido, hydrazido,[27] organometallic,[28] diazoalkyl [29] and imino ligands.[16c, 21,30-36] For organoimido derivatives, three types of reactions have been developed so far. All three reaction schemes are shown in Figure 6.

The first reaction (eq. 1), which was discovered by Matta, et. al., involves the reaction of phosphinimines with hexamolybdate. It demonstrates the direct functionalization of parent cluster.[30, 31] The second one (eq. 2), which was reported by Errington and Matta, et. al., involves the reaction of hexamolybdate with various isocyanates. The reaction is required to run in strictly anhydrous condition at higher temperature for prolonged time.[16c,21,32,33] The third method (eq. 3), reported by Errington, et. al., involves the reaction of aromatic diamines with hexamolybdate at harsh conditions but unfortunately no pure imidoderivative has been isolated.[34-36]

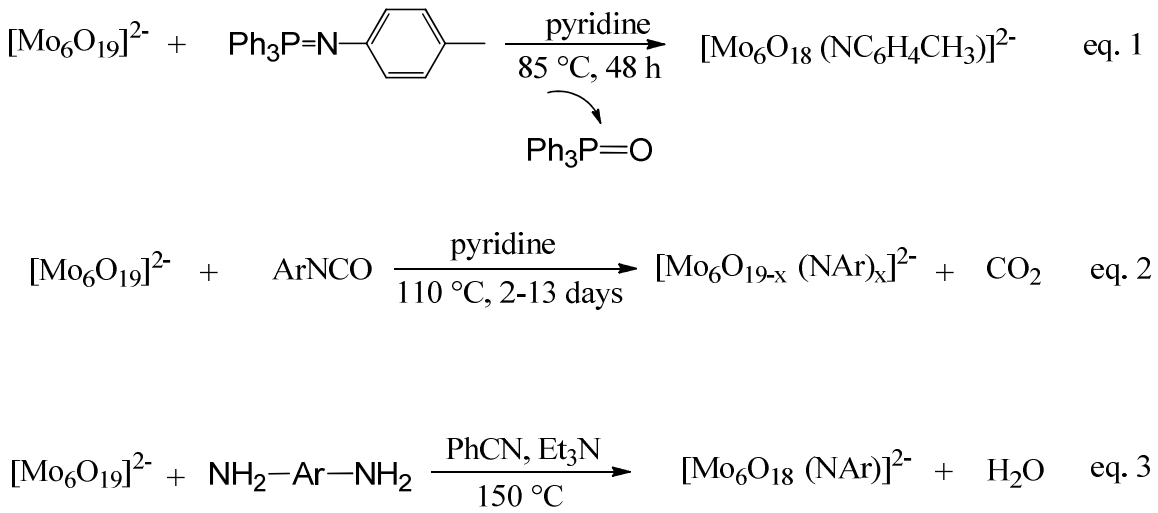

Figure 6. Three reaction schemes of organoimido derivatives.

All these above mentioned reactions require harsh conditions including higher temperatures and prolonged reaction times. But it has been demonstrated recently that one equivalent of dicyclohexylcarbodiimide (DCC) can facilitate the reaction of variety of aromatic amines with hexamolybdate under refluxing acetonitrile.[35] The enhancement of the rate of reaction is most likely due to the activation of the Mo-O_t bond, similar to activating effect on the carbonyl group in the synthesis of esters.[25b] Figure 7 shows the revised synthetic scheme of the reaction. All these derivatives have a short Mo-N bond length (~ 1.7 Å) with near linear Mo-N-C bond length (>170°).

Figure 7. Reaction of hexamolybdate with aromatic amine in presence of DCC.

The X-ray crystal structures of three different imido derivatives from three different aromatic amines namely, a) 2,6-dimethyl-4-iodoaniline, b) 2,6-dimethyl-4-ethynylaniline and c) 4-(N,N-diethyl) aminoaniline are shown in Figure 8.

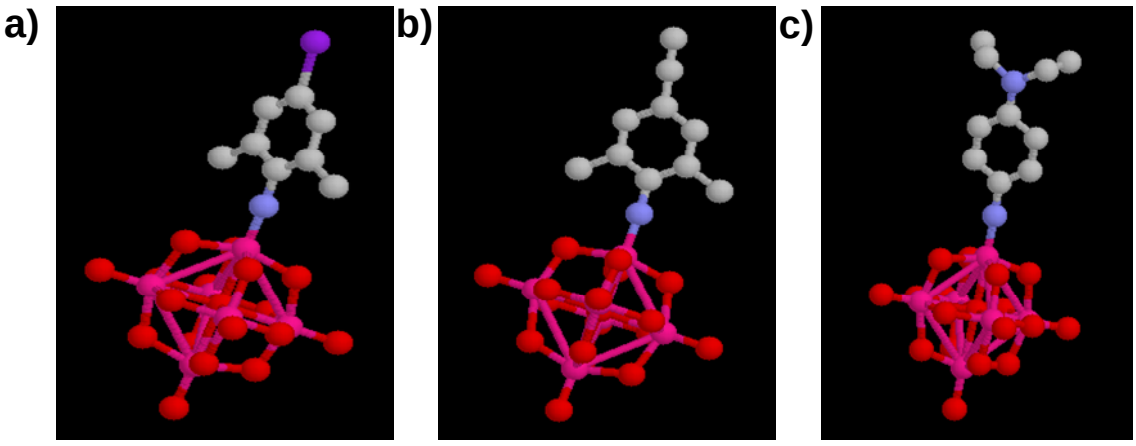

Figure 8. X-ray crystal structures of three $[Mo_5O_{18}(MoNAr)]^{2-}$ anions. a) Ar = 2,6-dimethyl-4-iodophenyl, b) Ar = 2,6-dimethyl-4-ethynylphenyl, c) Ar = 4-(N,N-diethyl) aminophenyl.

1.3. POM Containing Block Copolymers

Research on block copolymers has evolved from all organic systems in the early years to hybrid systems lately.[37] In particular metal-containing diblock copolymers (DCPs') have been actively pursued in recent years. The incorporation of metals into block copolymers not only affects the self-assembly process, but also brings about novel physical and chemical properties. For example, Manners has studied a variety of DCP's with one block containing ferrocenes.[38] Chan, [39] Schubert [40] and others [41] have explored DCP's containing transition metal complexes. While these studies are exemplary, they include only discrete mononuclear metal centers and most of the metals have been introduced as coordination complexes. Block copolymers containing metal-oxygen clusters especially POM has not been reported. A great deal of effort has been devoted in developing covalently bonded POM containing organic-inorganic hybrids,[42-60] among which a few examples involve POM-containing polymers.[42] Majority of research has been limited to composite materials where POM clusters are either embedded in a polymer matrix [42] or sandwiched between cationic polymers through layer by layer assembly.[43] Since Judeinstein reported the first POM-polymer hybrid,[44] increasing efforts have been devoted to develop variety of approaches to develop a unique set of materials. After Judeinstein, Lalot came up with the idea of making polymer-POM cross linked networks[45] and later on Stein with the functionalization of POM with silica.[46] Polystyrene having POM pendants by Matta[47] and POM containing polymer formed by metal-ligand

coordination have also been reported.[48,49] While most POM-containing polymers are based on an insulating polymer backbone, Peng, et. al. reported both main chain and side chain POM-containing conjugated polymers as shown in Figure 9 utilizing the imido functionalization and demonstrated that POM clusters as electron acceptors, in conjunction with organic π-conjugated segments as electron donors, may find applications as novel photovoltaic (PV) materials.[62] The functionalized imido-derivatives can be realized as the bedrock for rational synthesis of novel POM-organic hybrids. Such hybrid materials not only combine the advantages of organic materials, such as ease in processing and structural fine-tuning, but the close interaction of organic delocalized π-electrons with the cluster d-electrons may bring exciting synergistic effects. While all these developments are exciting, research on covalently bonded POM-organic hybrids are still in the stage of focusing on their primary structures. Morphological control or ordering on such hybrid materials is an uncharted territory which needs to be stressed.

1.4. Objectives

The objectives of this research account are to develop synthetic approaches for the preparation of block copolymers containing POM clusters, study their self-assembly processes leading to phase-separated nanostructures and explore their applications as new photovoltaic materials. POM clusters not only bring their rich electrochemical and photophysical properties into block copolymers, but also by virtue of their unique shape,

nanometer or near nanometer size and anionic nature impact significantly and unprecedentedly the self-assembly processes of block copolymers, leading to possibly new morphologies. It should be emphasized that POM clusters are not simply another different structural unit which can be incorporated into block copolymers, they are unique in their nanometer size and anionic nature. Introducing a nanometer size structural unit into a block copolymer has been shown to be an attractive approach to realize unique domain structures. For example, block copolymers containing polyhedral oligomeric silsesquioxane (POSS) (1.5 nm diameter) have been studied.[63] The aggregation tendency of POSS coupled with the self-organization of polymer blocks can result in hierarchically ordered hybrid structures such as hexagonally packed micropores plus phase-separated nanodomains.[64] Block copolymers containing ionic pendants constitute another important class of materials-polyelectrolyte block copolymers. A tremendous amount of work has been devoted to study their micellar structures in solutions.[65] The repulsive interactions between pendant ions tend to stretch the polyelectrolyte chains,[65e] making them rodlike.[65f] In addition, the polyelectrolyte block allows the modification or control on the self-assembly process through counter ions or another polyelectrolyte carrying opposite charges.[65a,66] POM clusters, being ionic and with nanometer size, are expected to impact the self-assembly of diblock copolymers in an unprecedented way. The specific aim would be at preparing two different diblock copolymers: one contains flexible blocks or coil-coil diblock while the other one is rod-coil one. Realizing that neither POM clusters, nor any charged nanoparticles have ever been covalently linked to a block copolymer, synthesizing such hybrid diblock copolymers and studying their self-assembly process

would be a conceptual advance in true sense. In addition to seek a thorough understanding of how POM clusters affect the self-assembly process of both coil-coil and rod-coil diblocks, we are curious to find out how POM clusters with rich electrochemical and photophysical properties can lead to functional rod-coil diblock copolymers. It has already been demonstrated as shown in Figure 9 that hybrid polymers based on POM clusters and organic π-conjugates exhibit efficient photoinduced charge separation. The limited charge transporting properties of such polymers however have hindered their PV performances. Since electrons transport through hopping among POM clusters while holes transport through aggregated conjugated segments, a polymer system which can segregate the two structural components may be able to provide the separate domains for different charge transport.[67] A rod-coil donor-acceptor type diblock copolymer with POM attached to the coil block can be considered as a potential candidate for such applications. The strong mutual interactions of liquid crystalline rod blocks, mostly extended π-conjugated systems, not only drive the formation of highly ordered phases, but also result in enhanced optoelectronic properties. Thus the motivation to such hybrid rod-coil diblock copolymers are two fold: to study their complex phase behavior and control the hierarchical orders and to explore such hybrids as photovoltaic materials. Though the self-assembly process of these hybrid diblock copolymers and their unique morphologies has been demonstrated, detailed and systematic study of morphological control requires extensive research. This account primarily focuses on the synthetic strategies to develop these hybrid diblock copolymers and their characterizations to establish the fundamental concept of metal cluster containing block copolymers.

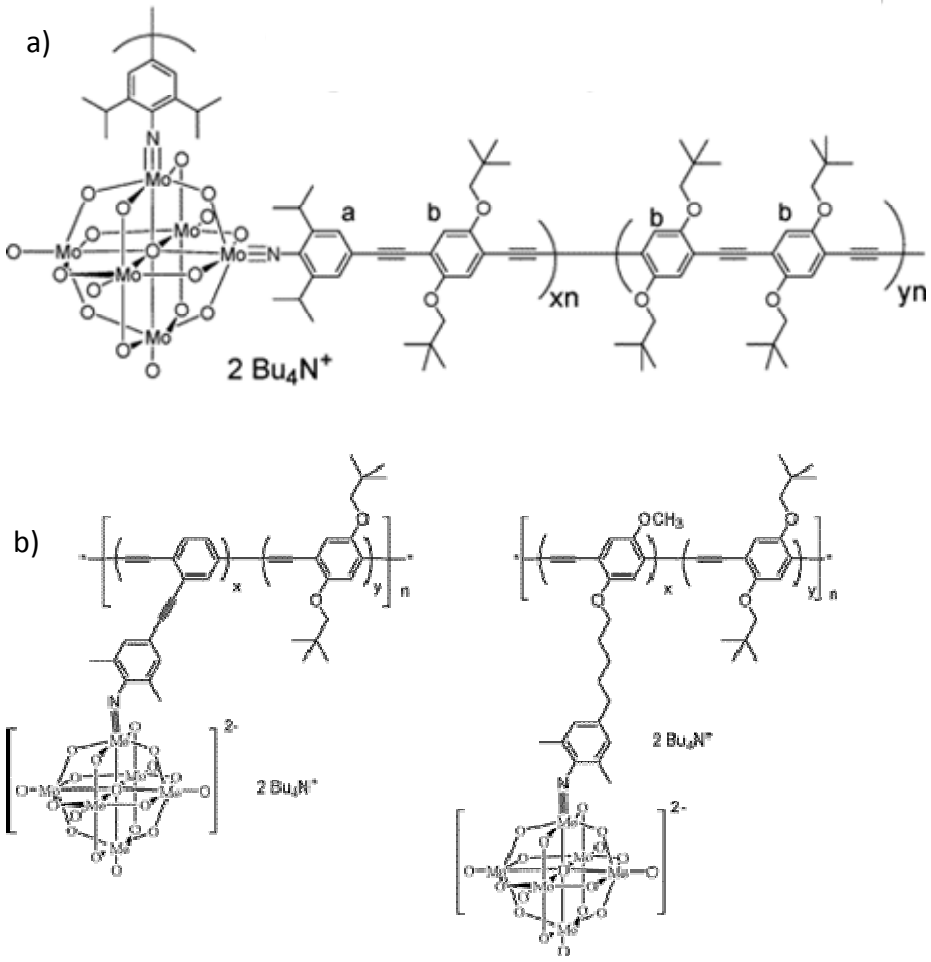

Figure 9. Conjugated polymers containing POM cluster a) Main chain POM containing conjugated polymer b) Side chain POM containing conjugated polymer

1.5. Synthetic Approaches

With these considerations in mind, we have set out to synthesize two different types of coil-coil DCP with POM clusters linked to one of the coil block and two different types of rod-coil DCP with POM clusters linked to the coil block. Atom transfer radical polymerization (ATRP), the most robust and widely applied controlled radical polymerization technique, was used to synthesize the flexible coil blocks. Polymer with narrow molecular weight distribution was the product and used as a macroinitiator by retaining the end functional Br- group for subsequent polymerization of other monomers. These polymer hybrids can be realized, in principle, by two different schematic pathways: the polymerization-hybridization (polymerization first) approach and the hybridization-polymerization (hybridization) approach. The approaches are demonstrated in Scheme 1a for coil-coil hybrid diblock and in Scheme 1b for rod-coil hybrid diblock copolymers. The first route involves the synthesis of precursor diblock copolymers with functional amine pendants on one block followed by the covalent linkage of the POM cluster. The second route initiates with the synthesis of hybrid monomers, which are in turn used directly for polymerization. Both the avenues enjoy some advantages at the same time inflict with some serious drawbacks. The former approach has better control over the degree of polymerization of each block with the flexibility of synthesizing polymer hybrids with varying clusters. There may be, however, a lack of control over the extent of cluster attachment. The latter approach while ensuring complete cluster functionalization on the coil block, demands the development of new chemistry: the living polymerization method of POM containing monomers has yet to be demonstrated

though living polymerization of styrene monomer using trivanadium substituted polytungstate type POM initiator has been reported.[61c] Though we have made efforts on both fronts concomitantly, our major focus was concentrated on exploring the first approach. For comparison purposes, the investigation of the second approach might be interesting, but only for the synthesis of coil-coil diblock copolymers.

Both the coil-coil DCPs and the rod-coil DCPs utilized one common coil block which was polymerized from amine-protected styryl-type monomer via ATRP method. This polymer was utilized as a macroinitiator to either polymerize the same block or 4-vinylpyridine monomer (4-VP) to form the second coil block. The vinylpyridine-based coil-coil diblock copolymer exhibits pH-dependent morphologies. Under different pH, the vinylpyridyl ring will be protonated to different extents, and thus modulating the interactions between the two blocks. A gradual transition from self-assembled domain structures to one homogenous phase is expected when the pH is lowered. For all these coil-coil DCPs the amine protected styryl type functionalized monomer is an important precursor and its polymerization via ATRP plays a significant role. Thus optimization of the ATRP conditions for this functionalized monomer is necessary. For the rod-coil DCP, two different rod blocks namely poly(phenylene vinylene) (PPV) and poly(3-hexylthiophene) (P3HT) have been chosen as they are among the most extensively studied conjugated polymers which show most promise in various molecular electronic devices. In the following chapter, besides optimizing the ATRP reaction conditions for the polymerization of amine protected styryl type functionalized monomer, the ATRP of POM cluster containing styryl type monomer was also demonstrated.

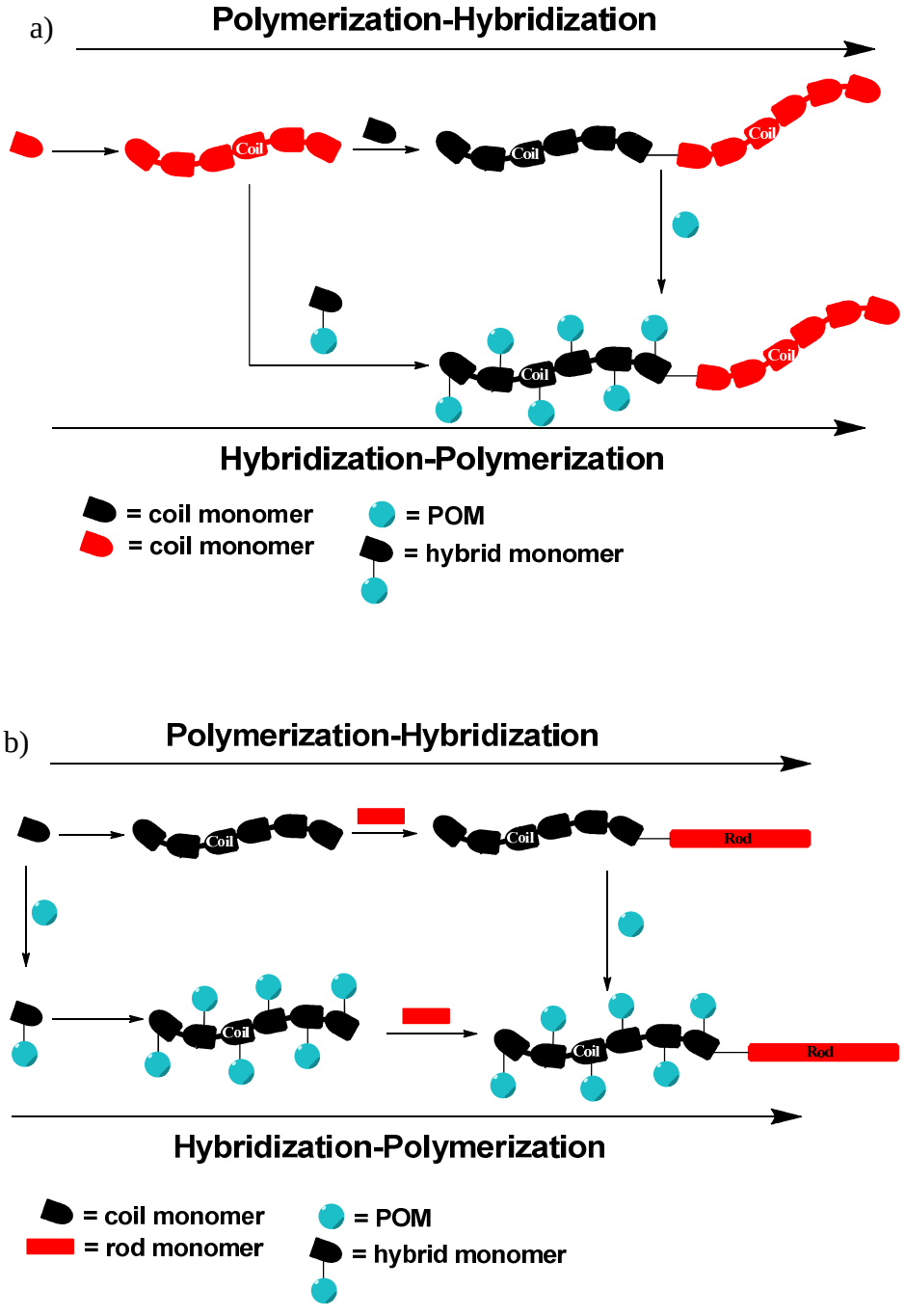

Scheme 1. Two synthetic routes each for a) coil-coil hybrid diblock copolymer and b) rod-coil hybrid diblock copolymer.

CHAPTER 2

ATOM TRANSFER RADICAL POLYMERIZATION OF FUNCTIONALIZED MONOMERS

2.1. Living Polymerization Method: ATRP

Free-radical polymerization is one of the major commercial processes for the production of high molecular weight polymers due to its versatility in polymerizing a wide variety of monomers using simple experimental conditions.[68] Nevertheless uncontrolled molecular weights combined with high polydispersities prevent the synthesis of well-defined polymers with narrow molecular weight distributions, high degree of chain-end functionalization and complex architectures.[69] Moreover the short lifetime of the propagating chain radicals restricts any kind of synthetic maneuver, end-functionalization or block copolymer synthesis. Over the last few decades living polymerization methods have been able to succeed tremendously which was otherwise unthinkable with conventional polymerization methods.[70] Though living anionic [71] and cationic [72] polymerization techniques have been instrumental in realizing numerous polymeric materials, their success story is somewhat dampened by their severe drawbacks in the limited choice of monomers and solvents, intolerance of variety of functional groups and sensitivity towards moisture and carbon dioxide. The development of controlled/living radical polymerization (CRP) over the last few decades has paved the way for the successful synthesis of various polymers and copolymers with precise composition, topology and functionality. [73] The rapid growth of CRP is the combination of the achievements of conventional free radical polymerization methods towards the

polymerization of various monomers along with their tolerance of variety of functional groups and the distinct features of ionic living polymerization methods of controlling molecular weight and chain-end functionalization. Despite the inevitable diffusion controlled termination reactions e.g. bimolecular radical coupling and disproportionation reactions, the minimal influence of these detrimental reactions upon the final product make CRP methods a powerful tool to craft a host of unique materials.[74] All the different CRP methods are based on the rapid dynamic equilibration between a miniscule amount of growing free radical chains or the active species and a large amount of various dormant species.

One such CRP method which stands out among its peers is atom transfer radical polymerization (ATRP) method [75] where the control is achieved through the dynamic equilibrium between propagating radicals and dormant halide-capped chains R-X established with the help of a transition metal catalyst. The general mechanism [76] for ATRP is shown in Scheme 2.

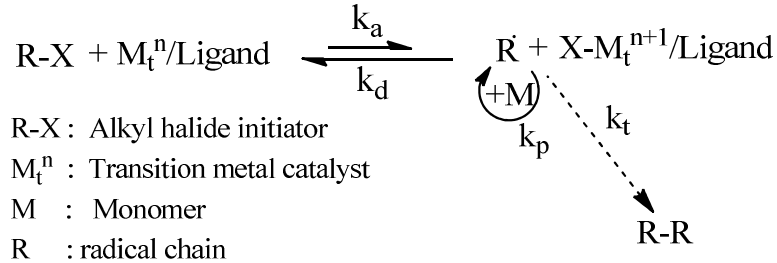

R-X : Alkyl halide initiator
M_t^n : Transition metal catalyst
M : Monomer
R : radical chain
k_a : activation rate constant
k_d : deactivation rate constant
k_p : propagation rate constant
k_t : termination rate constant

Scheme 2. General Mechanism of ATRP

2. 2. General Mechanistic Description of ATRP

Homolytic cleavage of an alkyl halide (R-X) initiator (dormant species) and a one-electron oxidation process catalyzed by a transition metal complex activator (M_t^n/Ligand: copper halide in presence of amine ligands) with concomitant abstraction of halogen atom from dormant species generates the radical and the higher oxidation metal complex deactivator (M_t^{n+1}/Ligand).[77] This process occurs with an activation rate constant of k_a.The radical can then propagates by the subsequent addition of monomer (M) with a propagation rate constant of k_p and terminates with another radical to form dead chain (R-R) or reversibly deactivated with a rate constant of k_d by the deactivator to get back the dormant chain. A very few polymer chains terminate during the initial, short, nonstationary stage of polymerization. This initial termination stage generates the oxidized metal complex or the deactivator as persistent radicals to minimize the stationary concentration of growing radicals and thereby lowering the termination event. The dynamic equilibrium between activation and deactivation steps is correlated to the equilibrium constant (k_{eq}) by the ratio of k_a/k_d. Each termination results in decrease in concentration of radicals with increase in deactivator concentration until a sufficiently high concentration of deactivator is formed to lower the rate of termination. This self-adjustment process during the initial stages of polymerization is called 'persistent radical effect' (PRE).[78] Due to this effect the equilibrium between the activation and deactivation steps is shifted strongly towards the dormant species so that $k_a << k_d$. In addition, fast deactivation of the active species in comparison to propagation ensures the growth of all polymer chains at the same rate with a controlled or living behavior. [79] In systems like

ATRP obeying the PRE, steady state of growing radicals can reach due to the activation-deactivation process, rather than the initiation-termination process observed in conventional free radical polymerizations.

2.3. Kinetics of ATRP

The rate of polymerization in ATRP is dictated by the ratio of activator to deactivator concentration according to eq.1.[80]

$$R_p = k_p [M] [R^{\cdot}] = k_p [M] k_{eq} [R\text{-}X] ([M_t^n/L]/ [XM_t^{n+1}/L])$$

$$k_{eq} = k_a/k_d \qquad \text{eq. 1}$$

ATRP follows first-order kinetics with respect to monomer, initiator and activator but negative first-order kinetics with respect to deactivator.[81] The polymerization rate increases with initiator concentration and depends on the ratio of activator/deactivator concentrations. So in principle, the absolute amount of catalyst concentration can be reduced without altering the rate of polymerization. Deactivator concentration plays a crucial role in adjusting the rate of polymerization and the polydispersity of the final polymer. Equation 2 shows how the polydispersity decreases with the increasing conversion rate, where p is the degree of conversion. This equation only holds well when the initiator is fully consumed and the degree of polymerization is very high. Otherwise, a Poisson term ($1/DP_n$) needs to be included in the equation where DP_n is the degree of polymerization. At the same time PD should be lower if k_p/k_d ratio is small, which means that faster deactivation of growing polymer chains results in lower PD. Polydispersity

should also decrease with increasing deactivator concentration at the cost of slower polymerization rates.[82]

$$PD = M_w/M_n = 1 + \left(\frac{[RX]_0 k_p}{k_d [D]} \right) \left(\frac{2}{p} - 1 \right) \qquad \text{eq. 2}$$

Another significant conclusion which can be derived from eq.2 is that the polydispersity increases for the shorter chain lengths or lower molecular weight polymers (higher initiator concentration) as DP_n is the ratio of the monomer concentration to initiator concentration derived from eq. 3.

$$DP_n = \frac{\triangle [M]}{[I_0]} \qquad \text{eq. 3}$$

Deactivation rate constant (k_d) depends on a number of factors including transition metal, ligand and the lability of the $X\text{-}M_t^n$ bond in the deactivator. The control of molecular weight is based on the fast initiation and deactivation allowing all the chains to grow almost the same time and maintaining a low concentration of radicals.

2.4. Individual Components of ATRP

ATRP is a multicomponent system comprises of monomer, an initiator with a transferable halogen atom, a transition metal catalyst with a suitable ligand.

Different types of monomers have been used including styrene, [83] acrylates, [75a] acrylamides [84] and acrylonitrile[8], etc. Each monomer possesses a unique K_{eq} using the same catalyst system for its active and dormant species which in turn determines the

polymerization rate. Each monomer has its own propagation rate. So a balance needs to be maintained between the concentration of radicals and rate of deactivation to control the rate of polymerization.

Fast initiation is a prerequisite for controlled ATRP reactions. Their major role is to determine the number of polymer chains. Generally alkyl halides (R-X) with activating α-substituents such as carbonyl or aryl are the best choice as an initiator. Another basic criterion of an initiator is that the halide group, X, must migrate selectively between radical chain and transition metal complex and so far, bromine or chlorine produces the best control over molecular weight.[86]

Arguably the most important component is the catalyst-ligand combination as it determines the position of the atom transfer equilibrium step. Several factors need to be taken into account while choosing an efficient transition metal catalyst e.g. the metal must possess two readily accessible oxidation states, high affinity towards halogen, and easily tunable activation rate constants for specific monomers. The metal should form strong complexes with ligand and can rearrange and expand coordination sphere to accommodate incoming halogens, etc.[75d] Copper catalysts are found to be the most reactive catalyst systems besides being versatile and less expensive.[87] The equilibrium constants should be so adjusted to avoid any type of side reactions like the outer-sphere electron transfer process or reduction/oxidation of radicals. Catalytic activity and selectivity mainly depends on ligands. Ligands are the key players in adjusting the redox potential of the metal for appropriate reactivity along with solubilizing the metal salt.[88] These ligands should not be involved in any sort of side reactions such as β-H

abstraction. Primarily nitrogen-based ligands are used in copper mediated ATRP.[89] Due to the unsuitable electronic effects and unfavorable binding constants, sulfur, oxygen and phosphorous based ligands are avoided. For copper based systems multidentate nitrogen ligands are used instead of monodentate ones as these ligands fail to promote controlled ATRP. Electronic and steric effects have profound influence on the catalytic activity. Strong electron withdrawing substituents on ligand and large steric hindrance around the metal center diminish the catalytic efficiency. Bridged or cyclic systems are better than linear analogues. The activity of nitrogen based ligands decreases with fewer number of coordinating N sites and higher number of linking carbon atoms in between the N coordinating sites. So the general order of activities of these ligands are as follows: teradentate (cyclic-bridged) > tertadentate (branched) > tetradentate (cyclic) > tridentate > tetradentate (linear) > bidentate. The nature of the N atom is crucial too and the order is pyridine ≥ aliphatic amine > imine. Some of the structures of ligands are shown in Figure 10.

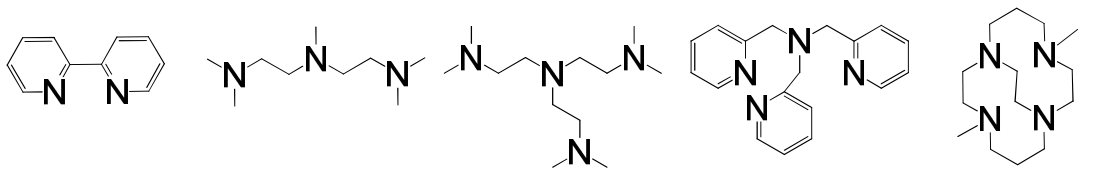

PMDETA: N, N, N', N'', N'''-pentamethyldiethylenetriamine

Me6TREN: Tris [2-(dimethylamino) ethyl] amine

TPMA: Tris (2-pyridylmethyl) amine

Cyclam-B: 4, 11-dimethyl-1, 4, 8, 11-tetraazabicyclo [6.6.2] hexadecane

Figure 10. Structures of different nitrogen based ligands.

According to the redox potentials of the Cu (I) and Cu (II) complexes with these amine ligands, enhanced catalyst activity is found with more reducing property. The higher the reduction potential, the higher the activity of the catalyst is.[90] The reactivity order of the ligands shown in Figure 10 is as follows: bipyridine < PMDETA < TPMA < Me6TREN < Cyclam-B.

2.5. Optimization of ATRP Reaction Conditions

The most commonly used ATRP catalysts and ligand combinations are the CuBr-PMDETA ligand system.[91] CuBr is the choice of catalyst over other copper halides e.g. CuCl as the halide exchange between the catalyst and polymer chain end is faster in the bromo system due to the labile C-Br bond.[92] However chain transfer/termination

processes for R-Br/CuBr systems exist which reduce the molecular weights at higher conversion and increase polydispersity. One of the major drawbacks of ATRP with the aliphatic amine ligands are their participation of various side reactions. In the course of reaction potentially active bromo terminated macromolecules can be converted to inactive macromolecules due to a possible chain transfer reaction to these aliphatic amine ligands. In addition, the amine ligands can react with the alkyl halides by a nucleophilic substitution reaction.[93] Another side reaction is the elimination reaction via an outer-sphere electron transfer (OSET) process induced by the Cu (II) species in the reaction system. In the OSET process the growing chain radicals are oxidized to carbocations by Cu (II) species followed by the loss of HX as shown in Figure 11.[94] One can predict the likelihood of the OSET process by considering the redox potential of the transition metal complexes and their halogenophilicities.[74] As a result well defined end functionalized polymer is difficult to obtain owing to these detrimental side reactions. Post-polymerization modification of end functional groups or diblock copolymer formation requires the end functional group to remain active. So there must be a trade-off between synthesis of higher molecular weight polymers and retention of active chain ends.

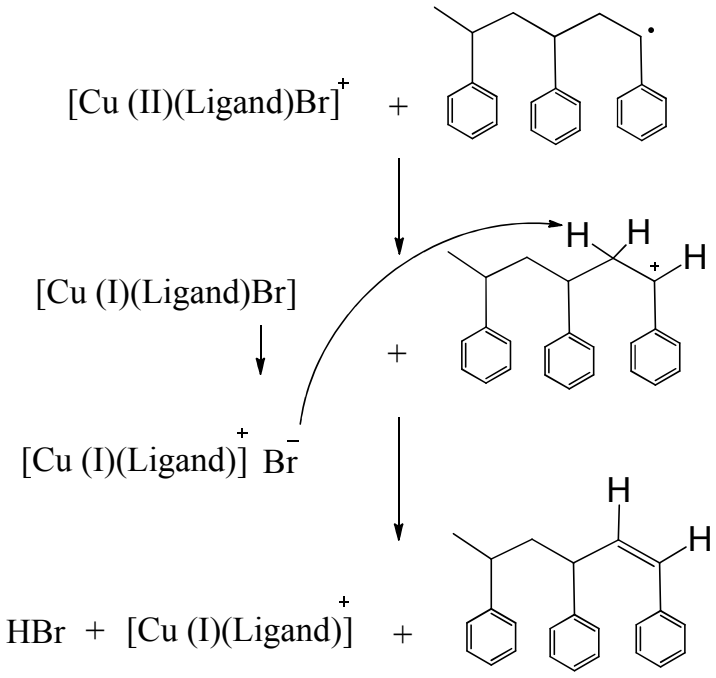

Figure 11. Possible mechanism of elimination by deactivator

Solvent also plays an important role in ATRP reactions. Choice of solvents is governed by multiple factors e.g. chain transfer to solvent, solvolysis of halogen ligands, etc. Polar solvents offer good control on the polymerization by solubilizing the catalyst complex as a homogenous catalyst system enhances the rate of polymerization and reduces the polydispersity. Polar solvents, however have drastically accelerate the above mentioned elimination side reactions, as well.[95] Non-polar solvents, though exert little effect on those elimination reactions, decrease the solubility of copper complexes especially Cu (I) complexes and reduce the polymerization rate. Although ATRP performs in a similar fashion whether or not the catalyst is soluble as the catalyst is not

bound to the growing chain, heterogeneous medium tends to result in higher polydispersity due to the lower concentration of Cu (II) and the slower deactivation process. In essence to obtain polymers with high end functionality for post-polymerization modification, a thorough understanding of the reaction kinetics is essential.

2.6. Design of Functionalized Monomers

In order to realize post polymerization functionalization and to construct building blocks for hybrid diblock copolymers through polymerization-hybridization approach, polymerization of an amine-protected styryl type monomer through ATRP has been designed. The structure of the monomer is given in Figure 12a. The amine group after deprotection of the phthalimide group and the chain end functional group would serve as handles for post polymerization reactions. If the active chain end functionality is retained for all polymers, it can be utilized to prepare block copolymers. A polyoxometalate cluster- containing styryl type monomer shown in Figure 12b has also been designed. The direct ATRP of this monomer may lead to the cluster-containing coil block in one step. In addition, it will facilitate in constructing hybrid diblock copolymers with complete cluster functionalization of all repeating units. The synthesis of POM containing monomer and its polymerization via ATRP for the development of hybrid diblock copolymer through hybridization-polymerization (hybridization first) approach will be discussed first followed by the synthesis and ATRP of amine-protected styryl type monomer for the

construction of hybrid diblock through polymerization-hybridization (polymerization first) approach.

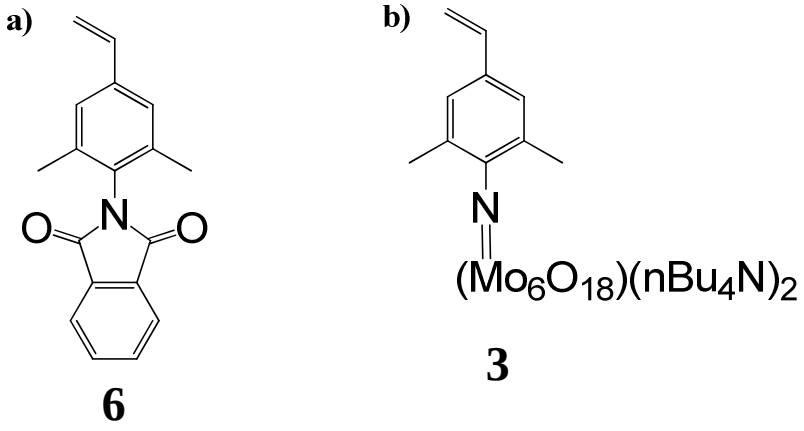

Figure 12. Structure of monomers for ATRP: a) amine protected styryl type monomer (6) and b) POM containing styryl type monomer (3)

2.7. Results and Discussion: Synthesis of the Coil Block using Hybridization-Polymerization Method

2.7.1. Synthesis of POM Containing Monomer and its ATRP Process

In this method a POM functionalized hybrid monomer is synthesized first, followed by its polymerization via ATRP to realize the coil block. The synthetic scheme for the preparation of POM containing hybrid monomer is shown in Scheme 3.

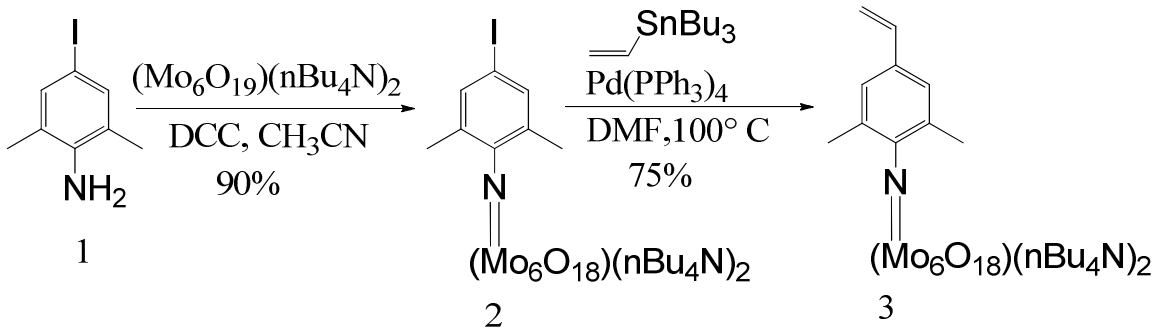

Scheme 3. Synthesis of POM containing monomer

The POM containing monomer 3 was synthesized in two steps via imido functionalization reaction of 4-iodo-2, 6-dimethylaniline (1) with the hexamolybdate cluster in the presence of DCC followed by the Stille coupling reaction. Realizing the synthetic challenge of converting the iodo functional group to vinyl group by Stille coupling reaction in the presence of free amines, the free amine was first capped with the molybdenum cluster by imido functionalization reaction according to a literature procedure to produce compound 2 in high yields. Compound 2 was then reacted with tributyl vinyltin in the presence of Pd (0) catalyst under standard Stille coupling conditions to give monomer 3 with a 75% yield. It was observed that the hexamolybdate moiety in compound 2 accelerated the coupling reaction presumably due to the electron withdrawing nature of the Mo≡N which activates the aryliodo group.

A mixture containing monomer 3 and styrene was then subjected to ATRP polymerization as shown on Scheme 4. Homopolymerization of the monomer 3 was difficult to achieve due to the steric bulkness of the repeating unit and the perceived poor solubility of the resulting polymer. The ATRP of the monomer mixture was carried out in DMF with the CuBr-PMDETA catalyst ligand combination at 110° C for 12 h. The reaction mixture after diluting with THF was passed through a neutral alumina column to get rid of the catalyst. Upon evaporation of the solvent, the crude product was precipitated out of methanol. The NMR spectra identified the product to be polystyrene. No signal corresponding to the cluster containing polymer was observed in the NMR. So, in order to investigate whether the cluster-containing monomer indeed polymerized, the alumina column was again eluted with DMF solvent. The eluted DMF solution was little cloudy. The solution was distilled off and the resulting solid was precipitated out from methanol. The resulting polymer which was believed to be compound 4 was completely insoluble in any solvent. So it was difficult to characterize it. It seemed the ATRP reaction occurred but due to the insoluble nature of the polymer, it was difficult to proceed further with it. Realizing the need for additional experiments we shifted our focus toward the second approach of making hybrid diblock copolymer i.e. polymerization-hybridization (polymerization first) method.

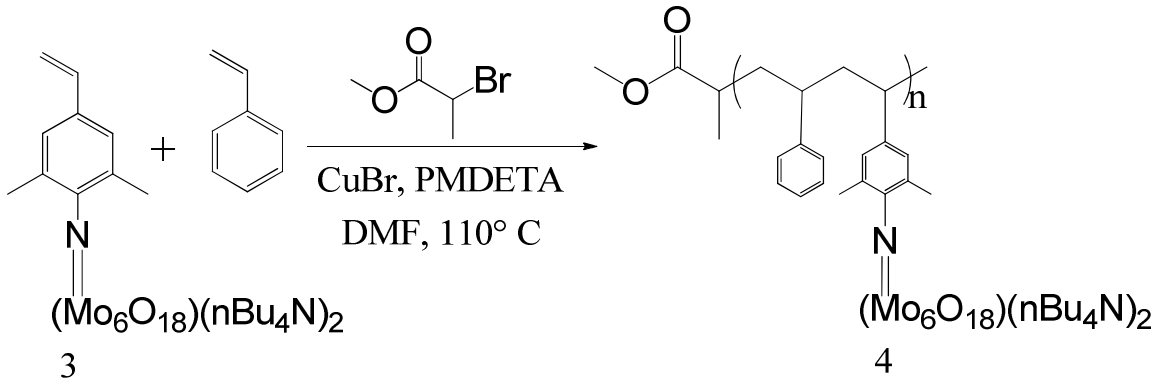

Scheme 4. ATRP of POM containing monomer.

2.7.2. Structural Characterization of POM Containing Monomer

^{1}H NMR spectra ($CDCl_3$, 400 MHz) of compound 2 and 3 are illustrated in Figure 13. All the ^{1}H NMR peaks can be assigned to the products. The vinyl protons in compound 3 at 5.27, 5.75 and 6.71 ppm are observed. The aromatic proton signal (signal f) is shifted upfield by 1 ppm in compound 3 compared to 2.

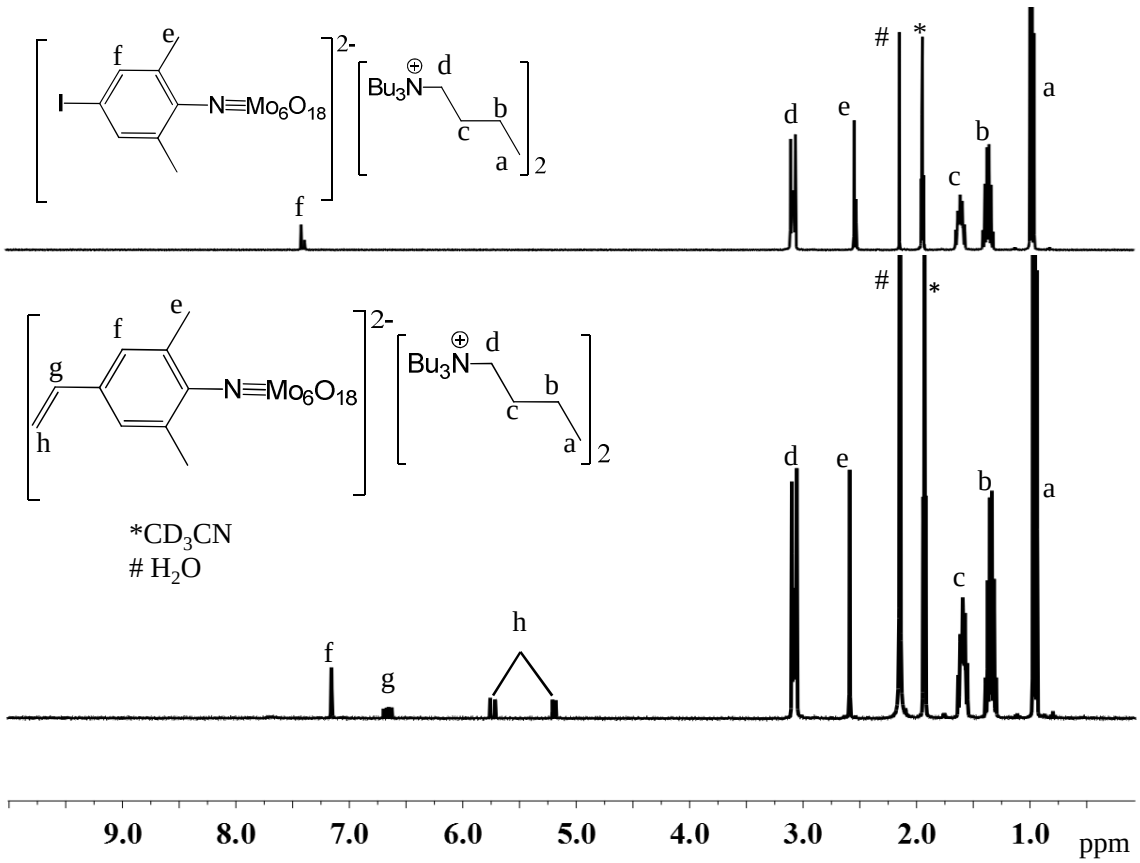

Figure 13. ^{1}H NMR spectra ($CDCl_3$, 400 MHz) of 2 (top) and 3 (bottom).

2.8. Synthesis of the Coil block using Polymerization-Hybridization Approach

2.8.1. Synthesis of Amine-Protected Styryl Type Monomer

The synthetic approach is shown in Scheme 5.

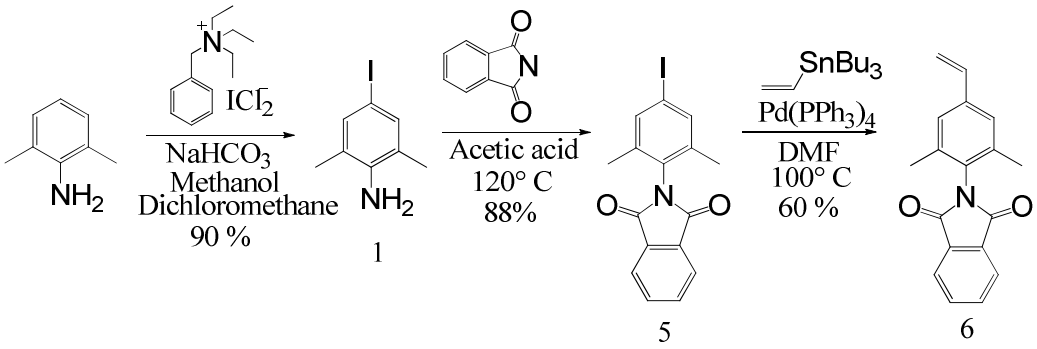

Scheme 5. The synthetic scheme of monomer 6.

Benzyltriethylammonium dichloroiodate was synthesized according to a literature method and was used for the iodination of 2, 6-dimethylaniline [96] followed by protection of the free amine group using phthalic anhydride to give compound 5.[97] Protection of the arylamine group is needed as the free amine group can act as a ligand and coordinate with the copper catalyst, thus interfering the ATRP process. Stille coupling reaction of 5 with tributyl vinyltin afforded the monomer 6 in 60 % yield.

2.8.2. Structural Characterization

The structures of the intermediates and monomer were confirmed by ^{1}H NMR and ^{13}C NMR. The ^{1}H NMR ($CDCl_3$, 400 MHz) spectrum and ^{13}C NMR ($CDCl_3$, 400 MHz) spectrum of monomer 6 are depicted in Figure 14 and 15 respectively.

The proton peaks around 5.27 ppm, 5.75 ppm and 6.67 ppm are corresponding to vinyl protons. Three distinct aromatic peaks are observed where the peak around 7.21 is due to the aromatic ring attached to the vinyl group. Two other peaks around 7.79 and 7.95 ppm are attributed to the phthalimide aromatic protons. The dominant alkyl proton signal at 2.03 ppm is assigned to the two phenyl-bonding methyl groups.

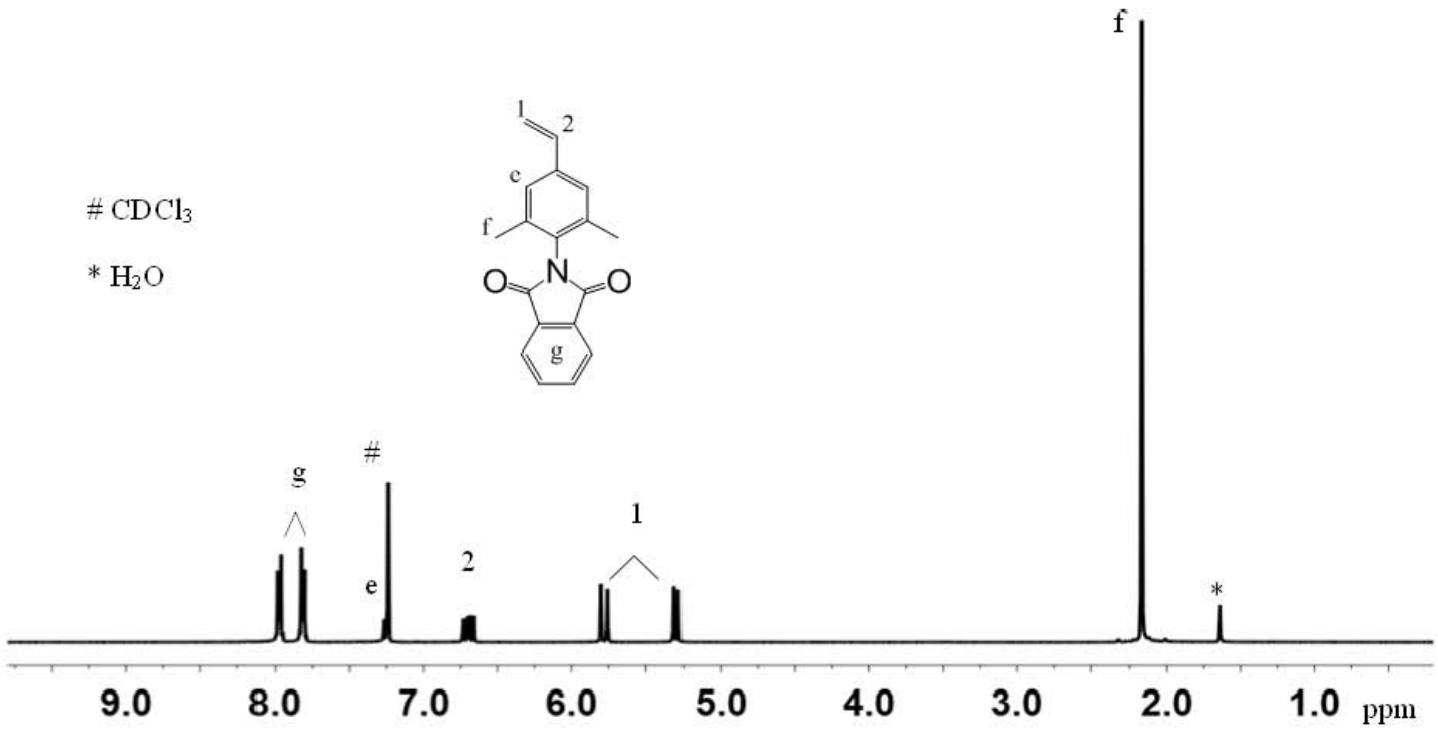

Figure 14. ^1H NMR spectrum ($CDCl_3$, 400 MHz) of monomer 6

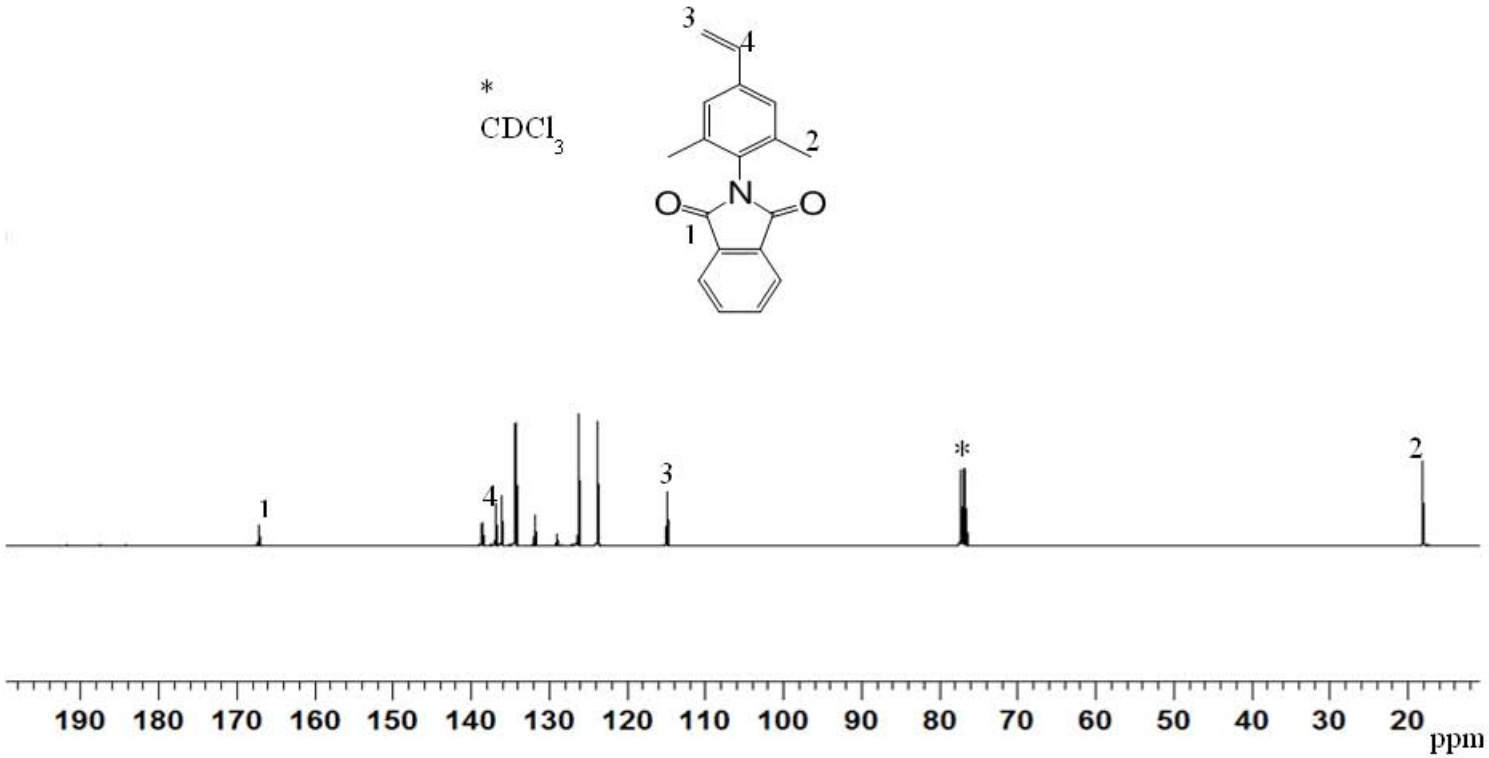

Figure 15. ^{13}C NMR ($CDCl_3$, 400MHz) spectrum of monomer 6

2.9. Synthesis of Polymer via ATRP

The reaction path for the polymerization of the monomer 6 through ATRP is shown in Scheme 6. CuBr was used as the catalyst and PMDETA as the ligand. Methyl-2-bromopropionate was employed as the initiator. The polymers were precipitated out from methanol several times.

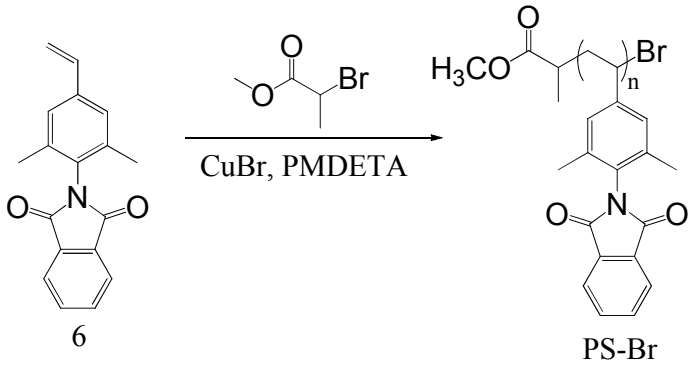

Scheme 6. ATRP of monomer 6.

2.10. Optimization of ATRP Conditions through NMR Analysis

To explore the optimized conditions under which the resulting polymers retain the end-functional group, monomer 6 was polymerized via ATRP under varied conditions. The three parameters which have been altered are temperature, solvent and stoichiometric ratio of the reactants. The list of different temperatures, solvents and stoichiometric ratios is shown in Table 3.

Table 3. Different reaction parameters for ATRP of monomer 6

	Molar Ratio (Monomer : Initiator: Catalyst: Ligand)		
	44:1:1:1		80:2:1:1
Temperature	95°C	110°C	110°C
Solvent	Anisole	Anisole	Anisole
	p-xylene	p-xylene	p-xylene

Primarily two different sets of molar ratios of the reagents were chosen. For each molar ratio two different solvents and temperatures were used. The monomer, initiator, catalyst and ligand molar ratio for the first set is in the order of 44:1:1:1. Anisole was the solvent of choice as it can dissolve the catalyst complex and form a homogenous solution to render a better control in polymerization. At a higher temperature the rate of polymerization increases because the ratio of k_p/k_t would be higher. However, some unavoidable side reactions can become dominant which could make the chain devoid of end functionality. We carried out ATRP of the monomer 6 at two different temperatures. The ^1H NMR spectra ($CDCl_3$, 400 MHz) of the reaction mixtures at different time intervals at a polymerization temperature of 95° C are shown in Figure 16. The reaction

mixture was passed through a short neutral alumina column and the solvent was evaporated before the NMR was taken.

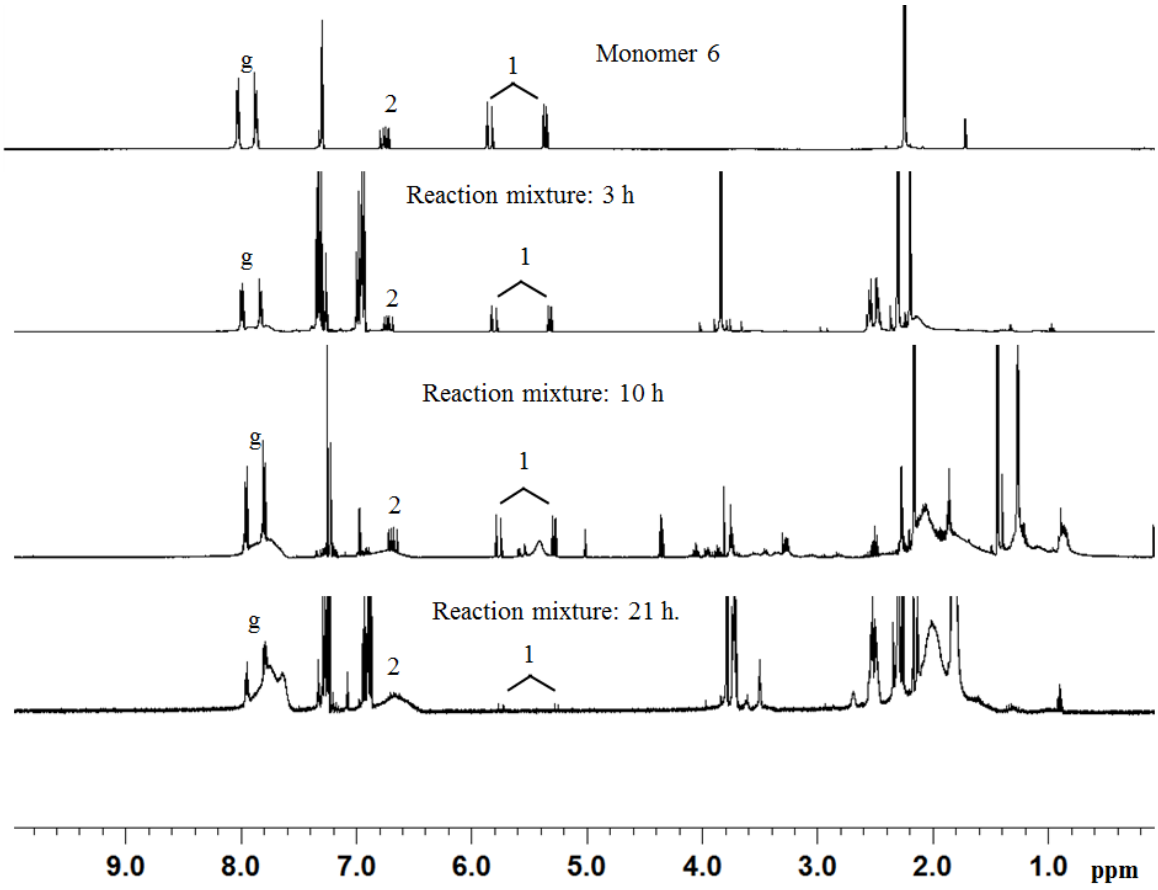

Figure 16. ^{1}H NMR spectra ($CDCl_3$, 400 MHz) of reaction mixtures at different time intervals.

The spectra of the monomer show three vinyl protons at 5.27 and 5.75 and 6.67 ppm. As the reaction progresses, the vinyl proton signals have gradually decreased. At 21h, the vinyl proton peaks almost disappeared with an appearance of a new broad peak at 6.67 ppm. The sharp aromatic peaks around 7.79 and 7.95 ppm (marked as g) corresponding to the phthalimide aromatic protons get broadened. These results indicated that the polymerization has really occurred. The reaction appears to be relatively slow as the significant vinyl protons remain even after 10 h. The reaction was stopped after 21 h and diluted with THF. The resulting reaction mixture was passed through the neutral alumina column to get rid of the copper catalyst. The solution was stripped off the solvent and precipitated the polymer from methanol. The precipitation process was repeated several times. The ^{1}H NMR spectra ($CDCl_3$, 400 MHz) of the final polymer is shown in Figure 17.

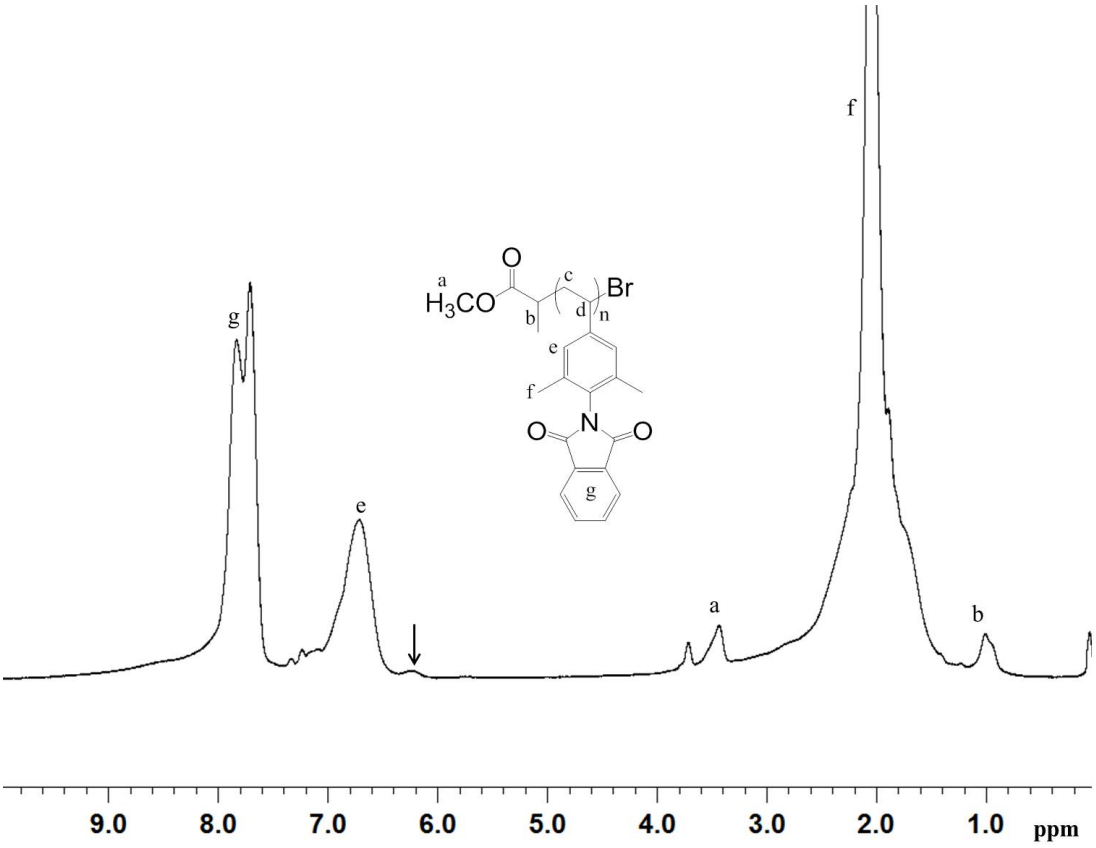

Figure 17. ^{1}H NMR spectrum ($CDCl_3$, 400 MHz) of pure polymer

The two broad overlapping peaks at 7.71 and 7.80 ppm (proton g) in Figure 17 correspond to the phthalimide unit whereas a broad peak around 6.65 ppm is attributed to the bridging phenyl ring protons (protons e). The broad and dominant alkyl signal at 2.03 ppm (proton f) can be assigned to the two phenyl bonding methyl groups. The initiating end methoxy signal (proton a) appeared at 3.42 ppm as a small broad signal and methyl fragment of the initiator (proton b) at 0.9 ppm. There is no signal observed corresponding to the proton associated with the end Br-bonding carbon in the region between 4.0 to 5.0 ppm. Instead one small but significant peak evolved (shown with black arrow) around

6.1-6.2 ppm region which can be attributed to the protons involving unsaturated dead end through elimination of HBr. It is evident from the spectrum that most of the chain ends are not active. It is likely that the reaction time is too long. At higher monomer conversions, the rate of propagation becomes slower while the rate of side reactions proceed at their normal rate as their rate is not dependent on the concentration of the monomer. Longer reaction time leads to higher conversions but with the loss of end group functionality.

Considering the sluggish nature of the reaction at the lower temperature and the loss of end functionality, the reaction temperature was raised to 110° C while the molar ratios of monomer to initiator to catalyst to ligand remain the same. The reaction was quenched after 5 h. The ^{1}H NMR spectrum ($CDCl_3$, 400 MHz) of the resulting polymer is shown in Figure 18. The proton signals are similar to the previous one. It is noteworthy to mention that by increasing the temperature from 95° C to 110° C the polymer formed in a short period of time. But once again no signals corresponding to the active chain end are observed, indicating that the majority of the polymers have lost the terminal bromide.

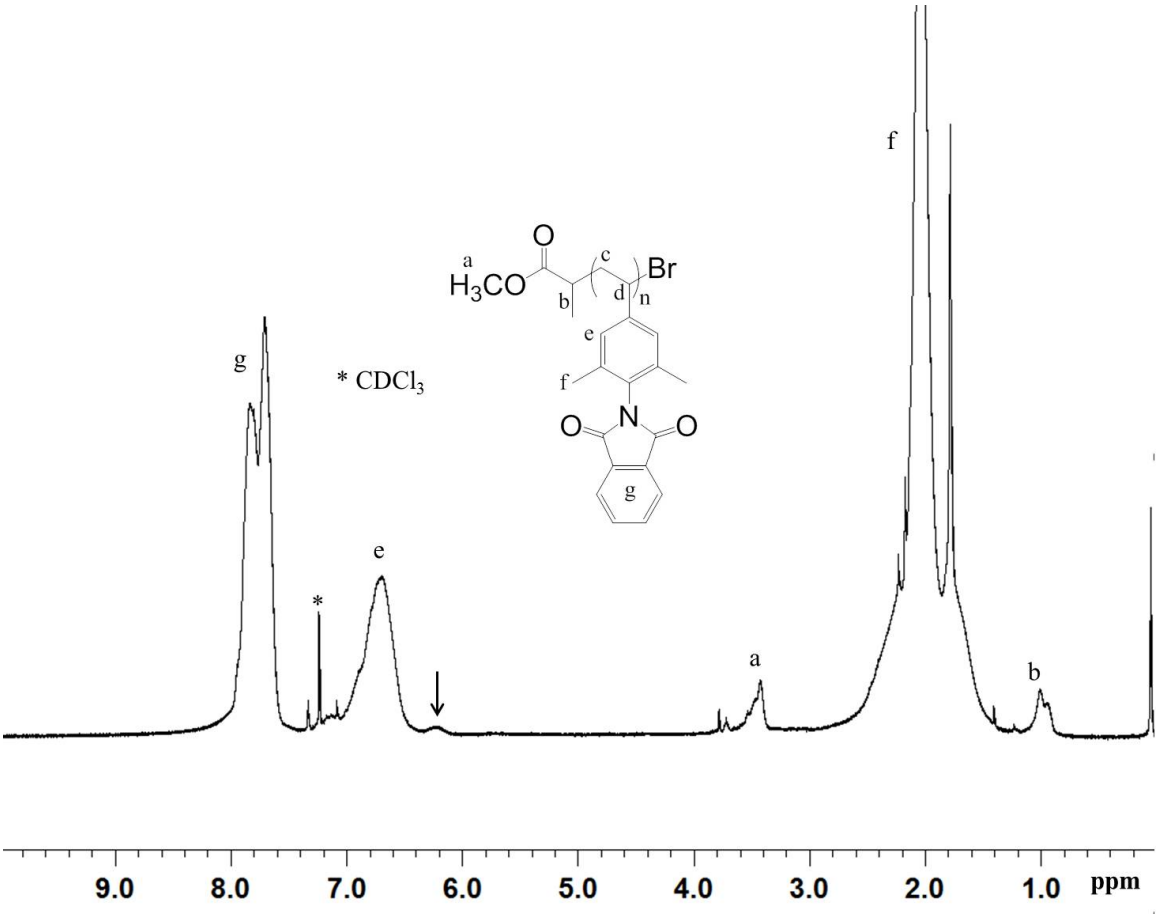

Figure 18. ^{1}H NMR spectrum ($CDCl_3$, 400 MHz) of pure polymer

The presence of dead polymer chains is significant at even shorter reaction time. It is unlikely that the concentration of the catalyst is too high. It is known [Cu (II)] complex can promote the elimination of HBr, rendering unsaturation at the chain end. Keeping that in mind, the molar ratio of the reaction mixture was changed so that the catalyst concentration remains low. The revised monomer: initiator: catalyst: ligand molar ratio was 80: 2: 1: 1. With this ratio, the monomer was again polymerized at two

different temperatures: 95° C and 110° C. Both the reactions were allowed to run for 5 h. The ^{1}H NMR spectra ($CDCl_3$, 400 MHz) of the two resulting polymers are shown in Figure 19.

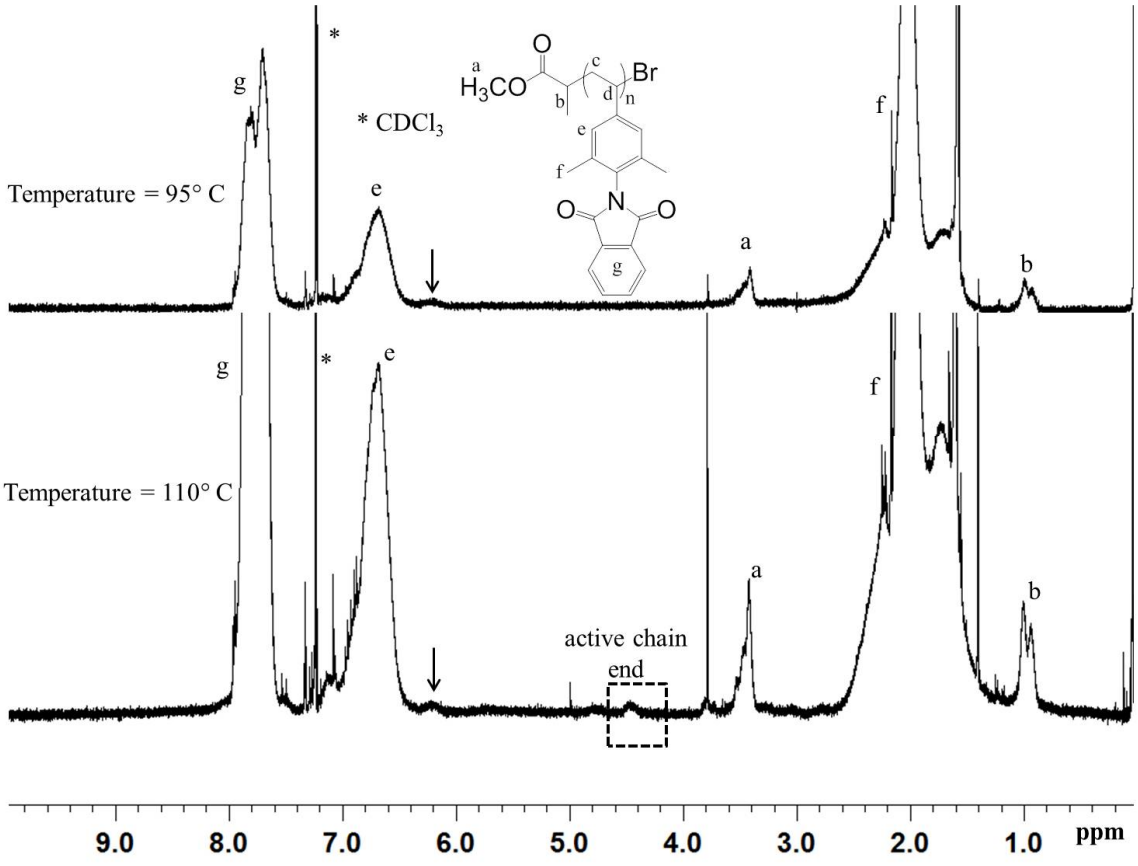

Figure 19. ^{1}H NMR spectrum ($CDCl_3$, 400 MHz) of pure polymer at two different temperatures

At 95°C, the polymer formed at a very shorter period of time as opposed to the previous case as shown in Figure 16. The probable reason might be the lowering of the deactivator concentration as it is inversely proportional to the rate of polymerization. At both temperatures dead chain proton signals are still present. The only difference is that at the higher temperature (110° C) the active chain end proton signal (proton attached to the Br-containing carbon) around 4.5 ppm (dotted box in Figure 19) is observed along with dead chain proton signals.

The results of these experiments revealed that changing molar ratio or temperature is not very effective in retaining majority of the active chain end functionality. Considering the fact that polar solvents are conducive to E1 elimination of alkyl bromides, we decided to change the reaction solvent from anisole to a non-polar p-xylene. First the molar ratio of 44:1:1:1 was chosen and the reaction was run at 110° C. The higher temperature was chosen because the catalyst system exhibits poor solubility in p-xylene. The ^{1}H NMR spectra ($CDCl_3$, 400 MHz) of the reaction mixture at different time intervals are shown in Figure 20. The vinyl proton signals (proton 1 and 2 in Figure 20) are decreasing gradually along with the broadening of the aromatic protons (g) during the course of the reaction. The reaction was quenched after 9 h. The ^{1}H NMR spectrum ($CDCl_3$, 400 MHz) of the resulting polymer is shown in Figure 21. The dead polymer chain is still dominant though a faint active chain end proton signal is visible (dotted box). The reactant ratio of monomer to initiator to catalyst to ligand molar ratio was then changed to 80:2:1:1. The reaction was quenched after 12 h. The ^{1}H NMR spectrum ($CDCl_3$, 400 MHz) of the crude polymer is shown in Figure 22. It is evident that the

active chain end proton signal (dotted box in Figure 22) is dominant over the dead chain end signal for the first time. This is the best reaction condition achieved so far although

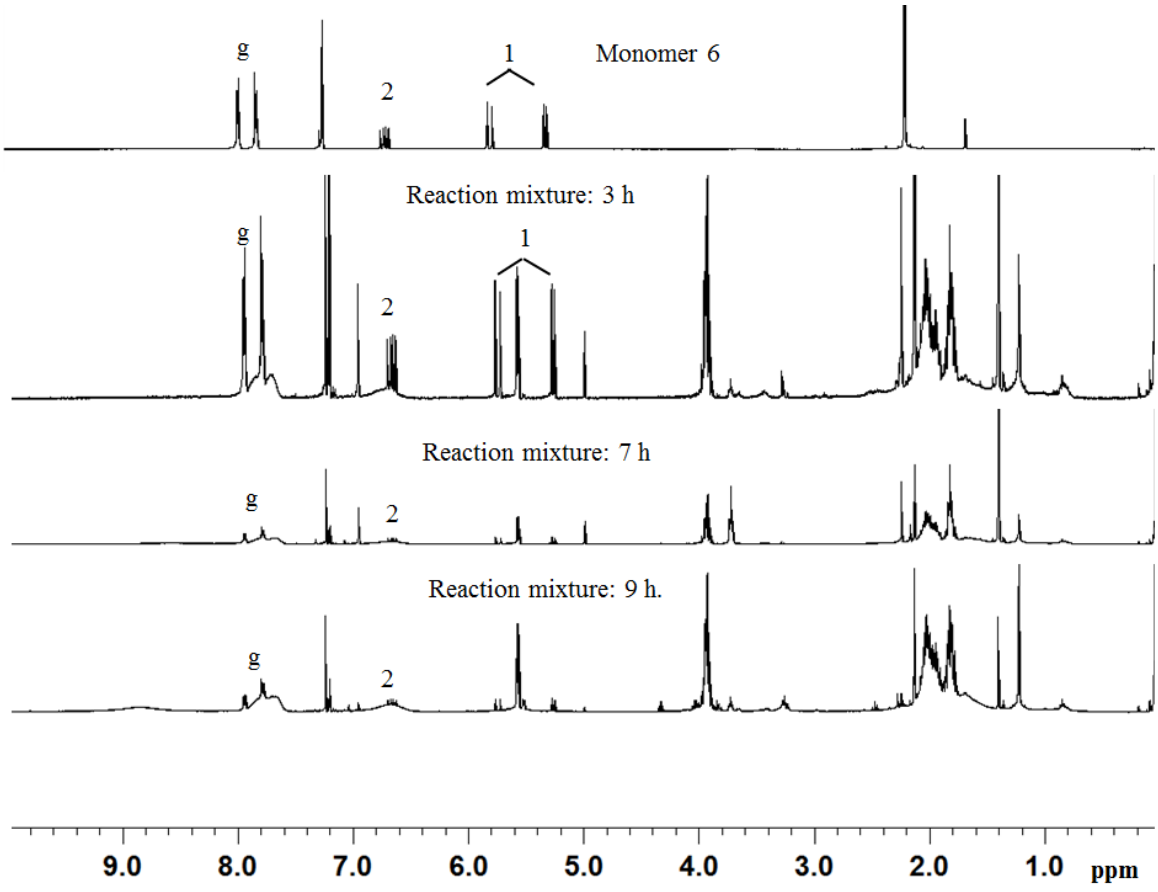

Figure 20. ^{1}H NMR spectrum ($CDCl_3$, 400 MHz) of reaction mixture at different time intervals

the dead chain end signal still persists. In order to minimize the dead chains, the reaction time is further shortened to 11 h. The ^{1}H NMR spectrum ($CDCl_3$, 400 MHz) of the crude polymer after 11 h is shown in Figure 23.

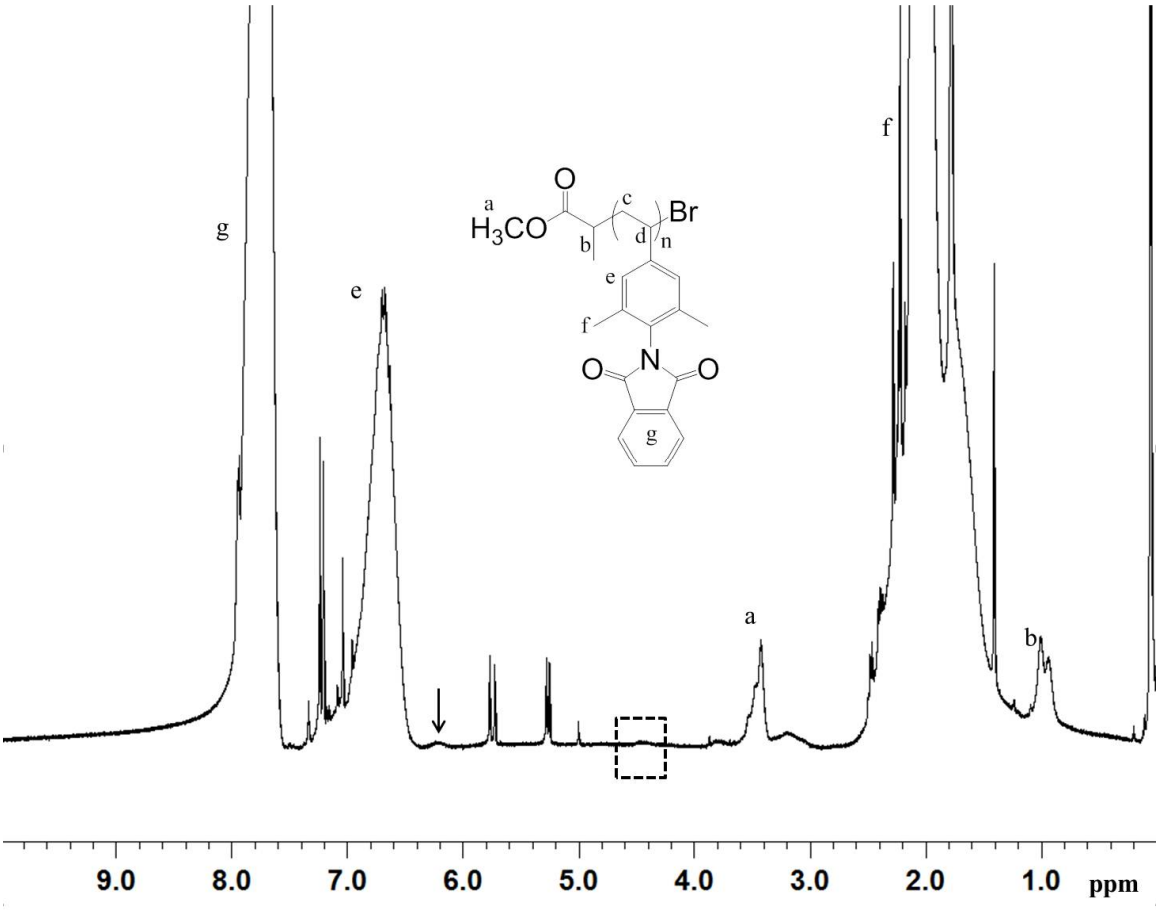

Figure 21. ^{1}H NMR spectrum ($CDCl_3$, 400 MHz) of crude polymer

It is obvious from the spectrum (Figure 23) that no dead chain proton signals are visible whereas the small but prominent peak at 4.45 ppm confirms that the majority of the polymer chains are still active i.e. majority of the polymer chain ends carry the bromo functionalized group. In summary, the ATRP of monomer 6 is best to run at 110° C in p-xylene with a reactant ratio of 80:2:1:1 (monomer: initiator: catalyst: ligand) and a reaction time around 11 h. Under such conditions, the overwhelming majority of the polymers obtained bear the active bromide end functional group.[98]

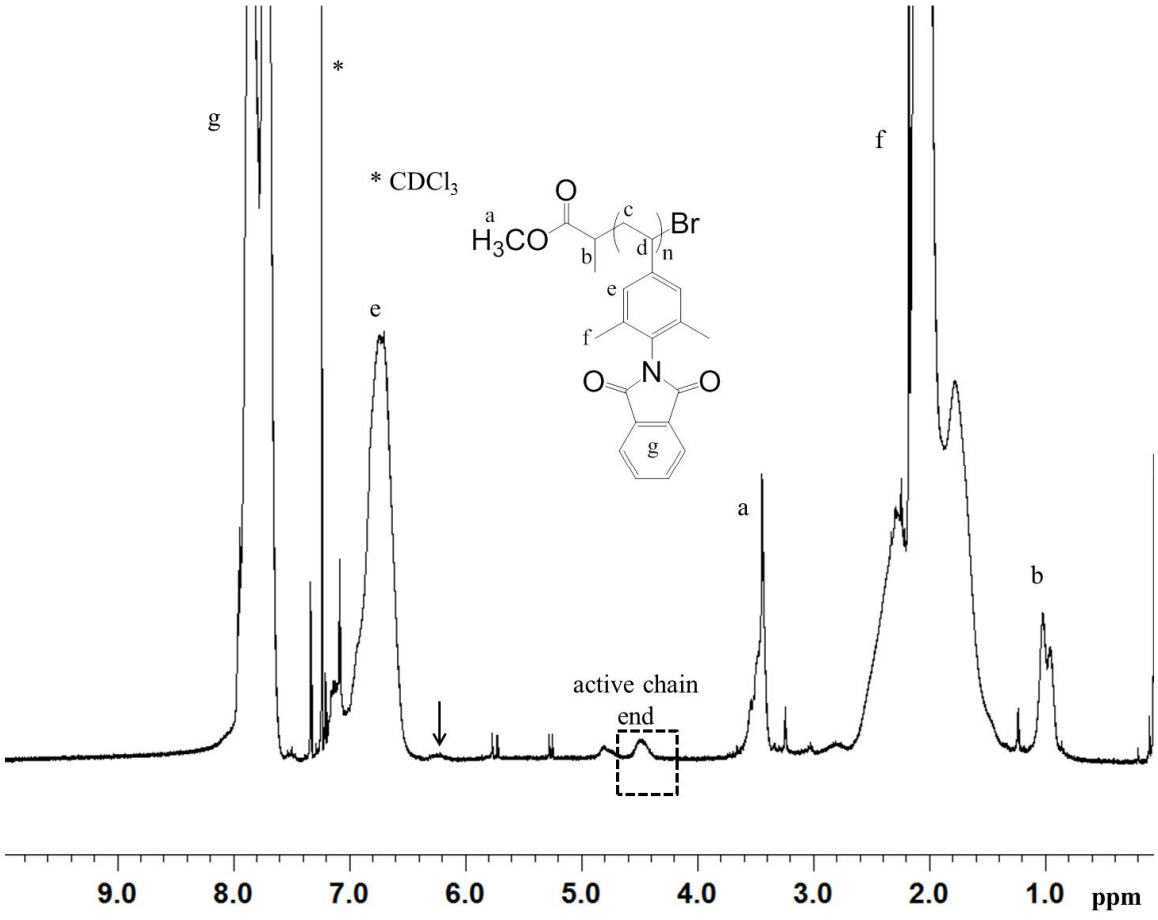

Figure 22. ^{1}H NMR spectrum ($CDCl_3$, 400 MHz) of crude polymer

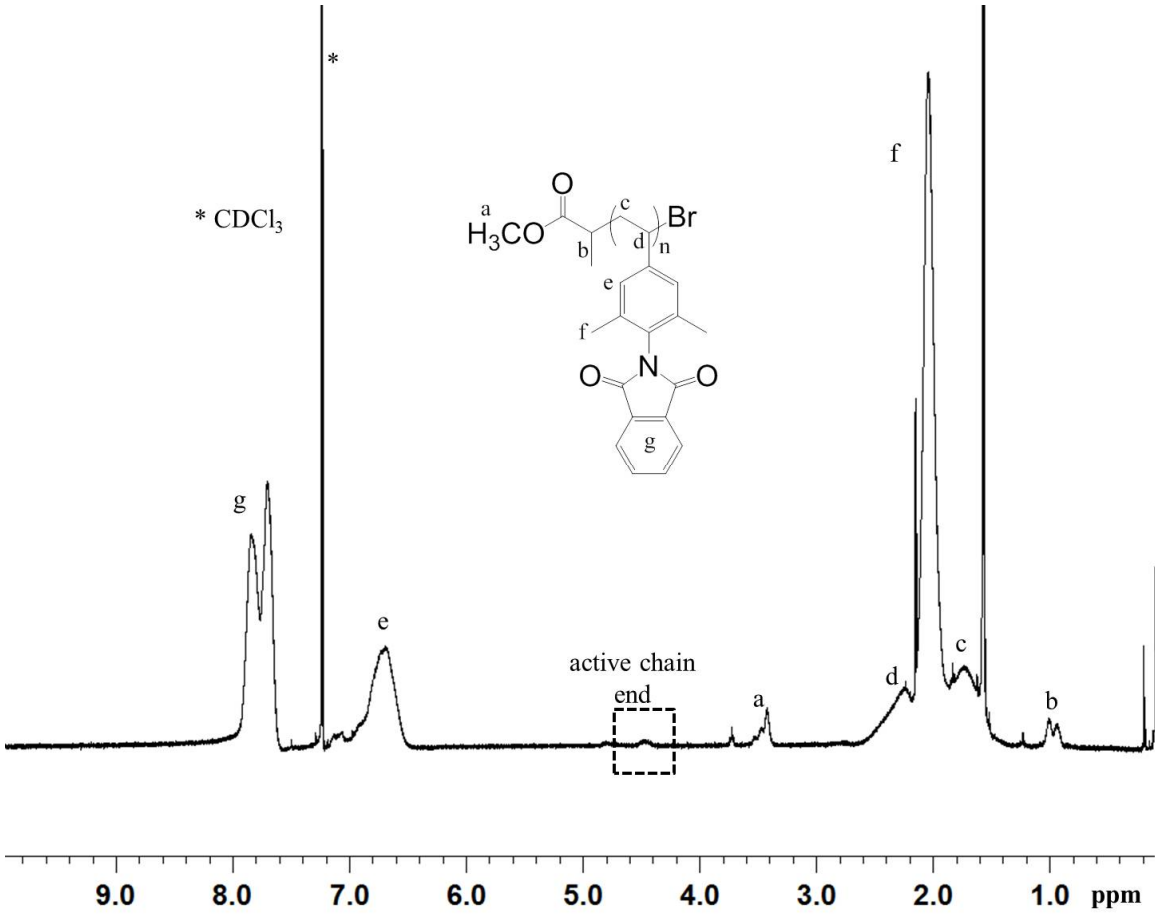

Figure 23. ^{1}H NMR spectrum ($CDCl_3$, 400 MHz) of crude polymer

2.11. Results and Discussion

2.11.1. Structural Characterization of the Polymers

The structure of the polymer synthesized via ATRP was confirmed by ^{13}C NMR spectroscopy besides ^{1}H NMR. The ^{1}H NMR spectrum ($CDCl_3$, 400 MHz) and ^{13}C NMR ($CDCl_3$, 400 MHz) of the polymer is depicted in Figure 24 and 25 respectively. All the

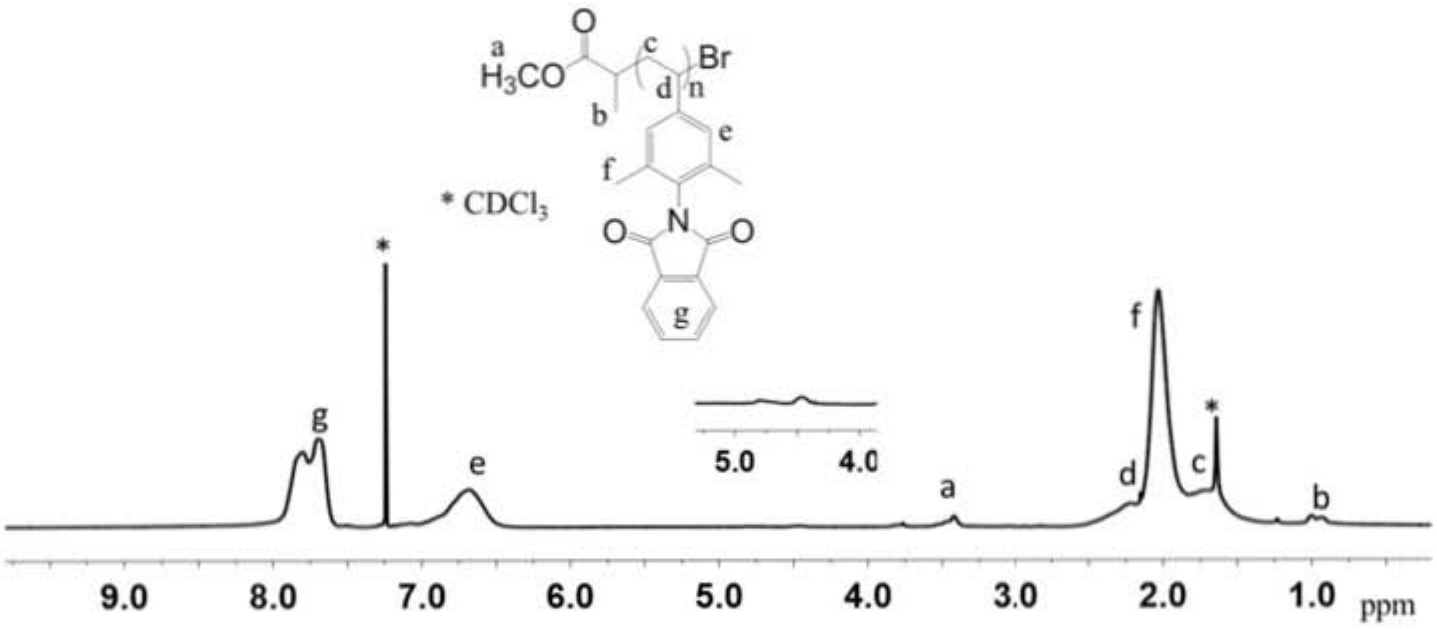

Figure 24. ^{1}H NMR spectrum ($CDCl_3$, 400 MHz) of polymer

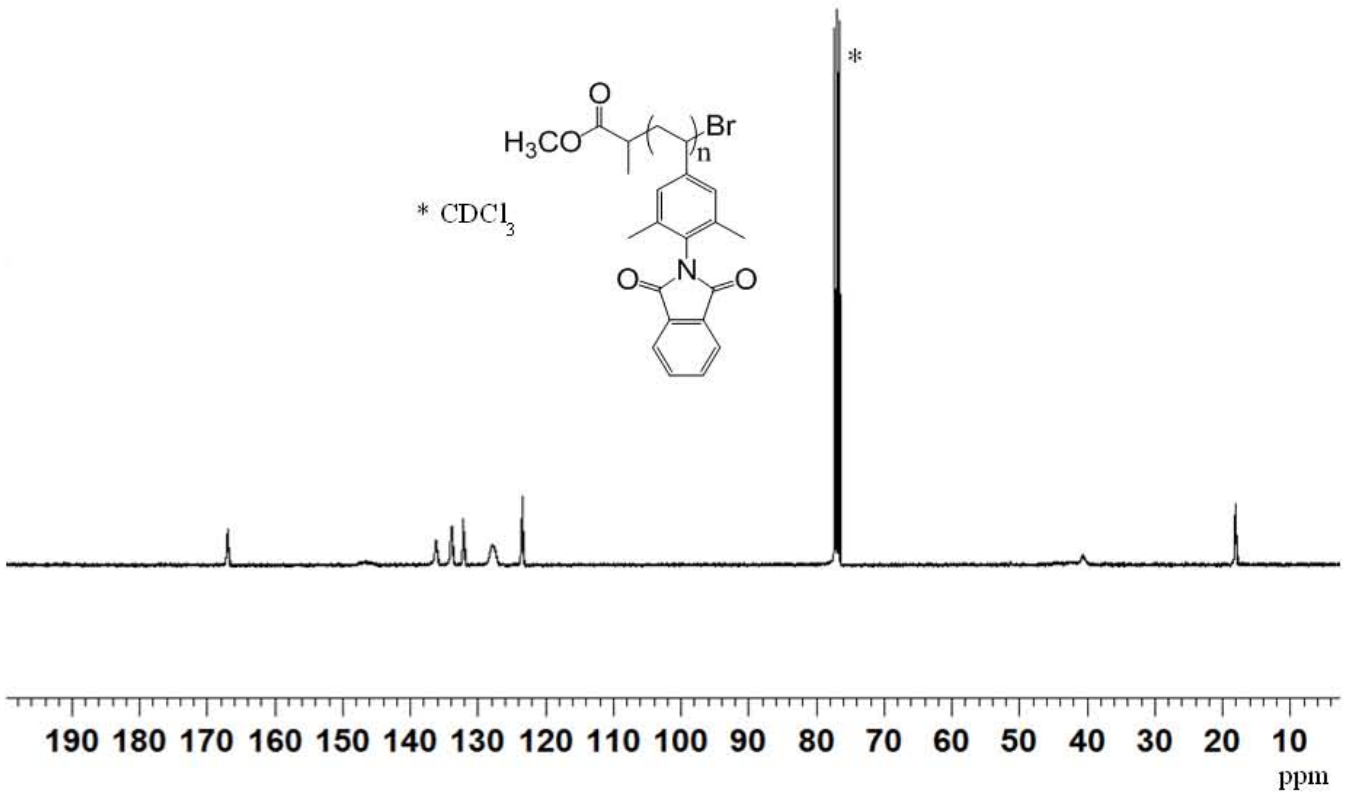

Figure 25. ^{13}C NMR spectrum (CDCl3, 400 MHz) of polymer

peaks of ^{1}H NMR can be unambiguously assigned to the polymer structure. End groups give small but clear signals. The initiating end gives methoxy signals at 3.42 ppm and methyl signals (b) around 0.9 ppm. Signals corresponding to propagating ends are not as clear. If one expands the region with chemical shits from 4.0 ppm to 5.0 ppm, one sees a clear signal around 4.43 ppm which can be assigned to the proton associated with the Br-bonding carbon. Using the integration ratio of a signal distinctively attributed to the repeating unit versus one to the end groups, one may calculate the degree of polymerization (DP) to be around 22. The carbon peak at 114 ppm in Figure 25 assigned as vinyl carbon in monomer 6 has disappeared in the polymer ^{13}C NMR spectra. The carbon peaks of the polymer are somewhat broadened too.

2.11.2. Molecular Weight Determination

The molecular weight of the polymer was determined by gel-permeation chromatography (GPC). The measurement was run at 30° C using THF as eluent and the molecular weight was calculated relative to polystyrene standards. The polymer has a number average molecular weight (M_n) of 2732 and a polydispersity (PD) of 1.10. The GPC trace is shown in Figure 26. The relatively narrow molecular weight distribution indicates the living nature of polymerization.

Realizing the relative nature of the molecular weight obtained from GPC, matrix-assisted laser desorption/ionization-time-of-flight (MALDI-TOF) mass spectrometry measurement was also carried out to get the absolute molecular weight and molecular

weight distribution. The MALDI-TOF spectrum is shown in Figure 27. The spectrum of the polymer shows a regularly distributed set of peaks with mass difference of one repeating unit (277.11). On the basis of molecular weights and intensities of peaks the calculated M_n is 4494 and which corresponds to an average degree of polymerization of 18, reasonably consistent with what obtained by ^1H NMR. The narrow molecular weight distribution of the polymer (PD= 1.10) confirms the living nature of the polymerization. It is to be noted that the molecular weight of the polymer obtained is not high. One plausible reason is the early quenching of the reaction in order to retain the active chain ends. Another probable reason is the lower rate of polymerization within the time span of the polymerization.

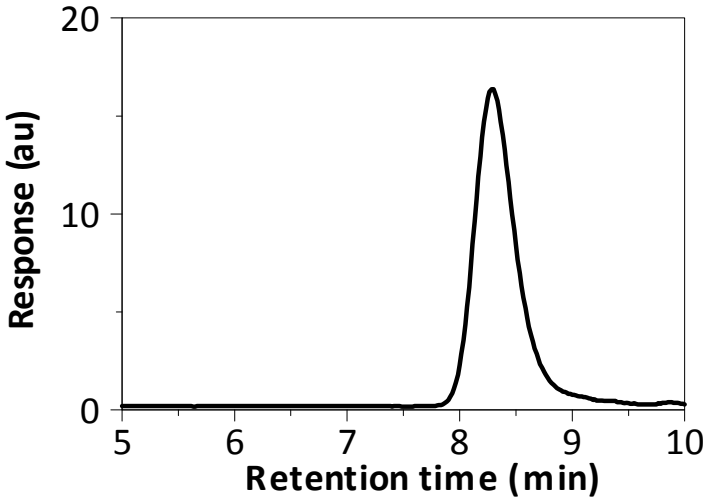

Figure 26. GPC trace of polymer using THF as the eluent

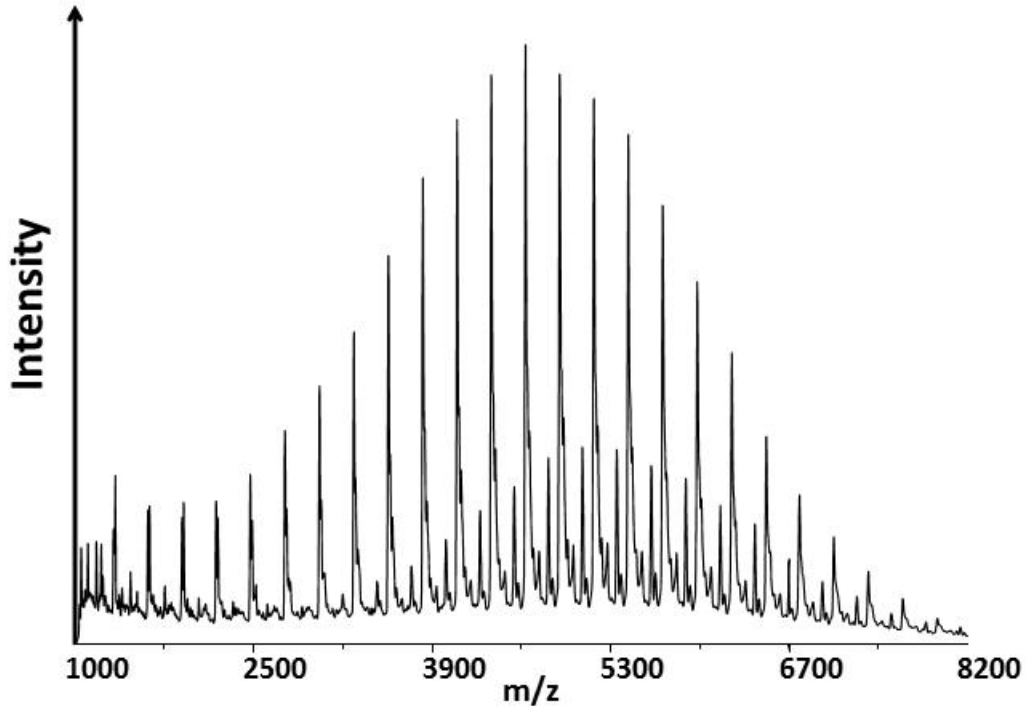

Figure 27. MALDI-TOF spectra of the polymer

2.12. Conclusions

Atom transfer radical polymerization (ATRP) method has been pursued to the successful polymerization of a novel amine-protected styryl type monomer. The amine group in the monomer was protected by phthalic anhydride to avoid any interference in the subsequent Stille coupling reaction and ATRP. The reaction conditions for ATRP have been optimized to realize the living nature of the polymer. Three basic parameters, namely, the reactant molar ratio, temperature and solvent were modified with CuBr and

PMDETA as the catalyst-ligand system. The reactions were monitored by ^{1}H NMR spectroscopy. Anisole being a polar solvent rendered the homogeneity of the reaction medium but provided poor end group control of the reaction. When ATRP was run in anisole, the majority of the polymer chains were devoid of the active bromo chain end functionality whether the reaction was run at 95°C or 110°C. The bromo end group was apparently eliminated as HBr which is favored in the polar medium. With p-xylene as the solvent, optimum reaction conditions were realized at 110°C and a lower reactant ratio. While majority of the polymer chains retain the active end functional group, the polymer molecular weights are only moderate due to the lower polymerization rate and shorter reaction time. The narrow molecular weight distribution of the polymer confirmed the living nature of the ATRP method. The direct ATRP of POM-functionalized styryl type monomer was also explored which resulted in an insoluble product.

2.13. Experimental Section

Materials. THF was purified by distillation over sodium pellets and benzophenone. CuBr was purified by washing consecutively with glacial acetic acid, absolute ethanol and diethyl ether, and then dried under vacuum. 2, 6-dimethyl aniline, N, N, N', N', N''-pentamethyldiethylenetriamine (PMDETA, 99%), methyl-2-bromopropionate and p-xylene were distilled in vacuo before use. All other chemicals were purchased either from Aldrich or Acros and were used as received unless otherwise stated.

Instrumentation. All reactions were conducted under protection of nitrogen. The ^{1}H NMR and ^{13}C NMR spectra were collected on a Varian INOVA400 MHz FT NMR spectrometer. All samples were referenced to the deuterated solvents. GPC measurements were performed at 30°C on a Waters system equipped with a Waters 410 differential refractometer, Waters 515HPLC pump and a styragel HR 4E column with THF as the eluent. The calibration curve was determined by the use of five polystyrene standards from 800 to 90,000. A Voyager DE Pro (Perceptive Biosystems/ABI) MALDI-TOF mass spectrometer was used for mass measurement operating in both linear and reflector mode. A mixture of silver trifluoroacetate/dithranol (1, 8-dihydroxyanthrone) (1:25 w/w) was used as the matrix.

4-iodo-2, 6-dimethylaniline (1). 2,6-dimethylaniline (10 g, 82.5 mmol), methanol (100 mL), methylene chloride (100 mL) and sodium bicarbonate (15 g, 178 mmol) were mixed in a two-neck round bottom flask and cooled in an ice-water bath. A yellow solution of benzyltriethylammonium dichloroiodate (32 g, 92 mmol) in methylene chloride (80 mL) was added dropwise to the above ice cooled solution while keeping the reaction temperature below 15°C. The resulting reaction mixture was stirred for 20 minutes in the ice water bath and another 30 minutes without the bath. The resulting mixture was washed with water and the organic layer was stripped off the solvent to get dark black solids which were purified by recrystallization from hexanes several times to yield compound 1 as a gray solid (18.5 g, 74.5 mmol, 90.3%, mp 50-51° C). ^{1}H NMR (400 MHz, CD_3CN, 25° C): δ 2.10 (s, 6H), 3.55 (s, 2H), 7.22 (s, 2H). ^{13}C NMR (400 MHz, CD_3CN, 25° C): δ 17.39, 79.25, 124.23, 136.56, 142.73.

Compound 2. A mixture of 4-iodo-2, 6-dimethylaniline (1.0 g, 4.05 mmol), dicyclohexylcarbodiimide (0.89 g, 4.36 mmol), hexamolybdate $[Mo_6O_{19}][Bu_4N]_2$ (5.6 g, 4.08 mmol) and acetonitrile (40 mL) was stirred under reflux for about 12 h. After cooled to room temperature, the resulting red-orange solution was filtered to remove the byproduct (N, N'-dicyclohexylurea). Absolute ethanol (20 mL) was then added into the filtrate. The product precipitated out of the solution as orange crystals and was collected by filtration. The product was washed successively with ethanol and diethyl ether several times and dried under vacuum to yield organoimido compound 2 as reddish orange crystals (5.5 g, 85%). ^{1}H NMR (400 MHz, CD_3COCD_3, 25 °C): δ 7.45 (s, 2H), 3.45 (t, *J* = 8.6 Hz, 16H), 2.58 (s, 6H), 1.83 (q, *J* = 7.9 Hz, 16H), 1.46 (m, 16H), 0.98 (t, *J* = 7.3 Hz, 24H).

Compound 3. Compound 2 (1.04 g, 0.652 mmol) and tetrakis (triphenylphosphine) palladium (0) (0.023 g, 0.019 mmol) were taken into a 2-neck flask. The flask was evacuated and backfilled with nitrogen three times. Tributyl (vinyl) tin (97%, 0.27 g, 0.83 mmol) and DMF were added dropwise to the flask with syringe. The resulting mixture was stirred at 100° C for 4 h and then poured into water. The solution was extracted with methylene chloride (3× 300 mL). The organic layer were combined and dried over magnesium sulfate. The solvent was evaporated to get a dark reddish liquid. The product precipitated out when cold ethanol was added to the liquid as reddish orange solid (0.73 g, 75%). ^{1}H NMR (400 MHz, $CDCl_3$, 25 °C): δ 7.17 (s, 2H), 6.66 (dd, *J* = 10.8 Hz, 17.6 Hz, 1H), 5.76 (dd, *J* =0.8 Hz, 17.6 Hz, 1H), 5.19 (dd, *J* = 0.8 Hz, 10.8 Hz, 1H), 3.10 (t, *J* = 8.6 Hz, 16H), 2.59 (s, 6H), 1.56 (q, *J* = 7.9 Hz, 16H), 1.34 (m, 16H),

0.96 (t, *J* = 7.3 Hz, 24H). Anal. Calcd. For $C_{42}H_{854}N_3O_{18}Mo_6$: C, 34.25; H, 5.68; N, 2.79; Mo, 38.18. Found: C, 31.33; H, 5.07; N, 2.50; Mo, 40.57.

Compound 5. 4-iodo-2, 6-dimethylaniline (1, 10 g, 36.4 mmol), phthalic anhydride (6.0 g, 36.4 mmol) and glacial acetic acid (180 mL) were combined and refluxed for 4 h. After cooled to room temperature, the precipitate was collected by filtration and washed with acetic acid, and then water. The product was dried under vacuum to produce 5 as white crystals (12.1 g, 32.1 mmol, 88%, mp 228-230° C). ^{1}H NMR (400 MHz, CD_3CN, 25° C): δ 2.12 (s, 6H), 7.56 (s, 2H), 7.80-7.83 (m, 2H), 7.95-7.98 9m, 2H). ^{13}C NMR (400 MHz, CD_3CN, 25° C): δ 17.90, 95.82, 124.04, 130.00, 131.96, 134.68, 137.55, 139.24, 167.03.

Compound 6. Compound 5 (8.95 g, 23.7 mmol), and tetrakis (triphenylphosphine) palladium (0) (0.522 g, 0.435 mmol) were added into a 100 mL two-neck flask. The flask was evacuated and backfilled with nitrogen three times. Tributyl (vinyl) tin, (97%, 7.75 g, 24.4 mmol) and DMF (10 mL) were then added dropwise to the flask with a syringe. The resulting mixture was stirred at 100 °C for 3 h and then poured into water. The solution was extracted with methylene chloride (3 × 300 mL). The organic layer was collected, washed with water (3 × 300 mL) and dried over magnesium sulfate. The solvent was evaporated to yield a yellow crude product, which was purified by column chromatography (silica gel, hexane/methylene chloride 4:1 as the eluent) to afford compound 6 as a white solid (4.00 g, 60%, mp 186-188 °C). ^{1}H NMR (400 MHz, $CDCl_3$, 25 °C): δ 7.95 (m, 2H), 7.79 (m, 2H), 7.21 (s, 2H), 6.71 (dd, *J* = 10.8 Hz, 17.6 Hz, 1 H), 5.78 (dd, *J* = 0.8 Hz, 17.6 Hz, 1H), 5.28 (dd, *J* = 0.8 Hz, 10.8 Hz, 1H),

2.14 (s, 6 H). ^{13}C NMR ($CDCl_3$, 400 MHz): δ 167.2, 138.6, 136.9, 136.1, 134.3, 131.9, 129.1, 126.3, 123.8, 115.0, 18.1. Anal. Calcd. For $C_{18}H_{15}NO_2$: C, 77.90; H, 5.45; N, 5.05. Found: C, 77.65; H, 5.33; N, 5.17.

PS-Br (ATRP of compound 6). Compound 6 (0.500 g, 1.803 mmol) and CuBr (0.006 g, 0.041 mmol) were added to flame-dried two-neck round-bottom flask. The flask was degassed and back-filled with nitrogen three times, and left under nitrogen. Then PMDETA (0.009 mL, 0.008 g, 0.041 mmol) was added via a gas-tight syringe, followed by *p*-xylene (0.900 mL). After addition, three freeze-pump-thaw cycles were performed and the mixture was allowed to stir at room temperature for 45 min under nitrogen. The solution became light green-colored. The flask was then placed into an oil bath at 110 °C and deoxygenated methyl-2-bromopropionate (0.005 mL, 0.007 g, 0.041 mmol) was added through a gas-tight micro liter syringe to initiate the polymerization. After 11 h, the contents of the flask were exposed to air to quench the polymerization. THF (30 mL) was then added to the flask to dissolve the polymer. The solution was then filtered through neutral alumina to remove the copper catalyst. The resulting colorless polymer solution was concentrated and twice precipitated into 10-fold excess of methanol. The white polymer was collected by vacuum filtration and dried under vacuum for 12 h (0.600 g). ^{1}H NMR (400 MHz, $CDCl_3$, 25 °C): δ 7.75 (br), 6.69 (br), 3.42 (br), 2.03 (br), 1.00 (br). ^{13}C NMR ($CDCl_3$, 400 MHz): δ 167.0, 145.9, 136.2, 133.9, 132.2, 127.8, 123.4, 40.4, 18.0. Anal. Calcd: C, 76.36; H, 5.41; N, 4.88. Found: C, 74.44; H, 4.67; N, 4.75. GPC: M_n= 2732, PD= 1.10. MALDI-TOF MS: M_n = 4494, PD = 1.10.

CHAPTER 3

SYNTHESIS OF COIL-COIL DIBLOCK COPOLYMERS WITH COVALENT ATTACHMENT OF POLYOXOMETALATE CLUSTERS TO THE COIL BLOCKS

3.1. Flexible Block Copolymer-Inorganic Hybrids

Introducing a nanometer size structural moiety into a flexible block copolymer has been an innovative way to develop a variety of self-assembled morphologies with ordered domain structures.[63-66,99] Controlling the self-assembled multiphase domain structures has been key in realizing their potential in multiple fields including materials science and pharmaceutical industries. The shape and size of the nanometer sized units has found to profoundly affect the self-organization process of the block copolymers. For instance, the polyhedral oligomeric silsesquioxane (POSS) containing block copolymers have been widely studied.[63,64] In one example where POSS was introduced as a pendant in a PMMA-b-PMA diblock copolymer as shown in Figure 28a. The aggregation of the POSS units along with the self-assembly of the PMMA-b-PMA diblock has resulted in hexagonally packed micro pores with phase-separated nanodomains. Block copolymers with ionic pendants constitute another important class of materials which are commonly known as polyelectrolyte block copolymers. A great deal of effort has been devoted to study the complex micelle formation of these ionic diblocks in solution.[65] Addition of inorganic salts, counter ions, and another polyelectrolyte carrying opposite charges can modify or control the self-assembly process of the polyelectrolyte block copolymer.[65a,66] In many cases addition of inorganic salts resulted in the shrinkage of micelle corona and

a)

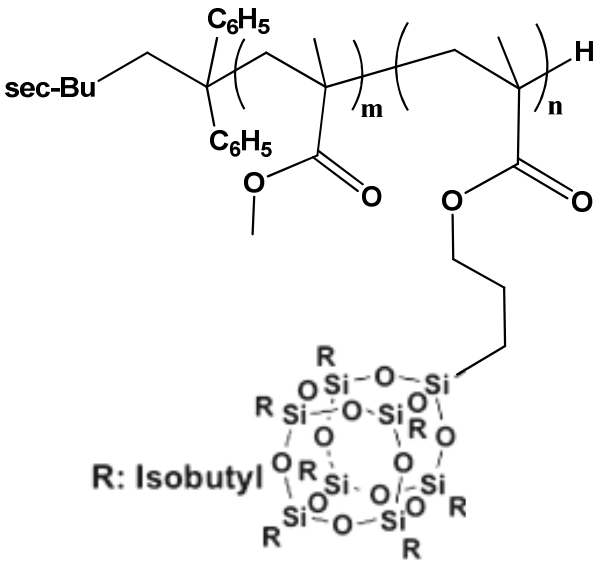

b)

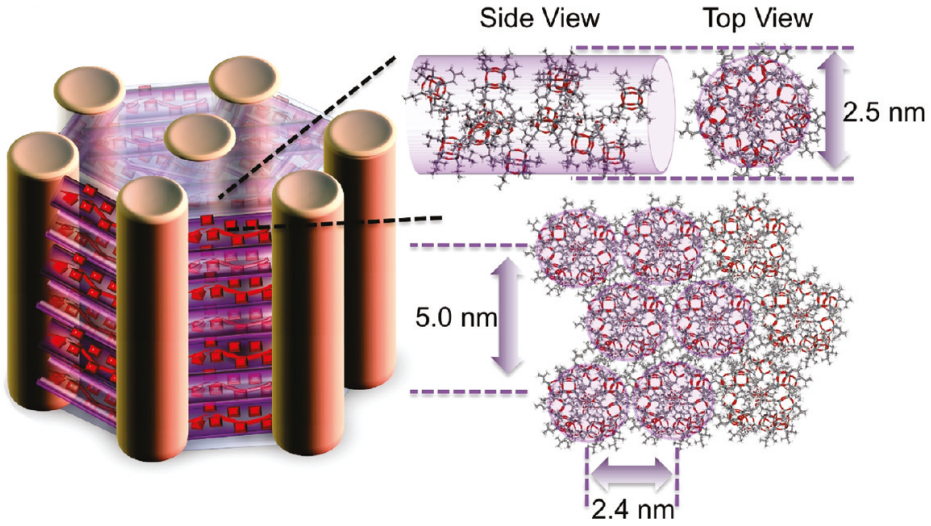

Figure 28. a) Structure of PMMA-b-PMAPOSS block copolymer b) Cartoon representation of thermally annealed morphology. Adapted with permission from Hirai, T.; Leolukman, M.; Jin, S.; Goseki, R.; Ishida, Y.; Kakimoto, M.; Hayakawa, T.; Ree, M.; Gopalan, P. "Hierarchical Self-Assembled Structures from POSS-Containing Block Copolymers Synthesized by Living Anionic Polymerization", *Macromolecules* **2009**, *42*, 8835. Copyright @ 2009, American Chemical Society.

the aggregation increases due to the electrostatic screening of repulsions between chains.[99] For a poly(acrylic acid)-*block* poly(methyl acrylate)-*block*-polystyrene (PAA-b-PMA-b-PS) polyelectrolyte triblock copolymer system it has been demonstrated that the micellar structure of the triblock copolymer can be controlled in solution by choosing organic diamine counterion of varying structures as shown in Figure 29.[65g] Three different diamines with different spacer length between the two amine end groups interact differently with the PAA blocks which induce the formation of disk-like micelles, cylindrical micelles or spherical micelles.

POM clusters being anionic in nature and by virtue of its nanometer size are expected to impact the self-assembly process of flexible diblock copolymers similarly as mentioned above. So a styrene monomer was copolymerized with the free amine protected styryl type functionalized monomer 6 (as synthesized in chapter 2) via ATRP to realize the first coil-coil diblock copolymer. The hybrid diblock copolymer was synthesized by reacting with polyoxometalate cluster through the polymerization-hybridization approach.

A second type of hybrid coil-coil diblock copolymer based on 4-vinylpyridine (4VP) was also synthesized. It is well known that the interaction between the two chemically linked blocks in a diblock copolymer plays a significant role in the self-assembly process. One way to tune the interaction between the two blocks is by adjusting the pH of the system. So the coil-coil diblock copolymer based on poly(4-vinylpyiridine)

(PVP) similar to PS-b-PVP can be envisioned. PS-b-PVP block copolymers have been prepared by both anionic living polymerization[39a] and ATRP.[39b,100] In our case we used ATRP to synthesize the diblock copolymer using free amine protected styryl type functionalized monomer 6 (as synthesized in chapter 2) along with 4-vinylpyridine. Likewise the hybrid diblock copolymer was realized by allowing the diblock copolymer to react with polyoxometalate cluster through polymerization-hybridization approach. Under different pH, pyridine will be protonated to a different extent, and thus by tuning the attractive interaction between the polystyryl type block and the PVP block a gradual transition from self-assembled domain structures to one homogenous phase is expected.

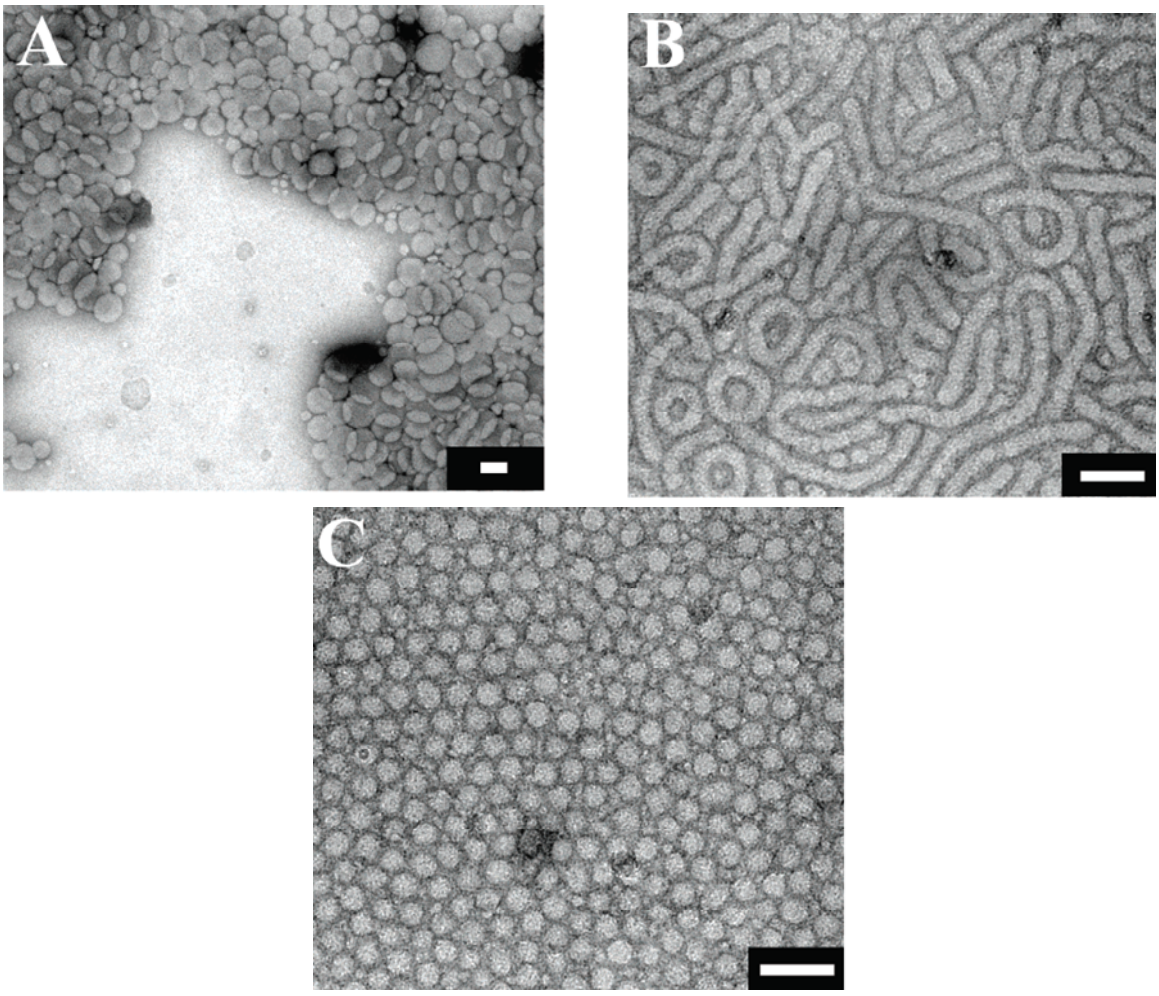

Figure 29. TEM images of micellar structure of triblock copolymer depending on diamine spacer length. A) disklike micelles, B) cylindrical micelles and C) spherical micelles. Scale Bar: 100 nm. Adapted with permission from Cui, H.; Chen, Z.; Wooley, K.L.; Pochan, D. J. "Controlling Micellar Structure of Amphiphilic Charged Triblock Copolymers in Dilute Solution via Coassembly with Organic Counterions of Different Spacer Lengths", *Macromolecules* **2006**, *39*, 6599. Copyright @ 2006, American Chemical Society.

3.2. Results and Discussion

3.2.1. Synthesis of Two different Coil-coil Diblock Hybrid

In order to obtain the first hybrid coil-coil diblock copolymer through polymerization-hybridization method the coil-coil diblock copolymer with free aryl amine pendant groups was synthesized followed by polyoxometalate cluster attachment. To synthesize the coil-coil diblock copolymer first of all styrene was polymerized via ATRP for certain amount of time to form one block and while the polystyrene chain is still active a mixture of styrene and amine-protected styryl type functionalized monomer 6 in 1:1 stoichiometric ratio were added into the same reaction vessel to polymerize further to form the second block of mixed monomers as shown in Scheme 7.

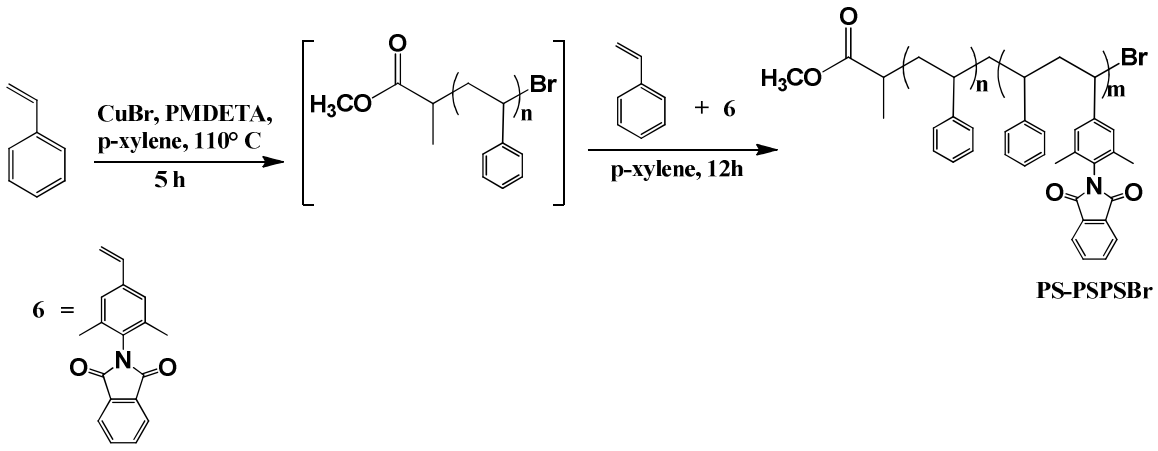

Scheme 7. Synthetic scheme of a PS-PSPSBr coil-coil diblock copolymer

The resulting coil-coil diblock copolymer PS-PSPSBr was then reacted with hydrazine hydrate according to Ing-Manske procedure[101] to obtain a diblock copolymer with pendant amine functional groups in the mixed monomer block by removing the phthalimide protecting group. The hybrid diblock was realized by reacting with excess hexamolybdate and DCC in DMF solvent as shown in Scheme 8. Excess free clusters were removed by precipitating the hybrid polymer from hot acetonitrile. The resulting cluster attached hybrid DCP or PS-Mo_6-PSPS is soluble in DMSO and DMF but insoluble solvents like chloroform, THF, acetonitrile, etc.

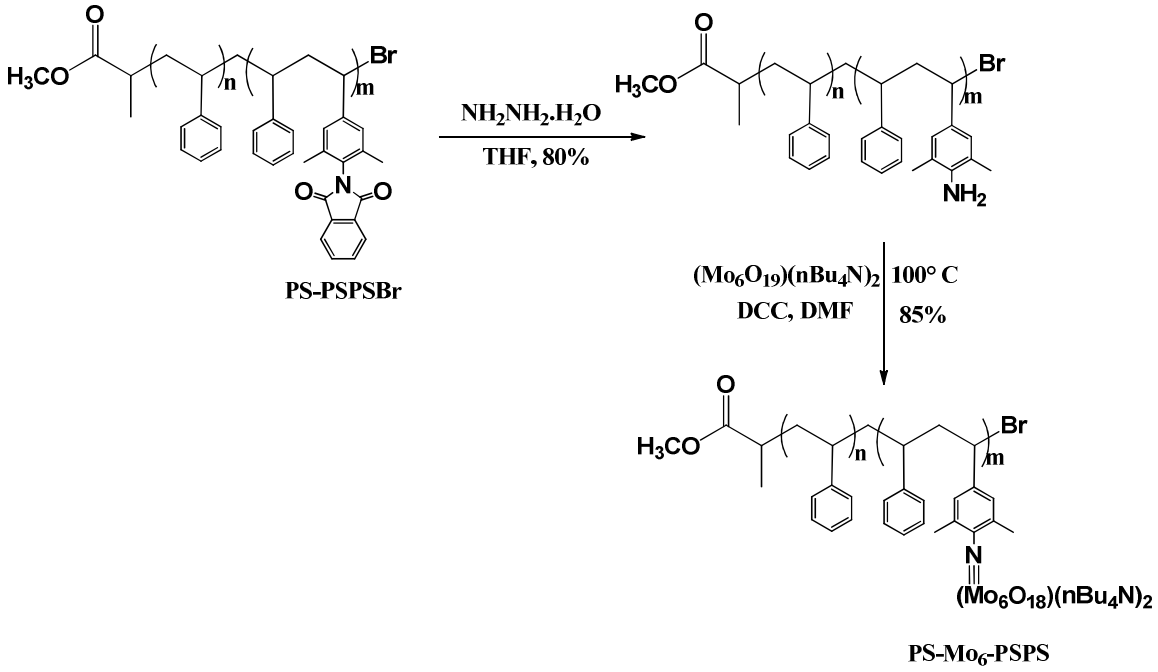

Scheme 8. Synthetic route for hybrid diblock copolymer

For the PS-P4VP coil-coil diblock copolymer, our initial attempt was to polymerize monomer 6 (as shown in Scheme 6 in Chapter 2), followed by the continuous polymerization of 4-vinylpyridine (4-VP) using ATRP as shown in Scheme 9. Unfortunately the reaction resulted in no diblock copolymer even after 12h due to the very slow polymerization rate of 4-VP. Considering the low solubility of reactants in p-xylene, DMF was used as the solvent which dissolved the reactants completely. But the polymerization rate was still very slow as shown in Figure 30, where the monomer peaks still dominate the ^{1}H NMR spectrum even after 12 h of reaction, indicating very low

monomer conversion. These results prompted us to investigate further into the details of the polymerization of 4VP via ATRP.

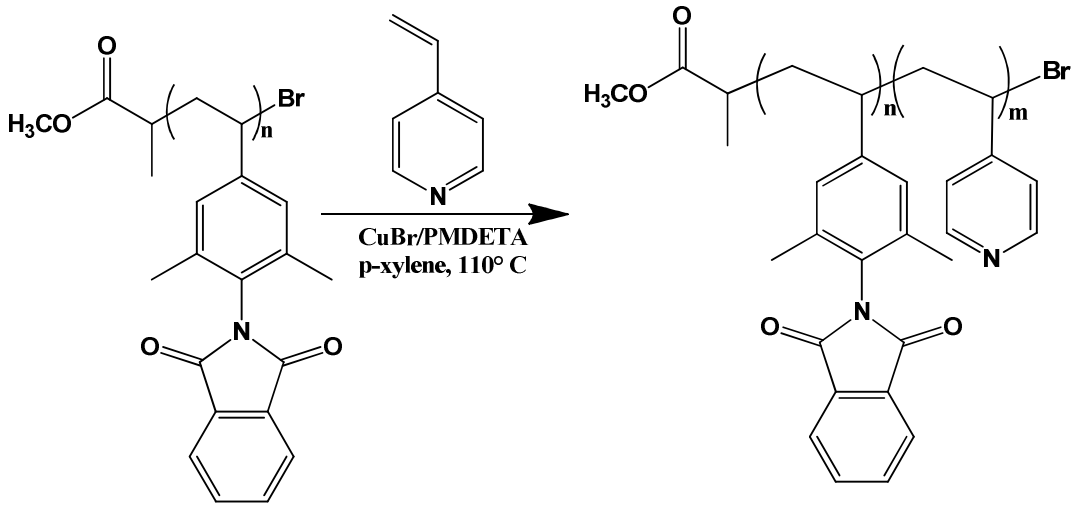

Scheme 9. ATRP of 4VP from macroinitiator

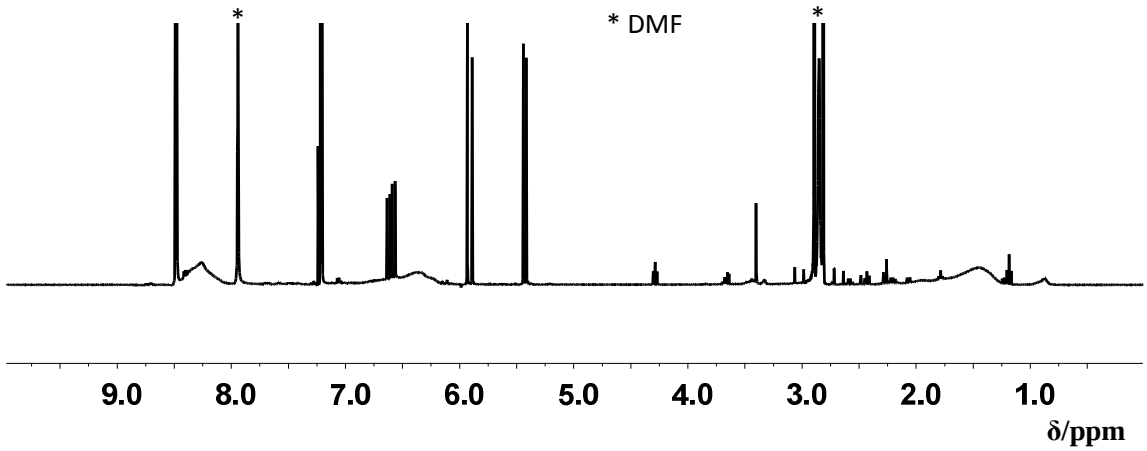

Figure 30. ^{1}H NMR spectrum ($CDCl_3$, 400 MHz) of ATRP reaction mixture of 4VP

ATRP of 4-VP poses a challenging task as both 4-VP and poly(vinylpyridine) (P4VP) are strong coordinating ligands which can compete for the binding of the copper catalysts in the polymerization system.[100] As the monomer is present in large excess over the ligand, complexation of pyridine with copper can occur resulting in pyridine-coordinated copper which is not a very effective catalyst-ligand system for ATRP. It has been shown that addition of 5 vol% pyridine to styrene can significantly slow down the ATRP of styrene with CuBr/dNbpy. [dNbpy: 4,4'- di(5-nonyl)-2,2'-bipyridine].[102] In addition to that the polymer solution remained green even after passing through an alumina column indicating the complexation of P4VP with copper. In order to avoid such detrimental effect on the polymerization of 4VP, Matyjaszewski et. al. emphasized on using a stronger binding ligand whose high complexation constant to copper is crucial in

the control of the polymerization method. Though PMDETA is a stronger binding ligand than bipyridine (bpy) type ligand, the competitive coordination of 4VP to copper was evident. When even stronger binding ligands like tris[2-(dimethylamino)ethyl]amine (Me_6TREN) was used in the ATRP of 4VP, the molecular weight increased linearly with conversion resulting in narrow polydispersities.[100,103] Two other factors contributed to the successful ATRP of 4VP in solution. First one deals with the choice of initiator and catalyst. In general k_d (deactivation rate constant) for ATRP as shown in eq. 2 is higher for alkyl bromide initiators and copper bromide catalyst systems compared to chloride based ones. However, for styryl type monomers the polymer chain ends are susceptible to nucleophilic substitution or elimination reactions which are more pronounced in nucleophilic monomers like 4VP. This type of substitution reactions known as pyridinolysis leads to the formation of pyridinium salts and branching as shown in Scheme 10.[104] The rates of the nucleophilic substitution reaction are determined by the nature of the halogen at the polymer chain end. The stronger C-Cl bond compared to C-Br and the inferior ability of the Cl atom as a leaving group in comparison to Br make it less susceptible for S_N2 type nucleophilic attack. So to preserve the living polymer chain throughout the course of the reaction and to obtain a narrow molecular weight distribution, alkyl chloride initiator along with CuCl system is preferred. Moreover it has been shown that the polymerization system involving Br has much darker green color than that with Cl indicating a significant amount of Cu(II) present in the solution.

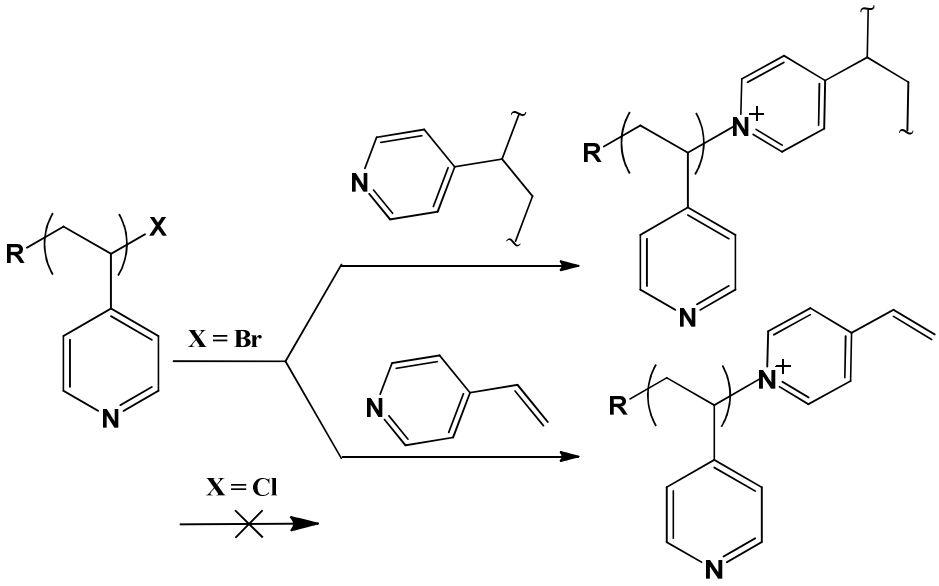

Scheme 10. Pyridinolysis of polymer chain end by 4VP and P4VP

The second one is the choice of solvent. It is important to carry out the polymerization in protic solvent like 2-propanol which not only solubilizes the polymer formed but also reduces the coloration of the polymerization system possibly through hydrogen bonding to 4VP/ P4VP, thus lowering the contamination of the catalyst.[100]

Considering all the facts about the ATRP of 4VP we changed the catalyst, ligand, initiator and solvent system for the polymerization of 4VP. In order to eliminate the possibility of above mentioned side reactions the macroinitiator was first synthesized to obtain a chloro–end functional polymer chain. The chloro end functionalized macroinitiator was obtained from the monomer mixture of styrene and compound 6 in 1:1 stoichiometric ratio in the presence of CuCl/PMDETA catalyst system and 1-chloro-1-

phenylethane initiator system as shown in Scheme 11. The reaction was optimized to ensure that the polymer chain remains active. The macroinitiator was then used to polymerize 4VP for the synthesis of coil-coil diblock copolymer. For the diblock copolymerization of 4VP as shown in Scheme12, Me_6TREN was synthesized according to literature procedures [105] and employed as the strong coordinating ligand along with CuCl as the catalyst. In addition, a high boiling point solvent 1-butanol was used as the

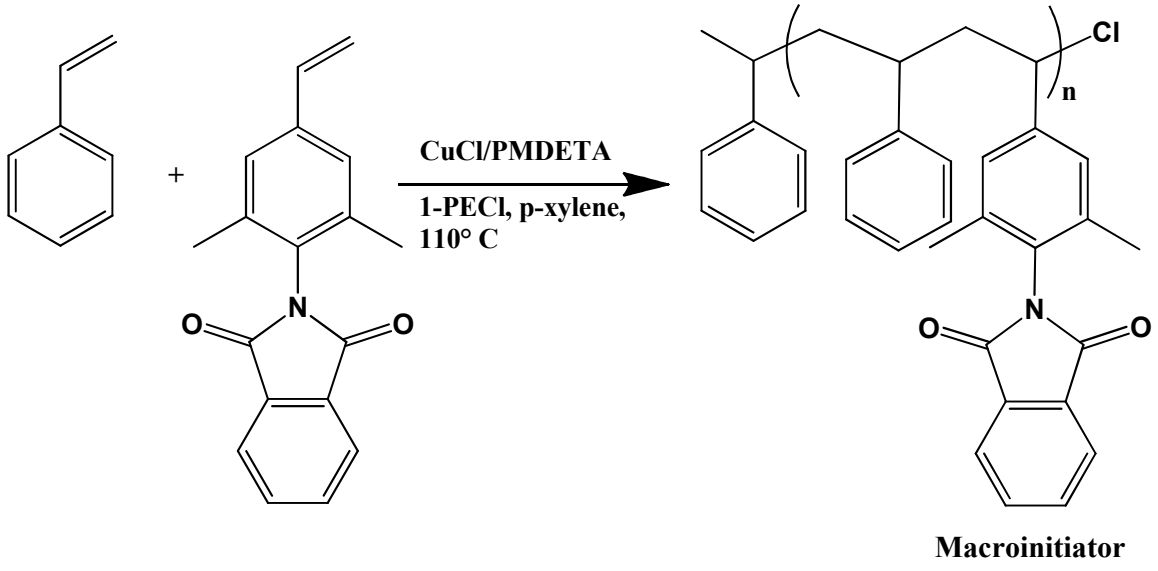

Scheme 11. Synthesis of macroinitiator via ATRP of styrene and monomer 6

protic solvent instead of the widely used 2-propanol so that the temperature of the reaction mixture can be better tuned. The reaction mixture turned to dark brown color after 1 h. The solution became viscous as the reaction progressed. As the resulting diblock copolymer is soluble in methanol, the reaction mixture was precipitated from hexanes after passing through a neutral alumina column. The product was precipitated out from the hexanes several times to obtain a light brownish white colored copolymer. The diblock copolymer was then reacted with hydrazine hydrate to remove the phthalimide protecting group. Finally the hybrid diblock copolymer was synthesized from the free amine functional group containing diblock copolymer by adding excess DCC and polyoxometalate cluster in DMF as shown in Scheme 13. The excess free clusters were removed by precipitating the polymer mixture from hot acetonitrile. The resulting hybrid diblock copolymer is soluble only in hot DMF and hot DMSO but completely insoluble in most other common organic solvents.

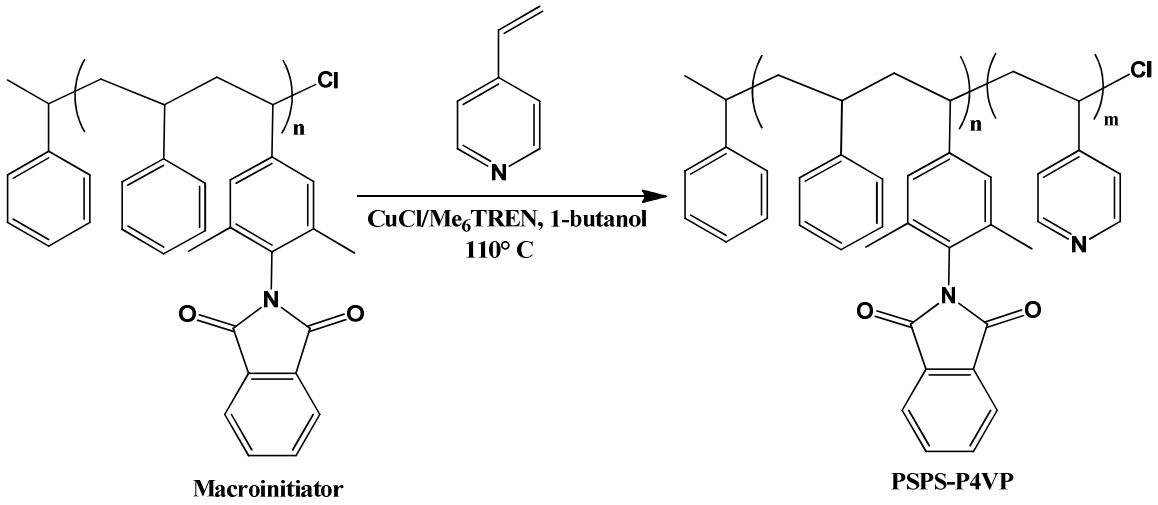

Scheme 12. ATRP of 4VP via ATRP from macroinitiator

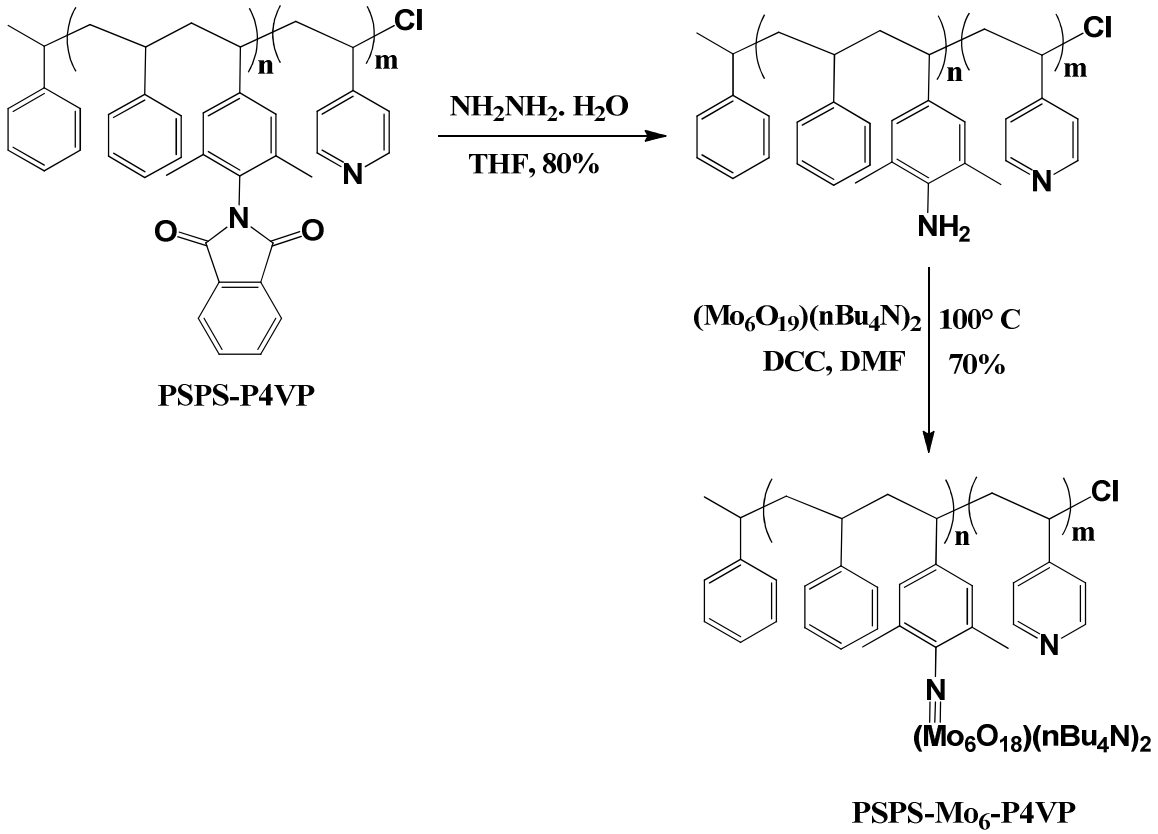

Scheme 13. Synthetic route for the PSPS-Mo_6-P4VP

3.2.2. Structural Characterizations

The structures of all the synthesized products were confirmed by ^{1}H NMR spectroscopy. The ^{1}H NMR spectra ($CDCl_3$, 400 MHz) of our first coil-coil diblock copolymer PS-PSPSBr is depicted in Figure 31. All the peaks are assigned unambiguously to the polymer structure. The methoxy (a) end group signals at 3.45 ppm and methyl (b) signals around 0.9 ppm are clearly visible. The propagating end group signals around 4.45 ppm related to the proton associated with the Br-bonding carbon is

perceived when the region with chemical shifts from 4.00 ppm to 5.0 ppm is expanded. As the aromatic proton signals of styrene monomer (h) and that of monomer 6 (e) are overlapped in the region between 6.3 ppm to 7.3 ppm it is difficult to calculate the degree of polymerization of each block.

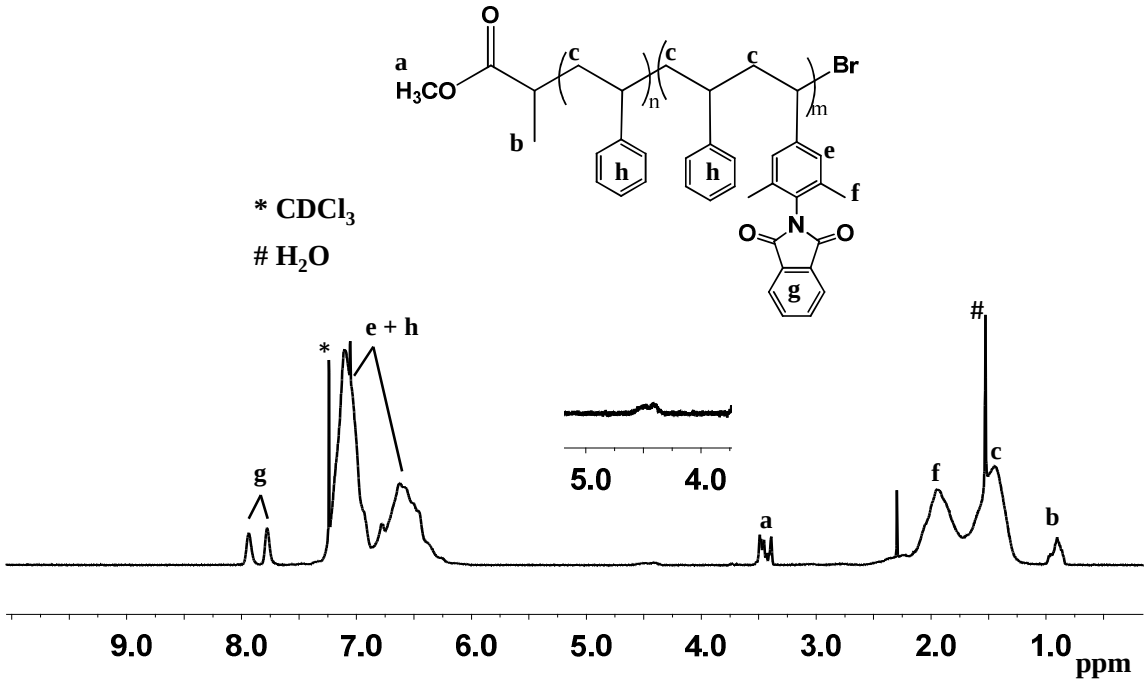

Figure 31. ^{1}H NMR spectrum ($CDCl_3$, 400 MHz) of diblock copolymer PS-PSPSBr

The complete removal of phthalimide protecting group is confirmed by the ^{1}H NMR spectrum as shown in Figure 32. For comparison the ^{1}H NMR spectrum of the diblock is also shown. The aromatic proton signal g is disappeared with the emergence of a new proton peak at 4.1 ppm corresponding to the free amine.

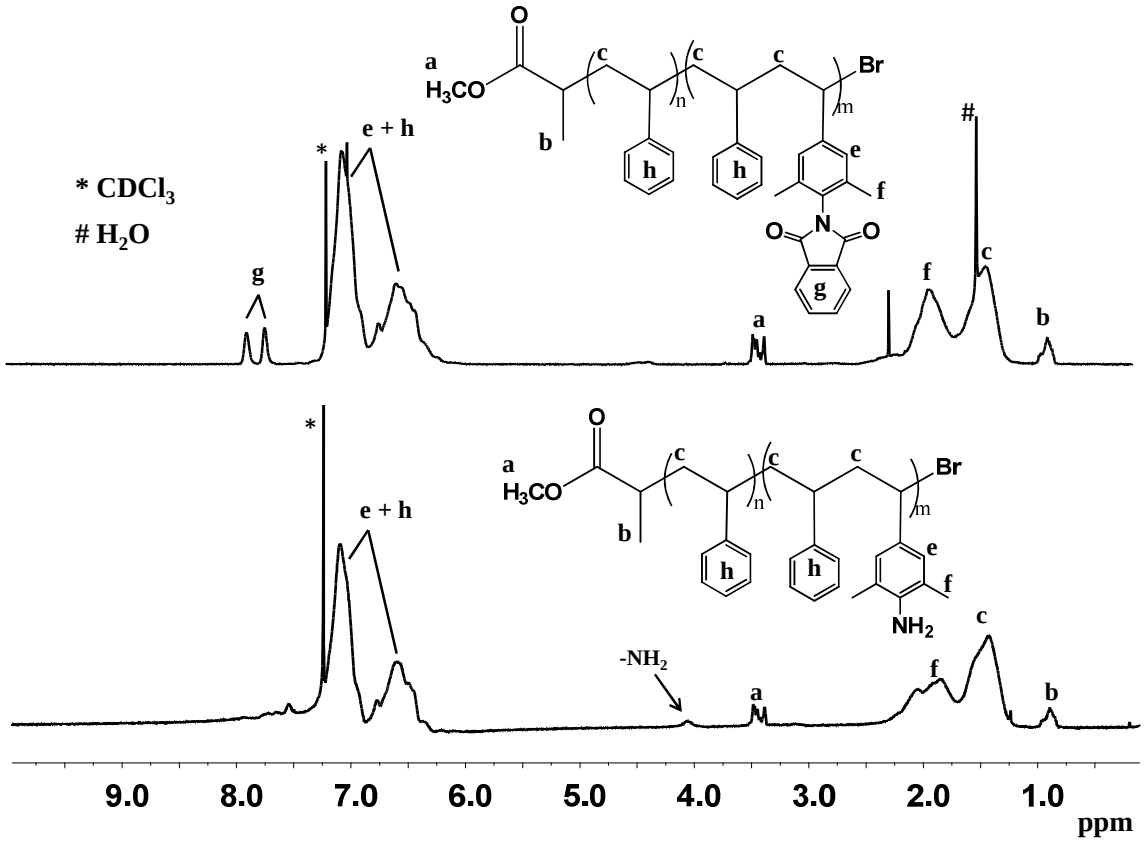

Figure 32. ^{1}H NMR spectrum ($CDCl_3$, 400 MHz) of PS-PSPSBr (top) and deprotected diblock copolymer(bottom).

The solubility of the hybrid diblock is very poor in chloroform. So the ^{1}H NMR spectrum of the hybrid was taken in DMSO-d_6 as shown in Figure 33. Weak aromatic proton signals are evident from the spectrum. The signals corresponding to the tetrabutylammonium counterion and the aliphatic signals from the organic part are overlapped in the region between 0.5 ppm to 2.2 ppm. Though one strong proton signal (a) corresponding to the –NCH_2- protons of the counterion at 3.3 ppm is clearly visible. It is difficult to estimate the number of cluster attachment per chain though the elemental analysis data of the hybrid diblock estimated the percentage of the cluster attachment.

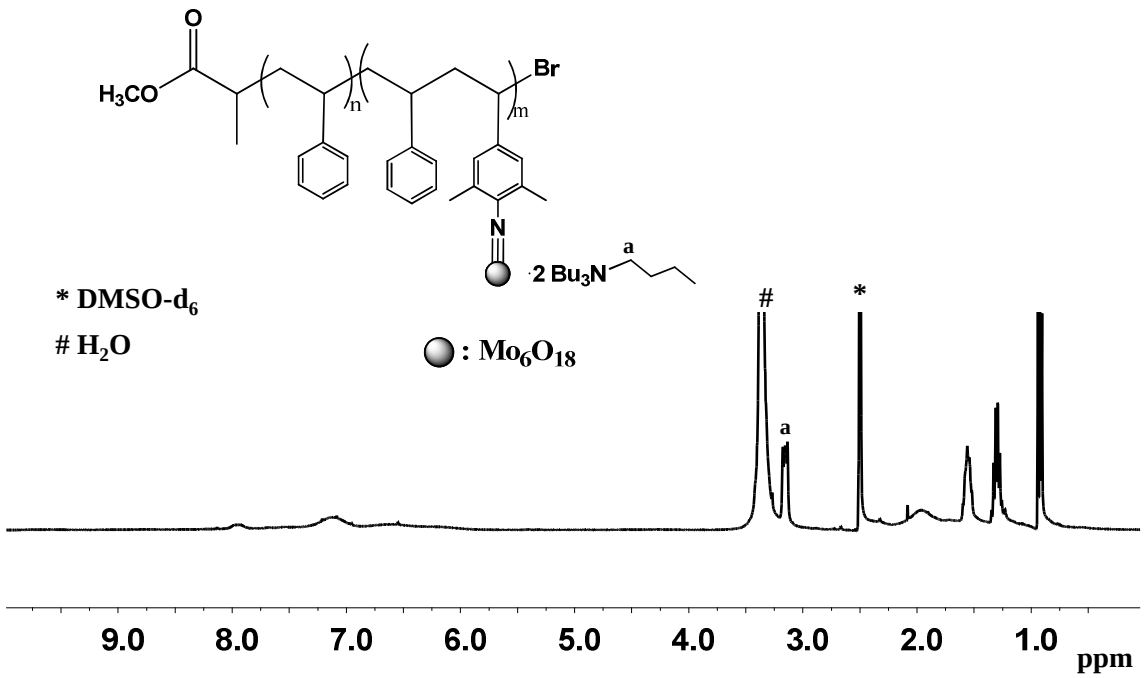

Figure 33. ^{1}H NMR spectrum (DMSO-d_6, 400 MHz) of hybrid diblock PS-Mo_6-PSPS

The ^{1}H NMR spectra ($CDCl_3$, 400 MHz) of the macroinitiator for the preparation of the second coil-coil diblock copolymer is depicted in Figure 34. All the peaks are assigned correctly to the polymer structure. The initiating end methyl (e) proton signals are clearly visible at 1.05 ppm. A clear signal at 4.4 ppm is assigned to the proton associated with the Cl-bonding carbon if the region between 4.0 ppm to 5.0 ppm is expanded. The aromatic proton signals of styrene (b) and that of the monomer 6 (a) overlapped between 6.2 ppm to 7.2 ppm region. The aromatic proton signals (c) corresponding to the phthalimide aromatic ring is evident. From the intensity of the aromatic peak signals it appeared that the two monomers are in 1:1 composition in the macroinitiator chain.

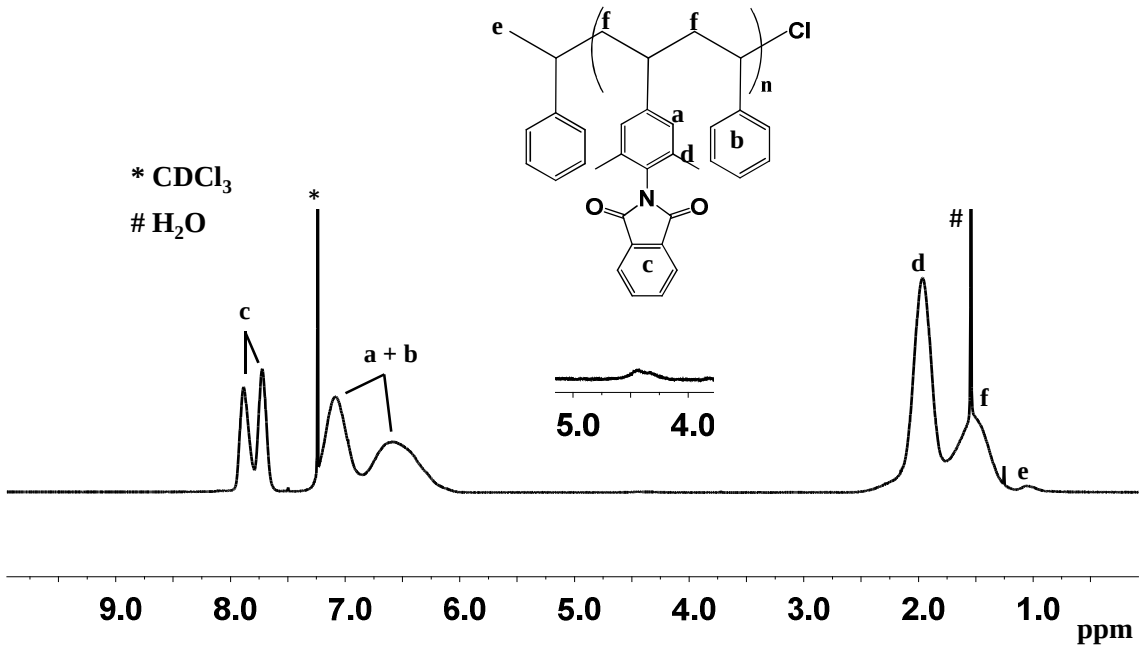

Figure 34. ^{1}H NMR spectrum ($CDCl_3$, 400 MHz) of macroinitiator

The ^{1}H NMR spectrum ($CDCl_3$, 400 MHz) of the second diblock copolymer PSPS-P4VP is shown in Figure 35. The proton signals from the macroinitiator are clearly visible. Two additional broad aromatic proton signals corresponding to the vinyl pyridine block appeared after the diblock copolymerization: one at 8.4 ppm (g) and another at 6.5 ppm (h). The small aromatic proton signals of the macroinitiator are easily distinguishable. Comparing the intensity of the aromatic proton signals between the vinylpyridine block and the macroinitiator block it can be concluded that the degree of polymerization of the vinylpyridine block is much higher than that of the macroinitiator.

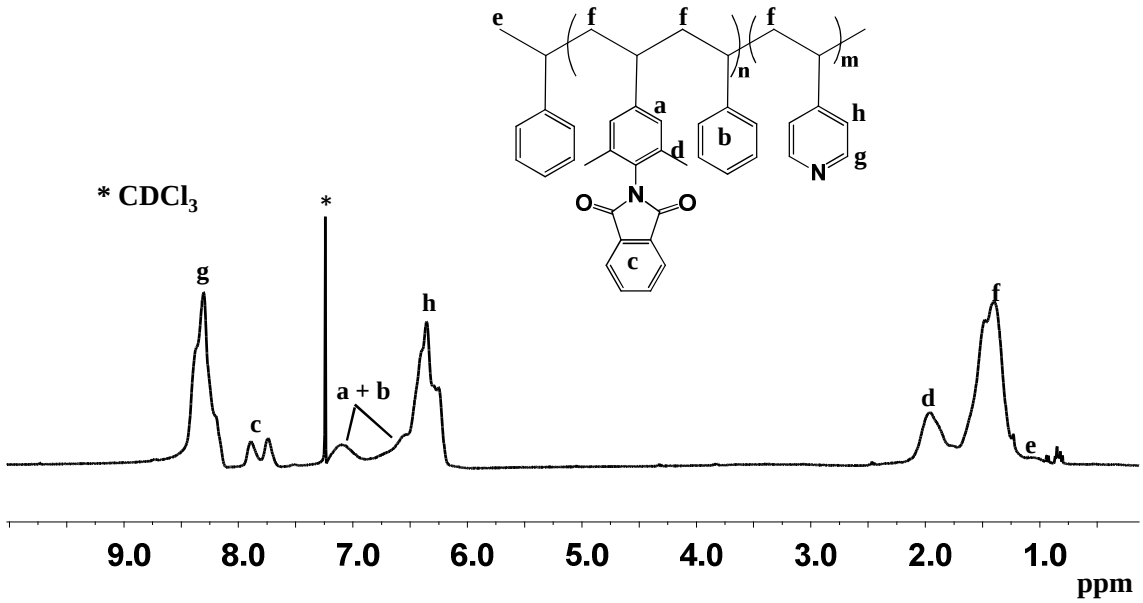

Figure 35. ^{1}H NMR spectrum ($CDCl_3$, 400 MHz) of diblock copolymer PSPS-P4VP

The ^{1}H NMR spectrum ($CDCl_3$, 400 MHz) of the deprotected diblock copolymer after complete elimination of the phthalimide protecting group is shown in Figure 36. The ^{1}H NMR spectrum ($CDCl_3$, 400 MHz) of the diblock copolymer is also shown for comparison. The proton signal c is completely missing.

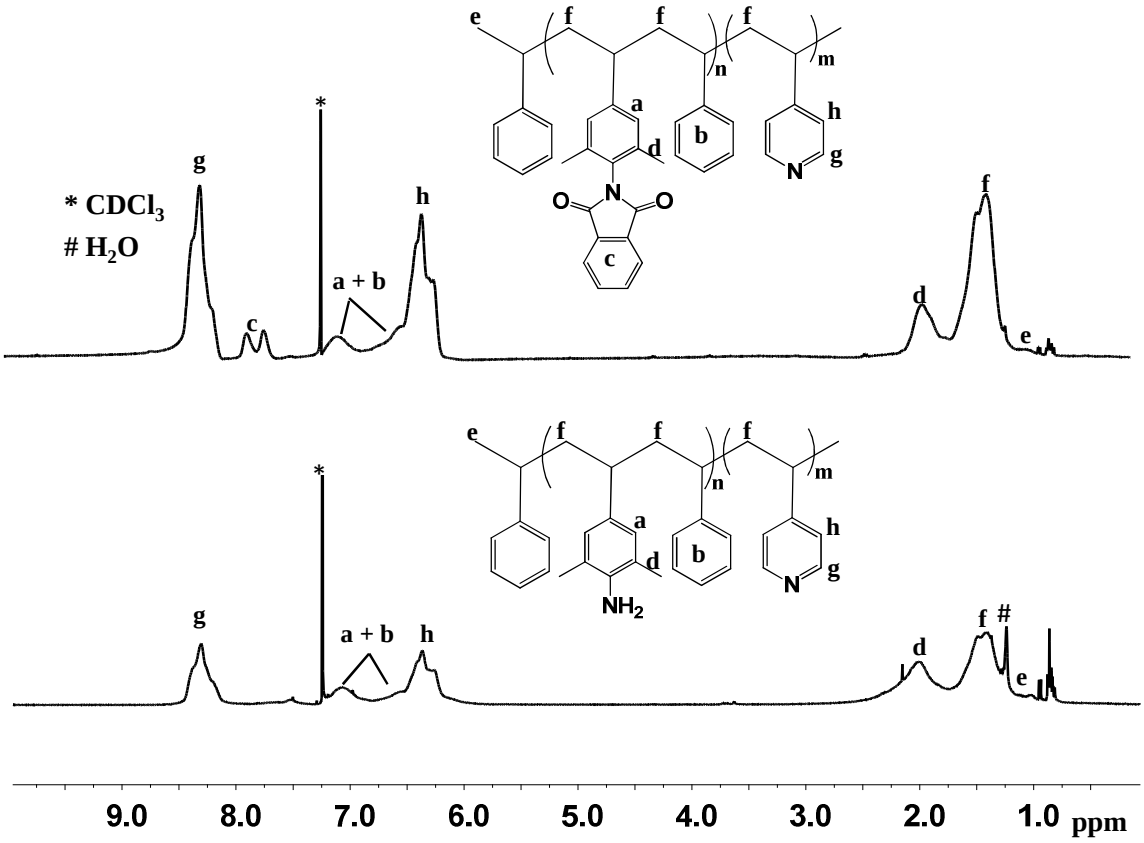

Figure 36. ^{1}H NMR spectrum ($CDCl_3$, 400 MHz) of diblock copolymer (top) and deprotected diblock copolymer (bottom).

The ^{1}H NMR spectrum (DMSO-d_6, 400 MHz) of the hybrid diblock copolymer PSPS-Mo_6-P4VP is shown in Figure 37. The weak but clear aromatic signals are clearly visible. The signals corresponding to the tetrabutylammonium counterion and the aliphatic signals from the organic part are overlapped in the region between 0.7 ppm to 2.2 ppm. The signal at 3.3 ppm (a) is corresponding to the –NCH_2- protons of the

counterion. The percentage of cluster attached to the diblock is estimated from the elemental analysis data though the number of cluster attachment per chain is not clear.

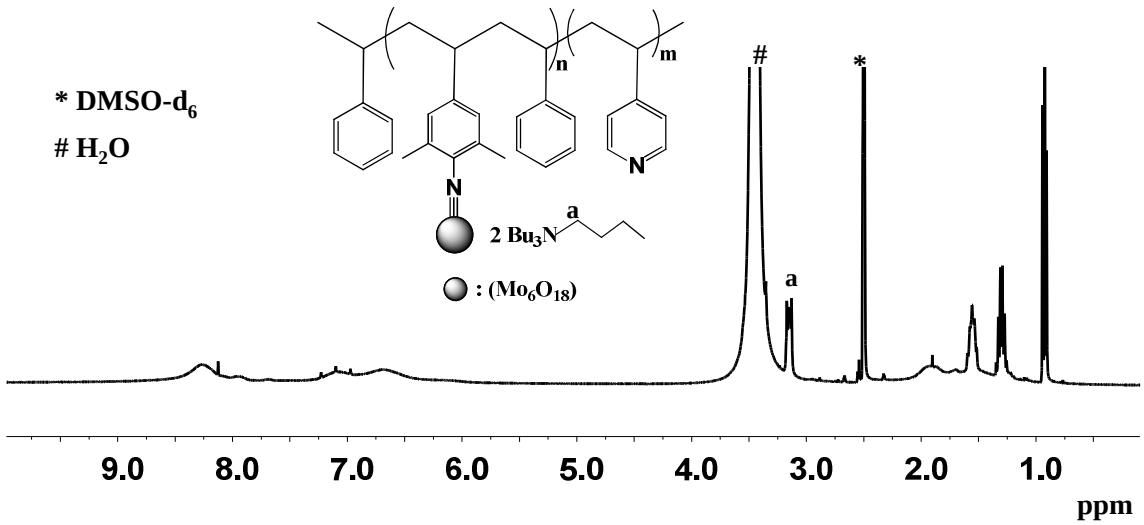

Figure 37. ^{1}H NMR spectrum (DMSO-d_6, 400 MHz) of hybrid diblock PSPS-Mo_6-P4VP

3.2.3. Molecular Weight Determination

The gel permeation chromatography (GPC) trace of the first coil-coil diblock copolymer PS-PSPSBr is shown in Figure 38. The measurement was done at 30°C using THF as the eluent. This coil-coil diblock copolymer has a number average molecular weight (M_n) of 3560 and a polydispersity (PD) of 1.2. The molecular weight distribution

is relatively narrow. Unfortunately no GPC data was available for the hybrid diblock copolymer PS-Mo_6-PSPS after cluster linkage due to its very poor solubility in any common organic solvents.

The GPC traces of the second coil-coil diblock copolymer and the chloro-functionalized macroinitiator are shown in Figure 39. The number average molecular weight (M_n) of the macroinitiator is 3800 with a polydispersity (PD) of 1.1 whereas the M_n for the diblock copolymer PSPS-P4VP is 6361 with a PD of 1.2. The high molecular weight and the lack of bimodal distribution of the GPC curve confirm the diblock copolymer formation. Similarly due to the poor solubility of the hybrid diblock PSPS-Mo_6-P4VP in common organic solvents no GPC data was generated after cluster attachment.

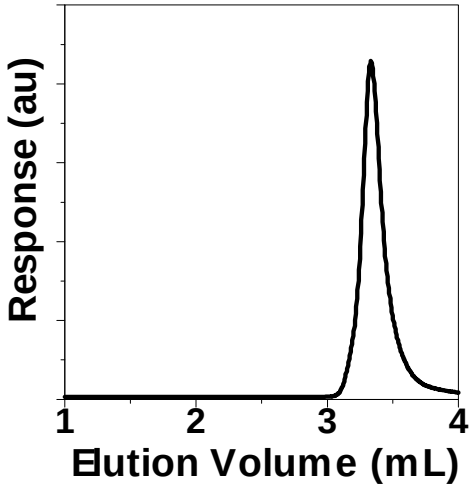

Figure 38. GPC trace of the PS-PSPSBr diblock copolymer using THF as the eluent.

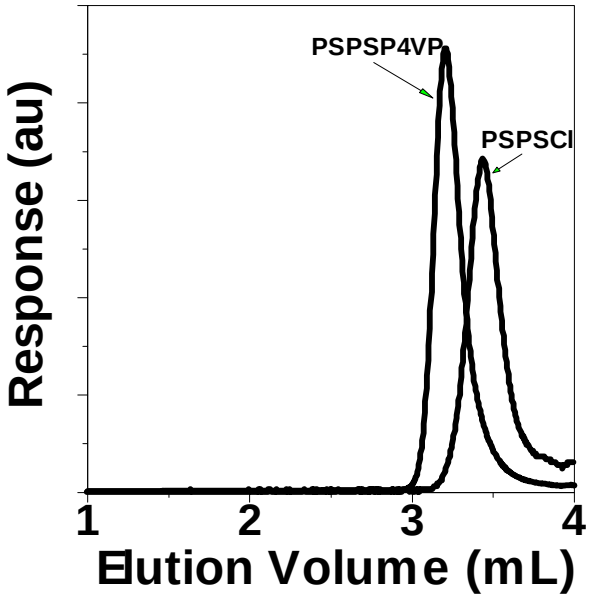

Figure 39. GPC traces of the macroinitiator PSPSCl and the diblock copolymer PSPSP4VP using THF as the eluent.

Matrix-assisted laser desorption/ionization-Time-of-Flight (MALDI-TOF) mass spectrometry (MS) measurements were carried out for the diblock copolymer as shown in Figure 40 to ascertain the absolute molecular weight. From the MALDI-TOF data the number average molecular weight (M_n) is calculated to be 4350 with a polydispersity

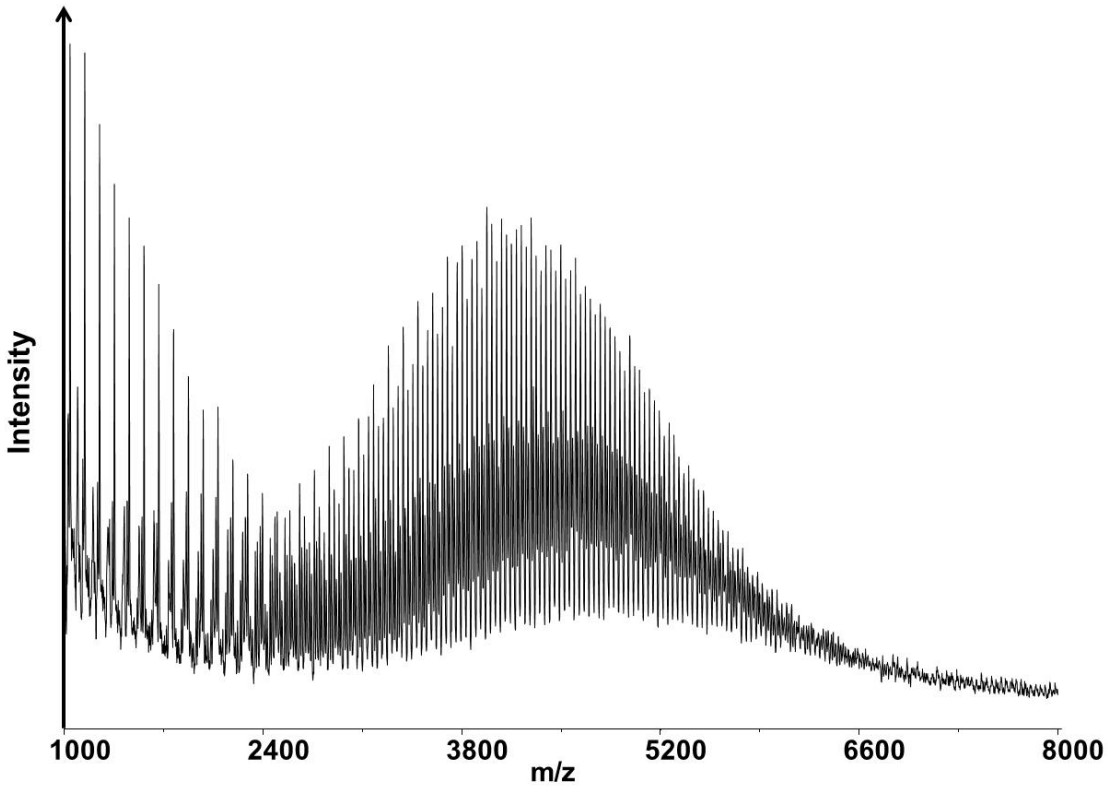

Figure 40. MALDI-TOF spectra of the PS-PSPSBr diblock copolymer

(PD) of 1.1 based on the molecular weights and the intensities of the peaks. MALDI – TOF measurement for the hybrid diblock PS-Mo_6-PSPS did not yield any peak whether using a positive or negative detection mode. This might either be due to the difficulty in vaporizing cluster attached diblock copolymers under MALDI conditions or due to the higher charge of the hybrid diblock making it impossible to show the high mass/charge signals. While MALDI measurements reveal the absolute molecular weight information about the first coil-coil diblock copolymer (PS-PSPSBr), the second diblock copolymer (PSPS-P4VP) and the macroinitiator (PSPSCl) were unable to produce any peaks. No signals were detected despite attempting different measuring conditions which includes various matrixes like dithranol, 2,5-dihydroxybenzoic acid (DHB) and cationizing agents.

3.2.4. FT-IR Spectroscopy Studies

Besides ^{1}H NMR spectroscopy, the covalent cluster attachment to the diblock is confirmed by the FT-IR analysis. The FT-IR spectra of the first coil-coil diblock copolymer (PS-PSPSBr) and the hybrid diblock (PS-Mo_6-PSPS) and free Mo_6 cluster are summarized in Figure 41. A sharp and intense peak at 1722 cm^{-1} of the diblock copolymer PS-PSPSBr due to the carbonyl stretching of the phthalimide protecting group is observed. Moreover two new peaks at 790 cm^{-1} and 950 cm^{-1} corresponding to the Mo-O stretching vibrations are clearly visible in the IR spectra of the hybrid. In addition to that a side/shoulder peak at 975 cm^{-1} which is attributed to the Mo-N stretching vibration

[62b] is easily detectable when the region is expanded as shown in the Figure 41. The FT-IR spectra of the second coil-coil diblock copolymer (PSPS-P4VP) along with the hybrid diblock (PSPS-Mo_6-P4VP) and free Mo_6 cluster are depicted in Figure 42. The diblock copolymer PSPS-P4VP exhibits an intense peak at 1722 cm^{-1} similar to the first coil-coil diblock due to the carbonyl stretching of the phthalimide protecting group. Two sharp peaks at 1598 cm^{-1} and 1417 cm^{-1} related to the characteristic ring vibration of pyridine can be distinguished.[106] Along with two small but significant peaks at 800 cm^{-1} and 950 cm^{-1} the hybrid diblock reveals a small shoulder peak at 975 cm^{-1} which can be assigned to the Mo-N stretching vibration. The appearance of this peak in both the hybrid diblocks is a clear evidence of the covalent attachment of the cluster to the two types of diblock copolymers.

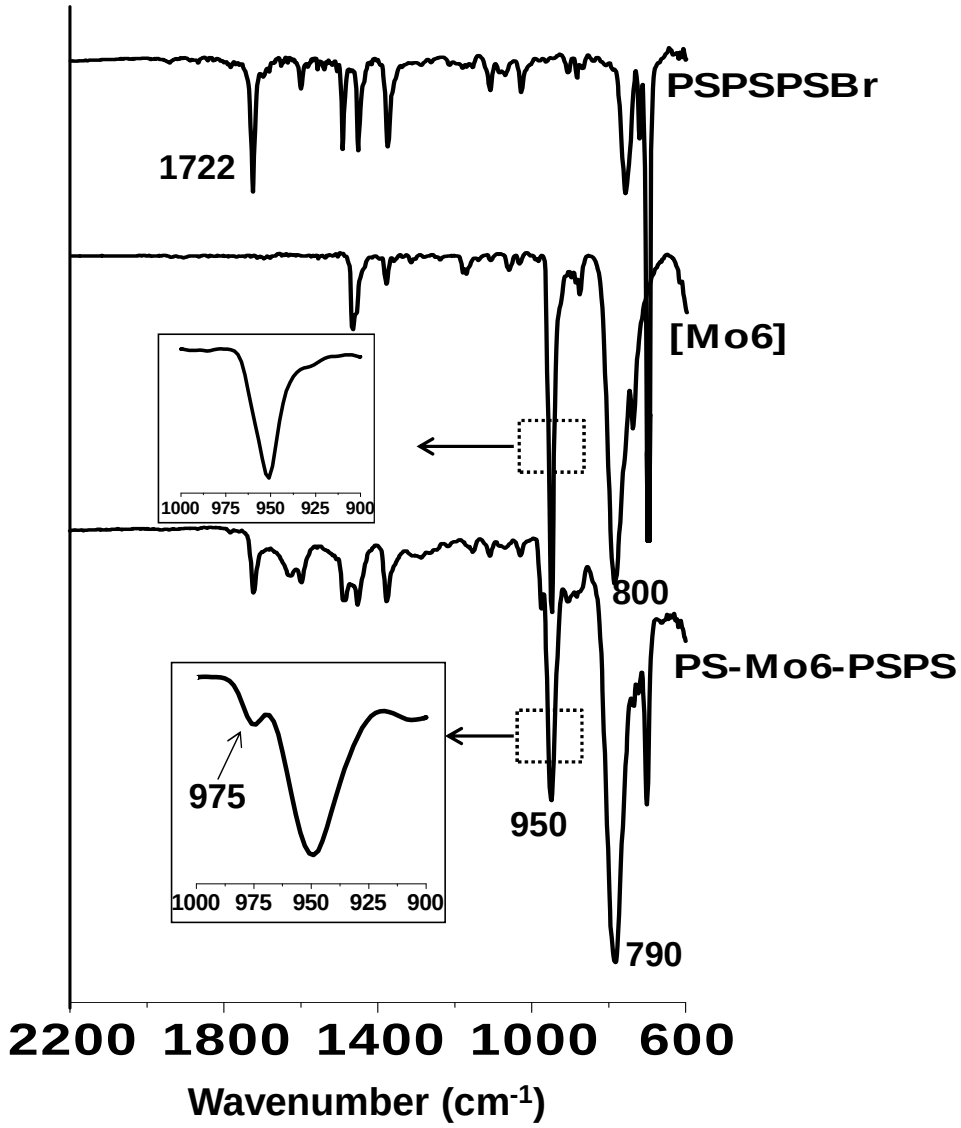

Figure 41. FT-IR spectra of diblock copolymer PS-PSPSBr (top), free Mo6 cluster (middle) and hybrid DCP (bottom).

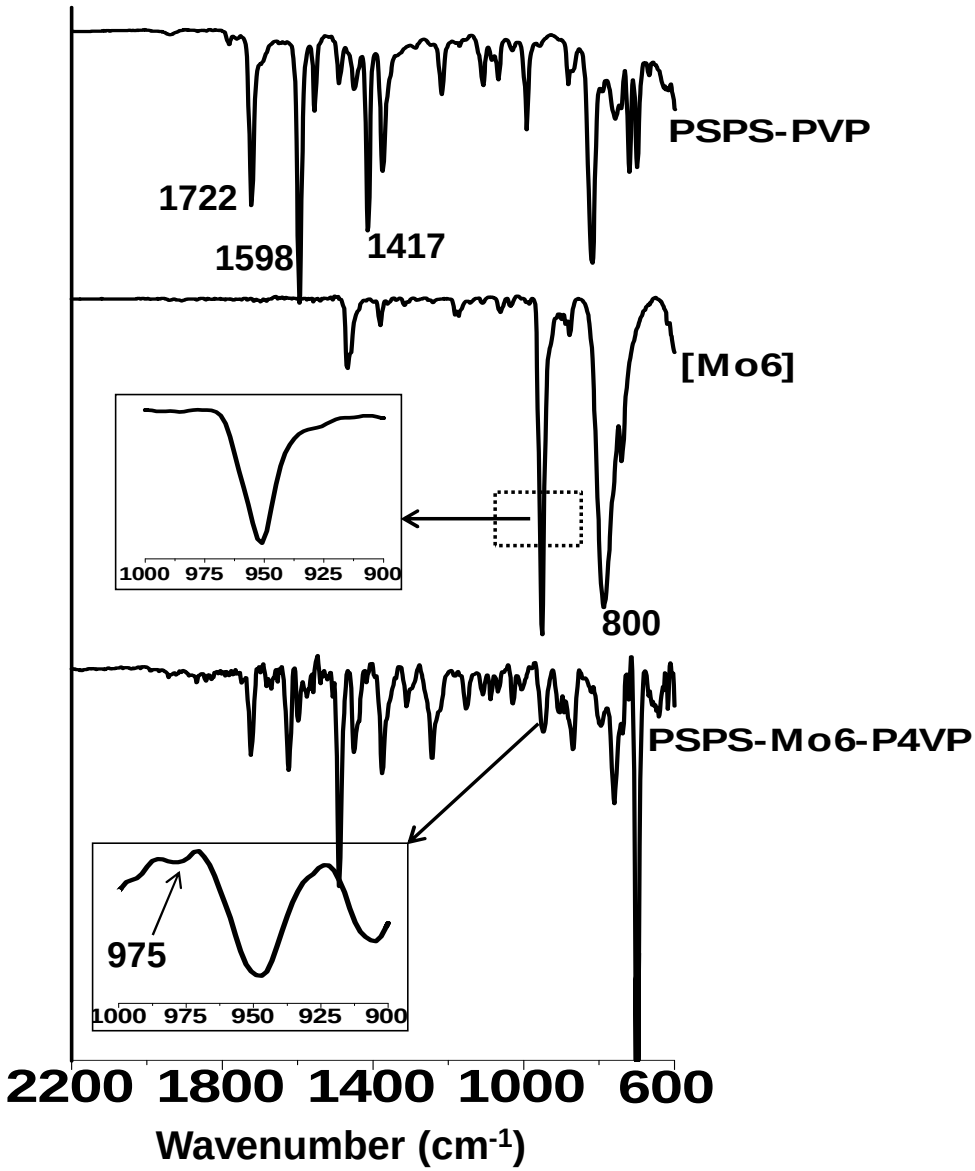

Figure 42. FT-IR spectra of diblock copolymer PSPS-P4VP (top), free Mo6 cluster (middle) and hybrid DCP (bottom).

3.2.5. Optical Properties

The absorption spectra of the PS-PSPSBr diblock copolymer and the hybrid diblock copolymer PS-Mo_6-PSPS are shown in Figure 43a. The diblock copolymer has a small absorption peak at 252 nm due to the π-π* transition of the styrene backbone. After cluster attachment, a new peak appeared at 370 nm which matches with the absorption spectrum of the imido-POM derivative of 2,6-dimethylaniline.[107] This peak can be assigned to the ligand-to-metal-charge transfer (LMCT) transition of the pendant imido-POM component and confirms the covalent cluster attachment through imido-functionalization of POM clusters. But the absorption spectra of the PSPS-Mo6-P4VP as shown in Figure 43b did not show any peak corresponding to the imido-POM derivatives.

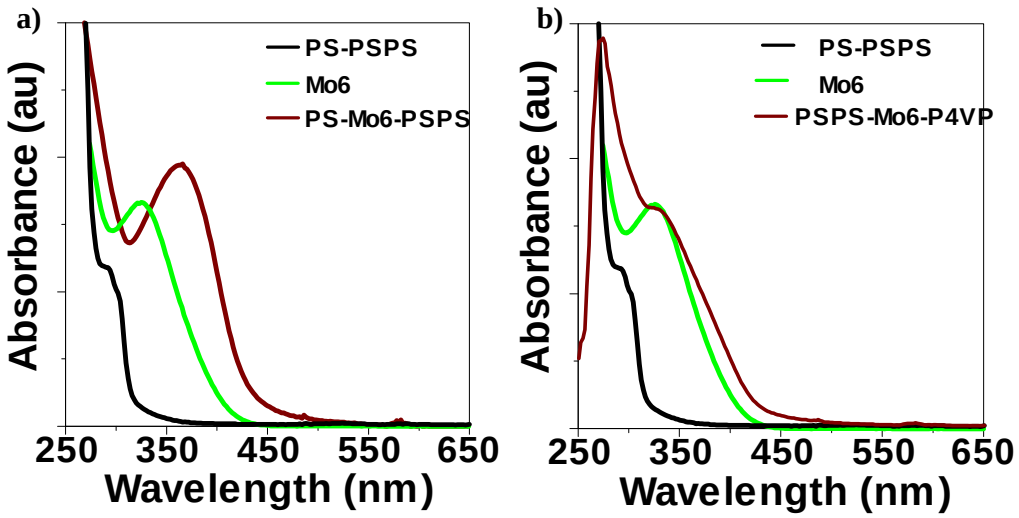

Figure 43. UV/Vis absorption spectra of a) diblock copolymer (PS-PSPS), free cluster (Mo6) and hybrid diblock copolymer (PS-Mo_6-PSPS) and b) diblock copolymer (PS-PSPS), free cluster (Mo6) and hybrid diblock copolymer (PSPS-Mo_6-P4VP)

3.2.6. Thin Film Morphologies

Film morphologies of the two diblock copolymers and the two hybrid diblock copolymers were studied using AFM. The topography and phase images of the PS-PSPS diblock copolymer and the hybrid PS-Mo_6-PSPS are shown in Figure 44 whereas the topography and phase images of the PSPS-P4VP diblock and the corresponding hybrid PSPS-Mo6-P4VP are shown in Figure 45. The diblock copolymers were dissolved in chloroform whereas the hybrid diblock copolymers were dissolved in DMF. The solutions were spin coated onto ITO glass slides at a speed of 600 rpm for 20 s and annealed at 120 °C for 10 min. The topography image and phase images for both the

diblock copolymers are featureless. But the phase images for the cluster attached hybrid diblock copolymers in both cases showed some aggregates throughout the film. These aggregates must have come from the clusters as they are absent in the diblock copolymers. No significant morphological pattern is observed for any of the films. These

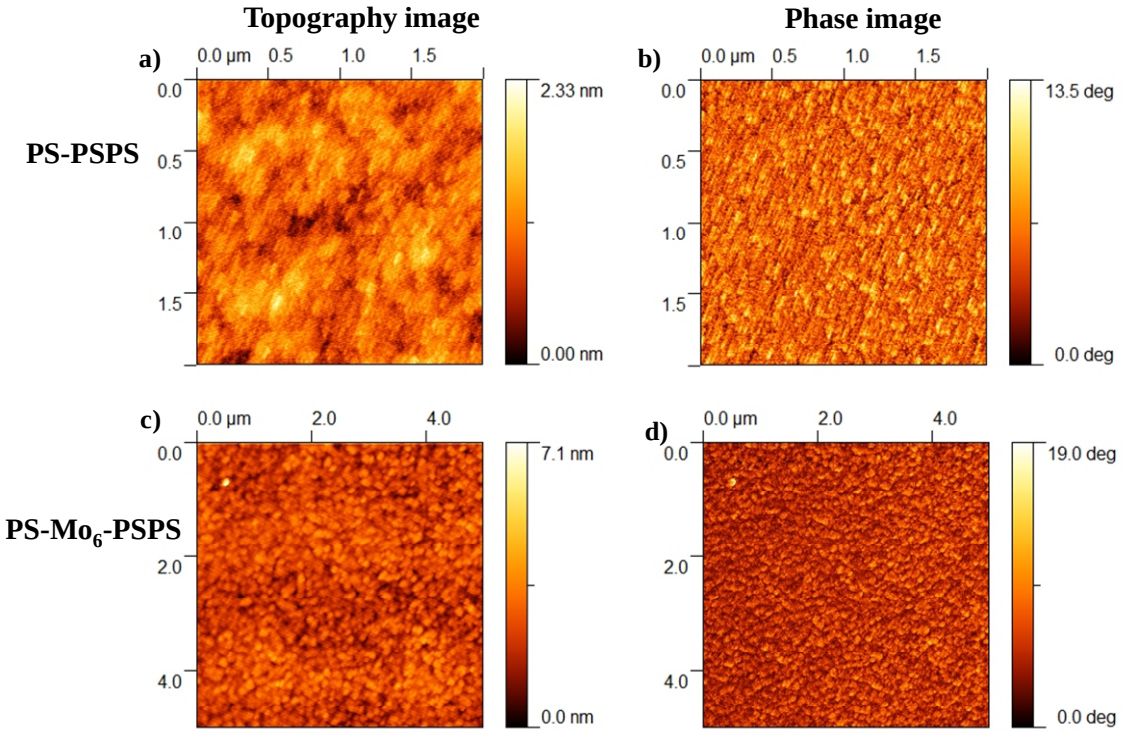

Figure 44. AFM images of diblock copolymer (PS-PSPS) film spin coated from chloroform on ITO glass. a) topography b) phase; AFM images of hybrid diblock copolymer (PS-Mo6-PSPS) film spin coated from DMF on ITO glass.

are the preliminary results. Further investigation into the morphology of these diblock copolymers and hybrid diblock copolymers are needed by changing different processing conditions.

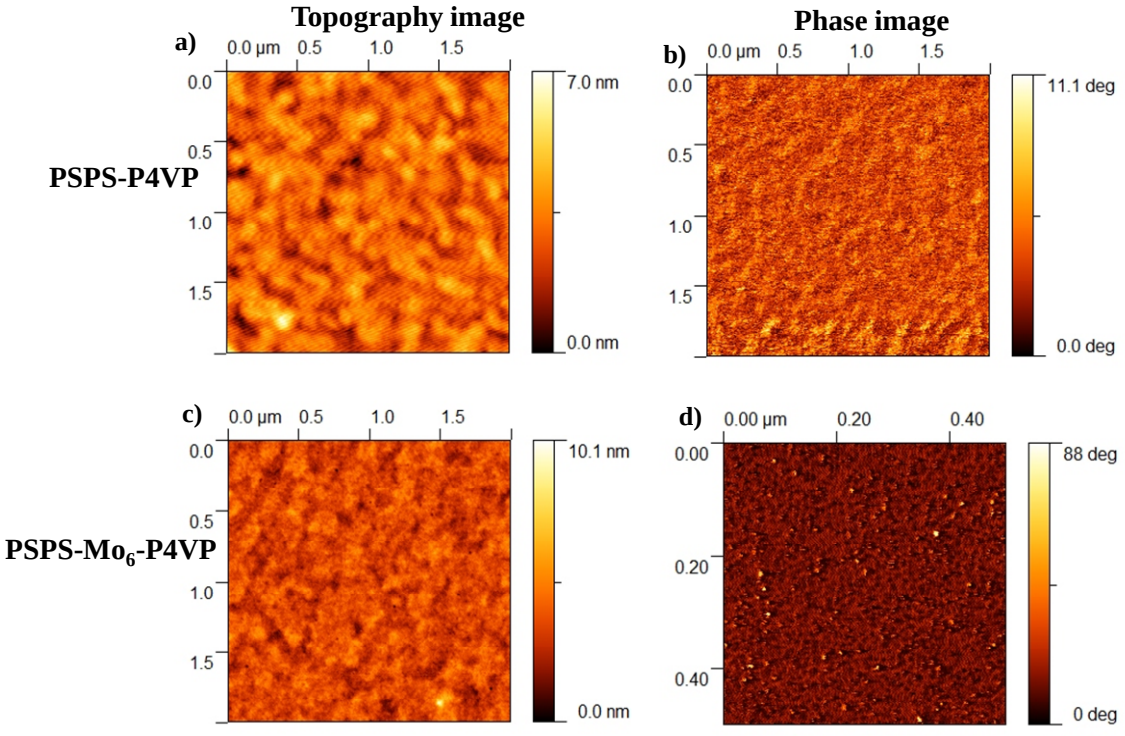

Figure 45. AFM images of diblock copolymer (PSPS-P4VP) film spin coated from chloroform on ITO glass. a) topography b) phase; AFM images of hybrid diblock copolymer (PSPS-Mo6-P4VP) film spin coated from DMF on ITO glass.

3.3. Conclusions

The first coil-coil diblock copolymers containing POM clusters have been synthesized successfully. GPC showed the formation of the two different diblock copolymers with narrow molecular weight distribution. IR and UV measurements were used to confirm the covalent cluster linkage. Initial AFM study showed cluster aggregates throughout the films in the phase images for both hybrid diblock copolymers.

3.4. Experimental Section

Materials. Tetrahydrofuran (THF) was purified by distillation over sodium pellets and benzophenone. CuBr and CuCl was purified by washing consecutively with glacial acetic acid, absolute ethanol and ethyl ether, and then dried under vacuum. N, N, N´, N´, N´-pentamethyldiethylenetriamine (PMDETA, 99%) was distilled in vacuo before use. Styrene was purified by vacuum distillation. 4-vinylpyridine (4-VP) was passed through a basic alumina column and distilled in vacuo and stored under -4° C. Me_6TREN was synthesized according to literature procedure. [105] All other chemicals were purchased either from Aldrich or Acros and were used as received unless otherwise stated.

Instrumentation. All reactions were conducted under the protection of nitrogen. The ^{1}H and ^{13}C NMR were collected on a Varian INOVA 400 MHz FTNMR spectrometer. All samples were referenced to the deuterated solvents. GPC measurements were performed at 30°C on a Tosoh Ecosec HLC 8320GPC system equipped with a

differential refractometer, UV detector, and styragel column with THF as the eluent. PSS (polymer standards service) WinGPC Unity version 7.5.0 system equipped with light scattering detector coupled to the Tosoh Ecosec system was used for analysis. The calibration curve was determined by the use of five polystyrene standards from 8000 to 90,000. FT-IR spectra were obtained from IR Affinity-1 FTIR-8400S instrument (Shimadzu Co.) using the attenuated total reflection (ATR) method (ZnSe crystal). UV-Vis absorption spectra were measured on a Hewlett-Packard 8452A diode array spectrophotometer. A Voyager DE Pro (Perceptive Biosystems/ABI) MALDI-TOF mass spectrometer was used for mass measurement, operating in both linear and reflector mode. Dithranol (1, 8-dihydroxyanthrone) was used as the matrix in all the measurements. AFM images were taken in air under ambient conditions using the intermittent contact mode on an Agilent 5500 AFM/SPM microscope.

Sample Preparation for AFM. Indium tin oxide (ITO) glass with a sheet resistance of 8-12 Ω/square was cut into 2 cm by 2 cm pieces. Then the ITO glass substrates were cleaned in an ultrasonic bath sequentially by hot detergent, hot deionized water, acetone and isopropyl alcohol, each for 15 min, and then dried in nitrogen stream. The diblock copolymers PS-PSPS and PSPS-P4VP were dissolved in chloroform at a concentration of 9mg/mL and 4 mg/mL, respectively. The hybrid diblock copolymers PS-Mo_6-PSPS and PSPS-Mo_6-P4VP were dissolved in DMF at a concentration of 3 mg/mL and 3 mg/mL, respectively. The chloroform and DMF solutions were spin coated onto pre-cleaned ITO glass substrate at 600 rpm for 20 s. Then the samples were annealed at 120 °C for 10 min in air.

Synthesis of PS-PSPSBr. CuBr (0.008 g, 0.060 mmol) was taken in a flame dried two-neck round bottom flask. The flask was degassed and back-filled with nitrogen three times, and left under nitrogen. Then PMDETA (0.012 mL, 0.010 g, 0.060 mmol) and styrene (0.500 g, 4.80 mmol) were added via a gas-tight syringe, followed by p-xylene (1.10 mL). After addition, three freeze-pump-thaw cycles were performed and the mixture was allowed to stir at room temperature for 45 min under nitrogen. The flask was then placed into an oil bath at 110°C and to which was added deoxygenated methyl-2-bromopropionate (0.013 mL, 0.020 g, 0.120 mmol) through a gas-tight microliter syringe. After 5 h, a mixture of styrene (0.275 mL, 0.250 g, 2.400 mmol) and monomer 6 (0.666 g, 2.400 mmol) in 1.00 mL p-xylene was added to the reaction mixture through a gas-tight syringe and let the reaction stir for another 12 h. After that the contents of the flask were exposed to air to quench the reaction. The reaction mixture was diluted with THF and the solution was filtered through neutral alumina to remove the copper catalyst. The resulting colorless polymer solution was concentrated and precipitated into 10-fold excess of methanol. The white polymer was collected by vacuum filtration and dried under vacuum for 12 h. (0.750 g). ^{1}H NMR (400 MHz, $CDCl_3$, 25°C): δ 7.94 (br), 7.78 (br), 7.10 (br), 6.62 (br), 3.43 (br), 2.28 (br), 1.94 (br), 1.42 (br), 1.90 (br). ^{13}C NMR ($CDCl_3$, 400MHz): δ 167.3, 145.1, 134.2, 132.1, 127.8, 125.5, 123.6, 51.4, 45.9, 44.0, 40.5, 37.1, 18.2, 16.3. Anal. Calcd. For $C_{424}H_{397}N_{10}O_{22}Br$: C, 83.9; H, 6.60; N, 2.31. Found: C, 86.93; H, 7.32; N, 0.69. GPC: M_n= 3560, PD= 1.2.

Deprotection of Phthalimide Group. PS-PSPSBr diblock copolymer (0.148 g, 0.049 mmol) was dissolved in freshly distilled THF in a two-neck flask. Then hydrazine

monohydrate (0.148 g, 2.96 mmol) was added dropwise into the above solution with constant stirring and the entire reaction mixture was refluxed for 48 h under nitrogen protection. The resulting solution was cooled to room temperature, and the white solid precipitate was filtered off. The filtrate was stripped off the solvent and precipitated from methanol to yield white colored solid product. (0.150 g). ^{1}H NMR (400 MHz, $CDCl_3$, 25°C): δ 7.10 (br), 6.60 (br), 4.05 (br), 3.43 (br), 2.01 (br), 1.44 (br), 0.88 (br).

Hybrid Diblock Copolymer. PS-Mo_6-PSPS. In a two-neck flask were added deprotected diblock (0.100 g) and DCC (0.04 g, 0.194 mmol). The flask was degassed and backfilled with nitrogen. Hexamolybdate cluster $[Mo_6O_{19}]^{2-}$. $2N(C_4H_9)_4^+$ (0.300 g, 0.219 mmol) dissolved in anhydrous DMF (1.00 mL) was then added into the flask and the reaction mixture was stirred at 100° C for 5 h. The resulting dark red solution was cooled to room temperature and the white solid precipitate (urea) was filtered off. The solvent was dried under vacuum and the resulting concentrated solution was poured into hot acetonitrile to yield the crude product, which was further washed with hot acetonitrile to get rid of any remaining free cluster. The resulting hybrid is an orangish-red solid (0.122 g). ^{1}H NMR (400 MHz, DMSO-d_6, 25°C): δ 7.09 (br), 6.54 (br), 3.16 (br), 1.93 (br), 1.56 (br), 1.29 (br), 0.90 (br). Molybdenum content: 27.91%

Macroinitiator. PSPSCl. Monomer 6 (0.500 g, 1.803 mmol) and CuCl (0.002 g, 0.023 mmol) were added to a flame dried two-neck round bottom flask. The flask was degassed and back-filled with nitrogen three times, and left under nitrogen. Then PMDETA (0.005 mL, 0.004 g, 0.023 mmol) and styrene (0.187 g, 1.803 mmol) were added via a gas-tight syringe, followed by p-xylene (0.960 mL). After addition, three

freeze-pump-thaw cycles were performed and the mixture was allowed to stir at room temperature for 45 min under nitrogen. The flask was then placed into an oil bath at 110°C and deoxygenated 1-chloro-1-phenylethane initiator (0.006 mL, 0.006 g, 0.045 mmol) was added through a gas-tight microliter syringe to initiate the polymerization. After 11 h, the contents of the flask were exposed to air to quench the polymerization. The reaction mixture was diluted with THF and the filtered through neutral alumina to remove the copper catalyst. The resulting colorless solution was concentrated and precipitated into 10-fold excess of methanol several times. The white macroinitiator was collected by vacuum filtration and dried under vacuum. (0.550 g). ^{1}H NMR (400 MHz, $CDCl_3$, 25°C): δ 7.88 (br), 7.72 (br), 7.08 (br), 6.58 (br), 1.96 (br), 1.54 (br), 1.04 (br). ^{13}C NMR ($CDCl_3$, 400MHz): δ 167.1, 135.9, 134.1, 132.4, 127.7, 125.6, 123.5, 40.3, 18.4. Anal. Calcd. For $C_{528}H_{469}N_{20}O_{40}Cl$: C, 81.6; H, 6.08; N, 3.61. Found: C, 81.84; H, 6.28; N, 3.31. GPC: M_n= 3800, PD= 1.1.

Synthesis of PSPS-P4VP. In a two-neck flask, CuCl (0.003 g, 0.033 mmol), Me_6TREN (0.018 mL, 0.066 mmol) and 1-butanol (0.65 mL) were added, followed by multiple free-pump-thaw cycles. The solution was the stirred for 30 min at 60°C. Then 4VP (0.500 g, 4.75 mmol) and the macroinitiator (0.100 g, 0.033 mmol) were added to the above green solution and several freeze-pump-thaw cycles were performed. Finally the entire reaction mixture was stirred at 110°C for 12 h. The color of the solution turned brown. After the reaction, the contents of the flask were exposed to the air to quench the polymerization. The reaction mixture was diluted with THF and the filtered twice through neutral alumina to remove the copper catalyst. The resulting faint brownish

solution was concentrated and precipitated into 10-fold excess hexanes. The light brownish solid diblock copolymer was collected by vacuum filtration and dried under vacuum. (0.60 g). ^{1}H NMR (400 MHz, $CDCl_3$, 25°C): δ 8.30 (br), 7.90 (br), 7.74 (br), 7.11 (br), 6.36 (br), 1.96 (br), 1.40 (br), 0.84 (br). Anal. Calcd. For $C_{738}H_{679}N_{50}O_{40}Cl$: C, 81.1; H, 6.26; N, 8.25. Found: C, 80.0; H, 6.82; N, 10.92. GPC: M_n= 3560, PD= 1.2.

Deprotection of Phthalimide Group. PSPS-P4VP diblock copolymer (0.100 g) was dissolved in freshly distilled THF in a two-neck flask. Then hydrazine monohydrate (0.500 g, 9.98 mmol) was added dropwise into the above solution with constant stirring and the entire reaction mixture was refluxed for 48 h under nitrogen. The resulting solution was cooled to room temperature, and the white solid precipitate was filtered off. The filtrate was stripped off the solvent and precipitated from hexanes to yield light brown colored solid product. (0.050 g). ^{1}H NMR (400 MHz, $CDCl_3$, 25°C): δ 8.30 (br), 7.08 (br), 6.36 (br), 2.02 (br), 1.45 (br), 0.88 (br).

Hybrid Diblock Copolymer. PSPS-Mo_6-P4VP. In a two-neck flask were added deprotected diblock (0.023 g) and DCC (0.011 g, 0.053 mmol). The flask was degassed and backfilled with nitrogen. Hexamolybdate cluster $[Mo_6O_{19}]^{2-}$. $2N(C_4H_9)_4^+$ (0.113 g, 0.083 mmol) dissolved in anhydrous DMF (1.00 mL) was the added into the flask and the reaction mixture was stirred at 100° C for 5 h. The resulting dark red solution was cooled to room temperature and the white solid precipitate (urea) was filtered off. The solvent was dried under vacuum and the resulting concentrated solution was poured into hot acetonitrile to yield the crude product, which was further washed with hot acetonitrile to get rid of any remaining free cluster. The resulting hybrid is a red solid (0.03 g). ^{1}H NMR

(400 MHz, DMSO-d_6, 25°C): δ 8.27 (br), 7.11 (br), 6.69 (br), 3.15 (br), 1.91 (br), 1.56 (br), 1.31 (br), 0.94 (br). Molybdenum content: 26.41%.

CHAPTER 4

SYNTHESIS AND OPTOELECTRONIC PROPERTIES OF A PPV-BASED ROD-COIL DIBLOCK COPOLYMER WITH POLYOXOMETALATE CLUSTERS COVALENTLY ATTACHED TO THE COIL BLOCK

4.1. Energy Demand and Organic Photovoltaics

From the dawn of human civilization, energy has been the key element to stimulate the life cycle of the living species. Starting from the stone age to rubbing the stones for fire to unearthing of coal from mines to spinning the water turbines for hydro-electricity to digging out of petroleum from wells, every human effort has broadened the spectrum of utilization of the natural energy resources. But due to the increasingly unorganized usage of these natural resources, the 'once abundant' resources have been facing the problem of rapid depletion. To cope up with this precarious situation, endeavors have been made since past few decades in the quest for inexpensive renewable energy sources. In this respect enormous research has been devoted for alternative efficient low cost energy source in the form of photovoltaic devices.[108] The easily available sunlight to produce energy opens up a new horizon for organic polymer based photovoltaics which has so far gained umpteen attentions. Since the advent of molecular thin film organic solar cell by Tang,[109] scientists have explored different materials ranging from small molecules, conjugated polymers, conjugated polymer blends, to molecule polymer bilayers, combinations of organic inorganic materials, etc. [110] New innovative synthetic designs have been implemented. Polymer-based solar cells are

lagging far behind in terms of power conversion efficiency compared to conventional silicon-based solar cells. The operating principle in organic photovoltaics is shown in Figure 46.[111] Inorganic photovoltaic materials where absorption of photon creates free charge carriers (electrons and holes), photoexcitation of polymeric counterparts generates bound electron-hole pairs (excitons), connected together by higher Coulombic binding energy. These excitons may diffuse to an interface like a donor-acceptor interface where dissociation to free electron and hole can occur. The free charges are then transported to the two opposite electrodes. Recombination of electrons and holes may occur if their transportation crosses paths which necessitate the existence of separate charge transporting pathways. Excitons have a limited diffusion length of around 10 nm. One way to achieve the donor-acceptor domain distribution in the desired size is the bulk

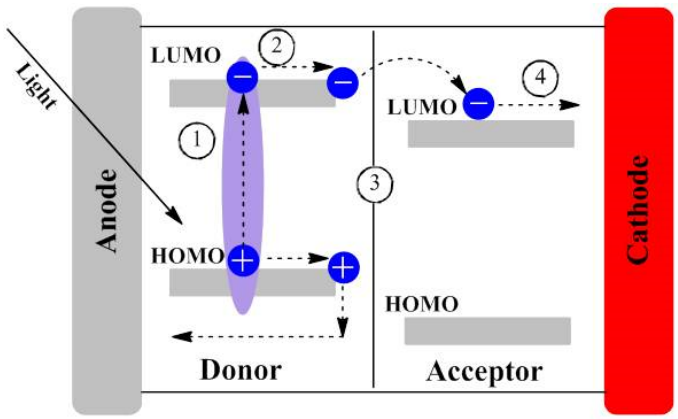

1) Photoexcitation to generate exciton
2) Exciton diffusion
3) Exciton dissociation at interface
4) Free charge transport towards electrode

Figure 46. Operating principles in organic photovoltaics (OPV).

heterojunction devices (BHJ) where the interfaces are distributed throughout the material.[110, 112] Efficiencies in the range of 5% have been achieved in the BHJ devices in the form of a blend of donor with acceptor.[113] One major drawback of these blends is the tendency for macrophase separation, where domain sizes can become too large to obtain efficient exciton dissociation. Realizing this shortcoming of blends and the importance of self-structuring and self-reorganization [114] processes, the concept of unique microphase-separation phenomenon of diblock copolymers (DCP's) [115] in an ordered nanometer sized domain structure is a huge leap towards achieving the goal of uninterrupted charge flow. Controlling the active layer morphology and interfacial structure on the 10 nm length scale of an exciton diffusion is critical to optimize device performance and rod-coil block copolymers are promising candidates in this regard.

4.2. Synthetic Approaches: Click Chemistry

A rod-coil diblock copolymer can be prepared in three primary approaches. The first one is diblock copolymer precursor approach where one can prepare a coil-coil diblock and then converts one of the coil blocks to a rod block. This is however restricted to certain polymer like PPP.[116] The second one is a divergent path where the coil block is formed from the rod block by a living polymerization method. [117,118] Though this method is applicable to variety of monomers, the presence of residual homopolymers due to partial functionalization of the starting rod polymer and the incomplete initiation of the second monomer's polymerization is a potential problem. The third one is a convergent

path where the coil block and the rod block are prepared separately before being joined together either by quenching [14b, 119] or condensation.[120] Majority of the rod-coil diblock copolymers have been synthesized by the convergent method as this leads to well-controlled block copolymers.

We followed the convergent approach of making the rod-coil diblock copolymer. The coil block is prepared by atom transfer radical polymerization (ATRP). The polymers produced by ATRP preserve the end functional bromide group which can be converted to other end groups through appropriate transformations. A variety of rigid conjugated blocks may be incorporated. At first we choose to focus on poly (phenylene vinylene) (PPV) conjugated system because PPV is not only one of the most extensively studied conjugated polymer system but also a polymer which has shown a lot of promise in various molecular devices such as light-emitting diodes, field-effect transistors and solar cells.[121] Instead of combining the two blocks together by quenching or condensation, we followed the route of click chemistry.[122-125]

As mentioned earlier in chapter 1 polymer hybrids can be realized, by two different mechanistic pathways: the polymerization-hybridization (polymerization first) approach and the hybridization-polymerization (hybridization) approach as shown in Scheme 1. We have made efforts on both fronts concomitantly. As the hybridization-polymerization (hybridization first) method demonstrated in chapter 2 needed further exploration due to the insoluble nature of the product, the second approach i.e. polymerization-hybridization (polymerization first) method was adopted for the synthesis of POM containing PPV based hybrid rod-coil diblock copolymer.

4.3. Results and Discussion

4.3.1. Synthesis of Rod-coil Hybrid

In this approach a rod-coil DCP with pendant free aryl amine was synthesized first, followed by cluster attachment to yield the hybrid DCP. To prepare the rod-coil DCP, an azide terminated coil block and an ethynyl functionalized rod block was developed. Then the two blocks were joined together through click chemistry in a convergent process of making rod-coil diblock copolymer. Phthalimide protected styrene based monomer 6 (structure shown in Figure 12) is the monomer of choice which was synthesized according to Scheme 5. The monomer was then subjected to atom transfer radical polymerization (ATRP) to produce the flexible coil block with CuBr as catalyst, PMDETA as ligand and methyl-2-bromopropionate as the initiator where the ratio of monomer to initiator to catalyst to ligand was 80:2:1:1 according to the synthetic route shown in Scheme 6. As described earlier the reaction conditions were optimized to obtain a coil block which retains majority of the bromo end functional group for subsequent modification. This bromo end functionalized coil block was then converted to an azide (shown in Scheme 14) group by the nucleophilic substitution reaction with sodium azide.[126]

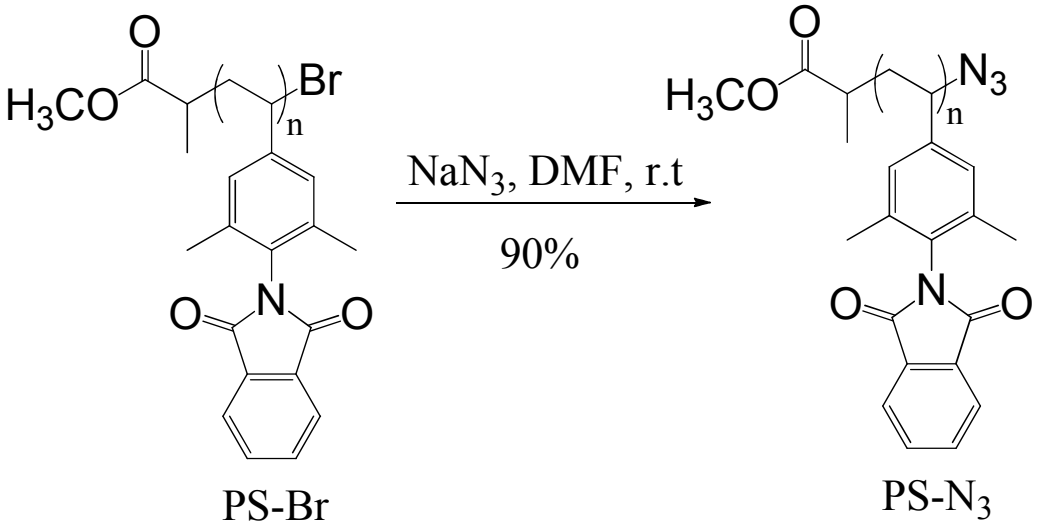

Scheme 14. Bromo- end functionalization with sodium azide

PPV blocks with well-defined lengths can be prepared using stepwise approach like the orthogonal pathway initially developed by Yu et.al, [127] which helped to realize the ethynyl terminated PPV block. In order to avoid the tedious stepwise process, a one-step approach was adopted. The synthetic scheme of ethynyl terminated PPV block is shown in Scheme 15. The monomer 9 was synthesized starting from the etherification of 2-methyl hydroquinone with 1-bromohexane to produce 7. Iodination of 7 yielded compound 8. The iodo group was converted to a formyl group by a literature procedure.[115d] PPV block with one terminal aldehyde group was synthesized in one step via Siegrist polycondensation of monomer 9, an approach demonstrated previously by Kretzschmann et.al. and Hadziioannou et.al.[115d, 1118b, 128] In this reaction the aldehyde

containing monomer 9 was first reacted with one equivalent of aniline to form an imine intermediate. Polycondensation of the intermediate was performed in the presence of base to form the imine end functionalized polymer. Hydrolysis with hydrochloric acid yielded the polymer PPV-CHO. This polycondensation reaction is highly stereoselective with no traces of Z-configuration. Generally, yields of Siegrist polycondensation reaction are lower. The intramolecular activation by the imine group enhances the reactivity of methyl group through its electronic effect. But the activation effect decreases with increasing chain length and finally reactivity approaches to a non-activated methylarene system. Due to this effect, a relatively narrow molecular distribution of the polymer is observed. The PPV-CHO was converted to ethynyl terminated PPV by the Horner-Wittig-Emmons reaction with compound 13. Compound 13 was successfully prepared in multigram quantities from 4-iodotoluene in three steps as shown in Scheme 16. Benzylic bromination [129] of 4-iodotoluene followed by Arbuzov reaction [130] with triethyl phosphite yielded compound 12. Then it was coupled with trimethylsilylacetylene in Sonogashira coupling reaction and subsequent desilylation with tetrabutylammonium fluoride [130] to obtain the targeted product.

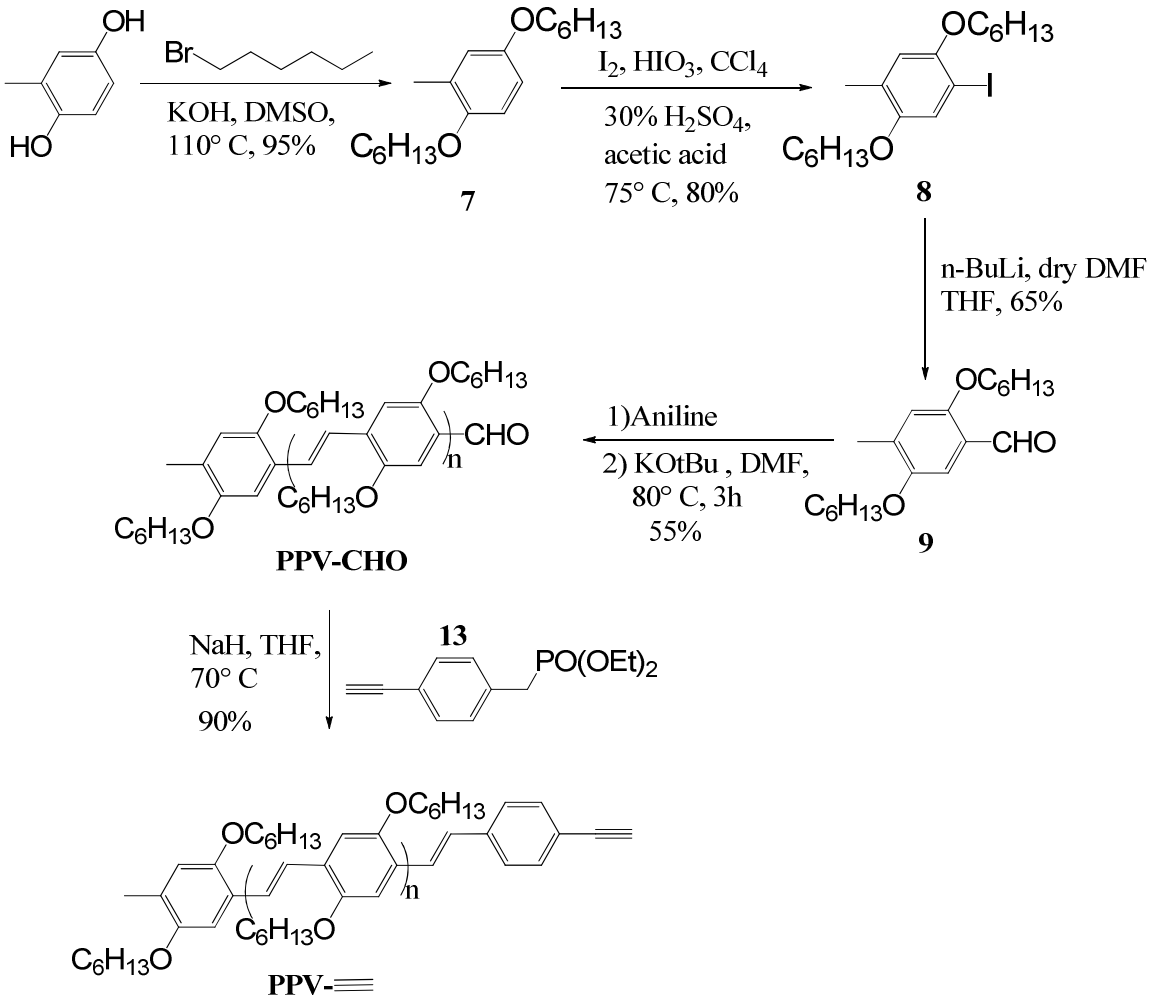

Scheme 15. Synthesis of ethynyl functionalized PPV

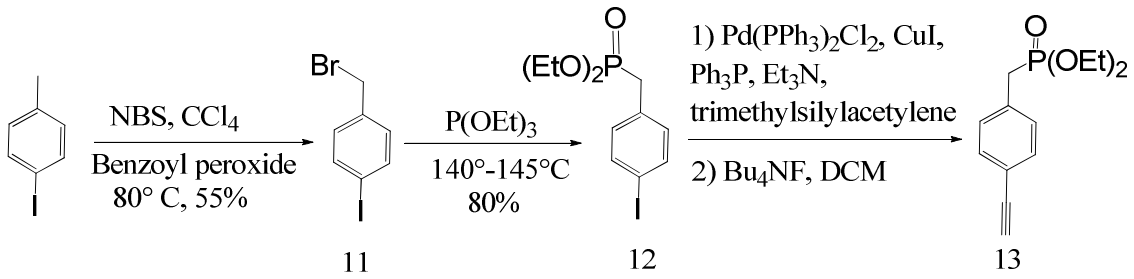

11 12 13

Scheme 16. Synthetic scheme of compound 13.

The azide terminated flexible coil block (PSN_3) and ethynyl terminated rigid block (PPV-≡) were joined together through click chemistry as shown in Scheme 17. While PSN_3 is soluble in common organic solvents such as, chloroform, dichloromethane, dimethylformamide (DMF), dimethyl sulfoxide (DMSO), acetone, tetrahydrofuran (THF), the PPV-≡ block is soluble only in chloroform, dichloromethane and THF. The click reaction was thus carried out in THF using CuBr and PMDETA catalyst-ligand combination. After completion the reaction mixture was passed through a neutral alumina column to get rid of copper. The resulting diblock copolymer PS-PPV was found to exhibit similar solubility to that of PPV block, making the separation of any unreacted PPV block difficult. To ensure complete reaction of PPV block, more than one equivalent of PSN_3 block was used. The unreacted PSN_3 block was easily removed by precipitating the mixture from acetone: PSN_3 is soluble in acetone but PPV is not.

The phathalimide protected amine group was made free with hydrazine hydrate according to Ing-Manske procedure to get a diblock (PS2-PPV) with pendant amine

functional groups dangling from each repeating unit.[101] It is noteworthy that the free amine pendant group is not very stable. So without delay, final cluster attachment was carried out in 1-methyl-2-pyrrolidinone (NMP) with excess hexamolybdate cluster and DCC as shown in Scheme 17. Both the cluster and PS-PPV diblock are soluble in NMP. Excess free clusters after the reaction were removed by precipitating the polymer from hot acetonitrile. The resulting cluster attached DCP or PS-Mo_6-PPV is soluble in NMP but partially soluble in chloroform and THF, and insoluble in most other organic solvents.

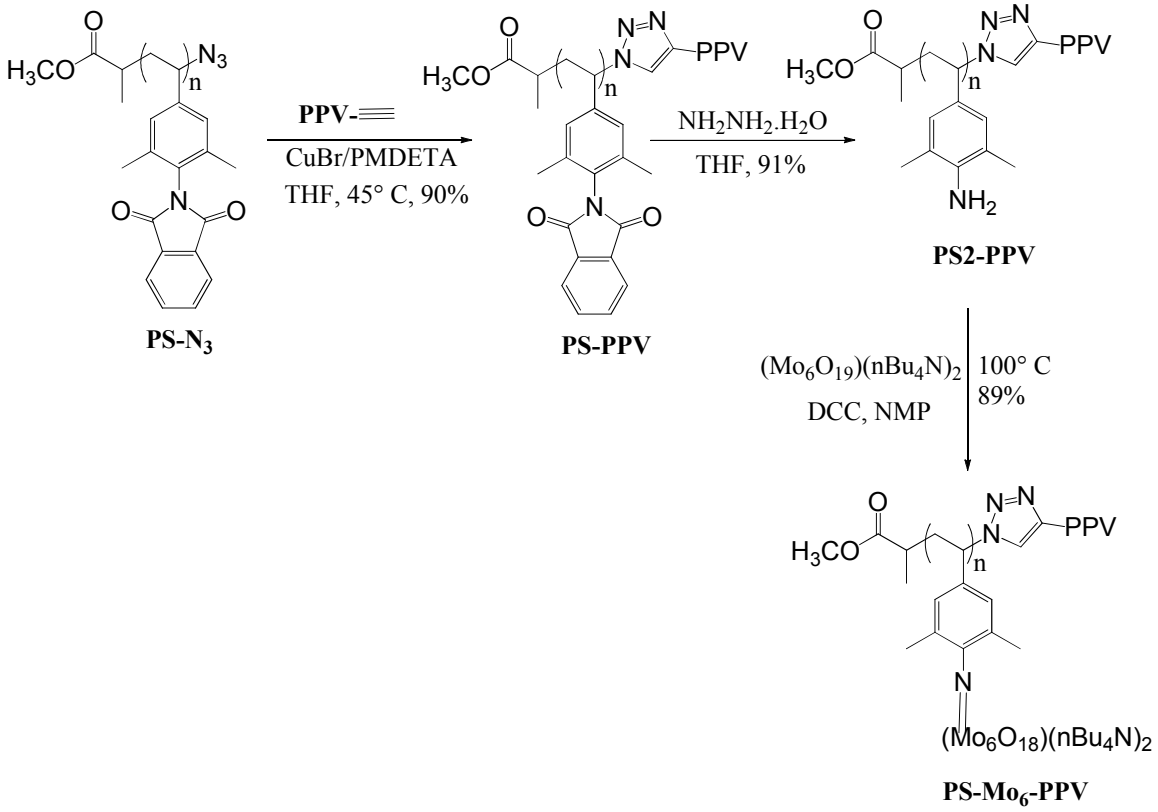

Scheme 17. Synthetic route for PS-PPV diblock and hybrid diblock

4.3.2. Structural Characterization

The structures of the synthesized products were confirmed by ^{1}H NMR spectroscopy. The ^{1}H NMR spectrum ($CDCl_3$, 400 MHz) and ^{13}C NMR ($CDCl_3$, 400 MHz) of the coil block (PS-Br) are depicted in Figure 24 and Figure 25 respectively. All the peaks of the polymer were assigned unambiguously. The ^{1}H NMR spectrum for bromo end functional polymer (PS-Br) and azide end functional polymer (PS-N_3) are

shown in Figure 47 for comparison. As expected the ^{1}H NMR spectrum for both polymers are identical except the signals corresponding to the proton at the end functional group. After expanding the region with chemical shifts of 4.0 to 5.0 ppm, a clear signal is observed around 4.43 ppm for PSBr which can be assigned to the proton associated with the Br-bonding carbon. After converting to azide, the signal shifted towards upfield to 3.95 ppm.

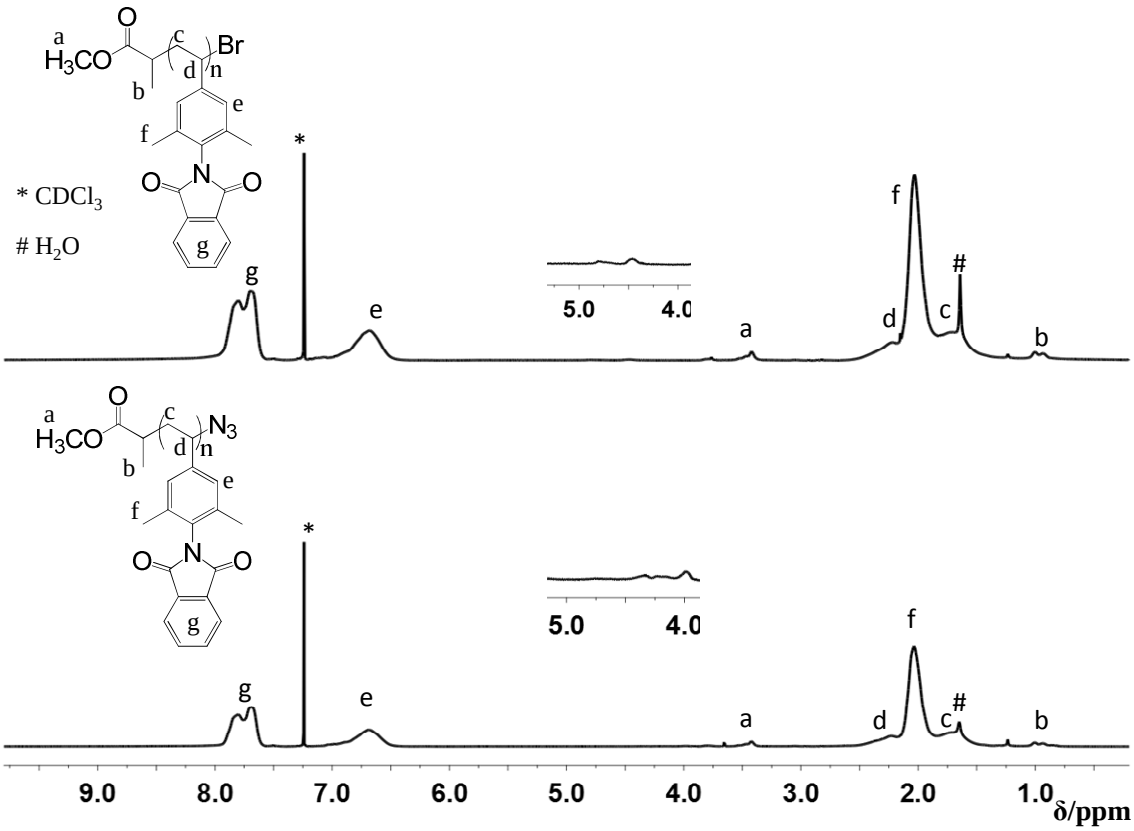

Figure 47. ^{1}H NMR spectrum ($CDCl_3$, 400 MHz) of PSBr (top) and PSN_3 (bottom)

The ^{1}H NMR spectra ($CDCl_3$, 400 MHz) of monomer 9 for the rod block and the two PPV polymers are shown in Figure 48 for comparison.

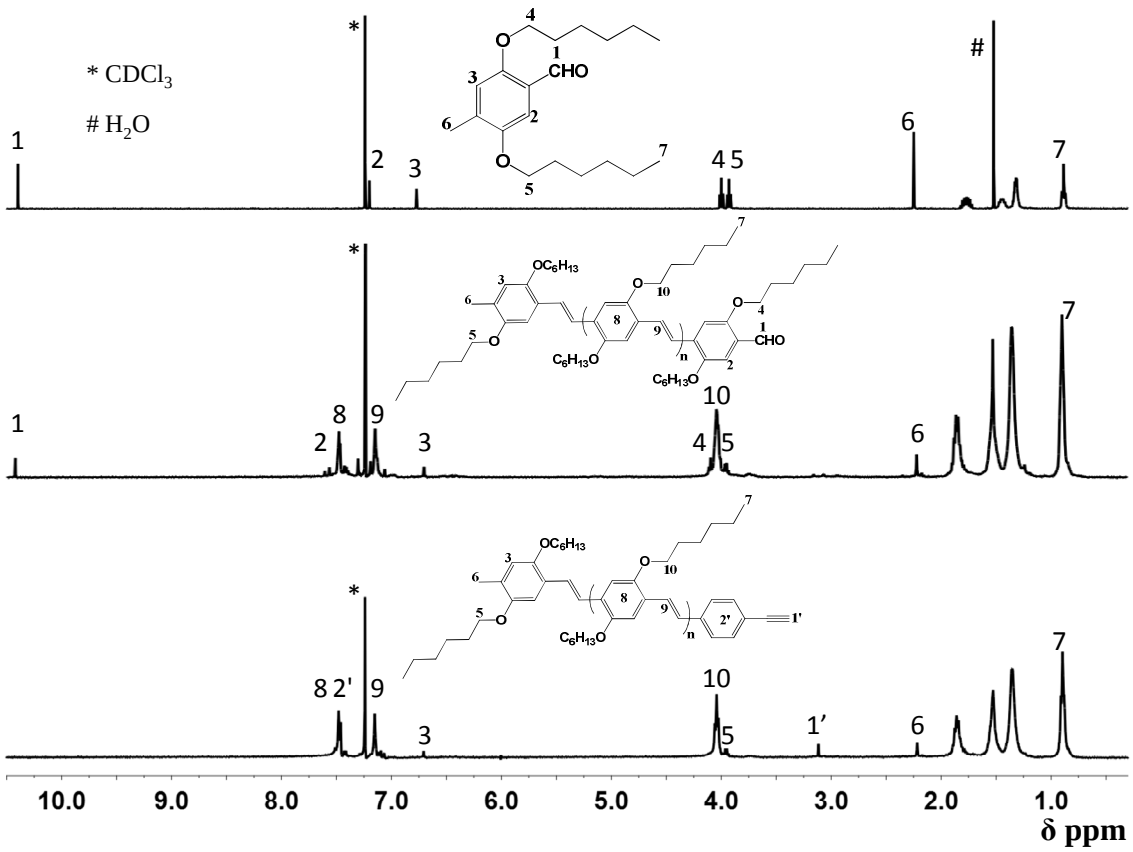

Figure 48. ^{1}H NMR spectrum ($CDCl_3$, 400 MHz) of monomer 9 (top) and two PPV blocks: PPV-CHO (middle) and PPV-≡ (bottom)

After polymerization, two major peaks appeared at 7.48 (8) and 7.15 (9), which are assigned to aromatic and vinyl protons, respectively. The methyl and aldehyde end groups (1 and 6) are clear. Other end group signals such as 2,3,4,5 are also visible. Using the integration ratio of signal 7 versus 1 (7:1= 76:1), the degree of polymerization can be calculated to be around 11. Signals associated with the –CHO end group such as 1, 2, 4 disappeared upon conversion to alkyne. Signals corresponding to the new end group, such as alkyne signal 1' (3.12) are clearly visible. Signals at the other end, such as 3, 5 are again clear with no change in chemical shift observed. Using the integration of signals 7 and 6 (7:6 = 60:2.5), a degree of polymerization of 11 is again obtained.

The ^{1}H NMR spectra ($CDCl_3$, 400 MHz) of click product (PS-PPV), deprotected diblock (PS2-PPV) and hybrid diblock (PS-Mo_6-PPV) are shown in Figure 49. The spectra of the 'clicked together' diblock copolymer is essentially a combination of the spectra of the two polymer blocks, except for the missing terminal alkyne proton signal (signal 1'). When the spectral region of 5-6 ppm is expanded, a signal around 5.15 ppm is observed which can be assigned to the proton associated with triazole binding carbon in the PS block.[125e] Using the integration of signals attributed distinctively to either block, n/m ratio can be calculated (where n and m are the degree of polymerizations of the PS and PPV block, respectively). For example using the integration of signals g (34) and 8(8), the n/m ratio is calculated to be 2.1 to 1 consistent with the degrees of polymerization of two blocks.

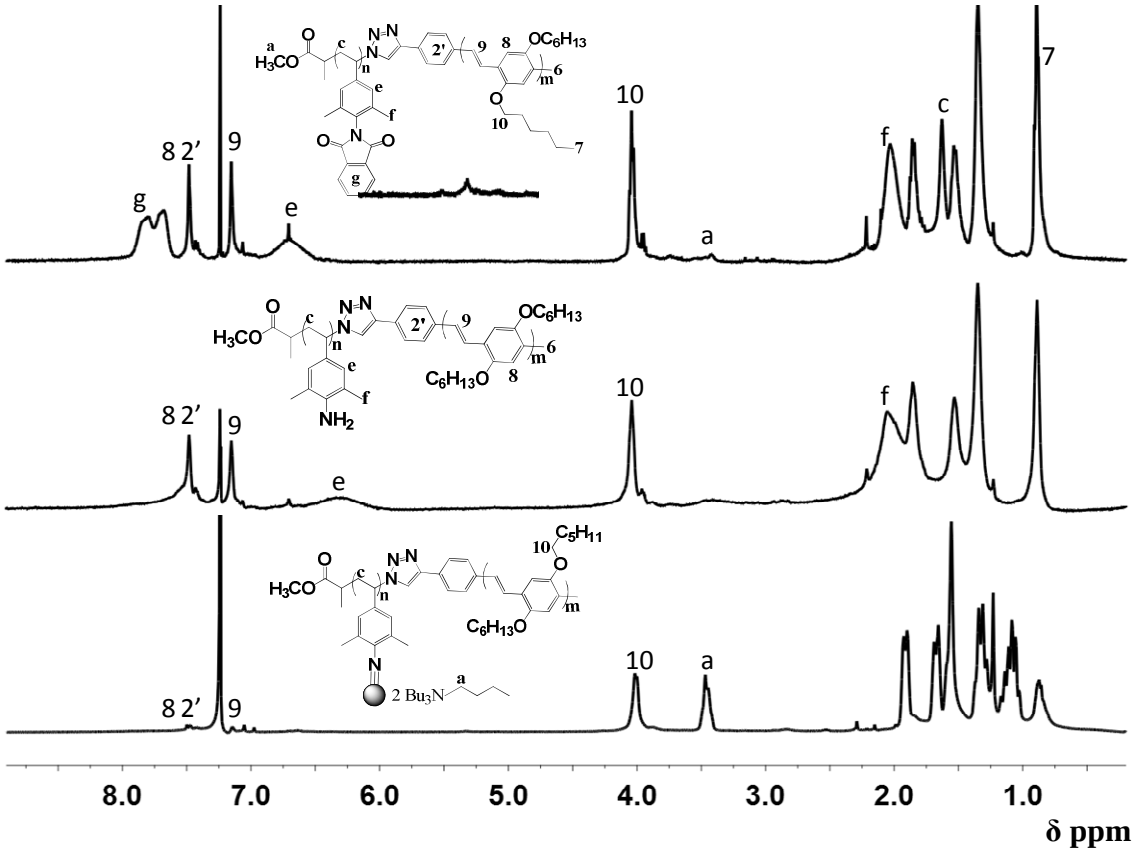

Figure 49. ^{1}H NMR spectrum ($CDCl_3$, 400 MHz) of PS-PPV DCP (top), deprotected DCP (middle) and the cluster attached DCP (bottom).

The complete removal of the phathalimide protecting group is confirmed by the ^{1}H NMR spectrum of the resulting polymer where signal g is completely missing (shown in Figure 49). The ^{1}H NMR spectrum of hybrid DCP was taken in $CDCl_3$. Because of its limited solubility, the spectrum reflects only the structures of those soluble DCPs. As

evidenced from Figure 49 rather weak aromatic signals are seen in the spectrum. The broad signals e and f seen in the ^{1}H NMR spectrum of the deprotected DCP have disappeared. Weak but discernible signals seen at 6.92 and 2.80 ppm are likely downfield shifted signals e and f, respectively. The hybrid DCPs which are soluble in chloroform are likely to have only short PS segments which may account for the unusually low intensity of proton signals associated with the PS segment. New signals corresponding to the tetrabutylammonium counterion, such as the one at 3.42 ppm, appeared in the ^{1}H NMR spectrum of the cluster-attached DCP. While signals overlap extensively in the 1.0 to 2.0 region and the aromatic region, in the 3.0 to 5.0 ppm range, two strong and well-resolved broad signals at 4.05 and 3.42 ppm are observed, which can be assigned to the -OCH_2- proton of the PPV block and the -NCH_2- protons of the tetrabutylammonium counterion, respectively. On the basis of their 1:1 integration ratio, the number of attached clusters can be estimated to be about one-fourth of the degree of polymerization of the PPV block, yielded about 3 POM clusters per PS block.

4.3.3. Molecular Weight Determination

The gel-permeation chromatography traces of the rigid PPV block, the PS block, the PS-PPV DCP, free cluster Mo_6, and the hydrid DCP are shown in Figure 50. All measurements were run at 30 °C using THF as the eluent. The coil PS block has a number average molecular weight (M_n) of 2732 and a polydispersity (PD) of 1.10 as already shown in Figure 16. The relatively narrow molecular weight distribution indicates the living nature of the polymerization. The PPV block has a Mn of 2208 and a slightly

larger PD of 1.27. Such a PD is consistent with literature reports.[118b] After "click" coupling, the PS-PPV DCP shows a M_n of 5900 and a PD of 1.22. No uncoupled PPV block or PS block is seen in the DCP's GPC trace, indicating a complete coupling reaction. Such a result also confirms that all the PS coil blocks prepared from the ATRP process possess the active Br end group. After cluster attachment, the resulting hybrid DCP shows a peak with a significantly shortened retention time. No peaks corresponding to the unreacted DCP and the free Mo_6 cluster are observed, indicating that all DCPs have reacted and free clusters have completely washed out. While it cannot be concluded that all amines have reacted and most likely that did not happen because of steric reasons, the narrow PD of the resulting hybrid DCP indicates that the extent of functionalization is fairly consistent among different DCP chains.

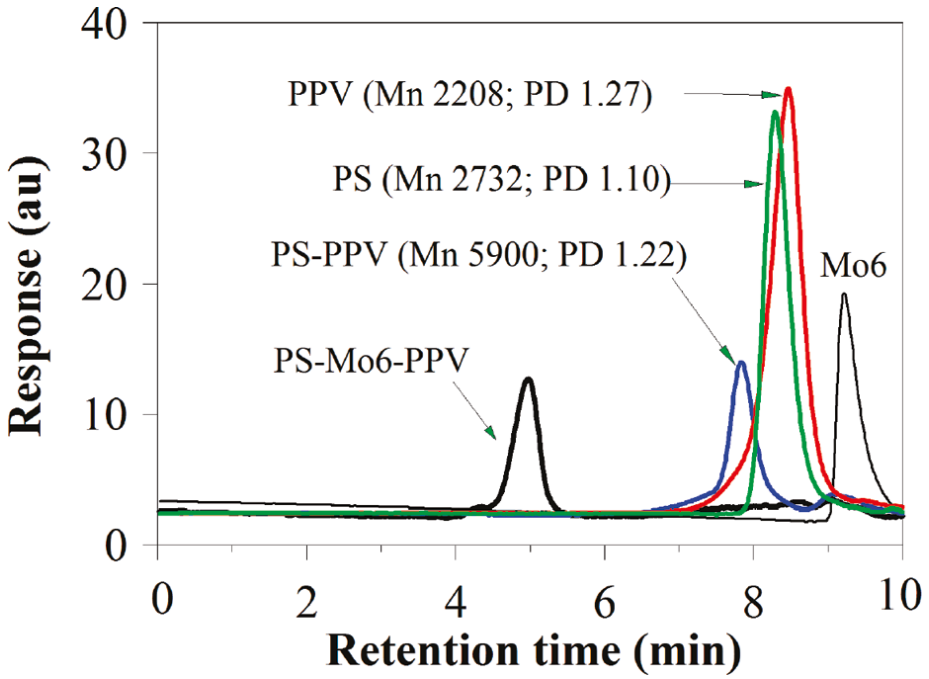

Figure 50. GPC traces of the PS-Br block, PPV-≡ block, PS-PPV DCP and the hybrid DCP using THF as eluent.

Realizing that GPC produces only a relative molecular weight (in relation to polystyrene standards), matrix-assisted laser desorption/ionization-Time-of-Flight (MALDI-TOF) mass spectrometry (MS) measurements were also carried out on all polymers to yield information on their absolute molecular weights and molecular weight distributions. MALDI-TOF spectrum of PS-Br has already been shown in Figure 27 from which M_n was calculated to be 4494 on the basis of molecular weights and the intensities of the peak. MALDI-TOF spectrum of PS-N_3 also depict a regularly distributed set of peaks with mass difference of one repeating unit (277.11) as illustrated in Figure 51, and the M_n of PS-N_3 is calculated to be 4596, which corresponds to an average degree of

polymerization (DP) of 18, reasonably consistent with the DP obtained by ^{1}H NMR. Both polymers (PS-Br and PS-N_3) show narrow molecular weight distributions with PD of 1.10 and 1.11, respectively, confirming the living nature of the polymerization. The MALDI-TOF spectrum of the PPV block shows one major peak at a mass/charge ratio of 2209.8, corresponding to 7 repeating units. The M_n and PD of PPV are calculated to be 2116 and 1.03, respectively. After being clicked together, the resulting DCP shows a M_n of 6644 and a PD of 1.04. The molecular weight of PS-PPV DCP matches very well with the theoretical value of 6712 (4596 + 2116) calculated based on the M_n's of the two blocks. Taking the distributions of the PS-N3 block and the PPV block and assuming a random reaction between them, the theoretical statistical molecular weight distribution of the PS-PPV DCP is calculated and shown in Figure 51 as well. The theoretical molecular weights and their distribution of the PS-PPV diblock copolymer as shown in Figure 51 are calculated depending upon the molecular weight and their intensities. Based on the MALDI-TOF mass spectrum of PS-N_3, its molecular weights (M_i (PS)) and mol fraction (X_i (PS)) can be obtained. Similarly, M_i (PPV) and X_i (PPV) can be obtained. Assuming a random reaction between the PS and PPV blocks, the mole fraction of the resulting PS-PPV diblock copolymer with a molecular weight of M_i(PS)+M_i(PPV) can be calculated as X_i(PS)X_i(PPV), from which the theoretical plot of molecular weight vs mole faction can be obtained. A nice match between the theoretical prediction and the actual experimental results can be observed, confirming the diblock copolymer formation. It is noted that a lower molecular weight distribution in the 1000-3000 range is observed, which was initially attributed to any unreacted PPV block. Repeated attempts in

chromatography separation failed to remove these low molecular weight components. Since GPC trace of PS-PPV does not show a corresponding low molecular distribution, it is possible that those low molecular weight components are fragments of PS-PPV, generated during the MS measurements. While MALDI-TOF measurements yield molecular weight information for the PS block, PPV block and the PS-PPV DCP, spectra of the cluster attached DCP revealed no peaks beyond a mass/charge ratio of 3000, whether using a positive or negative detection mode. The lack of high mass/charge signals may be due to the difficulty in vaporizing cluster-attached DCPs under the MALDI conditions or due to the simple fact that the hybrid DCP is highly charged (as each attached cluster carried a -2 charge).

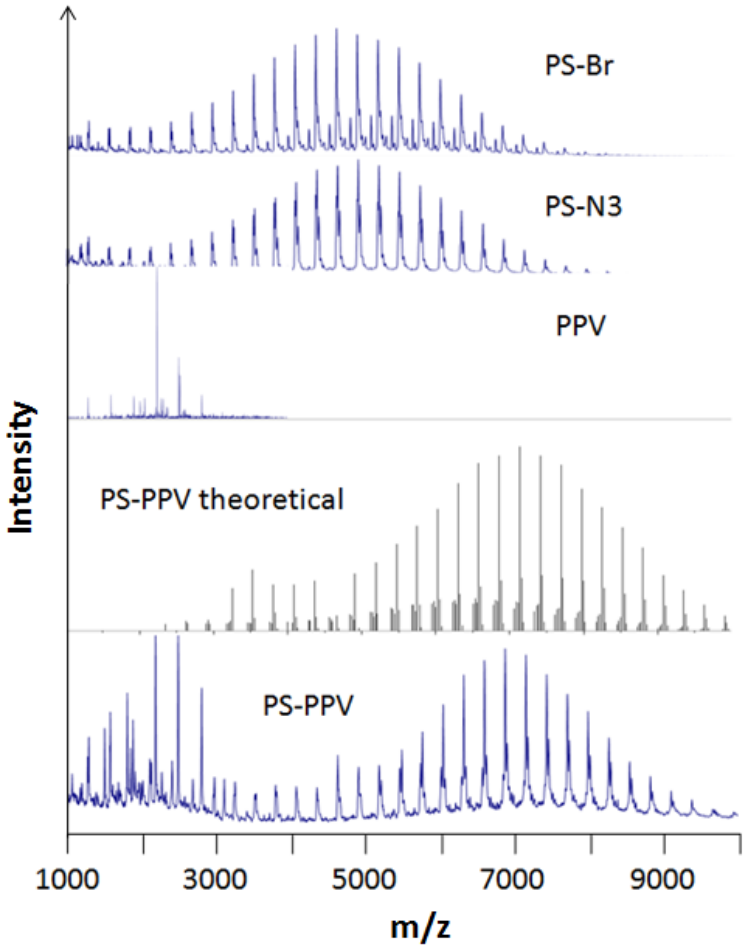

Figure 51. MALDI-TOF spectra of the PS block, the PPV block, and the PS-PPV DCP. The theoretical MW distribution is calculated based on the random statistical reaction of the two blocks with the known MW distribution.

4.3.4. Thermal Properties

Thermal properties of the two blocks, PS-PPV DCP and the hybrid DCP were studied by thermogravimetric analysis (TGA), and the results are shown in Figure 52. While both the cluster and the PS-PPV DCP are thermally stable up to 300°C, the hybrid

DCP started to decompose at a much lower temperature of 200°C. Weight loss continued until 530°C when no further loss is observed up to 700°C. A residual weight of 34% remains. For the free Mo_6 cluster, a similar no weight loss region from 530 to 700°C is observed, and the residual weight is 64%, which is consistent with its cluster anion content of 64%. The PS block, the PPV block, and PS-PPV, on the other hand, all started to degrade around 300°C and continued to lose weight up to 700°C. All these polymers have less than 8% residual weight at 700°C. It is thus reasonable to assume that at 700°C the thermally decomposed residue of the hybrid DCP is MoO_3, from which the weight percentage of Mo in the hybrid DCP can be calculated to be 22%. Using the DPs of 18 and 7, obtained from the above MALDI-TOF measurements, for the PS and PPV blocks, respectively, and assuming a complete phthalimide deprotection, a 22% Mo content in the hybrid DCP indicates that the number of attached clusters per PS block is between 3 (20% Mo) and 4 (23% Mo), quite consistent with the result obtained from ^{1}H NMR studies.

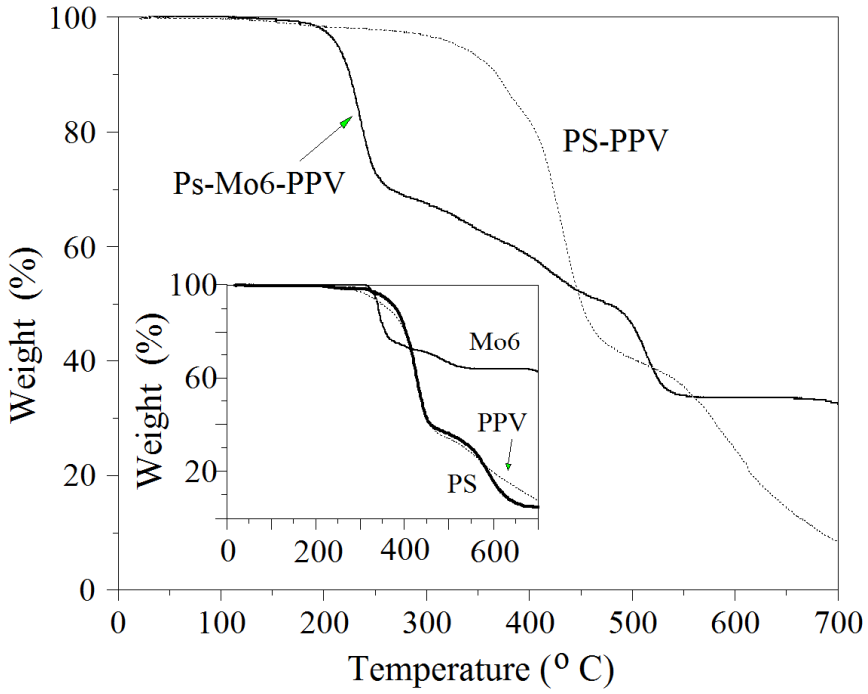

Figure 52. TGA thermograms of PS-Br, PPV-≡, PS-PPV DCP, $[Mo_6O_{19}]$. $2NBu_4$ cluster and the hybrid DCP.

4.3.5. FT-IR Measurements

Besides ^1H NMR and GPC, the covalent formation of PS-PPV diblock is evident by IR measurements, too. The azide stretching peak around 2100 cm^{-1} observed for the PSN_3 coil block as shown in Figure 53 is completely disappeared in the IR spectrum after PS-PPV diblock copolymer formation.

Both ^1H NMR and TGA analysis confirm the existence of clusters in the hybrid DCP, and GPC indicates that those clusters are attached covalently to the DCP polymer.

The cluster attachment is also confirmed by IR measurements. As shown in Figure 54, the PS-PPV DCP shows a sharp and intense peak at 1725 cm^{-1} which can be assigned to the carbonyl stretching of the phthalimide protecting group. After deprotection and cluster attachment, this peak is significantly weakened. On the other hand, new peaks at 798 and 953 cm^{-1}, which are characteristic Mo-O stretching vibrations, are shown clearly in the IR spectra of the hybrid DCP. A side/shoulder peak next to 953 cm^{-1} is detectable more clearly when expanded. This peak is attributed to the Mo-N stretching vibration.[62b] The observation of this peak is a good indication that Mo_6 clusters are attached to the coil block.

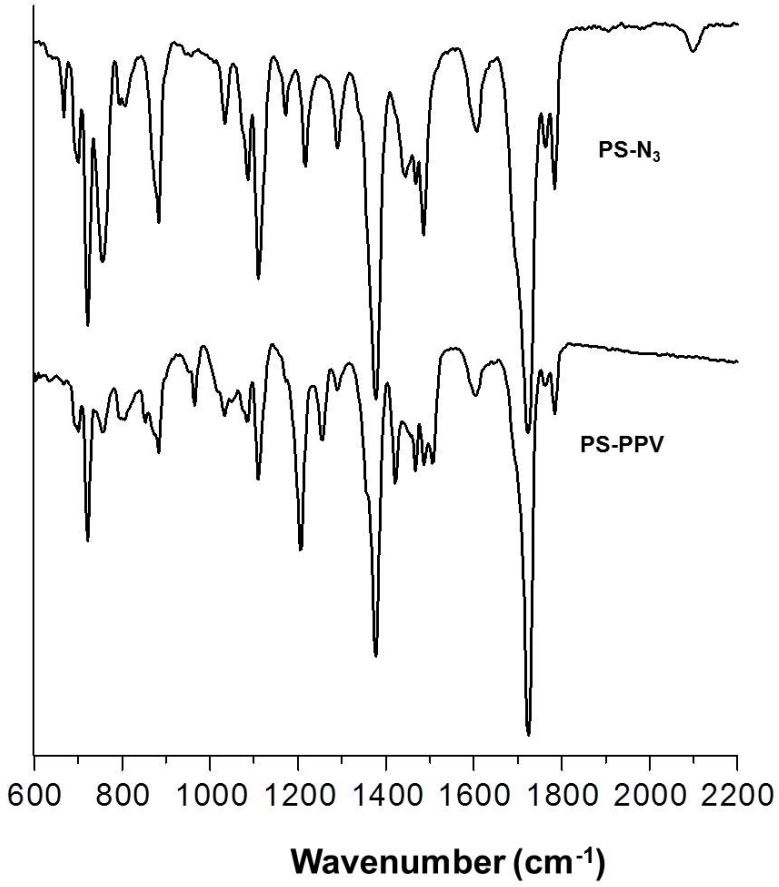

Figure 53. IR spectra of PS-N_3 and PS-PPV

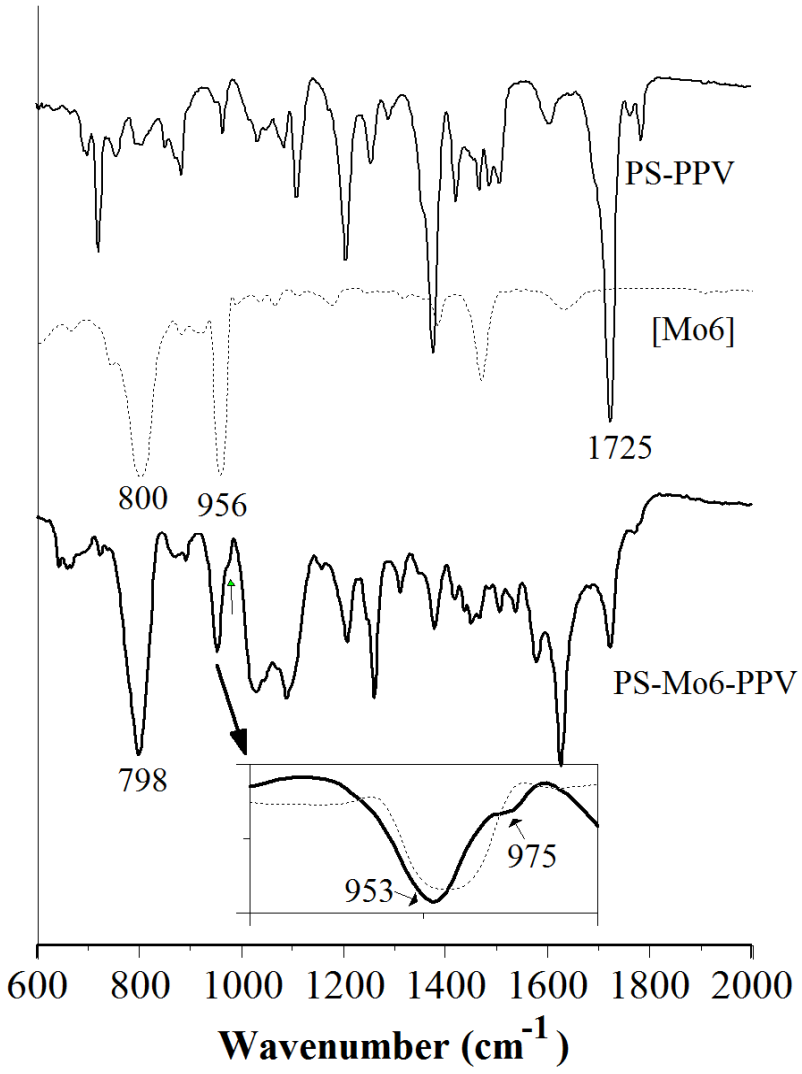

Figure 54. IR spectra of the PS-PPV DCP, free Mo_6 cluster and hybrid DCP.

4.3.6. Cyclic Voltammetry Studies

Cyclic voltammetry (CV) measurements of the DCP and hybrid DCP were carried out in acetonitrile using a Pt-disk working electrode coated with the respective polymer

film. Under identical conditions, a reversible oxidation wave at 0.32 eV is observed for the ferrocene/ferrocenium couple. As shown in Figure 55, the cyclovoltammogram of the hybrid DCP shows clearly a reduction process around -1.1 eV which does not exist in the precursor DCP, and is cathodically shifted compared to that of free [Mo_6]. This reduction process can be attributed to the imido-POM clusters, which are known to exhibit higher reduction potentials (more difficult to be reduced) than the freeMo_6 cluster.[16, 21] The clear observation of this reduction wave and the absence of reduction process of free clusters

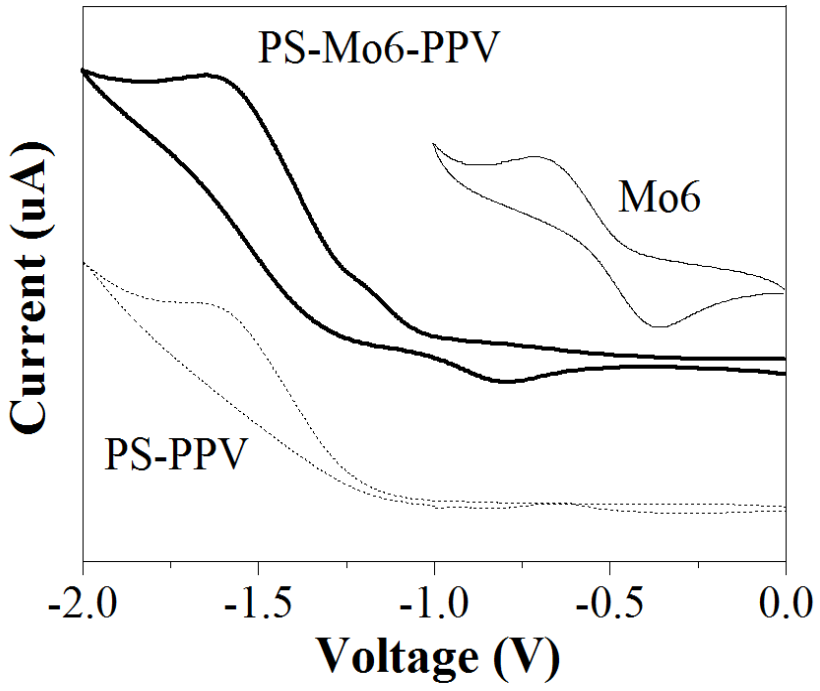

Figure 55. Cyclic voltammograms of the PS-PPV DCP, free Mo_6 cluster, and the hybrid DCP.

indicate that all POM clusters in the hybrid DCP are covalently bonded to the coil block through the imido Mo-N bond. Both the PS-PPV DCP and the hybrid DCP show a semi-reversible reduction process at around -1.5 eV, which is due to the reduction of the PPV block.

4.3.7. Optical Properties

The absorption spectra of the PS block, PPV block, a 1:1 PS/PPV mixture and the "click" coupled DCP is summarized in Figure 56. The absorption spectrum of the DCP closely matches that of the 1:1 PS/PPV mixture in both the UV and the visible region, indicating again a complete coupling between the two blocks. It also implies that there are minimal electronic interactions between the two blocks in their ground states. After cluster attachment, a new peak at around 370 nm appeared while the λ_{max} in the visible region is blue-shifted as illustrated in Figure 57. The new peak at 370 nm matches well with the absorption spectrum of the imido-POM derivative of 2, 6-dimethylaniline, [107]

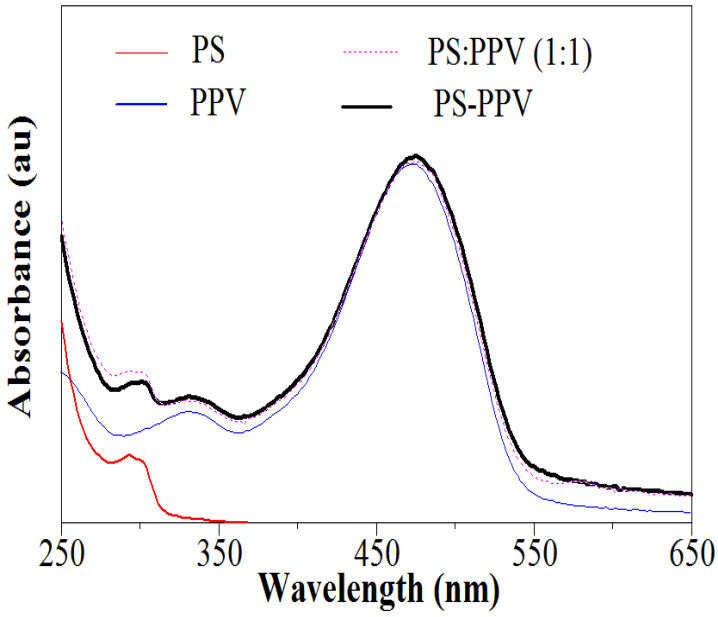

Figure 56. UV/Vis absorption spectra of PS-Br, PPV-≡, a 1:1 PS/PPV mixture and the PS-PPV DCP in dilute chloroform solutions.

and can thus be assigned to the ligand-to-metal charge-transfer (LMCT) transition of the pendant imido-POM component. The observation of this peak indicates clearly the formation of imido-functionalized POM clusters, again confirming the covalent cluster attachment. The absorption band in the visible region of the hybrid DCP is due to the π-π* transition of the PPV block. The slight blue shift of this band, compared to that of PS-PPV DCP, indicates that the attachment of POM clusters to the coil block has some effect on the effective conjugation length of the PPV block. It is possible that the bulky cluster-containing PS block may twist the bridging phenylene vinylene segment and thus decreases the effective conjugation length of the PPV block.

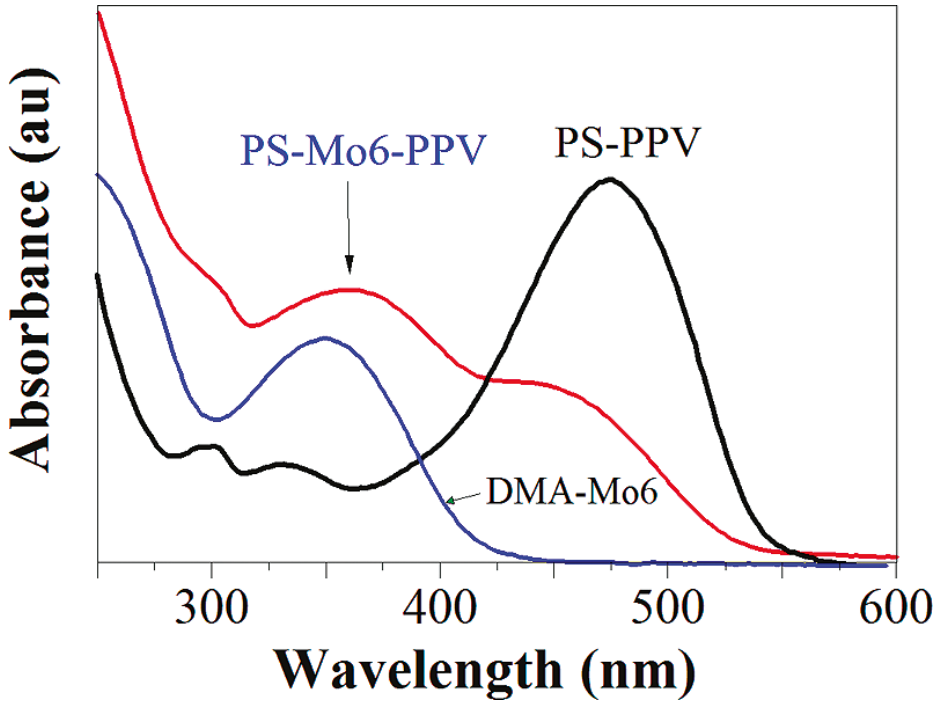

Figure 57. UV/Vis spectra of the PS-PPV DCP, the hybrid DCP, and the 2, 6-dimethylaniline functionalized hexamolybdate cluster in dilute chloroform solutions.

Both the DCP and hybrid DCP exhibit strong fluorescence in dilute solutions. Their fluorescence quantum yields are 0.21 and 0.19, respectively, indicating negligible fluorescence quenching in solution after cluster attachment. This observation is consistent with previous report on side chain POM-containing conjugated polymers where POM clusters exhibit inefficient fluorescence quenching when they are linked to the conjugated backbone through flexible alkyl bridges.[62b] In the hybrid DCP, the POMs are further away from the PPV donor and thus photoinduced electron-transfer from PPV to POM is

kinetically hampered. In the solid film, however, hybrid DCP does show much weaker fluorescence. Compared to PPV and PS-PPV, whose films show FL quantum yields of 0.48 and 0.34, respectively, hybrid DCP shows a fluorescence quantum yield of only 0.09, indicating the quenching of 74% of the PPV fluorescence when compared to PS-PPV. It is noted that while PS-PPV shows identical fluorescence to that of PPV in dilute solution, the emission of PS-PPV films is red-shifted by 15 nm while the hybrid DCP blue-shifted by 10 nm, as shown in Figure 58. Clearly, the PPV segments aggregate quite differently after the cluster attachment. Since the PPV emission in the hybrid DCP is not as red-shifted as that in PS-PPV, the observed fluorescence quenching of hybrid DCP may not be attributed to a better PPV π-stacking. The more plausible cause is the photoinduced electron transfer from the PPV exciton to the POM clusters. Such an electron transfer becomes facile in the solid state because of the close proximity of the donor PPV of one DCP and the acceptor POM clusters of another DCP. In other words, the inefficient intrapolymer photoinduced electron transfer in a dilute solution is replaced with efficient interpolymer electron transfer in the solid state, which accounts for the observation that the hybrid DCP is highly fluorescent in dilute solutions but exhibits much weaker fluorescence in the solid state.

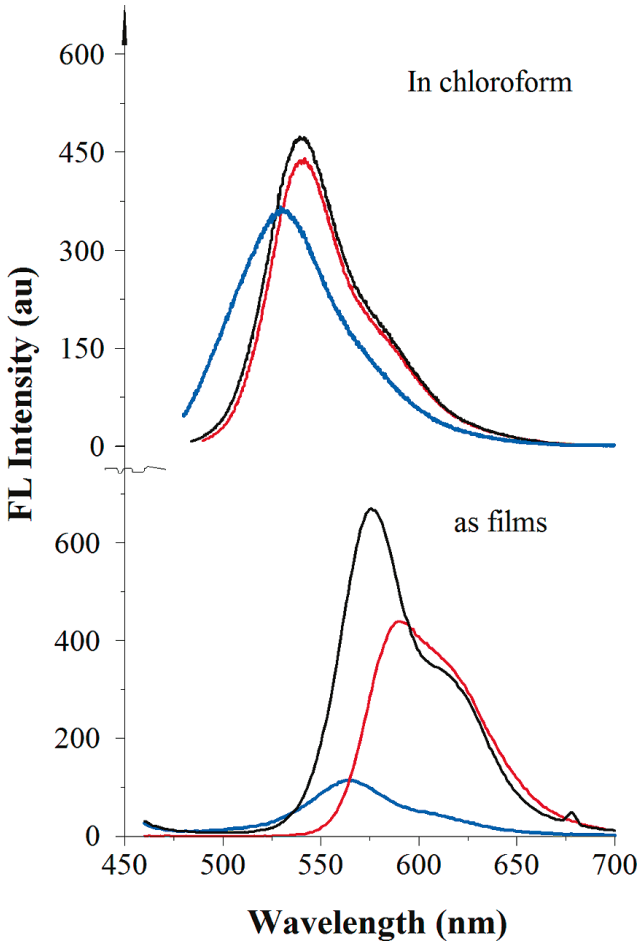

Figure 58. Fluorescence emission spectra of PPV (black), PS-PPV (red), and the hybrid DCP (PS-Mo6-PPV, blue) in dilute chloroform solutions and as solid films.

4.3.8. Thin Film Morphology

Film morphologies for the PS-PPV DCP and hybrid DCP were studied by AFM (atomic force microscopy) and SEM (scanning electron microscopy) measurements. Chloroform solutions of PS-PPV, and the hybrid DCP (1 mg in 1 mL chloroform) were spin-coated onto silicon wafer at a spin rate of 3000 and 1500 rpm. After drying in a

vacuum oven overnight, AFM was performed at tapping mode. The height and phase images at both spin rates for PS-PPV are shown in Figure 59.

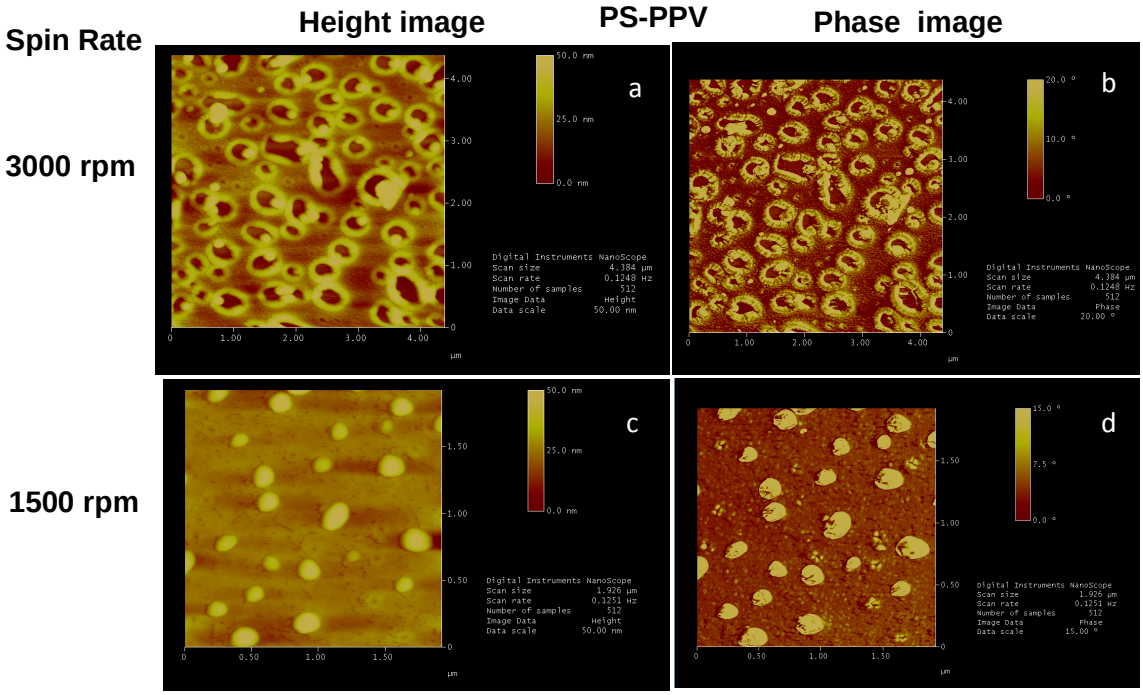

Figure 59. AFM height and phase images of PS-PPV. Height image: (a) higher spin rate, (c) lower spin rate; Phase image: (b) higher spin rate, (d) lower spin rate

The PS-PPV diblock copolymer at higher spin rate (300 rpm) exhibited a ring type irregular structure with a hollow at the center whereas at lower spin rate the diblock

formed globular structure scattered on the surface. The height and phase images at both spin rates for the hybrid are illustrated in Figure 60.

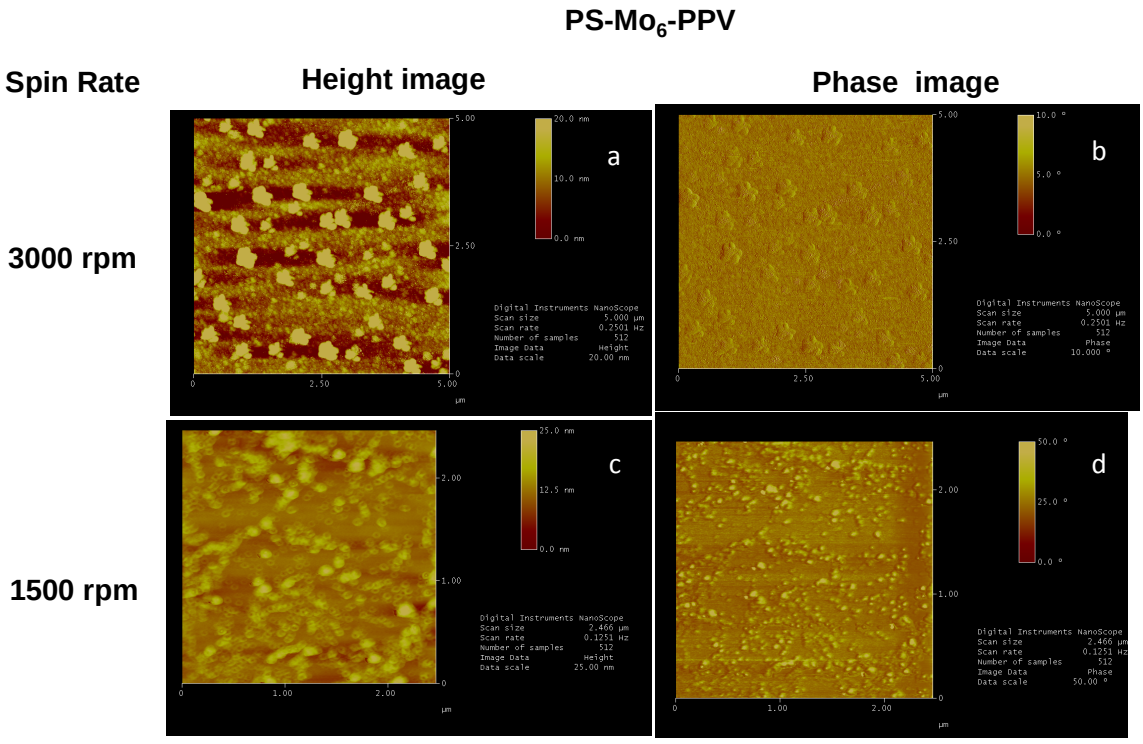

Figure 60. AFM height and phase images of PS-Mo_6-PPV. Height image: (a) higher spin rate (c) lower spin rate; Phase image: (b) higher spin rate, (d) lower spin rate

In contrast to the PS-PPV DCP, no distinct phase separated morphology was observed for the hybrid DCP both in higher and lower spin rate. AFM only provides an image of the surface topography. To get a clear idea about the samples at bulk scanning

electron microscope (SEM) can be a useful tool. The samples were prepared the same way as for AFM. After that the films were sputter-coated with a thin layer of gold/ palladium. Field-emission scanning electron microscope (SEM) XL30 (FEI Company, Hillsboro, OR) was used with an accelerating voltage of 15.0 kV. The SEM images of the PS-PPV films as shown in Figure 61 show interesting microporous structures.

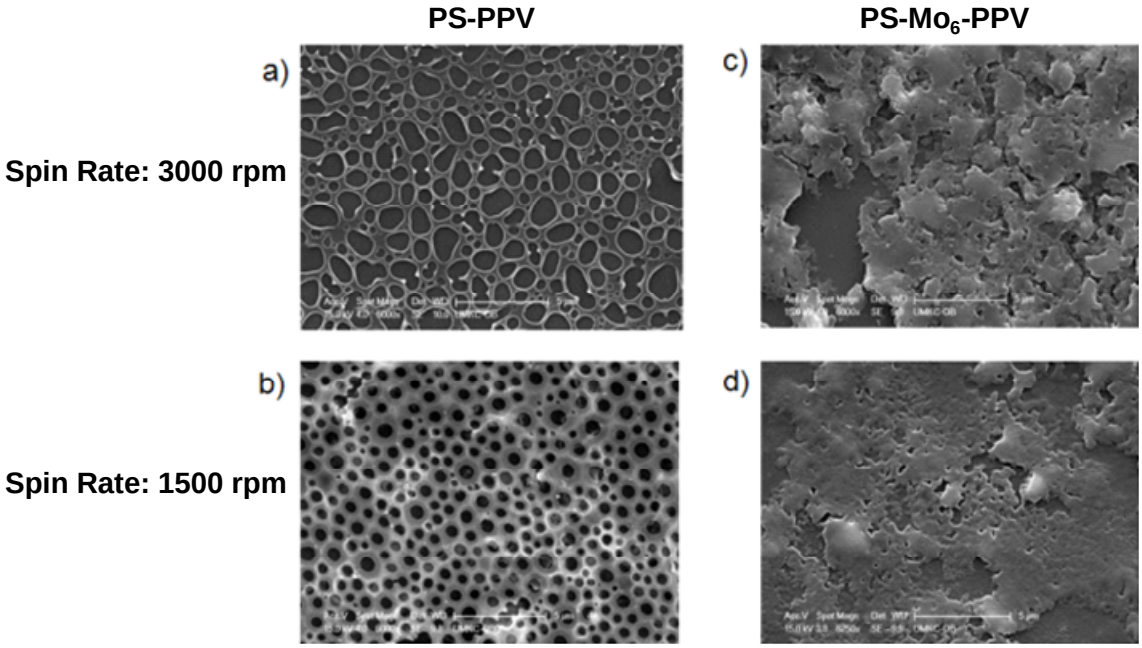

Figure 61. SEM images of PS-PPV films (a, b) and the hybrid DCP films (c, d), spin-coated at spin rates of 3000 rpm (a and c) and 1500 rpm (b and d).

At a high spin rate, the pores have irregular shape and varied sizes. At a spin rate of 1500 rpm, the pores show a regular spherical shape and much more uniform size. The

average diameter of the pores is around 500 nm. While a number of rod-coil diblock copolymers have been shown to give microporous films, [131] such morphologies are usually obtained by drop-casting with slow evaporation of the solvent. The formation of microporous films by spin-coating indicates that the PS-PPV DCP self-assembles rather quickly as solvent evaporates. This type of microporous structure is very similar to the so called "breath figure" structure.[132] During the fast evaporation of the volatile solvent the temperature drops to -6° C. The subsequent condensation of water from the moist environment onto solution surface results in the presence of isolated water droplets floating on the organic surface. The density of the droplets increases with the increasing diameter of the droplets. After some time rafts of non-coalescing droplets form and organize on the surface. These arrays do not coalesce rather sink into the solution of polymer when a second layer of droplets can be deposited on top of the first one. There are multiple theories which explain the absence of coalescence such as Marangoni convection or the instant precipitation of the polymer layer around the water droplets forming a solid envelope. The long range order of these bubble-arrays is driven by competing repulsive and attractive forces leading to a surface filled with water droplets stabilized by a solvated polymer layer. Upon further evaporation of solvent, viscosity of solution increases which in turn effectively locks the porous structure in place. Both open and closed bubble-arrays are observed and explained by the surface tension effect that opens up the bubble arrays if the connecting skin is very thin. Insights into the self-assembly process and the micropore formation mechanism require a detailed and systematic study of how the block sizes, solvent, polymer concentration, spin rate,

thermal treatment, and so forth affect the film morphologies. After cluster attachment, the resulting hybrid DCP yields films with very different morphologies. As shown in Figure 61 (c and d), spin-coating of a hybrid DCP solution gives films with an uneven surface and non-uniform coverage. While one sees pits in the film and some areas of aggregated lumps, the widespread pores seen in the DCP film are clearly missing. When the smooth film area is magnified, one sees no phase separated domains. It should be noted that the morphology of a spin-coated pristine film is formed through a kinetic process rather than a thermodynamic one, and thus it may be altered with time and temperature. The actual morphology depends on several factors like choice of solvent, annealing temperature, drying speed, and, above all, the degree of polymerization of each block. In our preliminary morphology studies, chloroform, a good solvent for both blocks, was used as the solvent. While no phase-separated morphologies were observed for either the PS-PPV DCP or the hybrid DCP films without prior thermal treatment, it remains to be seen whether spin coating from different solvents, under different spin rates and after thermal annealing at various temperatures will be able to create any new type of morphology.

4.4. Conclusions

The first POM-containing rod-coil DCP through the post-polymerization functionalization approach was successfully prepared. Click chemistry was used to join together a rigid PPV block and a flexible PS block to form the precursor DCP. Both GPC and MALDI-TOF measurements have confirmed the formation of the DCP with a narrow

molecular weight distribution. POM cluster attachment was carried out in NMP, a solvent in which both the precursor DCP and the Mo_6 cluster are soluble. The cluster attachment was confirmed by GPC, IR, CV, and optical spectroscopy. The hybrid DCP shows two absorption bands, one at 450 nm due to π-π^* transition of the PPV block, and the other at 370 nm attributable to the ligand-to-metal charge transfer transition of functionalized Mo6 clusters. Spin-coated PS-PPV films show microporous structures which are not observed in the hybrid DCP films. Significant fluorescence quenching is observed for the hybrid DCP because of photoinduced electron transfer from the PPV exciton to POM cluster, indicating its potential as photovoltaic materials. The film morphology was not the desired one for photovoltaic applications as the cluster attached DCP didn't exhibit any phase separation. POM-containing DCPs with different block structures, longer block lengths, different volume fractions of each block needed to realize the POM containing DCP as a potential candidate for photovoltaic applications.

4.5. Experimental Section

Materials. Triethylamine was distilled over CaH_2**.** THF was purified by distillation over sodium pellets and benzophenone. CuBr was purified by washing consecutively with glacial acetic acid, absolute ethanol and diethyl ether, and then dried under vacuum. N, N, N', N', N''-pentamethyldiethylenetriamine (PMDETA, 99%), aniline and 1-methyl-2-pyrrolidinone were distilled in vacuo before use. All other

chemicals were purchased either from Aldrich or Acros and were used as received unless otherwise stated.

Instrumentation. All reactions were conducted under protection of nitrogen. The ^{1}H NMR and ^{13}C NMR spectra were collected on a Varian INOVA400 MHz FT NMR spectrometer. All samples were referenced to the deuterated solvents. GPC measurements were performed at 30° C on a Waters system equipped with a Waters 410 differential refractometer, Waters 515HPLC pump and a styragel HR 4E column with THF as the eluent. The calibration curve was determined by the use of five polystyrene standards from 800 to 90,000. FT-IR spectra were obtained from samples dispersed on KBr pellets on an IR100 FT-IR spectrometer (Thermo-Nicolet Co.).UV-vis absorption spectra were measured on a Hewlett-Packard 8452A diode array spectrophotometer, and photoluminescence spectra were measured using a Shimadzu RF-5301PC spectrofluorophotometer. Fluorescence quantum yields for solution were determined using quinine sulfate in 1 N H_2SO_4 ($\varphi_{fl} \approx 0.55$) as the standard. For films, diphenylanthracene (dispersed in PMMA film with concentration less than 10^{-3} M, assuming PL efficiency of 0.83) was used as the standard. Cyclic Voltammetry (CV) studies were carried out in acetonitrile at room temperature under argon protection using a BAS Epsilon EC electrochemical station employing a 1 mm^2 Pt disk as the working electrode, silver wire as the reference electrode, and a Pt wire as the counter electrode. $[Bu_4N]PF_6$ was the supporting electrolyte, and the scan rate was 50 mV/s. Polymer films were cast from chloroform onto the Pt disk working electrode. Ferrocene was used as an internal standard. Thermal analyses were performed on Shimadzu TGA-60 at the heating

rate of 10°C/min. A Voyager DE Pro (Perceptive Biosystems/ABI) MALDI-TOF mass spectrometer was used for mass measurement operating in both linear and reflector mode. A mixture of silver trifluoroacetate/dithranol (1, 8-dihydroxyanthrone) (1:25 w/w) was used as the matrix. Field-emission scanning electron microscope (SEM) XL30 (FEI Company, Hillsboro, OR) was used with an accelerating voltage of 15.0 kV. A Multimode Nanoscope IIIa Atomic Force Microscope (AFM, Digital-Veeco instruments, CA) was used to observe the samples. J type of piezoelectric scanner with scan range of 100 ×100 μm^2 was selected. Oxide sharpened Si_3N_4 cantilevers having a nominal force constant of 0.08 N/m (OMCL TR400PS) were purchased from Olympus Ltd (Tokyo) and used in experiment. Contact/tapping Mode was employed to obtain AFM images. The scan rate was 0.5 Hz with the imaging force as low as possible and the resolution of images was 512×512 pixels. Height and defection data were recorded during experiment. Image formation and data analysis including D-banding and diameter were carried out using section analysis with Nanoscope Software 5.30 version.

Sample Preparation for AFM and SEM. One mg of each of the three polymer samples was dissolved separately in 1mL of chloroform solution inside a glovebox. Though PPV and PS-PPV were readily soluble in chloroform, hybrid DCP were heated at 50° C and stirred overnight under nitrogen protection to make a homogeneous solution. The solutions were filtered through 0.45 μm PTFE filter prior to spin coating on silicon wafers at spin rates of 3000 or 1500 rpm. All the films were dried in a vacuum oven overnight. For SEM only, the samples were sputter-coated with a thin layer of gold after drying.

Compound 7. 2-methyl hydroquinone (10.0 g, 80.5 mmol), 1-bromohexane (26.6 g, 161.0 mmol), potassium hydroxide (9.94 g, 177.2 mmol) and DMSO were combined and stirred at 110° C for 4 h. After cooled to room temperature, the reaction mixture was diluted with methylene chloride (300 mL) and poured into cold water (400 mL). The organic layer was collected and washed with aqueous KOH (1M, 100 mL), aqueous HCl solution (1M, 100 mL) and water (300 mL) respectively. The organic layer was collected, and after the evaporation of the solvent, yielded compound 7 as a dark red liquid. (22.4 g, 95 %). ^{1}H NMR (400 MHz, $CDCl_3$, 25 °C): δ 6.68 -6.75 (m, 3H), 3.88 (t, J=6.4 Hz, 4H), 2.23 (s, 3H), 1.73 (m, 4H), 1.47 (m, 4H), 1.35 (m, 8H), 0.93 (t, J= 7.2 Hz, 6H). ^{13}C NMR ($CDCl_3$, 400 MHz): δ 152.38, 150.98, 127.63, 117.86, 116.46, 111.71, 68.29, 66.84, 31.25, 29.05, 25.41, 22.26,13.19.

Compound 8. Compound 7 (5 g, 17.10 mmol), iodine (2.60 g, 10. 26 mmol), iodic acid (0.90 g, 5.13 mmol), sulfuric acid (6.25 mL, 30% w/w in H_2O), carbon tetrachloride (5 mL) and acetic acid (20 mL) were combined and refluxed for 4 h. The resulting reaction mixture was washed with saturated sodium bicarbonate (900 mL) to neutralize the solution. The entire reaction mixture was then extracted with methylene chloride (300 mL). The organic extract was washed with saturated sodium bisulfite (900 mL) followed by water. The organic layer was collected, dried over magnesium sulfate, filtered and evaporated the solvent to get a crude product. This was the recrystallized from methanol to get compound 8 as a white solid (5.75 g, 80%, mp 39-40°C). ^{1}H NMR (400 MHz, $CDCl_3$, 25 °C): δ 7.15 (s, 1H), 6.64 (s, 1H), 3.84-3.93 (m, 4H), 2.16 (s, 3H), 1.76 (m, 4H), 1.47 (m, 4H), 1.35 (m, 8H), 0.93 (t, J= 7.2 Hz, 6H). ^{13}C NMR ($CDCl_3$, 400

MHz): δ 152.05, 151.63, 128.06, 121.93, 115.39, 82.23, 70.18, 68.84, 31.14, 29.28, 25.74, 22.59, 16.44. 14.05.

Compound 9. Compound 8 (2.00 g, 4.78 mmol) was dissolved in dry THF (7 mL) and cooled to -10^{0}C in an ice-salt bath. n-Butyllithium (2.5M in hexanes) (2.86 mL, 7.17 mmol) was added drop wise to the above solution with a nitrogen filled syringe. The resulting mixture was stirred at -10°C for 15 min and then anhydrous DMF (2 mL) was added drop wise with a nitrogen filled syringe. The ice-salt bath was removed and the mixture was stirred for 1 h under nitrogen at room temperature. The reaction mixture was then poured in water (100 mL) followed by addition of 6N HCl (100 mL). The mixture was then extracted with methylene chloride (3 × 200 mL), washed with saturated $NaHCO_3$ (200 mL) and water (200 mL). The organic layer was collected and dried over magnesium sulfate. The solvent was removed to obtain yellow oil. This was purified by column chromatography (silica gel, hexanes/methylene chloride (2:1) as the eluent) to yield compound 9 as a white solid. (0.9 g, 59%, mp 41-42°C). ^{1}H NMR (400 MHz, $CDCl_3$, 25°C): δ 10.40 (s, 1H), 7.20 (s, 1H), 6.77 (s, 1H), 3.98 (m, 4H), 2.25 (s, 3H), 1.77 (m, 4H), 1.43 (m, 4H), 1.32 (m, 8H), 0.88 (m, 6H). ^{13}C NMR ($CDCl_3$, 400MHz): δ 189.47, 156.14, 151.30, 136.79, 122.89, 115.57, 108.16, 69.10, 68.42, 31.51, 29.17, 25.74, 22.59, 17.30, 14.02.

Compound 13. A mixture containing compound 12 (4.00 g, 11.3 mmol), trimethylsilylacetylene (1.33 g, 13.5 mmol), bis (triphenylphosphine) palladium (II) chloride (0.161g, 0.226 mmol), copper (I) iodide (0.148 g, 0.777 mmol), triethylamine (45 mL) and triphenylphosphine (0.059 g, 0.226 mmol) was stirred at 50°C under

nitrogen for 3 h and then extracted with methylene chloride (3 × 50 mL) followed by water (50 mL) wash. The organic layer was collected, dried over magnesium sulfate and evaporated the solvent to get a dark brown liquid. The liquid was then poured into hexanes (200 mL). The resulting mixture was washed with water (3 × 200 mL). The organic layer was then filtered through Celite 545 (Fisher Co.). Evaporation of solvent afforded 4.13 g of trimethylsilyl-protected precursor as a brownish red liquid, which was then desilylated by following procedure: tetrabutylammonium fluoride (1 M solution in THF, 20 mL) was added to a solution of trimethylsilyl-protected precursor (4.13 g) in methylene chloride (50 mL). The resulting mixture was stirred at room temperature for 1 h and was then poured into hexanes (200 mL). The resulting solution was then washed with water (3 × 200 mL). The organic layer was collected and again filtered through Celite 545 to get a yellow liquid. The liquid was dried over magnesium sulfate and evaporated the solvent to yield dark brown crude oil. The crude product was purified by flash chromatography (silica gel, ethyl acetate as the eluent) to yield compound 13 as yellow oil. (2.1 g, 74%). ^{1}H NMR (400 MHz, $CDCl_3$, 25°C): δ 7.42 (d, 7.6, J= 7.6 Hz, 2H), 7.24 (d, J= 8 Hz, 2H), 3.98 (m, 4H), 3.14 (s, 1H), 3.09 (s, 1H), 3.04 (s, 1H), 1.21 (t, J= 7 Hz, 6H). ^{13}C NMR ($CDCl_3$, 400MHz): δ 132.35, 132.26, 131.99, 129.54, 128.33, 120.43, 83.10, 62.03, 34.16, 32.79, 16.15.

PPV-CHO. Synthesis of Poly(2,5-Dihexyloxy-1,4-phenylenevinylene). Compound 9 (1.46 g, 4.68 mmol) was added into a two-neck flask. The flask was evacuated and backfilled with nitrogen three times. To the flask was added a sample of aniline (0.480 g, 5.15 mmol) with a nitrogen-filled syringe. The reaction mixture was

stirred at 60° C for 1.5 h. Potassium tert-butoxide (1.05 g, 9.36 mmol) was then added into the above mixture, followed by dry DMF (36 mL). The resulting reaction mixture was stirred at 80° C under nitrogen for 3 h. After being cooled down to room temperature, the solution was poured into mixture of 150 mL of 1 N HCl and 200 mL of $CHCl_3$ to hydrolyze the aldimine end group. After the mixture was stirred for 1 h, the organic layer was collected and washed with water until the aqueous phase was neutral. The organic layer was dried over sodium sulfate. After stripping off most of the solvent, the concentrated residue solution was poured into a large excess of acetone. The resulting dark red precipitates were filtered and dried at 50° C under vacuum to give 1.2 g of product (yield 55%). ^{1}H NMR (400 MHz, $CDCl_3$, 25° C): δ 10.43 (s, 1H), 7.48 (m, 16H), 7.15 (m, 14H), 6.71 (s, 2H), 4.04 (br), 2.22 (s, 3H), 1.84 (br), 1.53 (br), 1.35 (br), 0.89 (br). ^{13}C NMR ($CDCl_3$, 400 MHz): δ 189.2, 156.3, 151.1, 127.1, 123.0, 110.4, 69.5, 31.7, 29.5, 26.0, 22.7, 14.1. Anal. Calcd. For $C_{162}H_{244}O_{17}$: C, 78.91; H, 9.98. Found: C, 77.63; H, 9.92. GPC: M_n=2208, PDI=1.27. MALDI MS: M_n = 2116, PDI = 1.03.

PPV-≡. PPV-CHO (0.600 g) was added into a two-neck flask, and the flask was evacuated and then backfilled with nitrogen three times. Dry THF (20 mL) was then added, followed by sodium hydride (0.08 g, 3.33 mmol). After stirring at room temperature for 5 min, compound 13 (0.075 g, 0.297 mmol) in dry THF (5 mL) was then added dropwise to the above solution, and the resulting reaction mixture was refluxed for 16 h. The solution was then poured into water (50 mL) and extracted with chloroform. The organic layer was washed with water (100 mL) and dried over magnesium sulfate. After stripping the majority of the solvent, the concentrated solution was poured into

methanol to yield the polymer as red solids, which were dried at 50° C under vacuum (0.700 g, 90%). ^{1}H NMR (400 MHz, $CDCl_3$, 25° C): δ 7.48 (m, 19H), 7.15 (m, 12H), 6.71 (s, 2H), 4.04 (br), 3.12 (s, 1H), 2.22 (s, 3H), 1.86 (br), 1.53 (br), 1.36 (br), 0.90 (br). ^{13}C NMR ($CDCl_3$, 400 MHz): δ 151.1, 132.4, 127.6, 126.3, 124.8, 123.2, 110.4, 69.5, 31.7, 29.5, 26.0, 22.7, 14.1. Anal. Calcd. For $C_{169}H_{248}O_{16}$: C, 79.97; H 9.85. Found: C 76.40; H, 9.51. GPC: M_n=2208, PDI=1.27. MALDI MS: M_n = 2110, PDI = 1.03.

PS-N_3. PS-Br block (0.500 g, 0.164mmol), sodium azide (0.032 g, 0.492mmol), and DMF (4.00mL) were added in a two-neck flask. The resulting solution was stirred at room temperature for 14 h. The reaction mixture was then precipitated into cold methanol (50 mL). The white solid was collected by vacuum filtration and washed with water. The solid was dried under vacuum. (0.450 g). ^{1}H NMR (400 MHz, $CDCl_3$, 25° C): δ 7.80 (br), 7.71 (br), 6.65 (br), 3.37 (br), 2.03 (br), 1.70 (br), 0.93 (br). ^{13}C NMR ($CDCl_3$, 400 MHz): δ 167.0, 146.5, 136.3, 133.9, 132.2, 127.7, 123.5, 40.6, 18.1. Anal. Calcd. For $C_{328}H_{277}N_{21}O_{38}$: C, 76.90; H, 5.45; N, 5.75. Found: C, 75.40; H 4.89; N, 5.21. GPC: M_n=2700, PDI=1.10. MALDI MS: M_n=4537, PDI=1.11.

PS-PPV. PS-N3 (0.092 g, 0.031 mmol) and CuBr (0.005 g, 0.035 mmol) were charged to a two-neck flask. The flask was then evacuated and backfilled with nitrogen three times. PMDETA (0.007 mL, 0.006 g, 0.035 mmol) and freshly distilled THF (15 mL) were then added to the above mixture. To the resulting light yellow homogeneous solution was added dropwise a THF solution of PPV-≡ (0.060 g, 0.024 mmol in 15 mL of THF). The resulting red solution was stirred at 45° C for 24 h. The reaction mixture was filtered through neutral alumina to remove the copper catalyst. The resulting red solution

was concentrated and precipitated into methanol (100 mL). The crude red solid was collected by vacuum filtration and washed with acetone to remove excess PS-N_3. The red solid was dried under vacuum at 50° C (0.182 g, 90%). ^{1}H NMR (400 MHz, $CDCl_3$, 25° C): δ 7.78 (br), 7.65 (br), 7.43 (br), 7.11 (br), 6.6 (br), 3.99 (br), 2.17 (br), 1.99 (br), 1.81 (br), 1.60 (br), 1.54 (br), 1.30 (br), 0.85 (br). ^{13}C NMR ($CDCl_3$, 400 MHz): δ 167.0, 151.0, 136.3, 133.9, 132.2, 127.6, 123.5, 110.4, 69.4, 40.6, 31.7, 29.5, 26.0, 22.7, 18.1, 14.1. Anal. Calcd. For $C_{497}H_{525}N_{21}O_{54}$: C, 77.80; H, 6.91; N, 3.44. Found: C, 77.44; H, 6.96; N, 2.80. GPC: M_n=5900, PDI=1.22. MALDIMS: M_n=6644, PDI=1.04.

Deprotection of Phthalimide Group. PS-PPV DCP (0.050 g, 0.008 mmol) was dissolved in freshly distilled THF in a two-neck flask. Then hydrazine monohydrate (0.200 g, 3.99 mmol) was added dropwise into the above red solution with constant stirring, and the entire reaction mixture was refluxed for 13 h under nitrogen protection. The resulting solution was cooled to room temperature, and the light orange-white precipitate was filtered off. The orange color filtrate was stripped off the solvent and precipitated from methanol to yield an orange-red colored powder. (0.040 g, 91%). ^{1}H NMR (400 MHz, $CDCl_3$, 25° C): δ 7.41 (br), 7.11 (br), 6.25 (br), 4.04 (br), 3.45 (br), 2.06 (br), 1.85 (br), 1.54 (br), 1.35 (br), 0.89 (br).

Hybrid DCP (PS-Mo_6-PPV). In a two-neck flask were added deprotected DCP (0.030 g) and DCC (0.090 g, 0.436 mmol). The flask was degassed and backfilled with nitrogen. Hexamolybdate cluster, $[Mo_6O_{19}]^{2-}$. $2N(C_4H_9)_4^+$ (0.900 g, 0.659mmol) dissolved in NMP (4 mL) was then added into the flask, and the reaction mixture was stirred at 100° C for 12 h. The resulting dark red solution was cooled to room

temperature, and the white solid precipitate (urea) was filtered off. The solvent was distilled off from the dark filtrate solution under vacuum, and the resulting concentrated solution was poured into hot acetonitrile to yield the crude hybrid DCP, which was further washed with hot acetonitrile to get rid of any remaining free cluster. The resulting hybrid DCP is a brownish red solid (0.035 g, 89%). ^{1}HNMR (400MHz, $CDCl_3$, 25° C): δ 7.48 (br), 7.15 (br), 6.71, (br), 4.05 (br), 3.42 (br), 1.85 (br), 1.66 (br), 1.54 (br), 1.30 (br), 1.05 (br), 0.89 (br).

CHAPTER 5

SYNTHESIS AND THIN FILM MORPHOLOGICAL STUDIES OF P3HT-BASED ROD-COIL DIBLOCK COPOLYMER WITH POLYOXOMETALATE CLUSTERS COVALENTLY ATTACHED TO THE COIL BLOCK

5.1. Transition from PPV to P3HT as Conjugated Rod Block

While morphological diversities in coil-coil diblock copolymers (DCP) whose molecular shape closely matches Gaussian coil models are well understood, phase separation in rod-coil diblock copolymer remains more debated and intriguing. An increasing interest in rod-coil diblock copolymers for use in organic electronics is evident where importance of interface between two incompatible materials with different work functions is apparent. These diblock copolymers are promising in controlling the active layer morphology and interfacial structure in multicomponent devices on the 10 nm exciton diffusion length critical to device performances.[119b] Chemically connected donor-acceptor type blocks microphase separate into equilibrium ordered heterojunction structures driven by factors such as immiscibility or the crystallinity difference between two segments. In this connection PPV based rod-coil hybrid DCP has been documented in chapter 4 where PPV acts as the conjugated donor system and POM cluster acts as the electron acceptor. But limited molecular weight and lower hole mobility of PPV rendered very poor phase separated domains for useful application in PV devices. The microporous structures of DCP disappeared after attaching the POM cluster.[98] Besides PPV is highly susceptible to photo oxidation due to the reactive trans vinyl bonds in the

backbone which in turn leads to deterioration of photoconductivity and device performance.[133] So by changing the block structure especially the rod block structure phase separated morphology suitable for the PV devices can be achieved. Not only that by varying the length of rod blocks the size of the surfaces between donor and acceptor blocks, the exciton diffusion length and the shape of the domain through the photocharges percolate to the electrodes might be controlled. In this respect regioregular poly (3-hexylthiophenes) (P3HT) is extensively studied because of its good photo chemical stability and higher field-effect mobility (0.01-0.1 cm^2 V^{-1} s^{-1}) compared to PPV.[134] Its regular end to end arrangement of side chains allows efficient π-π stacking of the conjugated backbones making charge transfer efficient. [135] High solubility and good film forming properties make it attractive as a printable semiconducting polymer.[136] The electron transfer occurs through intra-chain and inter-chain transport in crystalline portion whereas amorphous region does the same through hopping and tunneling.[137] High regioregularity is required for the formation of highly ordered films with high charge carrier mobility.[138] Besides regioregularity, number average molecular weight and processing conditions affect the charge carrier mobility immensely.[139] It has been demonstrated that low molecular weight films exhibited low mobility due to domain boundaries or in other words due to the poor interconnection of highly aggregated domains whereas in higher molecular weight films small ordered regions are interconnected through the long chains and thus prevent the charge carriers from being trapped by disordered boundary regions. The charge carrier transport in low molecular weight and higher molecular weight P3HT has been illustrated in Figure 62 as proposed

by a chain-packing model. After thermal annealing the mobility in the low molecular weight films increased as a result of the ordering and overlap of the neighboring aggregated domains. So, by changing the conjugated system of the previously synthesized rod-coil diblock copolymer with varying sizes of regioregular polythiophenes, and if bicontinuous phase separated domains can be realized through self-assembly under various processing conditions for efficient charge transport, these hybrid rod-coil systems can be envisioned as a potent active layer in the fabrication of photovoltaic (PV) devices.

5.2. Synthetic Approaches for Rod-Coil Diblock Copolymer Hybrid

An important breakthrough in the development of polythiophene occurred in 1985 when the poly(3-alkylthiophene), a soluble, processable and stable polymer was achieved by the introduction of the alkyl group in the β-position of the thiophene ring.[140] The introduction of the long chain functional groups into the 3-position not only influences the solubility and processability but also control other physical, electronic and optoelectronic properties of polythiophene.[141] This 3-substituent breaks the C_2 symmetry of the thiophene structure. The 3-alkyl substituent in a thiophene ring can be incorporated into a polymer chain with two different regioregularities: head-to-tail (HT) and head-to-

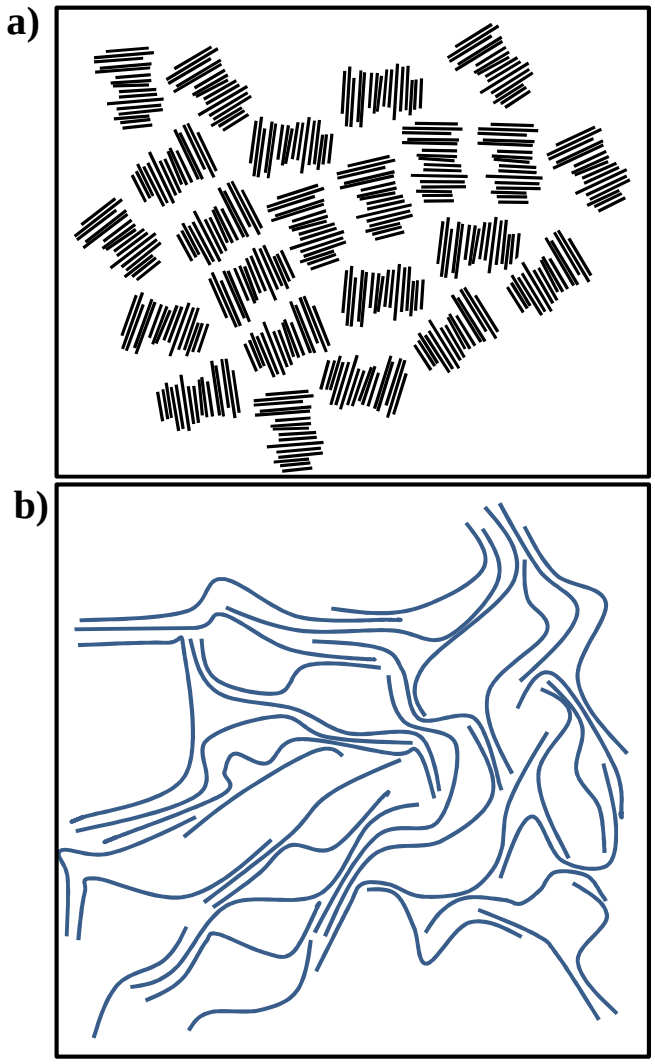

Figure 62. Chain-packing model of P3HT. a) Charge transport in low-MW and b) high-MW films. Charge carriers trapped on poorly connected aggregated domains in low-MW films. Long chains in high-MW bridge the ordered regions.

head (HH). This result in three types of dyad structures e.g. HH, HT and TT and four structurally nonequivalent, spectroscopically distinct triad regioisomers in polymer chain:

HT-HT, HT-HH, TT-HT and TT-HH as shown in Figure 63.[142] Head-to-head couplings are unfavorable due to the steric repulsion between both alkyl chains with the lone pairs of adjacent sulfur atoms.[143] Polythiophenes that contain significant amount of HH couplings are referred to as regioirregular, while polymers that bear only HT couplings are referred to as regioregular. Regioirregular polymers cannot adopt planar conformations mainly due to the repulsive interactions between the alkyl side chain and the sp^2 lone pair on the sulfur, which forces the backbone out of coplanarity. In addition to that irregular placement of alkyl groups prevents efficient solid-state packing causing defects and limits physical properties which in turn influence the photophysical phenomenon. In contrast, the planar backbone in the HT regioregular polymers increased the conductivity, non-linearity and other physical properties. Initially three general synthetic procedures for polythiophenes were developed which included electrochemical polymerization, [144] oxidative polymerization with $FeCl_3$[145] and polymerization by catalyzed dedihalogenation of 2,5-dihalo-3-alkylthiophene, such as nickel catalyzed coupling of thiophene Grignard reagents[140] or dihalothiophene monomers. [146] Though these methods lead to higher molecular weight polymers, regioregularity expressed as the percentage of HT-HT triads was rather low (usually between 50-60 %).

Recently with the modification of Grignard type polycondensation method poly(3-substituted)thiophenes was synthesized with almost exclusive HT couplings (>98%) in two steps.[147] Lithiation of 2-bromo-3-alkylthiophenes using LDA at cryogenic temperatures followed by transmetallation with $MgBr_2.Et_2O$ afforded only one metalated regioisomer. The lower temperature prevents the so called scrambling by metal-halogen

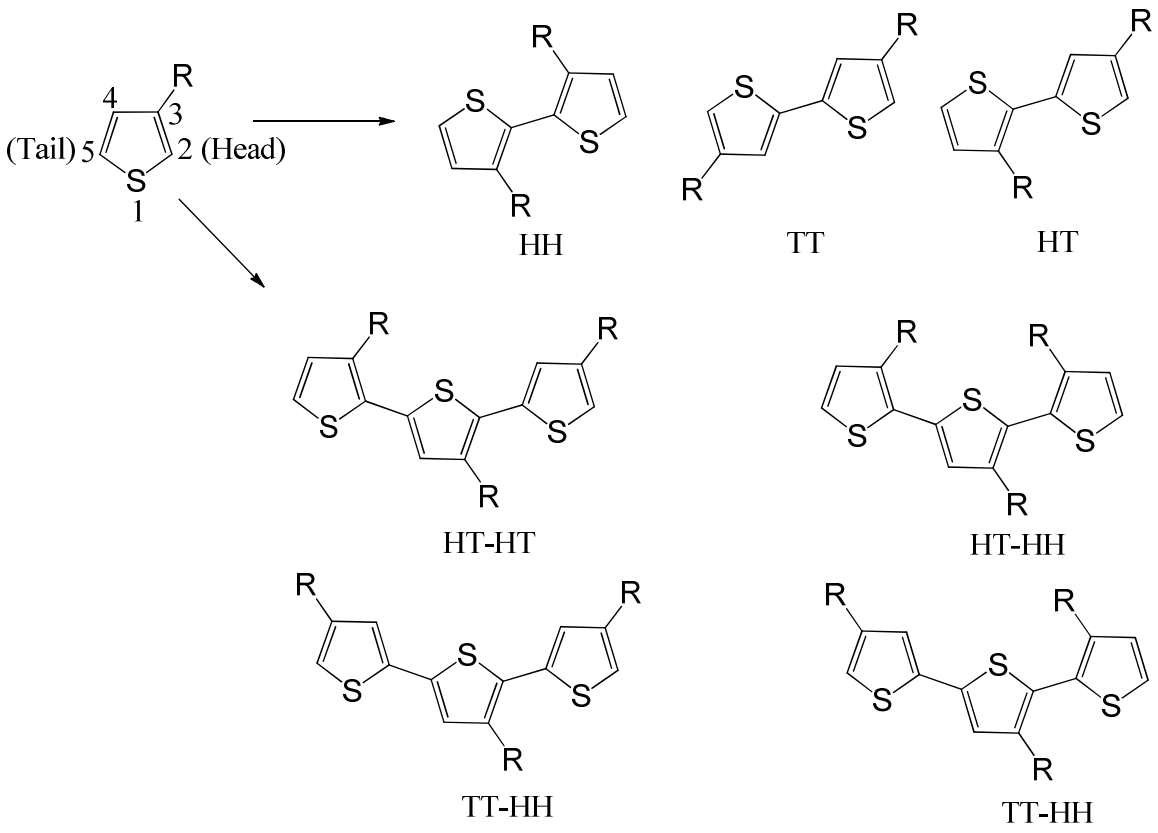

Figure 63. 3-substituted thiophene regioisomers: three dyads and four triads

exchange between lithiated aryl and heteroaryl halides.[148] The polymerization was achieved by Kumada coupling in head-to-tail fashion using Ni(dppp)Cl_2 (dppp = diphenylphosphinopropane).[149] Alternatively Rieke et al.[150] synthesized HT poly(3-substituted)thiophenes by the oxidative addition of Rieke Zn, noted as Zn*, to the 2,5-

dibromo-3-alkylthiophenes at cryogenic temperature to afford one regiochemical intermediate which was regioselectively polymerized in Negishi cross-coupling reaction.[151] The HT coupling percentage can be altered by the use of different nickel and palladium catalysts.[150a,d] The regioselective control was proposed to be based on the steric congestion at the reductive elimination step of the catalytic cycle. Besides these two above mentioned methods, regioregular poly(3-substituted)thiophenes can be synthesized using Stille [152] and Suzuki cross coupling[153] methods. In spite of these new advancements in synthesizing regioregular HT poly (3-alkyl)thiophenes, the synthetic procedures mentioned above have some drawbacks. The Grignard type polycondensation method requires highly purified materials especially the monomer, 2-bromo-3-alkylthiophene. Besides polycondensation methods or step growth process produces polymers with higher polydispersity along with uncontrolled molecular weight. In addition to that cryogenic temperature and long polymerization time are two other important requirements needed to be fulfilled. Though the purification of the monomer 2-bromo-3-alkylthiophene in the Rieke method is not tedious as the compound is the highest boiling fraction in the crude mixture, the method requires non-trivial preparation of Rieke zinc via alkali metal reduction of zinc halides, cryogenic temperatures and longer reaction times. The Suzuki and Stille coupling methods also suffered from many of the drawbacks similar to the above two methods. These methods are also not economically viable for the large scale synthesis. Keeping all these things in mind, McCullough et al. set out to describe a novel method as shown in Scheme 18 in

synthesizing HT-poly (3-alkylthiophenes) in a simple, fast, efficient and economical way.[154]

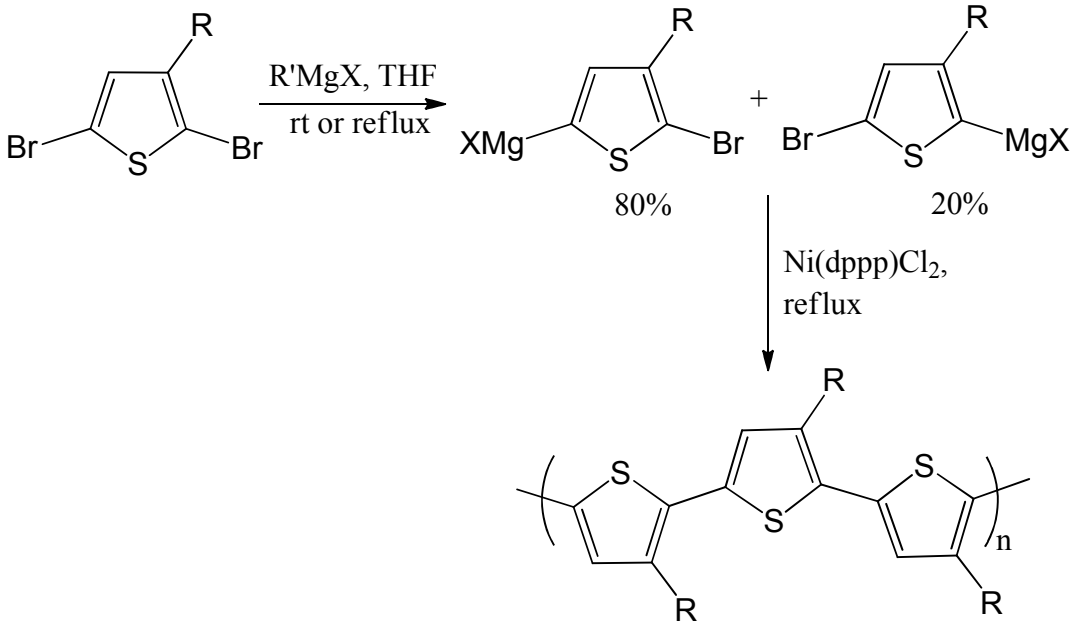

Scheme 18. Synthesis of HT-poly(3-alkylthiophene) by GRIM method.

The easy-to-purify 2,5-dibromo-3-alkylthiophene treated with 1 equivalent of commercially available alkylmagnesium bromide results in magnesium-bromine exchange, also referred to as Grignard metathesis or GRIM. The reaction proceeds with a moderate degree of regioselectivity leading to a mixture of regioisomers in the ratio of 80:20 regardless of the Grignard reagent used as shown in the Scheme 18. The Grignard

metathesis occurred due to the formation of a more stable Grignard reagent i.e. the thienyl Grignard reagent. This is then polymerized in presence of catalytic amount of Ni(dppp)Cl_2 to produce HT-coupled highly regioregular polythiophenes. To test the hypothesis of GRIM, the monomer was treated with variety of Grignard reagents followed by quenching with trimethylsilylchloride. The quenching results strongly support the magnesium-bromine exchange reaction. It is found that the use of methylmagnesium bromide leads to the best results for polymerization. The gaseous byproduct methyl bromide in the Grignard metathesis reaction helps in the complete formation of the intermediate regioisomers. The GRIM reaction occurs between temperatures as low as -40° C to refluxing conditions in THF. Lowering the temperature during the magnesium-halogen exchange results in the formation of the first isomer at the first step of Scheme 18 in higher proportion. Despite the regioselectivity of the metathesis step (80:20 mixture of isomers), degree of regioregularity displayed in resulting polymer is very high (99% HT-HT coupling). It has already been demonstrated that catalysts with sterically demanding ligands like dppp and dppe and small metal centers like Ni afford poly(3-alkylthiophenes) with a high degree of regioselectivity whereas less bulky and labile ligands combined with larger metal centers like Pd result in regiorandom poly(3-alkylthiophenes).[150a,d] Advantages of this new GRIM method are manifold. Easy and quick preparation and purification of thiophene monomers and the corresponding Grignard reagents are cheap and easy to handle. The reaction can be carried out at large scales without the use of cryogenic temperatures. The process is economically viable shunning the use of expensive $MgBr_2$ and $ZnCl_2$.

It has been elucidated that the nickel catalyzed regioregular polymerization of alkyl thiophenes proceed by a chain growth mechanism rather than the widely accepted step growth mechanism.[155] The degree of polymerization increases with conversion and can be predicted by the molar ratio of monomer to nickel initiator. So the polymerization is essentially a living system rendering low polydispersities. In a step-growth polymerization method one would expect a fast disappearance of the monomer and increase of molecular weight at the end of the reaction. But relatively high molecular weight polymers formed almost immediately as the reaction starts based on the experimental results. The mechanism of this chain growth polymerization is outlined in Scheme 19.[156] The monomer 1 generated in situ from 2,5-dibromo-3-hexylthiophene reacts with the nickel catalyst to yield the organonickel compound 2. The reductive elimination of 2 forms as associated pair [3·4] consists of the tail-to-tail dimer and Ni (0). This associated pair is proposed to form by coordination of 1,3-bis(diphenylphosphino)-propane-nickel (0) to the thiophene ring in a η^2 - or η^4 - bonded fashion similar to the reported Ni(0)-η^2 arene complex.[157] After the initial oxidative addition steps of dimer 4 to the nickel center compound 5 generated. Subsequent growth of the polymer chain occurs by monomer insertion one at a time as illustrated in the reaction cycle where the Ni(dppp) moiety is always attached to the polymer chain as end group such that additional Grignard reagents can be added resulting in end-capping of polymer with various functional groups. This phenomenon supports the fact that the Ni(dppp)Cl_2 acts as an initiator rather than a catalyst. The molecular weight of the polymer can be predicted by the molar ratio of monomer to Ni(dppp)Cl_2 which means 1 mol of Ni(dppp)Cl_2 initiates

one polymer chain. The increase of molecular weight with the conversion supports the living nature of the system. According to the mechanism, only one tail-to-tail coupling or

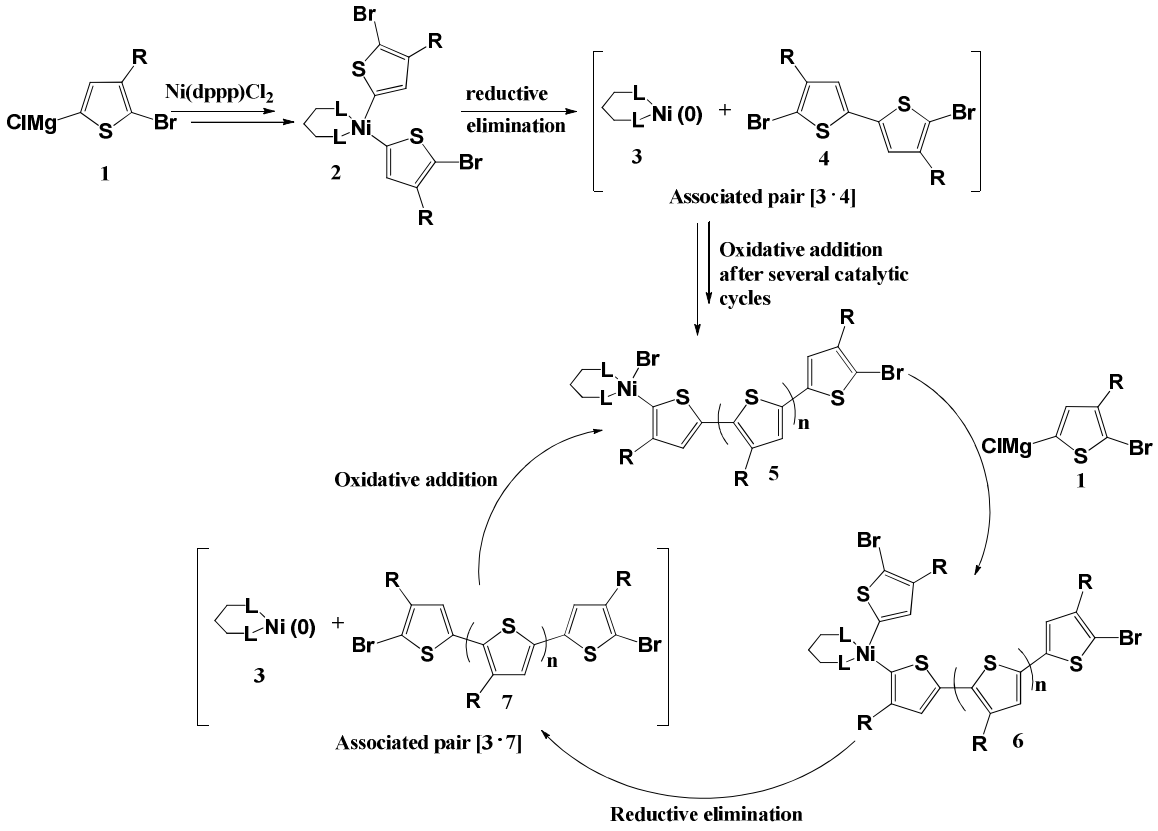

Scheme 19. Proposed mechanism for GRIM polymerization method

structural defect per polymer chain is generated during the course of the reaction.

The importance of end group functionalization in the synthesis of diblock copolymers and other applications prompted to develop a method of controlling the end group composition of regioregular polythiophenes in the GRIM method. While a great deal of work has been devoted to the modification and variation of side chains of regioregular HT polythiophenes, [158] less attention has been directed to the nature and control of the end groups of such polymers.[159] Typical GRIM polymerization yields polymer having one end group composition either H or Br. As the mechanism demonstrated above shows the polymerization to be chain growth instead of step growth, proper reaction conditions needs to be found to cap or terminate the chain end to yield an end-functionalized poly(3-alkylthiophenes). So simple addition of another Grignard reagent would terminate the polymer growth by end capping polymers and provide a simple one-pot method to control the end group composition of the HT polymer with various functional groups as shown in Scheme 20.[160] It is interesting to note that some Grignard reagents produce mono-capped product while others produce di-capped one. Mono or di capped product is neither the function of the concentration of the Grignard reagent nor the reaction time with the Grignard reagent. It is found that double or triple bond containing Grignard reagents produce mono-capped product while the rest yield di-capped polymer. Thorough examination of the mechanism revealed that after the reductive elimination to produce mono-capped polymer and reactive Ni (0), they form an associative pair and undergoes oxidative addition followed by reaction with another mole of Grignard reagent to yield the di- capped product. In the case of alkenyl or alkynyl

Grignard reagents, the unsaturated group can react with reactive Ni (0) to form a stable π-complex [161] which prevents further reaction with the bromine end group of the polymer.

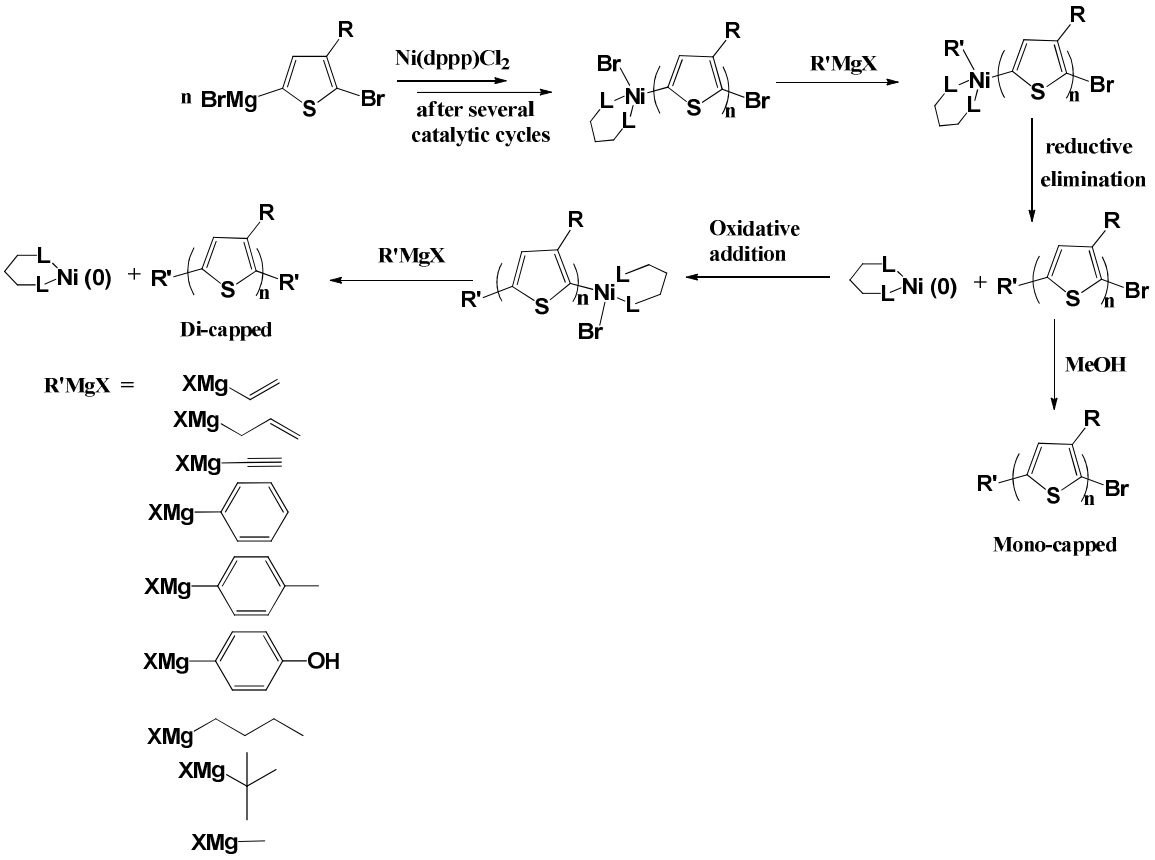

Scheme 20. Proposed mechanism of end-capping of P3HT.

So similar to the PPV based rod-coil diblock copolymer systems convergent approach has been pursued to synthesize the P3HT based rod-coil diblock copolymer

where the coil block synthesized using living radical polymerization method is coupled to the end-functionalized rod block. As discussed earlier the rod block is synthesized by GRIM method followed by in situ end group functionalization with ethynyl group. The azide functionalized flexible block was then joined separately to the alkyne functionalized three different molecular size P3HT rod blocks through click chemistry.

As the hybridization-polymerization (hybridization first) approach as shown in Scheme 4 is restricted by the unsuccessful ATRP of the hybrid monomer, rod-coil diblock copolymer hybrid was realized by polymerization-hybridization (polymerization first) approach. This route involves the synthesis of precursor diblock copolymers with functional amine pendants on coil block followed by the covalent linkage of POM cluster. Though this approach has better control over the degree of polymerization of each block but the number of cluster attachment is limited by the steric bulk of these inorganic charged species. In order to realize these compounds as active photoactive materials in photovoltaics, solar cell devices had been prepared to study the efficiency of these organic-inorganic hybrid materials.

5.3. Results and Discussion

5.3.1. Synthesis of Rod-coil Block

In this approach a rod-coil DCP with pendant free aryl amine was synthesized first, followed by cluster attachment to yield the hybrid DCP. To prepare the rod-coil DCP, the azide terminated coil block and the ethynyl functionalized rod P3HT block was

developed. Then the two blocks were joined together through click chemistry. The coil block remained same as synthesized via ATRP of monomer 6 according to Scheme 6 followed by the modification of the end-functionality to azide group as illustrated in Scheme 14. The synthetic route of three different molecular size P3HT rod block is shown in Scheme 21.

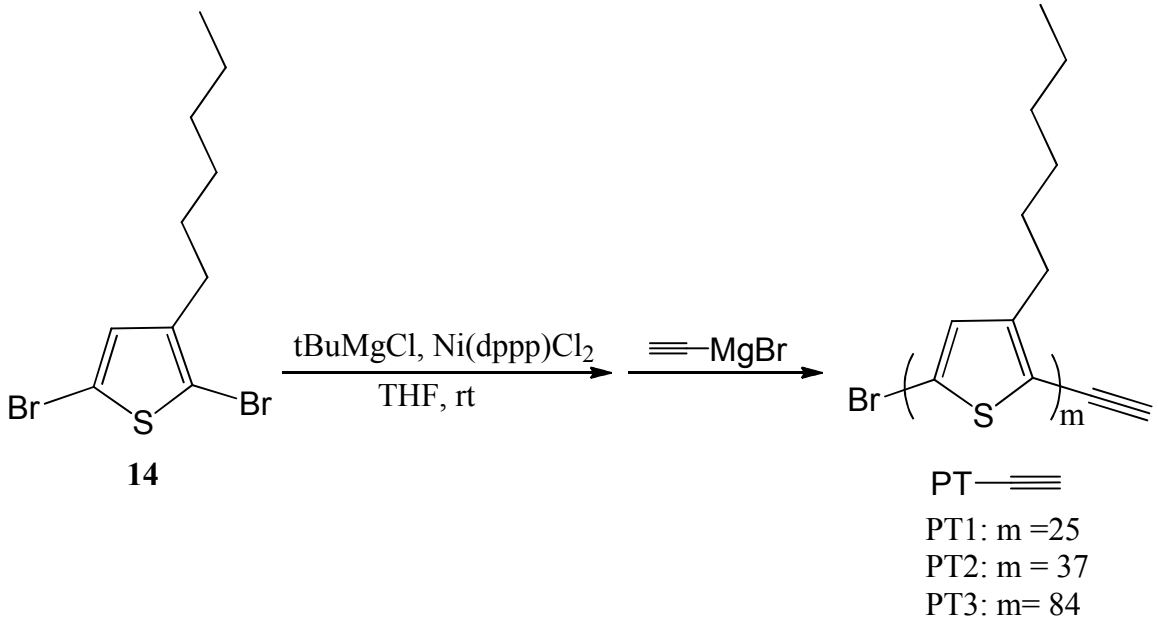

Scheme 21. Synthesis of three ethynyl terminated PT block

Commercially available 3-hexylthiophene is brominated with N-bromosuccinimide (NBS) according to a literature procedure [154a] to yield the dibromo-3-

hexylthiophene monomer 14. Then the monomer is polymerized via Grignard metathesis polymerization (GRIM) to obtain regioregular poly (3- hexylthiophene) (P3HT) with reasonably narrow molecular weight. Initially tert-butylmagnesium chloride was added to produce the 2-bromo-5-magnesiobromo-3-hexylthiophene intermediate and then polymerization initiated with the addition of nickel catalyst to form the living chain. While the polymer was still in solution a second Grignard reagent namely ethynylmagnesium bromide was introduced to cap the polymer and produce regioregular P3HT with ethynyl end functionalized polymer. As explained earlier mono-capped polymer was the product. Three different ethynyl end-functionalized P3HT were synthesized by varying the catalyst concentration. The molecular weight is a function of monomer to Ni(dppp)Cl_2. Here the Ni(dppp)Cl_2 acts as an initiator rather than catalyst. As catalyst loading decreased higher molecular weight regioregular P3HT obtained with narrow molecular weight distribution. The three molecular size P3HT polymers are designated as PT1, PT2 and PT3 in order of increasing molecular weight. All the PT polymers were purified by soxhlet extraction starting with methanol (to dissolve unreacted monomers), followed by hexanes (to dissolve oligomers and catalyst) and finally with chloroform. The red chloroform extract was collected and evaporated to get the pure polymers.

The azide terminated flexible coil block (PSN_3) and three ethynyl terminated rigid block (PT-≡) were joined together through click chemistry as shown in Scheme 22.[162] While PSN_3 is soluble in common organic solvents such as, chloroform, dichloromethane, dimethylformamide (DMF), dimethyl sulfoxide (DMSO), acetone,

tetrahydrofuran (THF), and so forth all the PT-≡ blocks are soluble only in chloroform, dichloromethane and THF. The click reaction was thus carried out in THF using CuBr and PMDETA catalyst-ligand combination to get three diblock copolymers: PS-PT1, PS-PT2 and PS-PT3. After completion the reaction mixtures were passed through a neutral alumina column to get rid of copper. The resulting diblock copolymers PS-PTs were found to exhibit similar solubility to that of PT blocks, making the separation of any unreacted PT blocks difficult. To ensure complete reaction of PT block, more than one equivalent of PSN_3 block was used. The unreacted PSN_3 block was easily removed by precipitating the mixture from acetone as PSN_3 is soluble in acetone but PT is not.

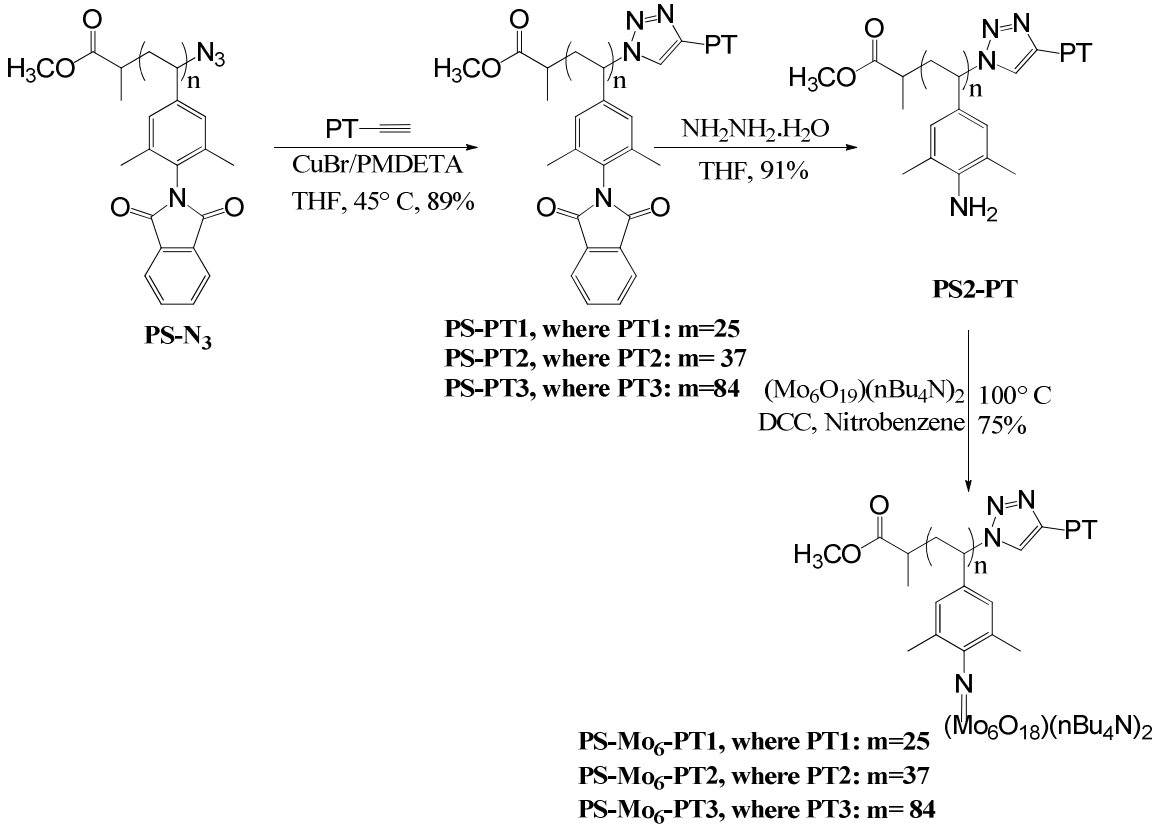

Scheme 22. Synthetic routes for three PS-PT blocks and corresponding hybrid blocks.

The next step was the deprotection of the phathalimide protected amine group which was carried out with hydrazine hydrate according to Ing-Manske procedure to get three different diblocks (PS2-PT) with pendant amine functional groups dangling from each repeating unit. The final cluster attachment was carried out in nitrobenzene solvent with excess hexamolybdate cluster and DCC as shown in Scheme 22. Though the cluster is easily soluble in nitrobenzene, PS2-PT diblocks require some heating to make them dissolve in this solvent. After the completion of the reaction the product along with the

byproduct DCU precipitated out from the solution on cooling while the excess free cluster was still in solution. The precipitated products were then washed in chloroform which solubilized the cluster attached diblocks leaving behind the DCU. The resulting cluster attached DCPs or PS-Mo_6-PT1, PS-Mo_6-PT2 and PS-Mo_6-PT3 are soluble in soluble in chloroform, THF, toluene and insoluble in most other organic solvents.

5.3.2. Structural Characterization

The structures of the synthesized products were confirmed by ^{1}H NMR and ^{13}C NMR ($CDCl_3$, 400 MHz) spectroscopy. The ^{1}H NMR spectrum ($CDCl_3$, 400 MHz) of all the three rod blocks (PT-≡) are depicted in Figure 64. All the peaks of the polymers were assigned unambiguously. After GRIM polymerization and subsequent end functionalization one small but sharp peak around 3.5 (2) ppm appeared for all three polymers which can be assigned to the terminal alkyne protons. Sharp aromatic proton signal around 6.9 (1) ppm is also clearly visible. Along with other hexyl side chain signals, one peak around 2.8 (3) ppm corresponding to the end methyl group of hexyl chain and another at 0.9 (4) ppm are prominent. It should be noted that one sharp aromatic peak around 6.9 ppm and one sharp α-methylene proton peak of side hexyl chain around 2.8 ppm clearly indicates that degree of regioregularity is almost 98 % as majority of the linkage is of H-T type. Formation of very little amount of regiorandom polymer can’t be avoided.

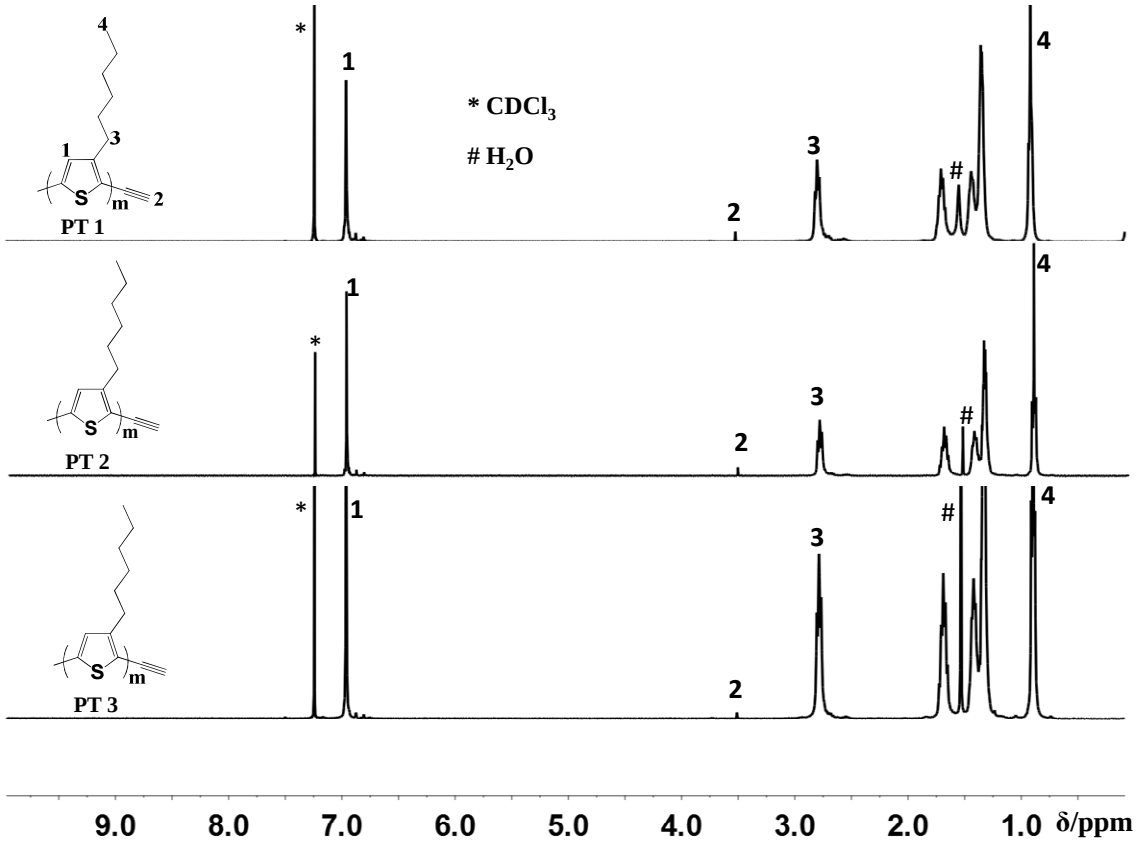

Figure 64. ^{1}H NMR spectrum ($CDCl_3$, 400 MHz) of PT1 (top), PT2 (middle) and PT3 (bottom)

The higher degree of regioregularity of the three rod PT blocks is also confirmed by the ^{13}C NMR spectrum ($CDCl_3$, 400 MHz) as shown in Figure 65. The four sharp aromatic peaks at 139.9 ppm, 133.7 ppm, 130.4 ppm and 128.4 ppm denote the HT-HT

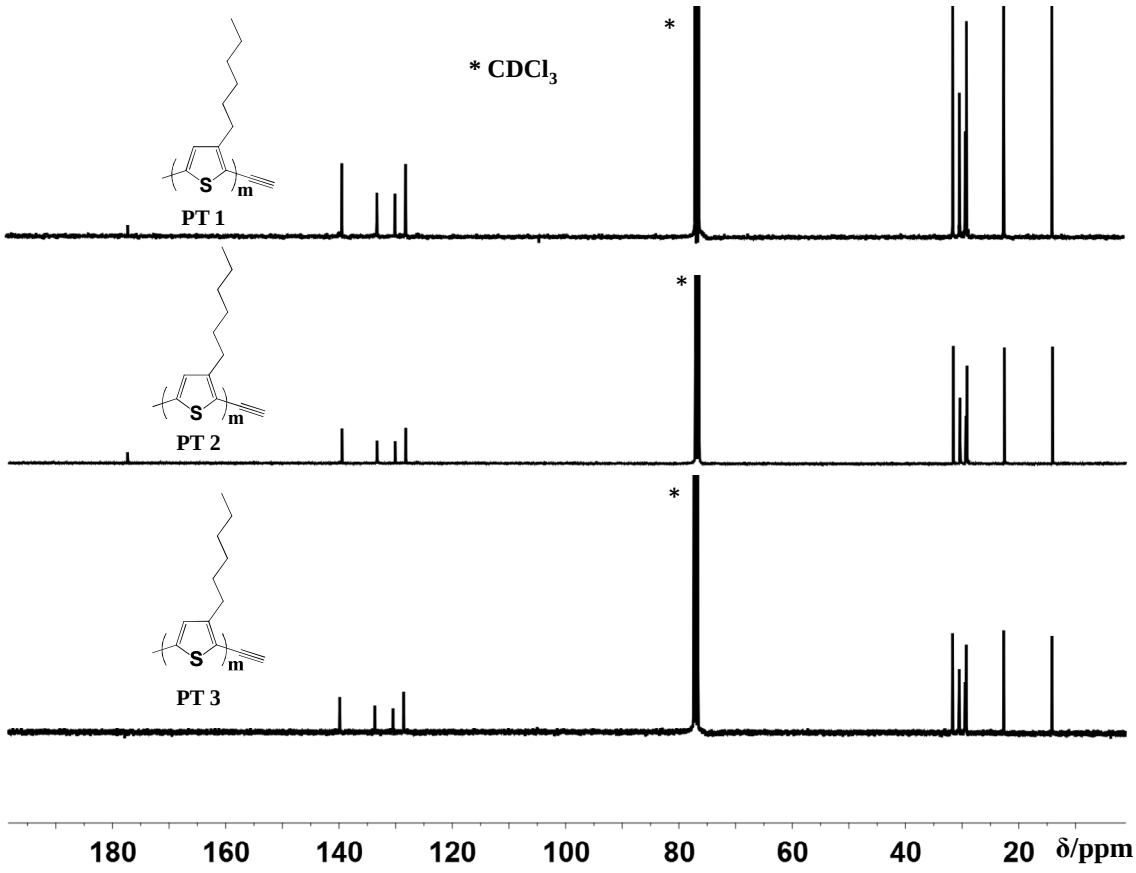

Figure 65. ^{13}C NMR spectrum ($CDCl_3$, 400 MHz) of PT1 (top), PT2 (middle) and PT3 (bottom)

coupling of the polythiophene backbone. These peak assignments are consistent with the literature assignments of HT regioregular P3HT.[150a] After diblock copolymer formation

through click chemistry the ^{1}H NMR spectrum ($CDCl_3$, 400 MHz) of all three PS-PT blocks (PS-PT1, PS-PT2 and PS-PT3) are exhibited in Figure 66. It is evident from the spectra that the click reaction occurred as the terminal alkyne at 3.5 ppm is completely missing. The broad proton peaks a, b and f are the signals related to the PSN_3 coil block as described earlier.

The ^{1}H NMR spectrum ($CDCl_3$, 400 MHz) of the three individual deprotected diblocks and their corresponding cluster attached hybrid polymers starting from the lowest molecular size diblocks to highest molecular size ones are shown in Figure 67, 68 and 69, respectively. The diblock copolymers are also shown for comparison. The complete removal of the phthalimide protecting group in all three diblocks are confirmed by the ^{1}H NMR spectrum of the resulting polymer where proton signal 'a' is completely missing (shown in Figure 67, 68, 69). While the small signal 'b' of the PS block is still discernible in lowest and medium molecular size deprotected diblocks in Figure 67 and 68, respectively, it is difficult to trace the signal in the highest molecular weight deprotected diblock as seen in Figure 69. After deprotection the signal 'b' appears to be shifted upfield. On the contrary, the proton signals corresponding to the PT blocks are very clear in all the deprotected diblock copolymers.

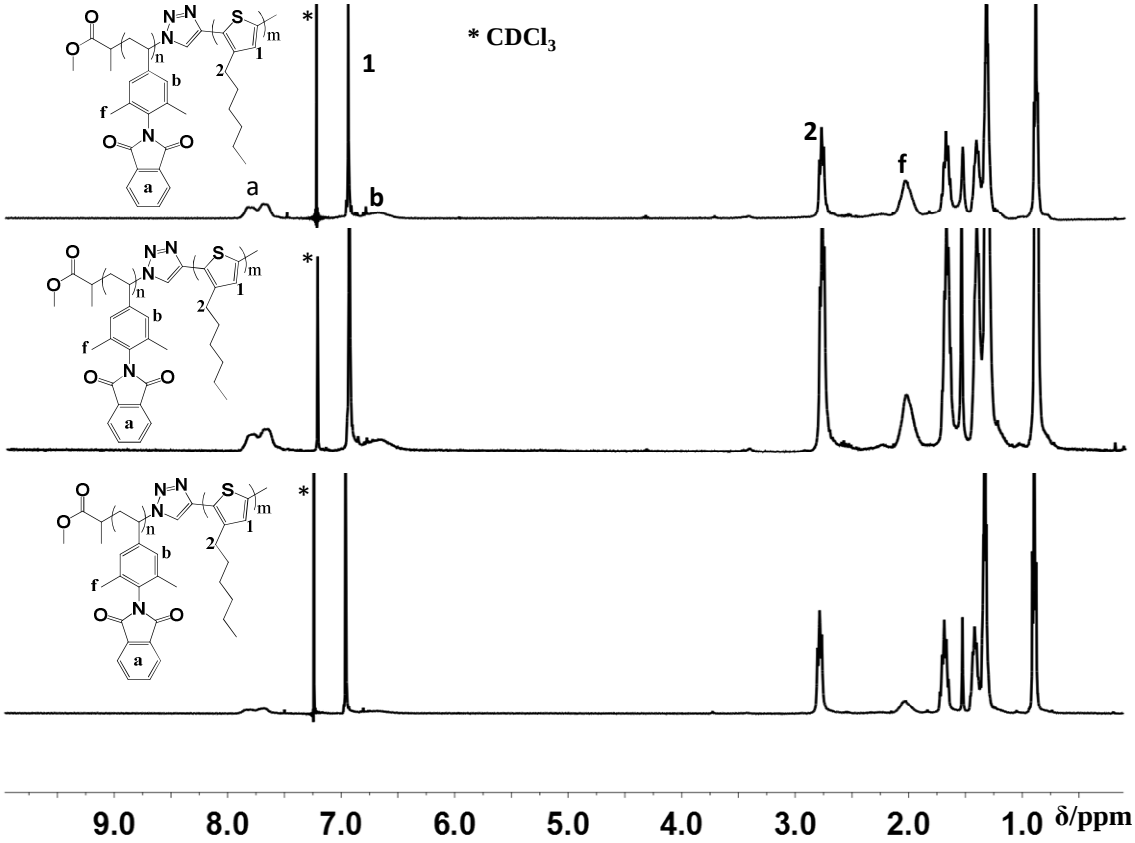

Figure 66. ^{1}H NMR spectrum ($CDCl_3$, 400 MHz) of diblock copolymer PS-PT1 (top), PS-PT2 (middle) and PS-PT3 (bottom).

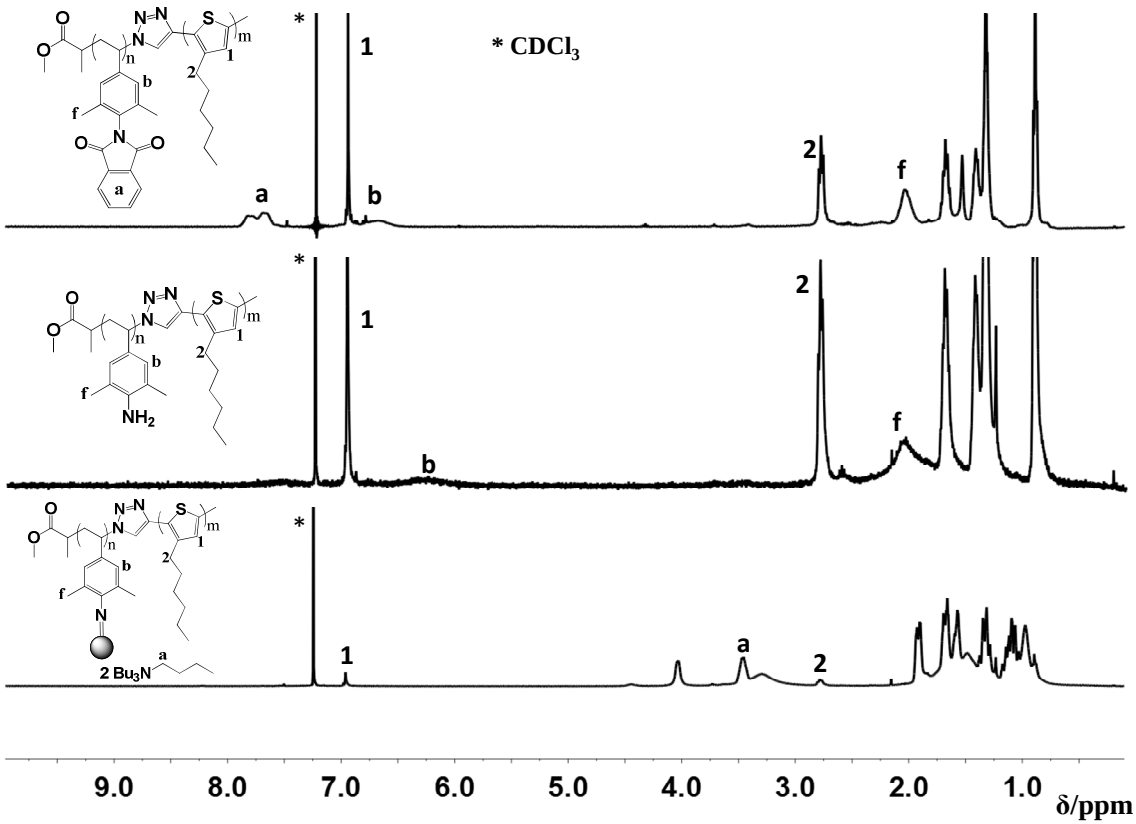

Figure 67. ^{1}H NMR spectrum ($CDCl_3$, 400 MHz) of diblock copolymer PS-PT1 (top), deprotected diblock PS2-PT (middle) and hybrid PS-Mo_6-PT1 (bottom).

After cluster attachment the proton signals from the PS block has almost disappeared. Short PS chain segments may be responsible for this unusually low intensity proton signals. The small but prominent PT proton signals are clearly visible. New signals corresponding to the tetrabutylammonium counterion, e.g. at 3.42 ppm, appeared in the ^{1}H NMR spectrum of the cluster-attached DCP. The cluster counterion proton signals and the hexyl chain proton signals of the PT blocks overlap in between the 1.0-2.0

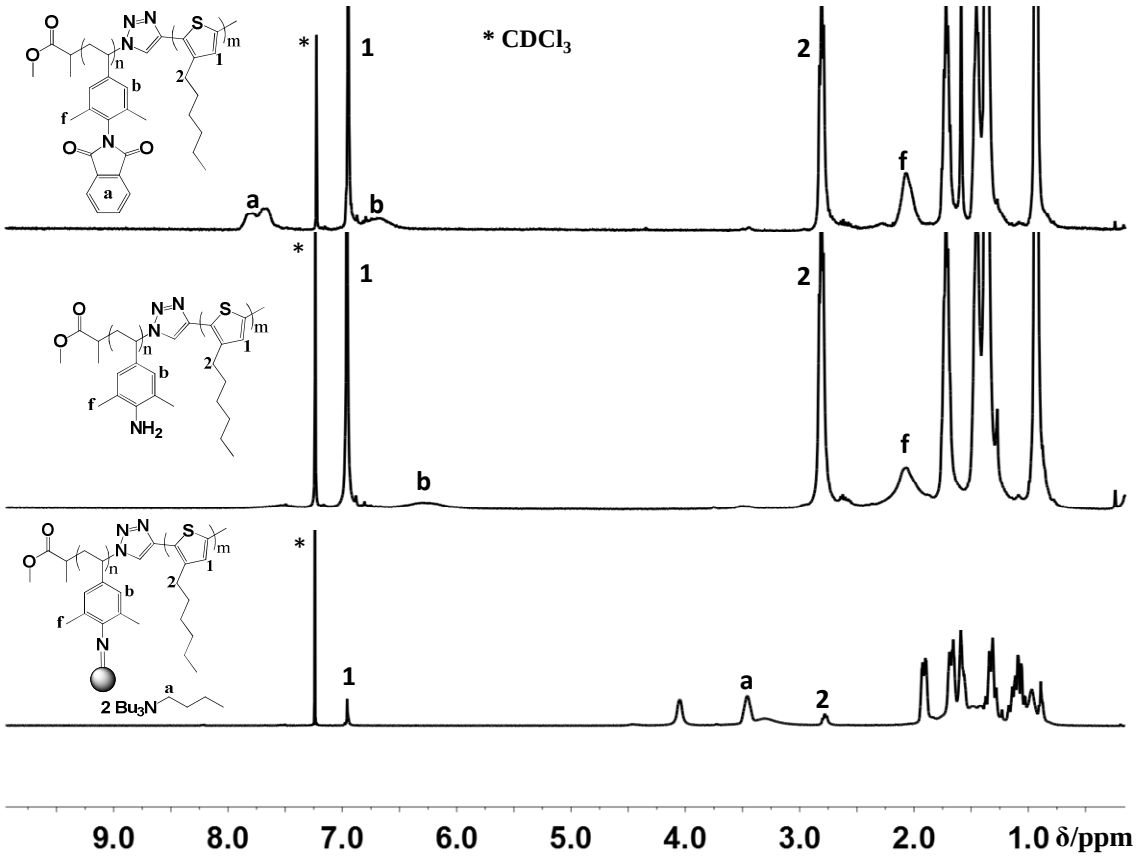

Figure 68. ^{1}H NMR spectrum ($CDCl_3$, 400 MHz) of diblock copolymer PS-PT2 (top), deprotected diblock PS2-PT (middle) and hybrid PS-Mo_6-PT2 (bottom).

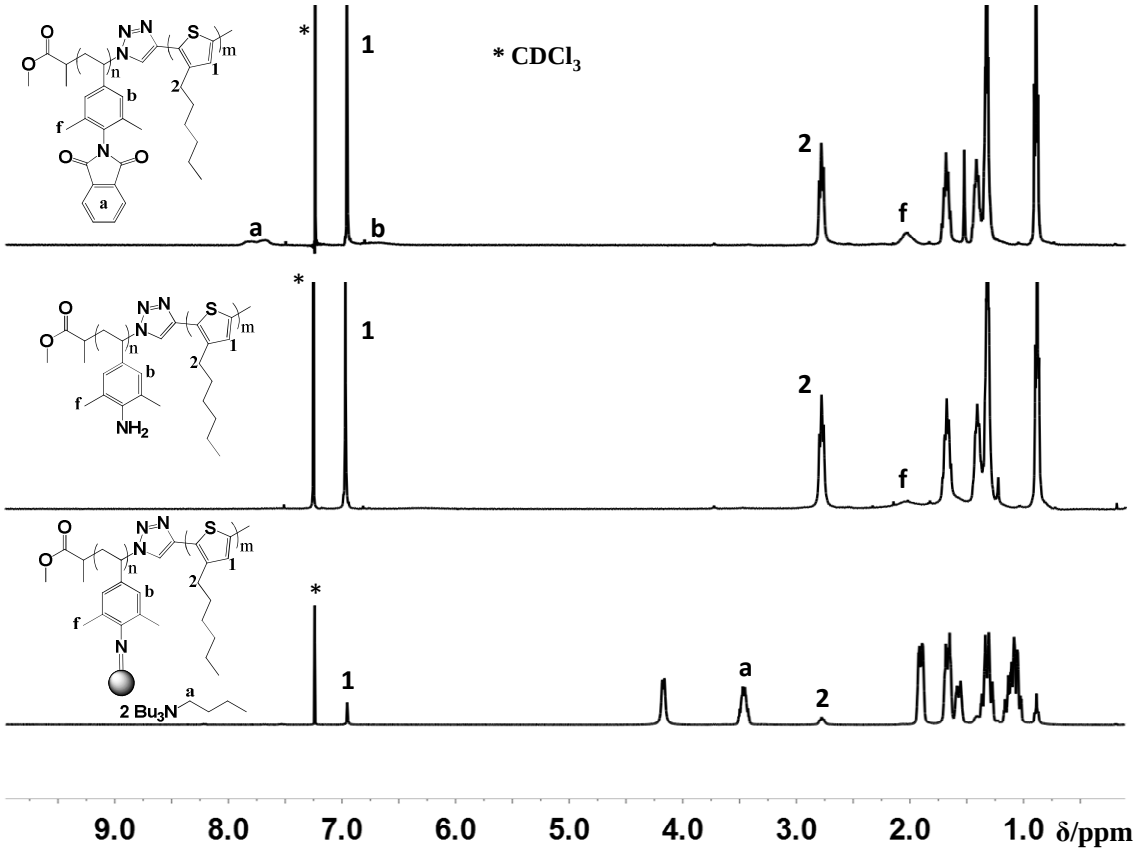

Figure 69. ^{1}H NMR spectrum ($CDCl_3$, 400 MHz) of diblock copolymer PS-PT3 (top), deprotected diblock PS2-PT (middle) and hybrid PS-Mo_6-PT3 (bottom).

ppm region. The well-resolved broad signal at 3.42 ppm can be assigned to the -NCH_2- protons of the tetrabutylammonium counterion.

5.3.3. Molecular Weight Determination

The three different molecular size PT blocks and the formation of their corresponding diblock copolymers are confirmed by the gel-permeation chromatography or GPC. All measurements were run at 30 °C using THF as the eluent. The shift of the GPC traces for the three different PT blocks towards shorter elution time assured the incerement in the molecular weight. The GPC curves are shown in Figure 70. The number average molecular weights (M_n) and polydispersity (PD) of the PT blocks are as follows: PT1 (M_n = 6634, PD = 1.1), PT2 (M_n= 8810, PD =1.2) and PT3 (M_n = 16150, PD =1.2). The relatively narrow molecular weight distribution indicates the living nature of the polymerization. The molecular weight determination of P3HT's by GPC using polystyrene standards is erroneous. GPC is based on correlating the hydrodynamic volume of the randomly coiled polymer chains with polymer molecular weight. Conjugated systems adopt a rodlike conformation in solution, so GPC tends to overestimate the molecular weight and it can be off by a factor of 1.5-2.0.[163] It can be noted that each PT blocks have a small shoulder peak of higher molecular weight which would be formed after quenching with methanol, not during polymerization as explained in the literature.[164] Formation of these small amount of higher molecular weight polymer during quenching is best accounted for by disproportionation of the P3HT-Ni(II)-Br complex, followed by reductive elimination of P3HT-P3HT.This may be due to the change of a ligand of the P3HT-Ni(II)-Br complex after addition of methanol as shown in Scheme 23. The GPC traces of the individual diblock copolymers DCP's along with their PS-N_3 and PT blocks are shown in Figure 71. No uncoupled PPV block or PS block can

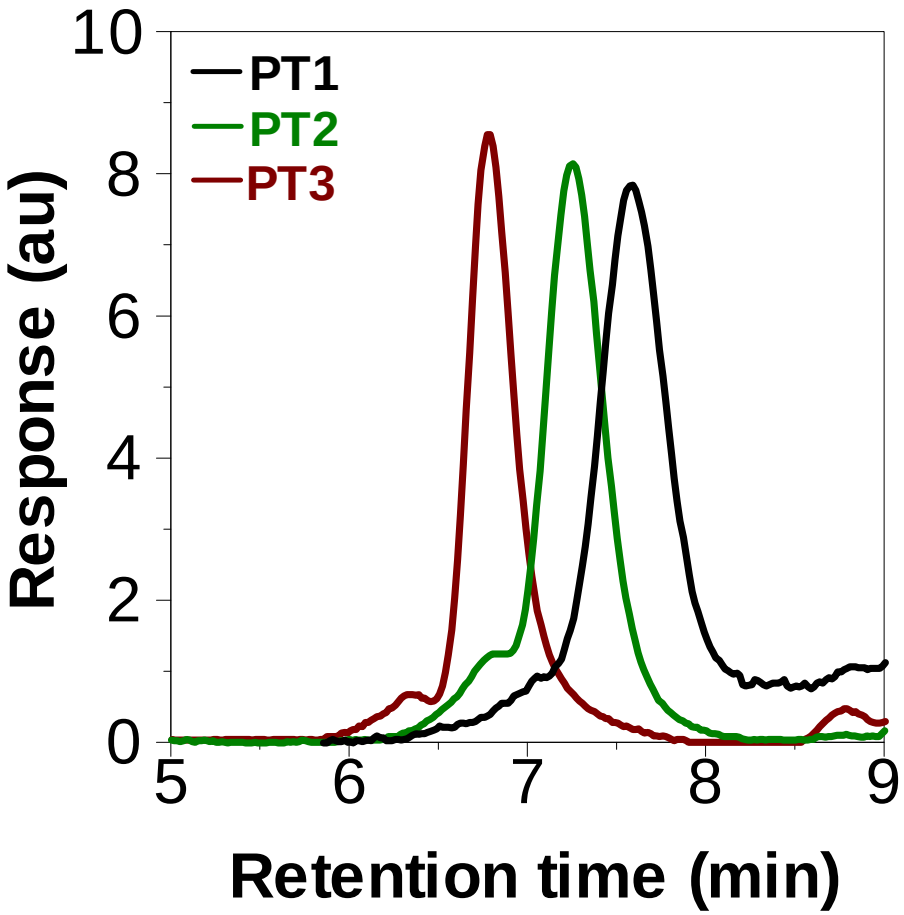

Figure 70. GPC traces of the PT1 (black), PT2 (green) and PT3 (brown) block from RI detector using THF as eluent.

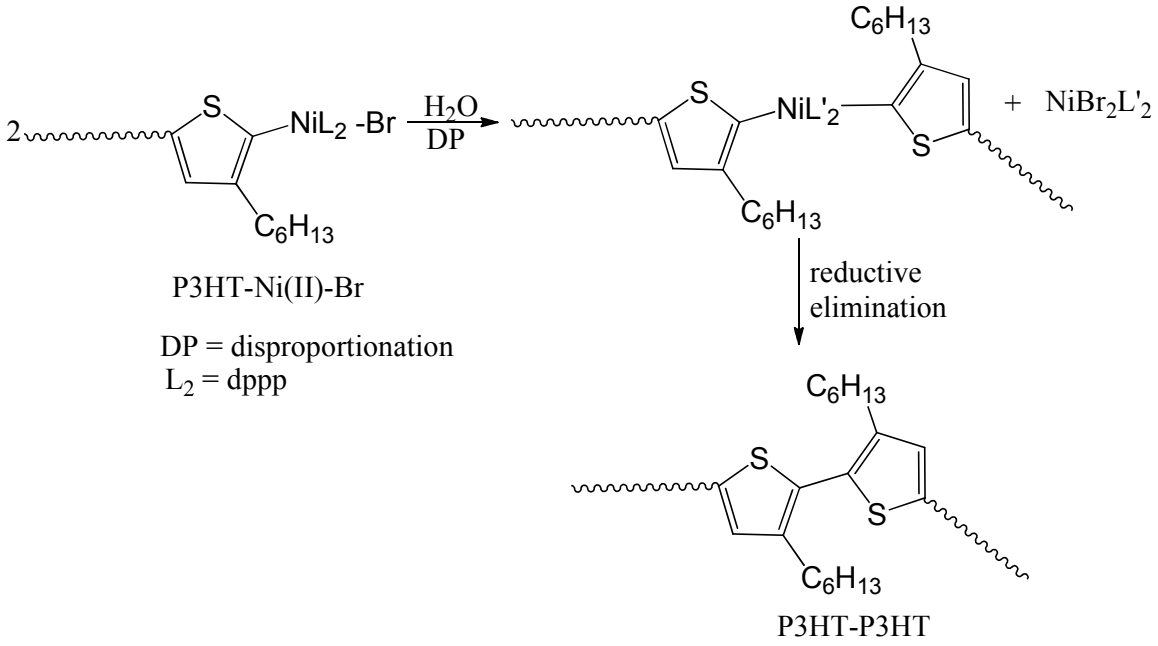

Scheme 23. Synthetic pathway for the formation of higher molecular weight shoulder peak in GPC trace of P3HT.

be seen in the DCP's GPC trace, indicating a complete coupling reaction. Such a result also confirms that all the PS coil blocks prepared from the ATRP process possess the active Br end group. The number average molecular weights (M_n) and polydispersity (PD) of the PSPT DCP blocks are as follows: PSPT1 (M_n = 8396, PD = 1.3), PSPT2 (M_n= 10550, PD =1.3) and PSPT3 (M_n = 18798, PD =1.3). Unfortunately the hybrid diblock copolymer didn't show any GPC traces using the RI detector. But when the light scattering (LS) detector was used for the free cluster, PSN_3 coil block, PT rod blocks, PS-PT DCPs and hybrid DCPs as shown in Figure 72, the hybrid DCPs eluted out of the column very fast due to their unique hydrodynamic volume. The sharp peaks of the

hybrid DCPs' (blue) are well separated from the rest of the polymer peaks which also confirmed the formation of covalent linkage between cluster and the DCPs. It is evident from the GPC curves of the hybrid diblock that there is no unreacted DCP and free cluster left in the system indicating complete reaction and complete removal of free clusters.

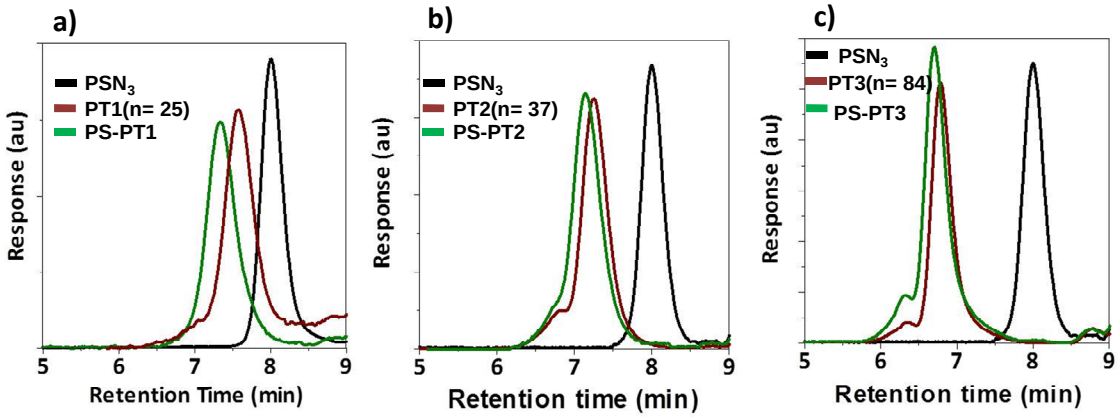

Figure 71. GPC traces of the DCPs, PTs and PSN_3s from RI detector using THF as eluent. a) PSN_3 block (black), PT1 block (red), PSPT1 (green); b) PSN3 block (black), PT2 block (red), PSPT2 (green); c) PSN_3 block (black), PT3 block (red), PSPT3 (green).

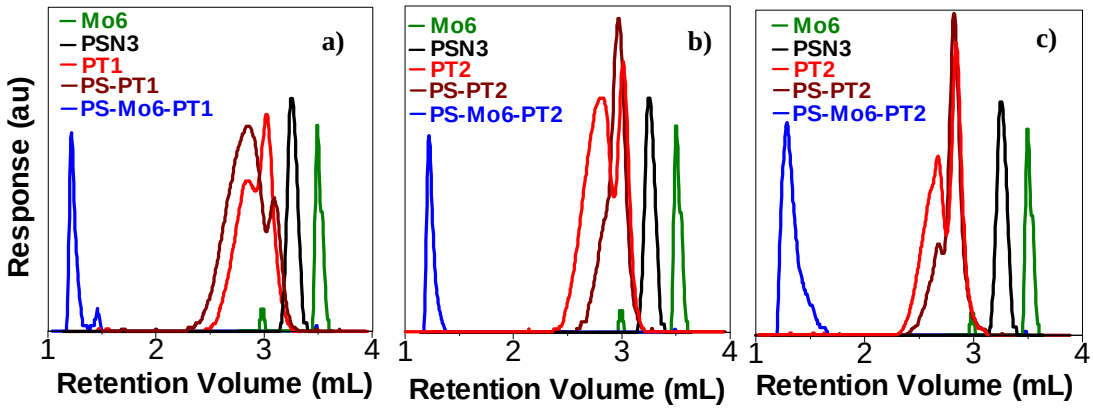

Figure 72. GPC traces of free cluster (green), PSN3 (black), PT blocks, PS-PT DCPs'and hybrid DCPs'from LS detector using THF as eluent. a) PT1 block (red), PS-PT1 (brown), PS-Mo6-PT1 (blue); b) PT2 block (red), PS-PT2 (brown), PS-Mo6-PT2 (blue); c) PT3 block (red), PS-PT3 (brown), PS-Mo6-PT3 (blue);

Matrix-assisted laser desorption/ionization-Time-of-Flight (MALDI-TOF) mass spectrometry (MS) measurements were also carried as illustrated in Figure 73 to yield information on their absolute molecular weights and molecular weight distributions. Sample preparation was somewhat critical in obtaining these spectras. Though dithranol was used for both PT1 and PT2 blocks, a different matrix namely terthiophene was used to get the mass spectra of PT3 block. A solution of terthiophene (75mg/mL) in THF and a solution of polymer (5mg/mL) in THF are mixed in 10:1 ratio and spotted on the sample well. All three PT polymers depict a regularly distributed set of peaks with mass difference of one repeating unit (166.30). The M_n of three PT blocks is calculated to be as follows: PT1 (M_n = 4230.04, which correspond to an average degree of polymerization (DP) of 25), PT2 (M_n =6243.97, which correspond to an average degree of polymerization (DP) of 37) and PT3 (M_n = 14018.99, which correspond to an average

degree of polymerization (DP) of 84). All of them show narrow molecular weight distributions with PD of 1.04, 1.05 and 1.01, respectively, confirming the living nature of the polymerization.

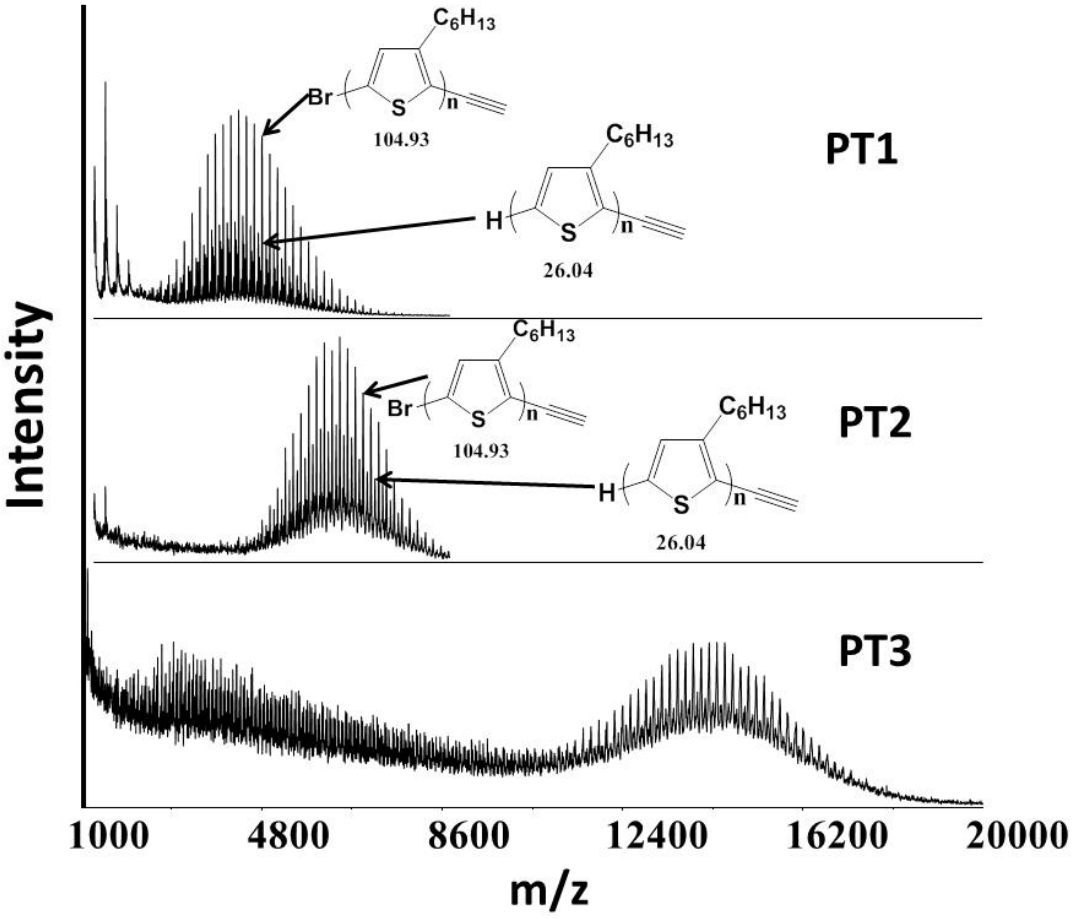

Figure 73. MALDI-TOF spectra of the three PT blocks: PT1 (top), PT2 (middle) and PT3 (bottom).

MALDI is a very powerful technique for end-group analysis and structure confirmation for PT systems. For PT1 and PT2 in Figure 73 it is evident that there exist two significant types of signal peaks per repeat unit. The difference between each type of end group is found to be 166 Da. Masses of each peak can be accurately expressed by (166n + 79.9 + 25) and (166n + 1 + 25) where n is equal to the number of repeating units. So it can be concluded that the polymer samples has two major end group configurations. The peak corresponds to (166n + 79.9 + 25) is the polymer chain terminated by bromine atom at one end and alkyne functionality on the other end. The peak corresponding to the (166n +1+ 25) refers to the polymer chain capped with a hydrogen atom at one end and the alkyne functional group on the other end. For PT3 polymer, end groups are not very clear from the spectra. Though the individual PT blocks revealed nice MALDI spectra, the spectra of PS-PT DCPs' were unavailable as it was difficult to get them fly in the ionization conditions. Similar to the PS-PPV systems, spectra of the cluster attached DCP revealed no peaks whether using a positive or negative detection mode. The lack of high mass/charge signals may be due to the difficulty in vaporizing cluster-attached DCPs under the MALDI conditions or due to the simple fact that the hybrid DCP is highly charged (as each attached cluster carried a -2 charge).

5.3.4. FT-IR Characterization

All the polymers are also characterized by the IR spectroscopy. The FT-IR spectra of all three PT rod blocks are summarized in Figure 74. Two characteristic peaks are evident from the spectra. A broad peak around 2950-2850 cm^{-1} corresponds to the aliphatic C-H stretching while a small sharp peak at 3350 cm^{-1} corresponding to the alkyne C-H stretch confirms the end functionality. After click reaction of these PT blocks with the azide end functionalized PS blocks the alkyne C-H stretching peak disappeared which are illustrated in Figures 75, 76 and 77 for all three diblock copolymers. The PS-PT DCPs' show a sharp and intense peak at 1720 cm^{-1} which can be assigned to the carbonyl stretching of the phthalimide protecting group of the PS block. This peak is significantly weakened after deprotection. For comparison IR spectra of Mo_6 cluster is also shown. Two new peaks at 798 and 953 cm^{-1}, which are characteristic Mo-O stretching vibrations, are clearly observed in the IR spectra of the hybrid DCP similar to the spectra of the free cluster. In addition to that a side/shoulder peak next to 953 cm^{-1} at around 975 cm^{-1} is detectable more clearly when expanded. This peak is attributed to the Mo-N stretching vibration.[62b] This clearly indicates that Mo_6 clusters are covalently attached to the coil block.

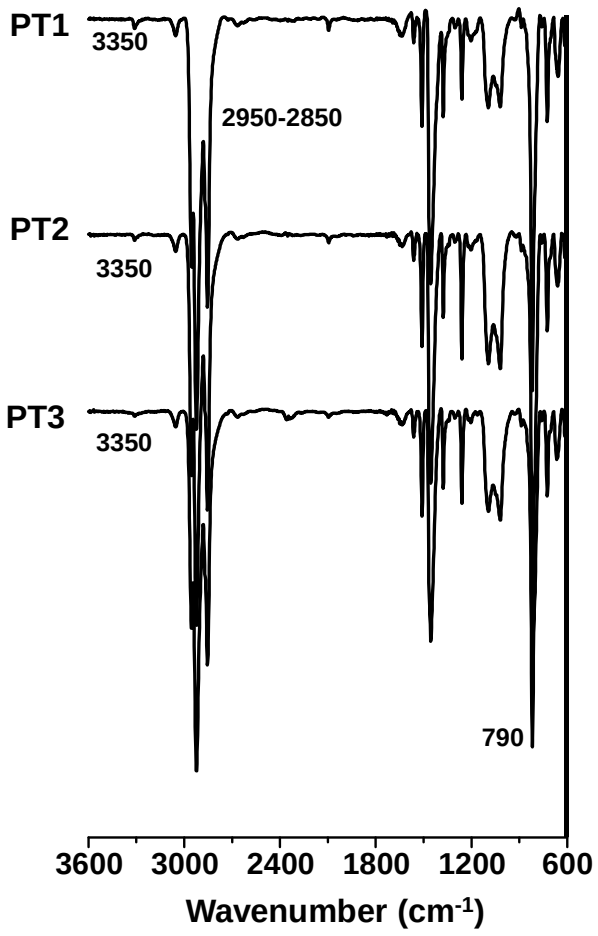

Figure 74. FT- IR spectra of the three PT blocks: PT1(top), PT2 (middle) and PT3 (bottom).

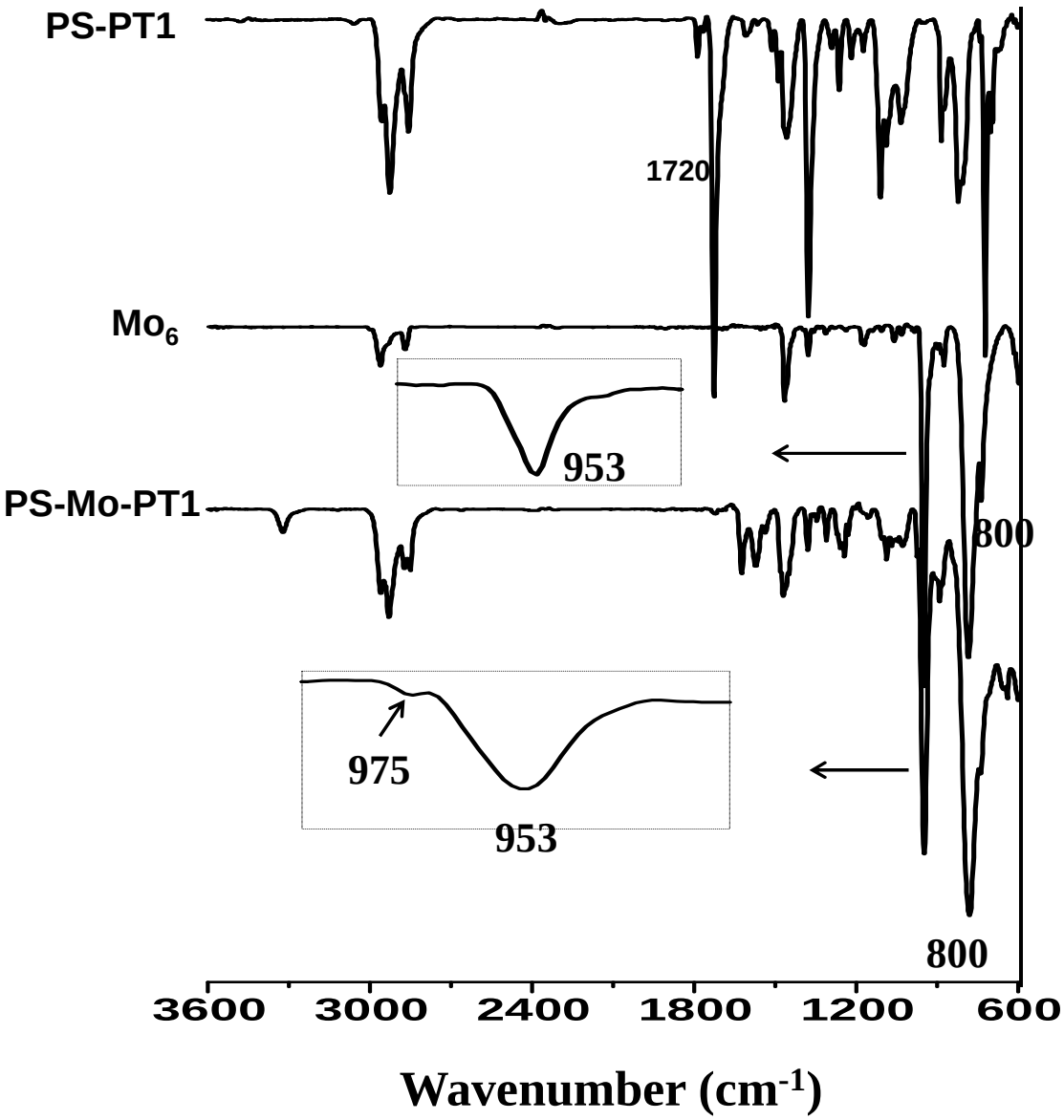

Figure 75. FT-IR spectra of diblock copolymer (PS-PT1) (top), free Mo_6 cluster (middle) and hybrid DCP (bottom).

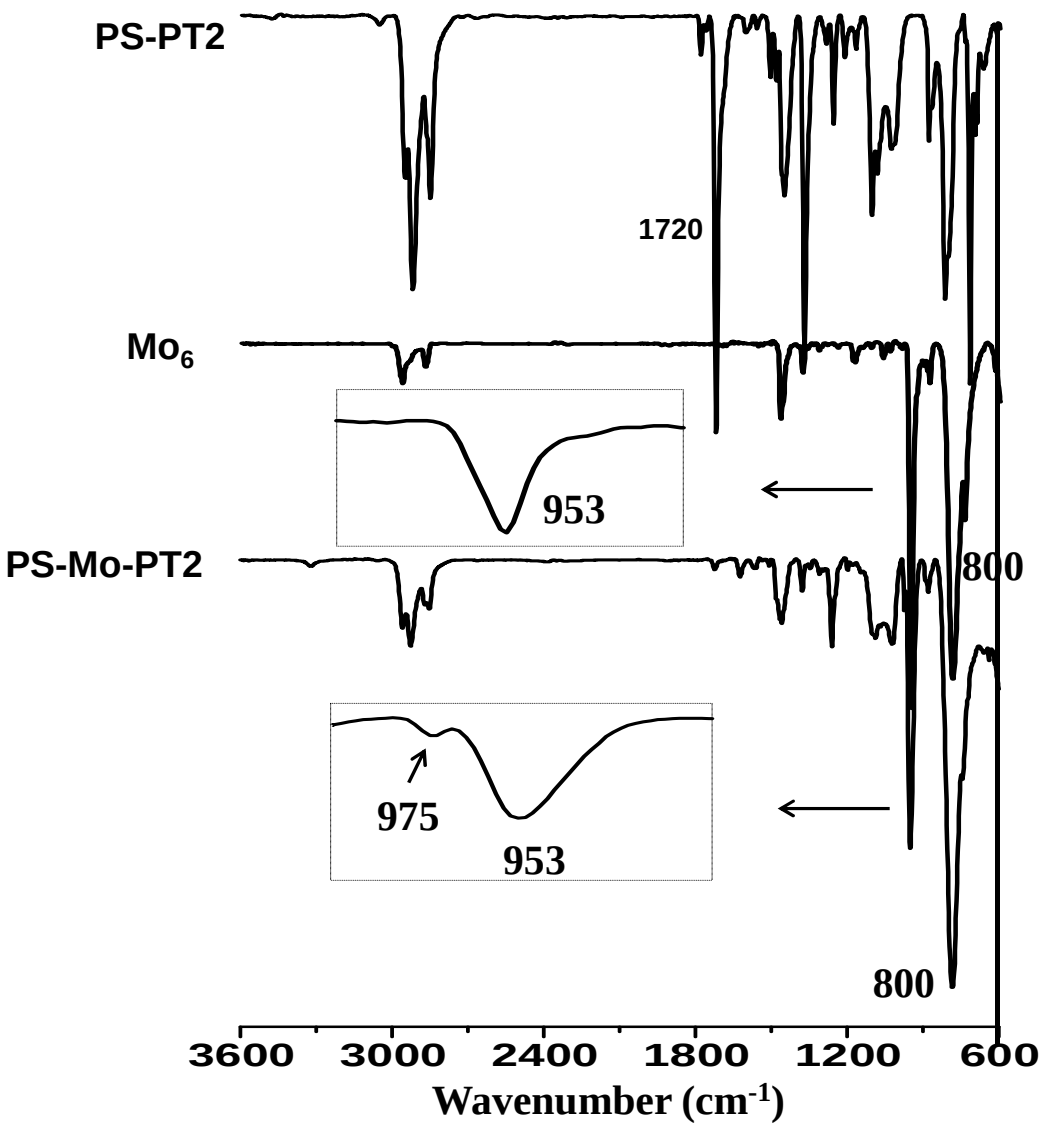

Figure 76. FT-IR spectra of diblock copolymer (PS-PT2) (top), free Mo_6 cluster (middle) and hybrid DCP (bottom).

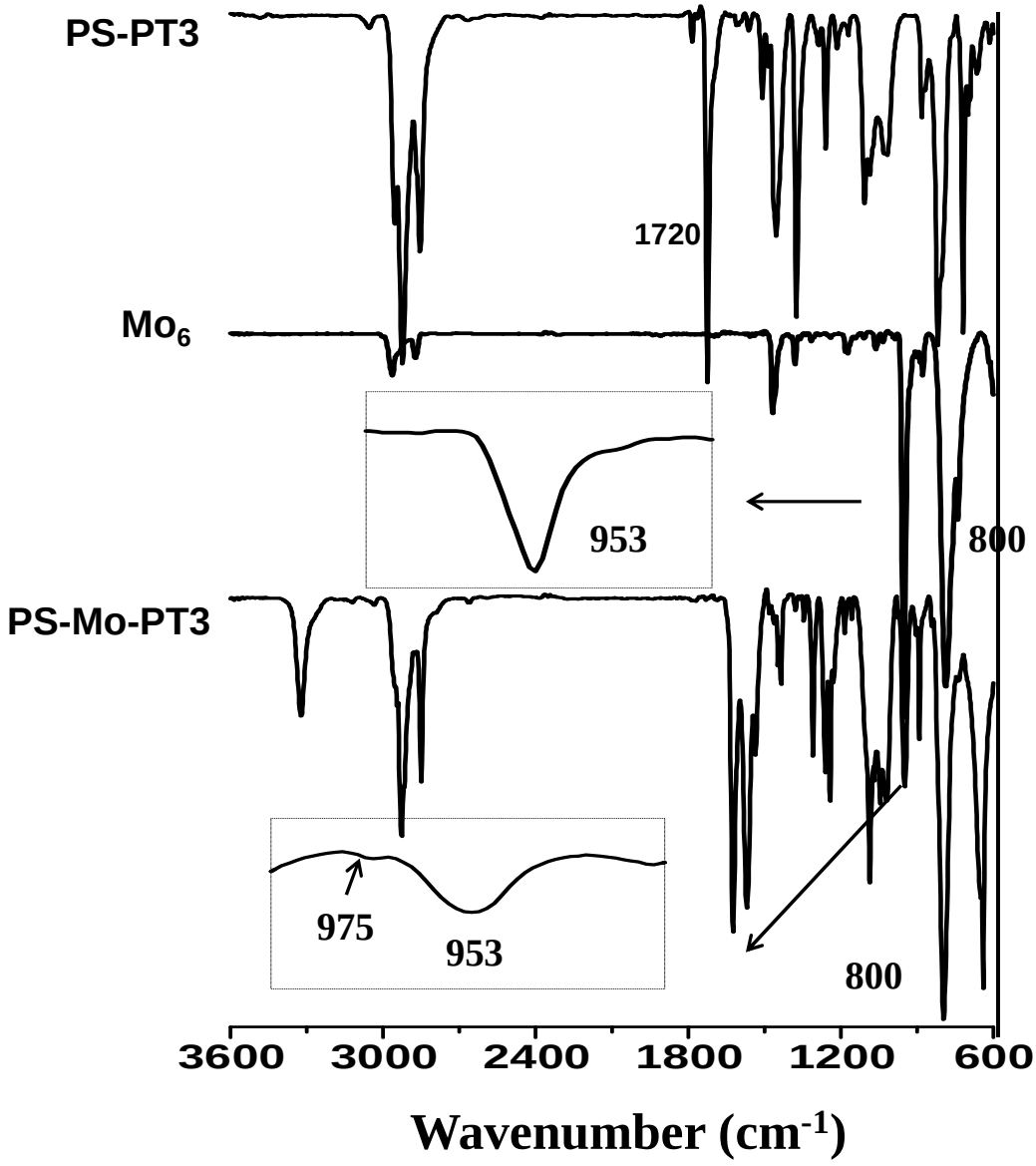

Figure 77. FT-IR spectra of diblock copolymer (PS-PT3) (top), free Mo_6 cluster (middle) and hybrid DCP (bottom).

5.3.5. Thermal Properties

Thermal properties of all the three PT blocks and their corresponding DCPs' and hybrid DCPs' were studied by thermogravimetric analysis (TGA). It is evident that all the three PT blocks, three DCPs' and the cluster are thermally stable upto 300°C while the hybrid DCP started to decompose at a much lower temperature of 200° C as shown in Figure 78 a), b) and c) for the lower molecular weight systems, medium molecular weight systems and higher molecular weight systems, respectively. This early degradation in the hybrid diblocks cannot be accounted for the cluster counterion loss as the cluster itself is stable over 300°C. This can be attributed to the free amine groups in the coil block which left unreacted in the hybridization step. These unreacted amine groups made the hybrids unstable resulting in early degradation. The initial degradation loss is different for the three hybrid diblock copolymers. The PS-Mo-PT1 has the lowest initial loss and the PS-Mo-PT3 has the highest initial loss while the PS-Mo-PT2 hybrid remained in between. This might be due to the amount of free amine groups in the coil block of these hybrids. Though the coil block for all the three hybrids is same, the extent of cluster attachment is different for the three different diblock copolymers. As the PS-Mo-PT3 hybrid has the lowest amount of cluster attachment, the highest amount of unreacted free amine is responsible for the highest initial degradation loss. Similarly as the PS-Mo-PT1 hybrid has the highest amount of cluster attachment, the initial degradation loss is the least. For PS-Mo-PT1 hybrid DCP, weight loss continued until 550° C when no further loss is observed up to 700° C. A residual weight of 42% remains. For the free Mo_6 cluster, a similar no weight loss region from 530 to 700° C is observed, and the residual weight is

64%, which is consistent with its cluster anion content of 64%. But PS-Mo-PT2 and PS-Mo-PT3 hybrid DCPs' continued to lose weight even after 550° C and the residual weight is 32% and 12%, respectively. Not only that, for the three PT blocks and their corresponding PS-PT blocks, though started to degrade after 300° C and continued to lose weight till 700° C, a significant amount of residue still left even after 700° C. So it is thus difficult to assume that at 700° C the thermally decomposed residue of the hybrid DCP is only MoO_3 due to the incomplete degradation of the DCP's at this temperature. Consequently weight percentage of Mo in the hybrid DCP cannot be calculated using the TGA data unlike of the hybrid PS-PPV systems. The molybdenum content obtained from the elemental analysis clearly indicates that cluster attachment is highest in PS-Mo-PT1 hybrid of 33.5% and lowest in PS-Mo-PT3 of 6.3% whereas PS-Mo-PT2 contains around 29.1% of molybdenum. So using the degree of polymerization of the coil block as 18 and assuming complete phthalimide deprotection, the number of attached cluster per PS coil block for PS-Mo-PT1 hybrid of 33.5% Mo content is 6, for PS-Mo-PT2 hybrid of 29.1% Mo content is 5 and for PS-Mo-PT3 hybrid of 6.3% Mo content is 1.

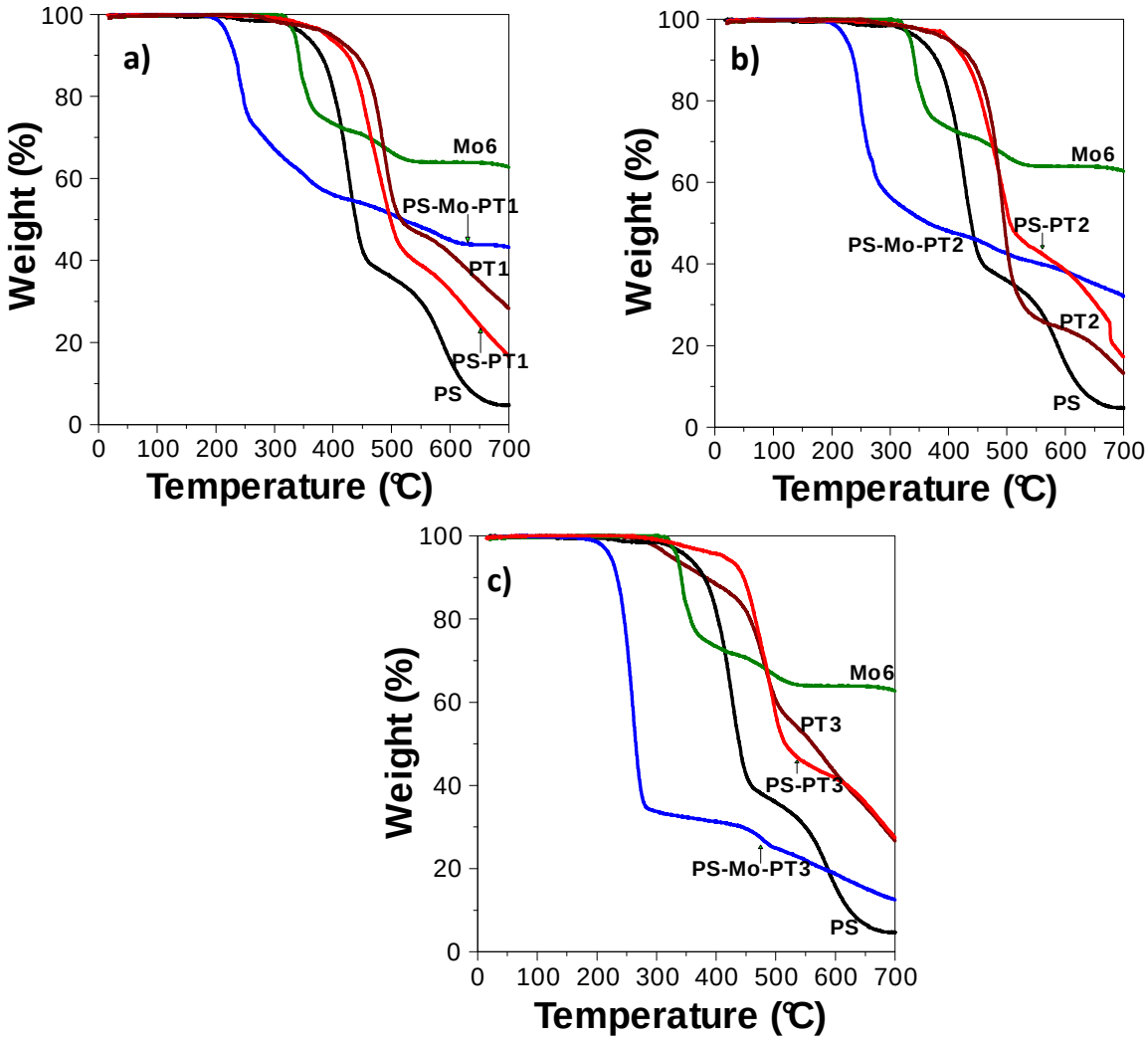

Figure 78. TGA thermograms of coil PS block, PT blocks, PS-PT DCPs', $[Mo_6O_{19}]$. $2NBu_4$ cluster and the hybrid DCP. a) lowest molecular weight systems, b) medium molecular weight systems and c) highest molecular weight systems.

The thermal properties of all the polymers and diblocks were also investigated by differential scanning calorimetry (DSC). The measurements were carried out under nitrogen atmosphere with heating and cooling rates of 10° C/min. All the melting and crystallization temperatures were determined from the second heating and cooling cycles.

First heating and cooling cycles were performed only to eliminate the thermal history. The DSC thermograms for all three PT rod blocks are shown in Figure 79. All the PT samples exhibited one sharp endothermic or melting peak (T_m) and one sharp exothermic or crystallization peak (T_c). The T_m and T_c peaks for all the polymers are given in Table 4. It is interesting to note that with increasing molecular weight the melting point of the polymers increases. Several factors can be responsible for this depression of melting point with molecular weight.[165] These two are related as shown in equation 4,

$$\frac{1}{T_m} - \frac{1}{T^0_m} = \frac{R}{\Delta H^0_m}\frac{2}{n} \qquad \text{eq. 4}$$

T^0_m = melting temperature of perfect crystal, R = gas constant, ΔH^0_m = heat of fusion per mole of crystalline monomer, n = average number of monomers per chain.

It has been shown that the decrease in melting point is not only governed by the decrease of molecular weight but also related to the change in morphology with molecular weight. In addition to that the degree of crystallinity of the three different sizes P3HT chains can also be calculated from the equation 5,

$$\phi_c = \frac{\Delta H_m}{\Delta H^0_m} \qquad \text{eq. 5}$$

ΔH_m = heat of fusion, ΔH^0_m = 99.0 J/g is heat of fusion of ideal perfect crystal.[166]

The heat of fusion or melting enthalpies of PT1 is 19.02 J/g, PT2 is 23.25 J/g and PT3 is 62.30 J/g from which the degree of crystallinity can be calculated to be 19.2%, 23.5% and 63% for PT1, PT2 and PT3, respectively. It can be seen that with the decrease

of molecular weight from PT3 to PT1, the enthalpy of melting along with degree of crystallinity decreases. The glass transition temperatures (T_g) of all the PT blocks are not very clear in the Figure 79 but they can be clearly visible when expanded as shown in Figure 80. The T_g is not a thermodynamic property of a polymer, and thus is dependent of the processing history combined with differences in molecular weight and regioregularity. As a result wide spectrums of T_g values are reported for P3HT in literature, such as 5.8, -14, 24, 12 and -3°C.[167] In the present case, the T_g values are almost same for all three PT blocks at around -7°C to -5° C.

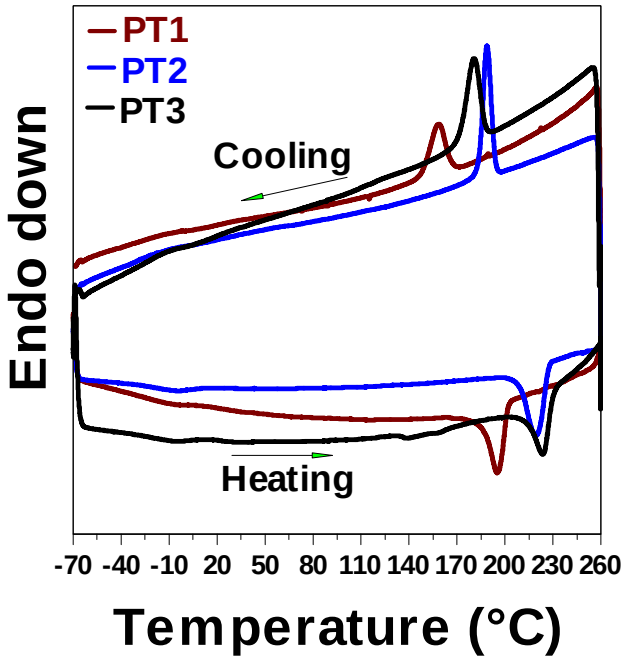

Figure 79. DSC thermograms of three different size PT blocks at a scan rate of 10°C/min.

The DSC thermograms of the three diblock copolymers (PS-PTs) are shown in Figure 81. All the diblocks show a sharp melting endotherm and a crystallization exotherm similar to the PT blocks. The T_m and T_c values are given in Table 4. The melting temperatures decrease with decrease in molecular weight. But it was difficult to observe any significant endo- or exothermic peaks for all three the hybrid PS-Mo-PTs diblock copolymers.

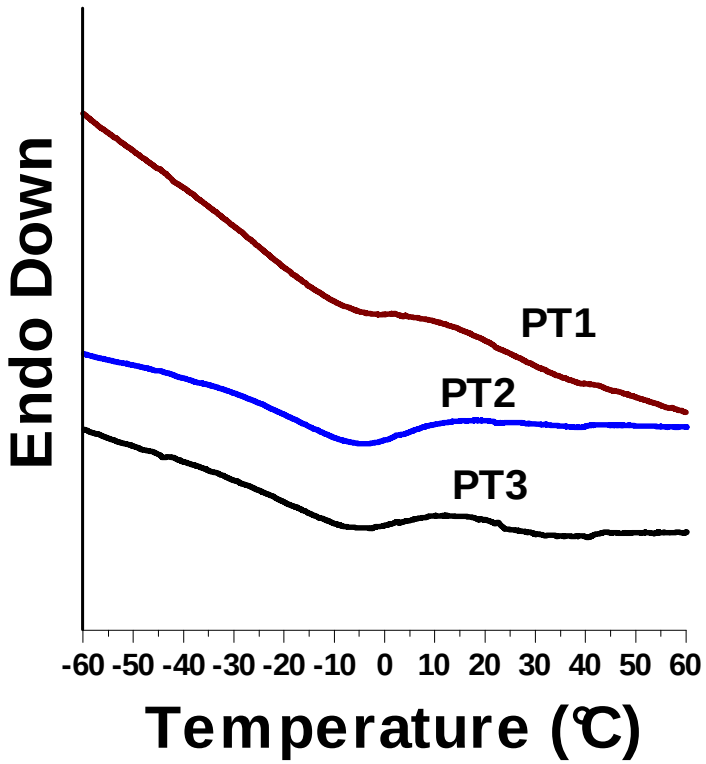

Figure 80. The DSC thermograms showing the T_g of three PT block

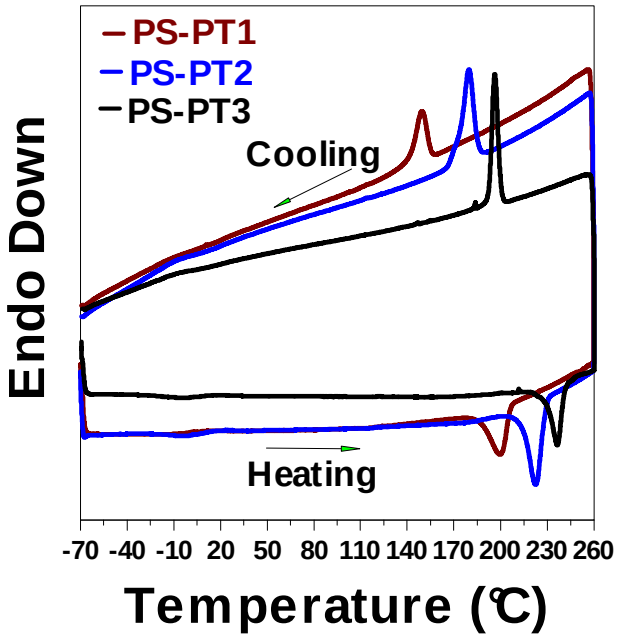

Figure 81. DSC thermograms of three different size PSPT blocks at a scan rate of 10°C/min.

5.3.6. Optical Properties

The UV-Vis absorption spectra of the three different size PT blocks in two different solvents namely, chloroform and toluene are elucidated in Figure 82. The absorption band at 450 nm in both the solvents is due to the π-π* transition of the PT backbone. It is also noted that though there is not much difference between the absorption

Table 4. Melting and crystallization temperatures for PT blocks and diblocks

	T_m°C (onset)	T_c°C (onset)
PT1	188.2	172
PT2	210.0	197
PT3	211.69	195
PS-PT1	191.57	159
PS-PT2	215.04	192
PS-PT3	227.28	205

spectra in toluene from PT1 to PT3. This slight shift can be attributed to the increased conjugation length with increased molecular weight of the PT blocks.

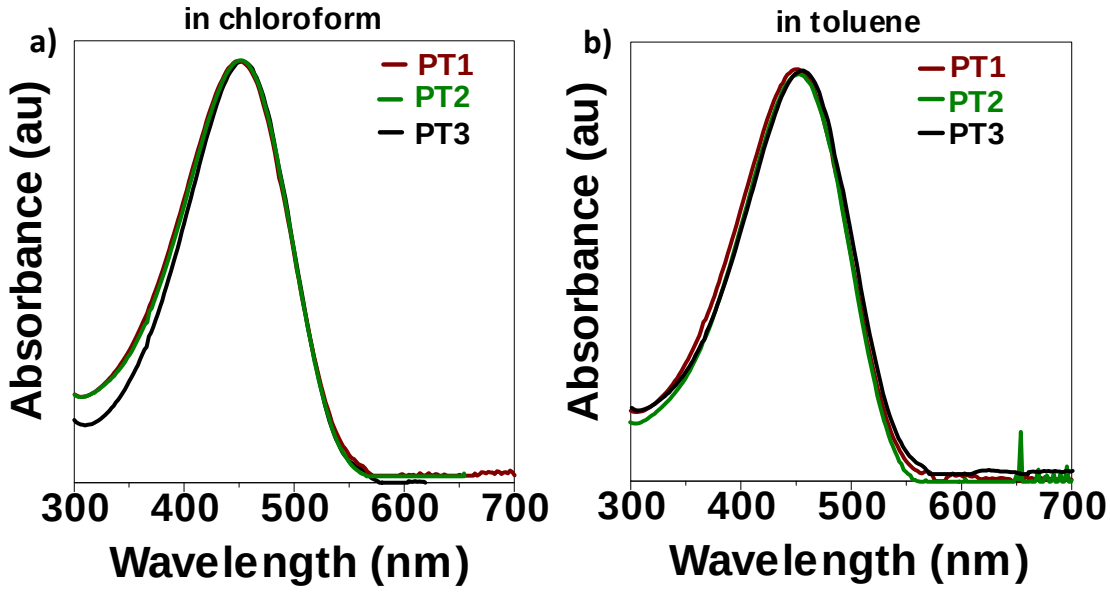

Figure 82. UV-Vis spectra of three different size PT blocks in two different solvents a) chloroform, b) toluene

After diblock copolymer formation the absorption spectra of the three different diblocks (PSPT) matches exactly with their corresponding PT blocks in both chloroform and toluene as shown in Figure 83 for PT1, in Figure 84 for PT2 and in Figure 85 for PT3.

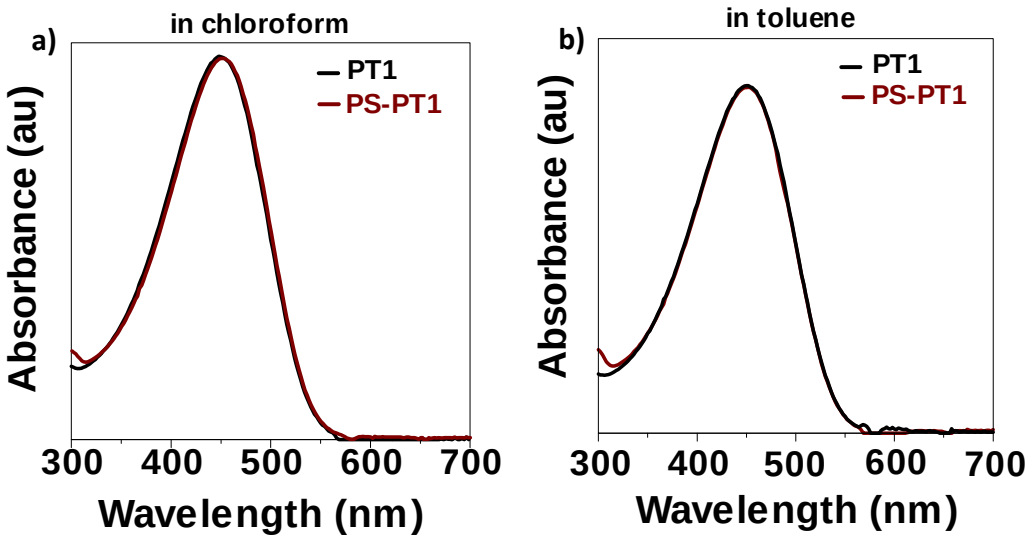

Figure 83. UV-Vis spectra of PT1 block and the corresponding diblock PS-PT1 in a) chloroform and b) toluene solution

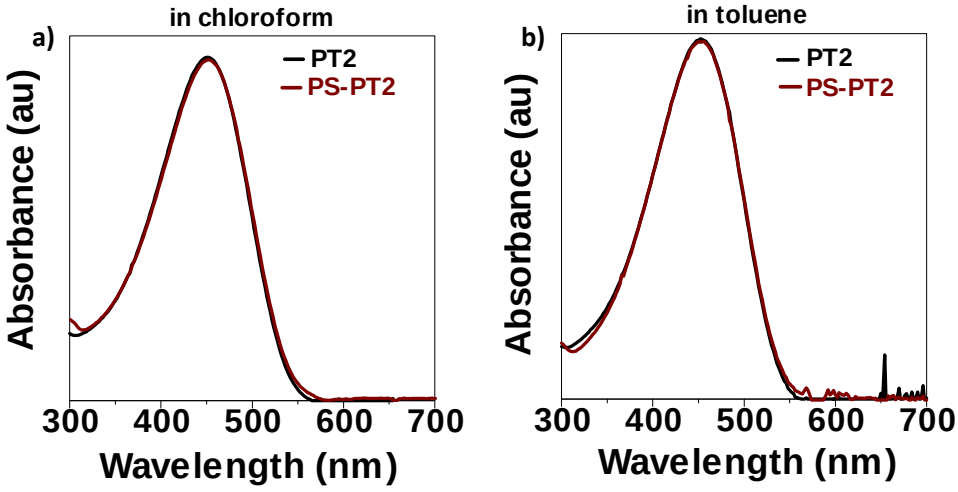

Figure 84. UV-Vis spectra of PT2 block and the corresponding diblock PS-PT2 in a) chloroform and b) toluene solution

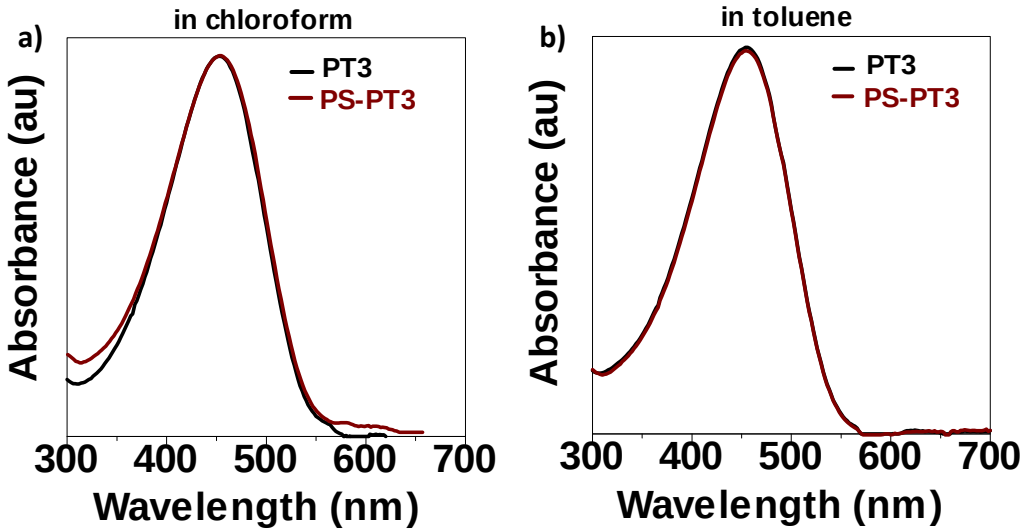

Figure 85. UV-Vis spectra of PT3 block and the corresponding diblock PS-PT3 in a) chloroform and b) toluene solution

After cluster attachment it is evident that a new peak appeared at around 350 nm in both chloroform and toluene solutions as shown in Figures 86-88 which can be assigned to the ligand-to-metal charge-transfer (LMCT) transition of the pendant imido-POM component. This peak indicates clearly the formation of imido-functionalized POM clusters. The LMCT peak is prominent in both Figure 86 for the low molecular weight hybrids and in Figure 87 for medium molecular weight hybrids whereas a little broadening of the hybrid absorption spectra compared to the DCP spectra without any noticeable peak is observed in Figure 88 for the highest molecular weight hybrids. In

addition, a little blue shift of the π-π* transition compared to the diblock is observed only for PS-Mo-PT1 in both chloroform and toluene. It is possible that the bulky cluster group may twist the conjugated system and decrease the effective conjugation length. The effect of this kind of twist by bulky cluster groups has minimized in PS-Mo-PT3 hybrids due to the higher molecular weight of the PT block compared to the PS block and lower cluster attachment. The absorption spectra of all the three different size hybrid films formed from chloroform and toluene are also shown in Figure 86-88. It can be seen that a major peak at 520 nm with a shoulder peak of 560 nm is evident for the PS-Mo-PT1 film whereas for PS-Mo-PT2 and PS-Mo-PT3 films the major peak red-shifted to 550 nm with the small shoulder peak around 600 nm. The broadening and red-shifting of the absorption peaks with respect to their absorption spectra in solution can be the result of molecular aggregation forming larger crystallites in the films.

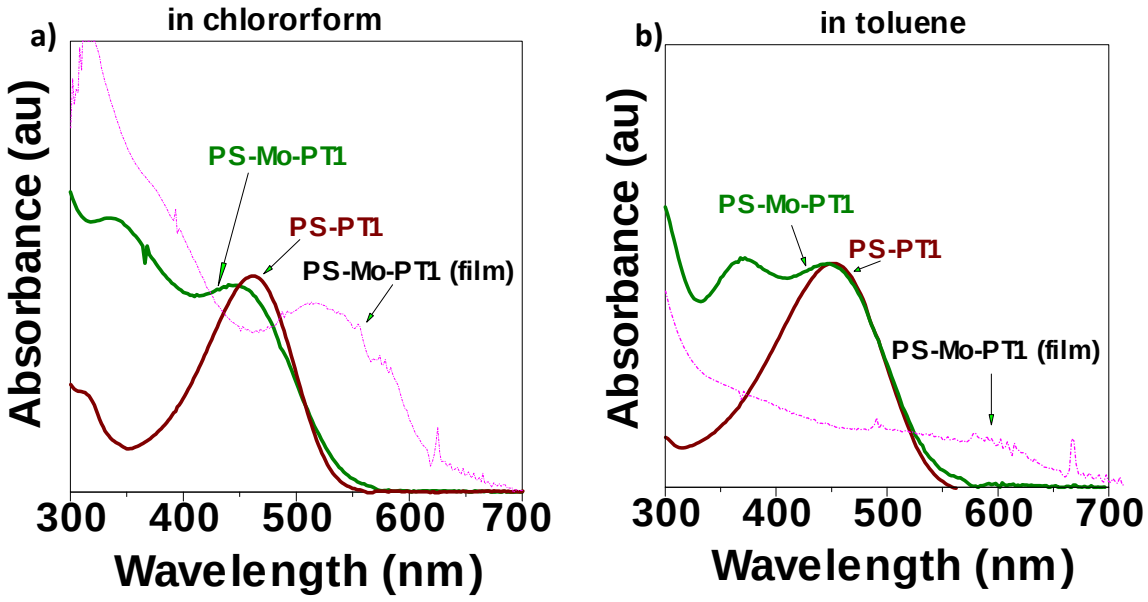

Figure 86. UV-Vis spectra of PS-PT1 block (solution) and PS-Mo-PT1 (solution and film) in a) chloroform and b) toluene.

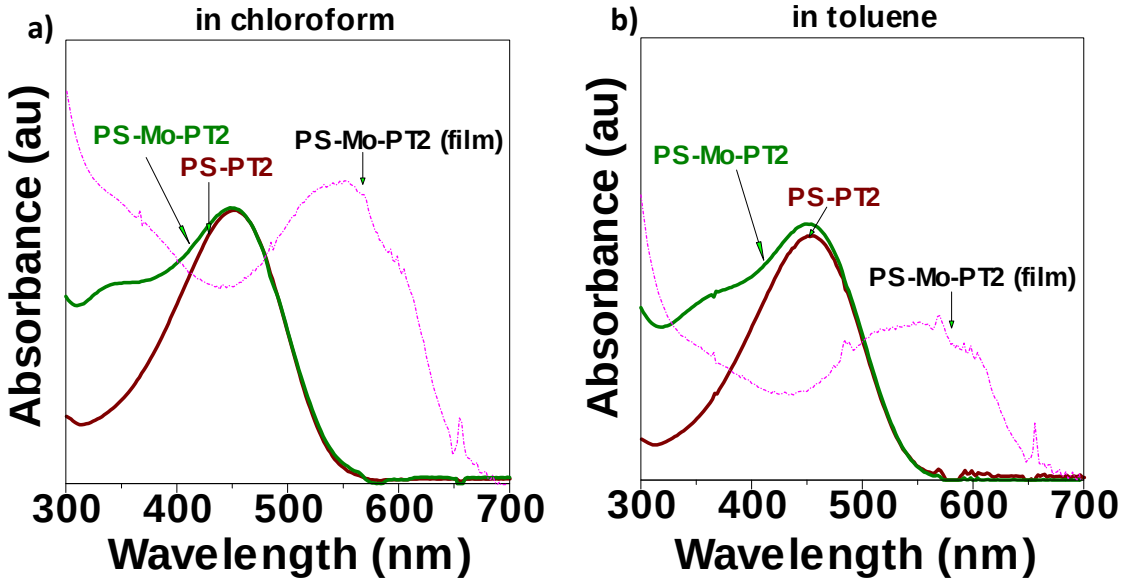

Figure 87. UV-Vis spectra of PS-PT2 block (solution), and PS-Mo-PT2 (solution and film) a) chloroform and b) toluene

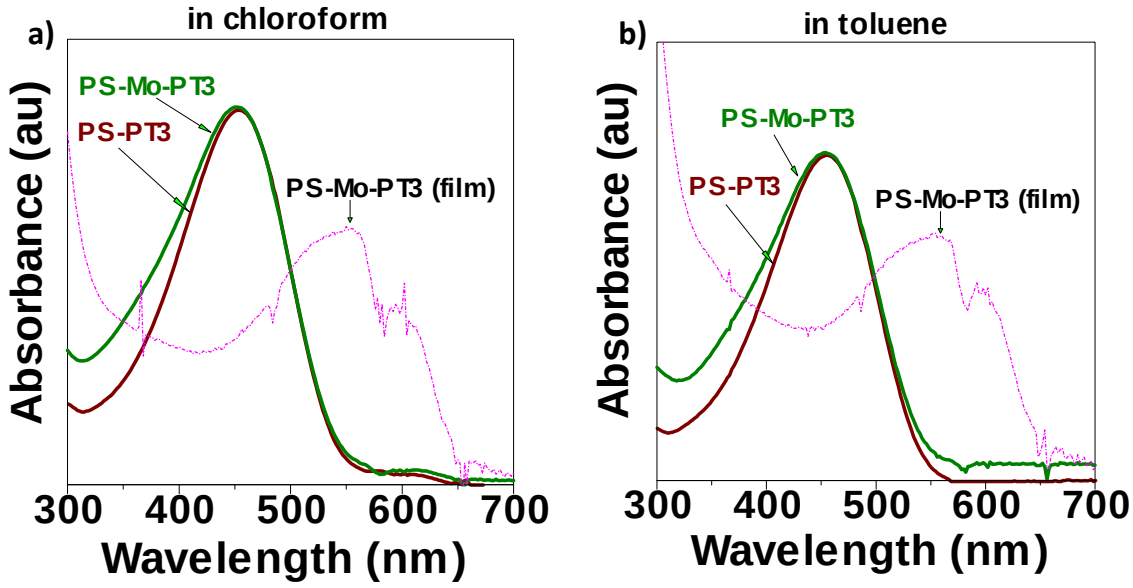

Figure 88. UV-Vis spectra of PS-PT3 block (solution), and PS-Mo-PT3 (solution and film) a) chloroform and b) toluene

All the PT blocks, diblock copolymers and hybrid diblocks show little fluorescence in both dilute chloroform and toluene solutions under the excitation of 450 nm. The photoluminescence spectra of all three PT blocks are shown in Figure 89 and the quantum yield values are shown in Table 5. The emission spectra shows a peak at 580 nm with a little broadening of the peak and a very little shoulder peak at 620 nm. These spectral profiles are corresponding to the intra-chain excitations. Strong vibrational motions of P3HT moiety corresponding to torsional twisting and chain stretching cause many vibrational electronic states in its ground state as well as change of its

conformational structure from a rigid planar excited structure to a flexible ground state structure. These motions led to broadened emission spectra with a shoulder peak.[168] The fluorescence quantum yield of the PT blocks and the diblock copolymers are not very high which are in good agreement with literature.[169] One of the reasons for the lower fluorescence quantum yields of PT based systems in solution might be due to several non-radiative deactivation processes. Twisted nature of conjugated segments due to torsional vibrations in solutions can be one such process.[169] The fluorescence spectra for all three hybrid diblock copolymers in both chloroform and toluene solution are shown in Figure 90 for lowest molecular weight hybrid, in Figure 91 for medium molecular weight hybrid and in Figure 92 for highest molecular weight hybrid. These spectra are not corrected for absorption. After cluster attachment there is little or negligible fluorescence quenching in both chloroform and in toluene as evident from the quantum yield. In contrast, the thin films of all the polymer samples exhibited nearly zero fluorescence quantum yields.[169] There are several explanations for this large drop in fluorescence in solid state compared to the solution photoluminescence of polythiophene systems. One explanation invoked the concentration quenching considerations which are observed when a planar ground state molecule is in close face-to-face proximity with a planar excited state molecule. In this case the excitation energy is shared intermolecularly, forming a new excited species called excimer, which can deactivate non-radiatively. In addition to that these strong interchain interactions in solid state which extend the ground state conjugation across several chains enables the electron cloud delocalization in two-dimension.[170] This non-radiative interchain interactions coupled with intersystem

crossing caused by the heavy atom effect of sulfur are believed to be responsible for the low quantum yield values of films.[171] Another alternative explanation is the polaron (charged species) formation following light absorption. It's been observed that both neutral emissive singlet states and charged polaron species are formed in solid states. Charge generation in P3HT films is found to be an intrinsic single photon process made possible by the strong interactions between chains leading to large delocalization of the excited state.[172]

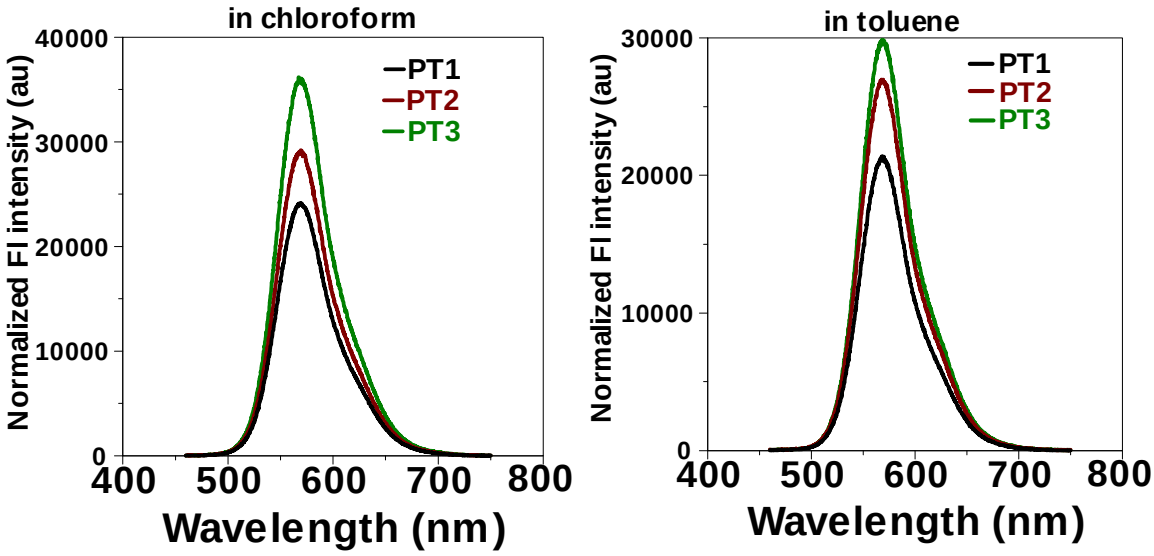

Figure 89. Fluorescence emission spectra of PT1, PT2 and PT3 in two different solvents a) chloroform and b) toluene solution.

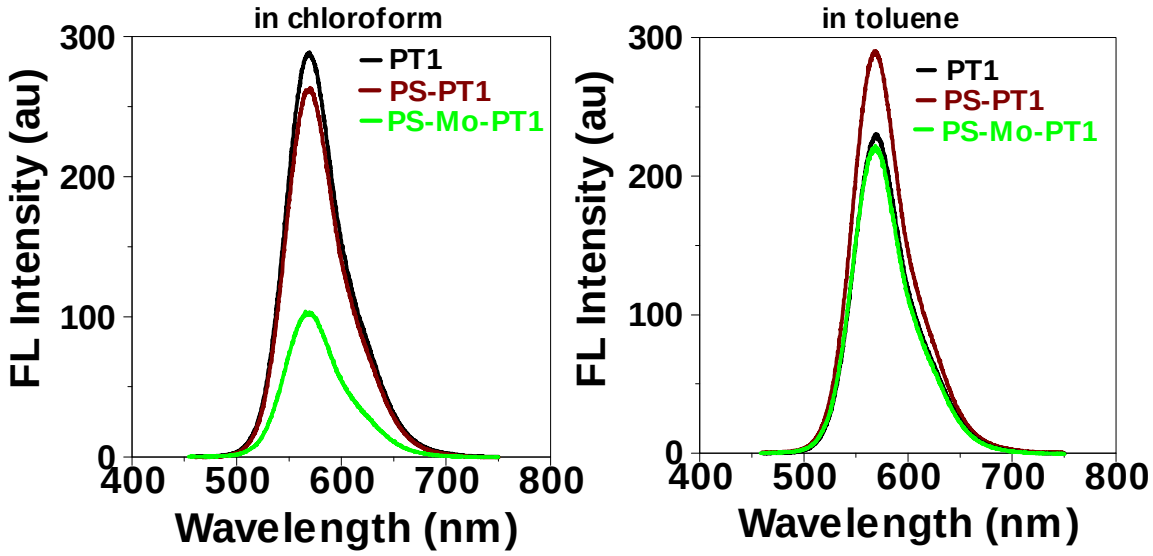

Figure 90. Fluorescence emission spectra of PT1, PS-PT1 and hybrid diblock in two different solvents a) chloroform and b) toluene solution.

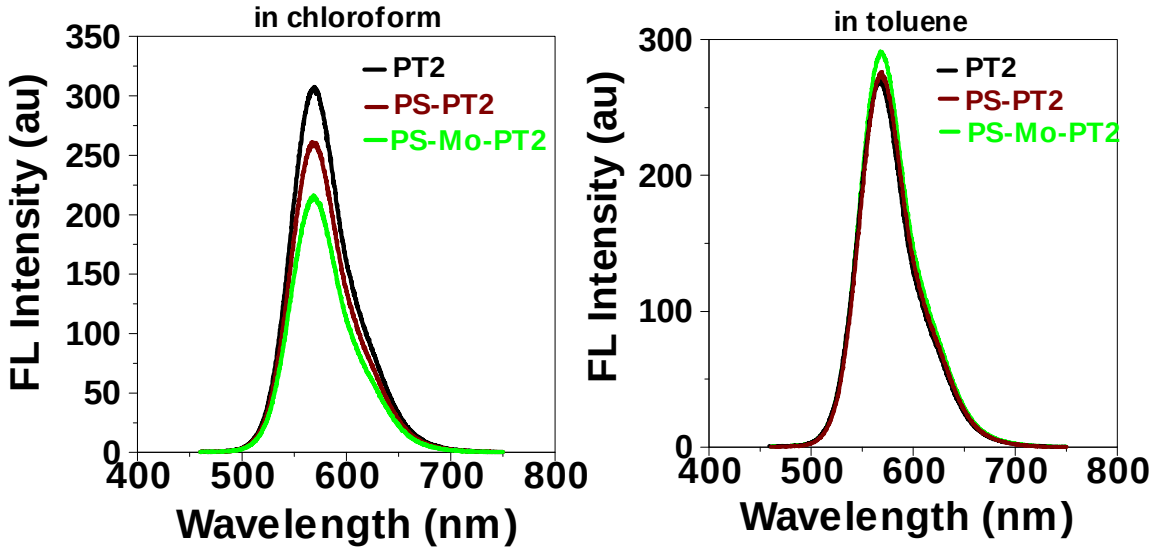

Figure 91. Fluorescence emission spectra of PT2, PS-PT2 and hybrid diblock in two different solvents a) chloroform and b) toluene solution.

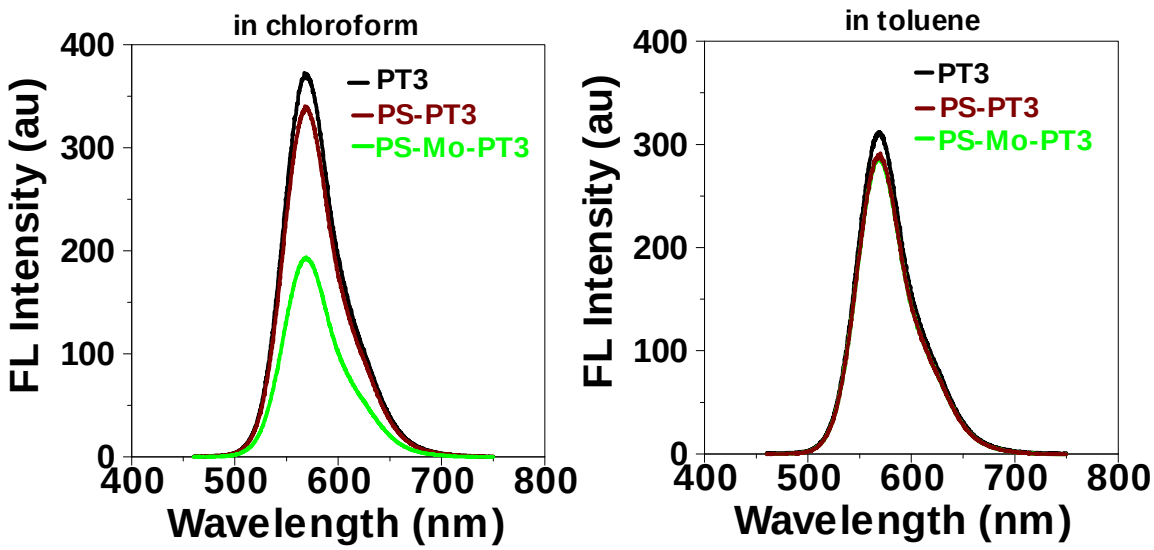

Figure 92. Fluorescence emission spectra of PT3, PS-PT3 and hybrid diblock in two different solvents a) chloroform and b) toluene solution

Table 5. Quantum yields of PT blocks, DCPs and hybrid DCPs in chloroform and toluene solution

Quantum Yields						
	Chloroform			Toluene		
	PT	PS-PT	PS-Mo-PT	PT	PS-PT	PS-Mo-PT
1	0.09	0.08	0.09	0.08	0.10	0.08
2	0.11	0.09	0.09	0.10	0.10	0.08
3	0.13	0.12	0.06	0.11	0.11	0.10

In order to reveal the excitation behaviours of these diblock copolymers, ultrafast time-resolved fluorescence dynamics of all three hybrid diblock copolymers in solution were investigated. Generally upon photoexcitation, the excited states of the P3HT moiety within the diblock copolymers follow self-trapping (dynamic localization) of excitons by nuclear motion within 100 fs[173], exciton relaxation [i.e. energetically downhill excitation energy transfer (EET), or downhill resonant energy transfer (RET)] and migration (i.e. EET between segments with comparable energy).[173a] It was reported that the energetically downhill EET occurs in less than 1 ps to several ps after photoexcitation,[173,174] while the EET between segments with comparable energy at the bottom of the density of states occurs within a much slower time scale (between 10 ps to 100 ps).[168a,173a,174a,175]

Figure 93 and 94 show the short- and long- time fluorescence dynamics for hybrid diblock copolymers PS-Mo-PT1, PS-Mo-PT2 and PS-Mo-PT3 in solution at emission wavelengths of 580 nm and 620 nm, respectively, under the excitation at 400 nm. The fitting results are compiled in Table 6. The short-time fluorescence (< 8000 fs) reveals the dynamics of photo-induced ultrafast initial processes. For the short-time fluorescence dynamics, a fast decay component of 692 fs and 804 fs for PS-Mo-PT1 at 580 nm and 620 nm, respectively, and 6.3 ps for PS-Mo-PT3 at 580 nm were observed. These fast decay components were ascribed to energetically downhill EET from high energy segments to low energy segments within the P3HT moiety, as typically occurs in a time

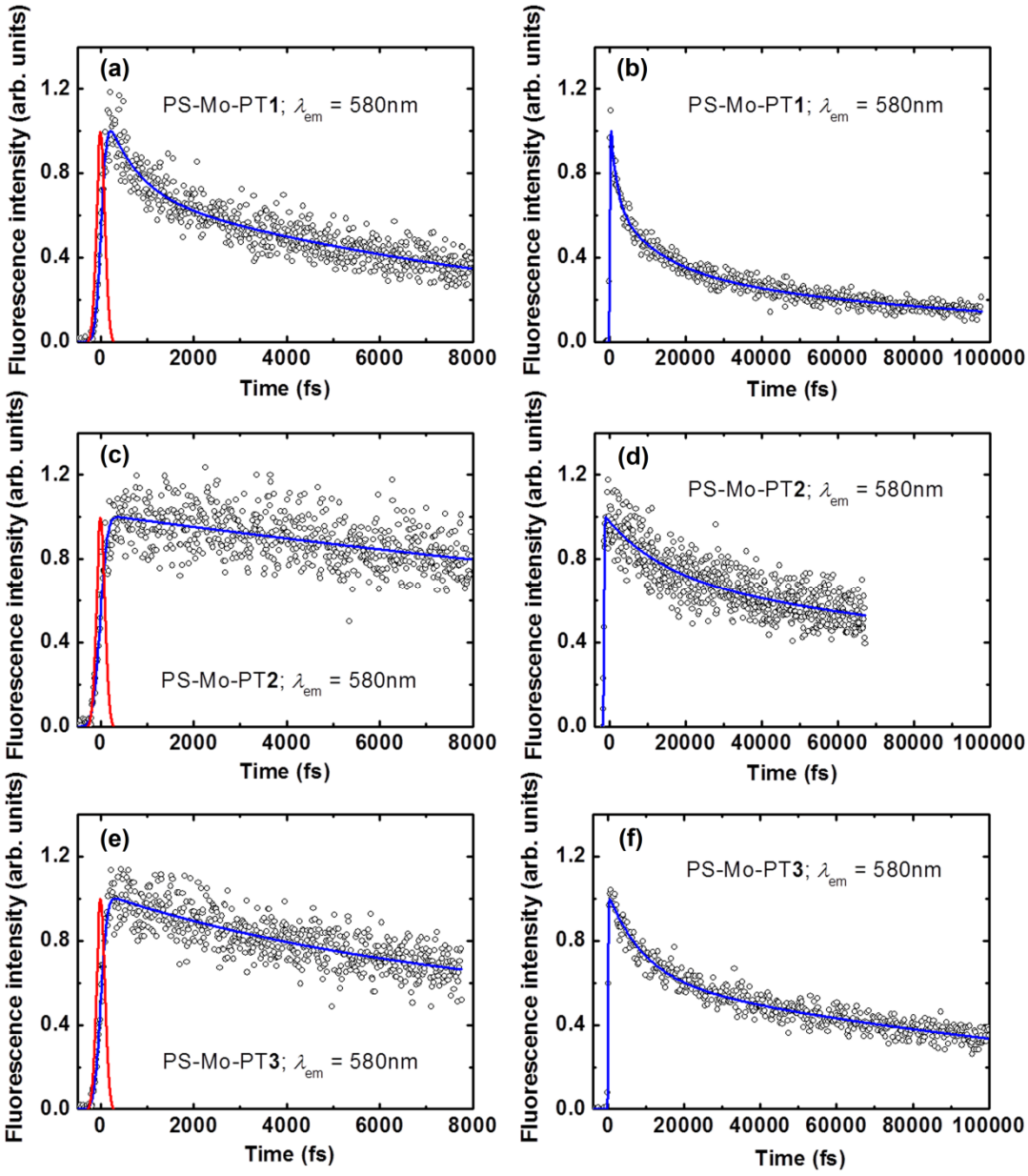

Figure 93. Short-time (a,c,e) and long-time (b,d,f) fluorescence dynamics of the hybrid diblock copolymers PS-Mo-PT1, PS-Mo-PT2 and PS-Mo-PT3 in chloroform solution with emission at 580 nm and excitation at 400 nm. The red lines are plotted instrument response function and blue lines are the fitted curves.

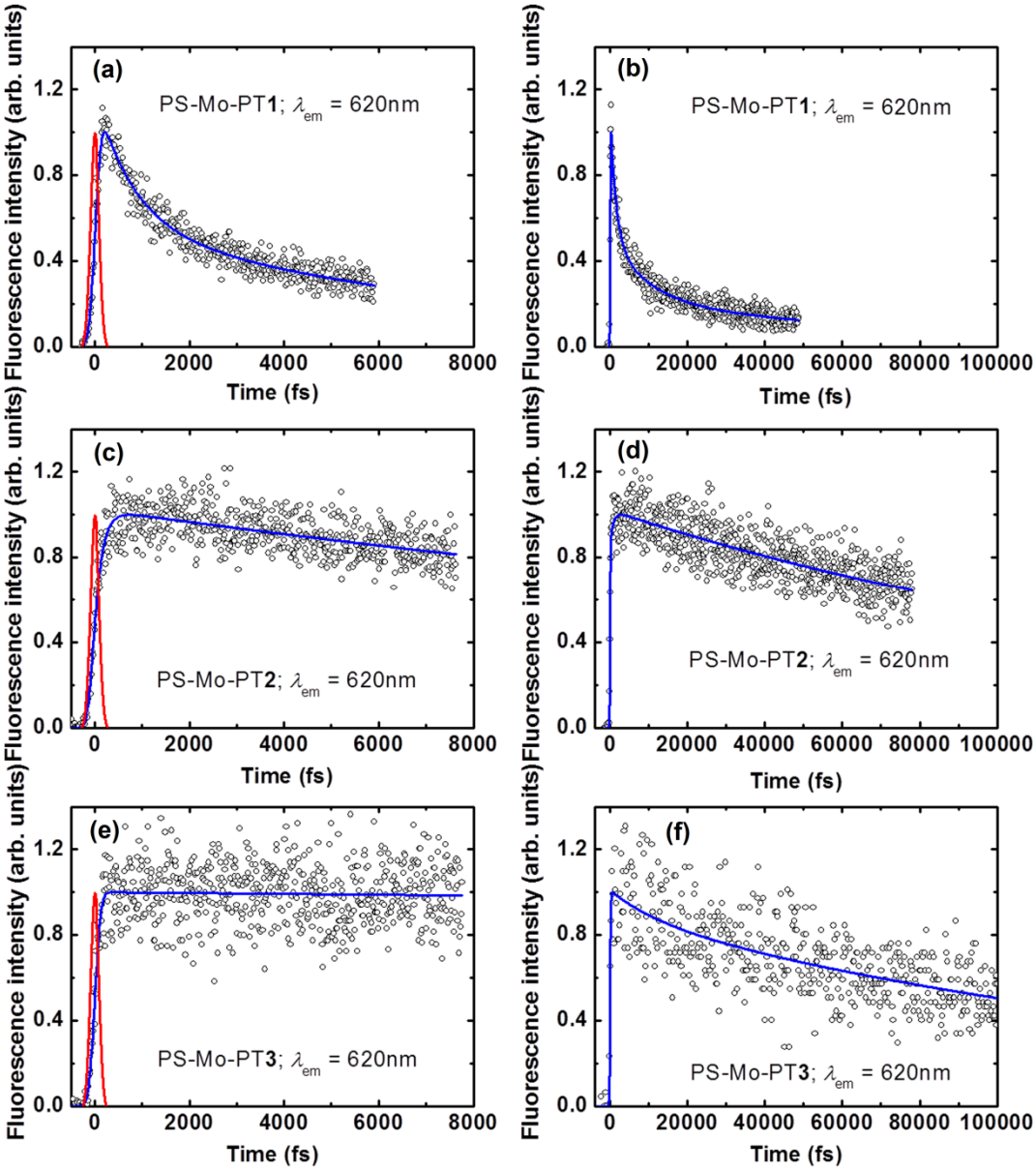

Figure 94. Short-time (a,c,e) and long-time (b,d,f) fluorescence dynamics of the hybrid diblock copolymers PS-Mo-PT1, PS-Mo-PT2 and PS-Mo-PT3 in chloroform solution with emission at 620 nm and excitation at 400 nm. The red lines are plotted instrument response function and blue lines are the fitted curves.

Table 6. Multi-exponential fitting parameters for the fluorescence dynamics of the hybrid diblock copolymers in chloroform with excitation at 400 nm. The sign of minus represents a rising behavior.

emission@	sample	time	τ_1 (fs)	A_1 (%)	τ_2 (ps)	A_2 (%)	τ_3 (ps)	A_3 (%)
580 nm	PS-Mo-PT**1**	short-time	692	37.5	11	62.5		
		long-time	1760	40	13	30	115	30
	PS-Mo-PT**2**	short-time	40	-15.5	34	84.5		
		long-time			16	30	233	70
	PS-Mo-PT**3**	short-time			6.3	40	67	60
		long-time			9.5	38.8	160	61.2
620 nm	PS-Mo-PT**1**	short-time	804	51.4	8.5	48.6		
		long-time	1500	55.0	9.8	27.0	90	18.0
	PS-Mo-PT**2**	short-time	153	-56.6	33	43.4		
		long-time	797	-15.0	170	85.0		
	PS-Mo-PT**3**	short-time	29	-6.0	496	94.0		
		long-time			13	12.0	179	88.0

scale of sub-ps to several ps.[173a,174] It is worth noting that an ultrafast rising component of 40 fs and 153 fs for PS-Mo-PT2 at 580 nm and 620 nm, respectively, and 29 fs for PS-Mo-PT3 at 620 nm was observed. It has been reported that strong excitation self-trapping by the phonon mode and the intramolecular vibrational energy redistribution can happen within 100 fs or sub 100 fs for P3HT and other polymers and oligomers.[168a,c,176] However, such ultrafast processes were usually hard to be directly observed because of their time scales which are shorter than the instrument response function (IRF) (~ 255 fs, FWHM) of the measurement.[168a] The observed ultrafast rising component in the present case might suggest energy transfer process from S_2 excited states to the S_1 excited states. The relatively slow decay within time scale of 11 ps to 67 ps for PS-Mo-PT1, PS-Mo-PT2 and PS-Mo-PT3 at 580 nm and of 8.5 ps to 33 ps for PS-Mo-PT1 and PS-Mo-PT2 at 620 nm can be assigned to the EET between segments of comparable energy. The EET between segments of comparable energy was reported to occur in a time scale of 10 ps to 100 ps.[168a, 173a, 174a, 175] The slow decay of 496 ps (with large error) for PS-Mo-PT3 at 620 nm might be designated to the lifetime of the fluorescence from S_1 to S_0.[168a,173a]

The long-time fluorescence (upto 100,000 fs) was mainly aimed to extract the fluorescence lifetimes usually within relatively longer time scale. The fast decay component of 1760 fs and 1500 fs for PS-Mo-PT1 at 580 nm and 620 nm, respectively, corresponding to the energetically downhill EET from high energy segments to low energy segments within the P3HT moiety, was observed. The ultrafast rising component of 797 fs for PS-Mo-PT2 at 620 nm might be ascribed to the energy transfer from S_2 excited states to the S_1 excited states. The decay component of 13 ps, 16 ps and 9.5 ps for

PS-Mo-PT1, PS-Mo-PT2 and PS-Mo-PT3, respectively, at 580 nm, and 9.8 ps and 13 ps for PS-Mo-PT1 and PS-Mo-PT3, respectively, at 620 nm can be assigned to either downhill or iso-energetic EET. Considering the system error for the short- and long-time measurement, these data were in proximate agreement with short-time fluorescence dynamics results. The slow decay of 115 ps, 233 ps and 160 ps for PS-Mo-PT1, PS-Mo-PT2 and PS-Mo-PT3, respectively, at 580 nm, and 90 ps, 170 ps and 179 ps for PS-Mo-PT1, PS-Mo-PT2 and PS-Mo-PT3, respectively, at 620 nm can be assigned to the lifetime of the fluorescence from S_1 to S_0.[168a, 173a]

Figure 95 shows the anisotropy initial decay of the emission of PS-Mo-PT1, PS-Mo-PT2 and PS-Mo-PT3 at both 580 nm and 620 nm. These emission anisotropy decays were fitted by a function with two-exponential components and the results are compiled in Table 7. In line with the previous results for P3HT solution, the ultrafast component from 138 ps to 226 ps for all three hybrid diblocks and slow component of 20 ps for PS-Mo-PT1 at emission of 580 nm can be attributed to EET among segments, while the slow component from 202 ps to 796 ps for PS-Mo-PT2 and PS-Mo-PT3 might be attributed to the dipole moment rotation diffusion.[168a] For the anisotropy initial decay at emission of 620 nm, an ultrafast depolarization process within a time scale of 82 fs to 142 fs and a slow component in 11.7 fs to 460 ps were observed. The ultrafast depolarization (82-142 fs) suggested a strong and ultrafast reorientation of excited state dipole moments which was induced by the energy transfer process originated form the exciton delocalization via energy vibrational relaxation or redistribution.[168a] The slow depolarization process of 11.7 ps for PS-Mo-PT 3 was attributed to EET.[168a] From all these measurements it can be

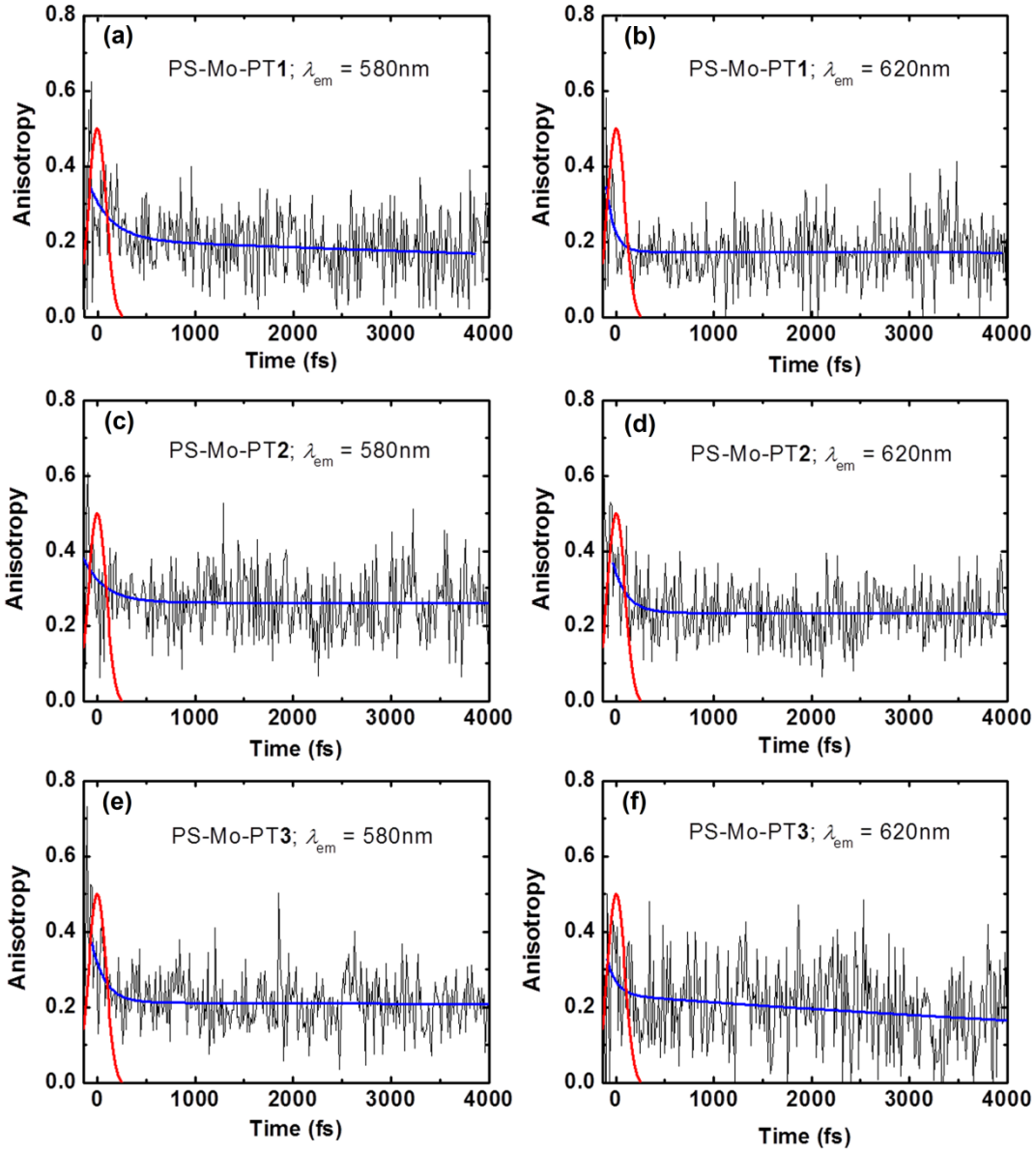

Figure 95. Anisotropy decay profiles for the emissions at both 580 nm (a, c, e) and 620 nm (b, d, f) of the hybrid diblock copolymers, PS-Mo-PT1, PS-Mo-PT2 and PS-Mo-PT3 in chloroform under the excitation at 400 nm. The res lines are plotted instrument response function and blue ones are fitted curves.

Table 7. Bi-exponential fitting parameters for the fluorescence anisotropy decay of the diblock copolymers PS-Mo-PT(1–3) in $CHCl_3$ with excitation at 400 nm

emission @	sample	τ_1 (fs)	A_1 (%)	τ_2 (ps)	A_2 (%)
580 nm	PS-Mo-PT**1**	226	0.140	20	0.210
	PS-Mo-PT**2**	215	0.137	796	0.261
	PS-Mo-PT**3**	138	0.160	202	0.210
620 nm	PS-Mo-PT**1**	82	0.170	392	0.170
	PS-Mo-PT**2**	142	0.131	460	0.234
	PS-Mo-PT**3**	97	0.100	11.7	0.230

concluded that the energy transfer from the P3HT donor to the acceptor in solution is not very efficient. The ultra-fast time resolved fluorescence dynamics study of all these hybrid diblock copolymers in film is required further to explain the behavior.

5.3.7. Thin Film Morphology

The film morphology of the three different size PS-PT blocks and their corresponding hybrid PS-Mo-PT blocks were studied in chloroform and toluene in order to understand the effect of molecular size of the film deposited from solvents of varying boiling points on the morphology. The films were spin coated from the solvents onto indium tin oxide (ITO) glass slides and dried under vacuum which is followed by thermal

annealing at around 170°C for 6 h. The spin coating on ITO glass enabled to realize the conducting images in addition to the topography and phase images. The topography, phase and conducting images of the three diblock copolymers PS-PT1, PS-PT2 and PS-PT3 spin coated from chloroform and toluene are shown in Figure 96 and in Figure 97, respectively. Topography and phase images of these films deposited from both the solvents are not very well resolved. But the white conductive regions in the conducting images are clearly discernible by using the conductive cantilever tip of AFM. It is important to note that the lowest molecular size diblock PS-PT1 has the highest conductive region covering the entire ITO glass whereas the medium molecular size diblock PS-PT2 and highest molecular size diblock PS-PT3 has almost negligible conductivity for the films spin coated from chloroform. On the contrary, the films deposited from toluene exhibit a complete opposite trend. Here the highest molecular size diblock PS-PT shows the maximum conductive region which decreases for medium molecular size diblock and become negligible for lowest molecular size diblock PS-PT3. One plausible reason for this contrasting behavior lies within the evaporation rate of the solvents during spin coating. In the low boiling chloroform solvent the non-equilibrium state is trapped by fast drying as the highest molecular size diblock has limited time to organize itself into a well-ordered arrangement while the lower molecular size diblock is able to rearrange itself into ordered structure resulting in highly conductive regions. In toluene the highest molecular size diblock experience sufficient time to arrange into ordered equilibrated structure due to the slow evaporation of high boiling toluene resulting in higher conductive regions.

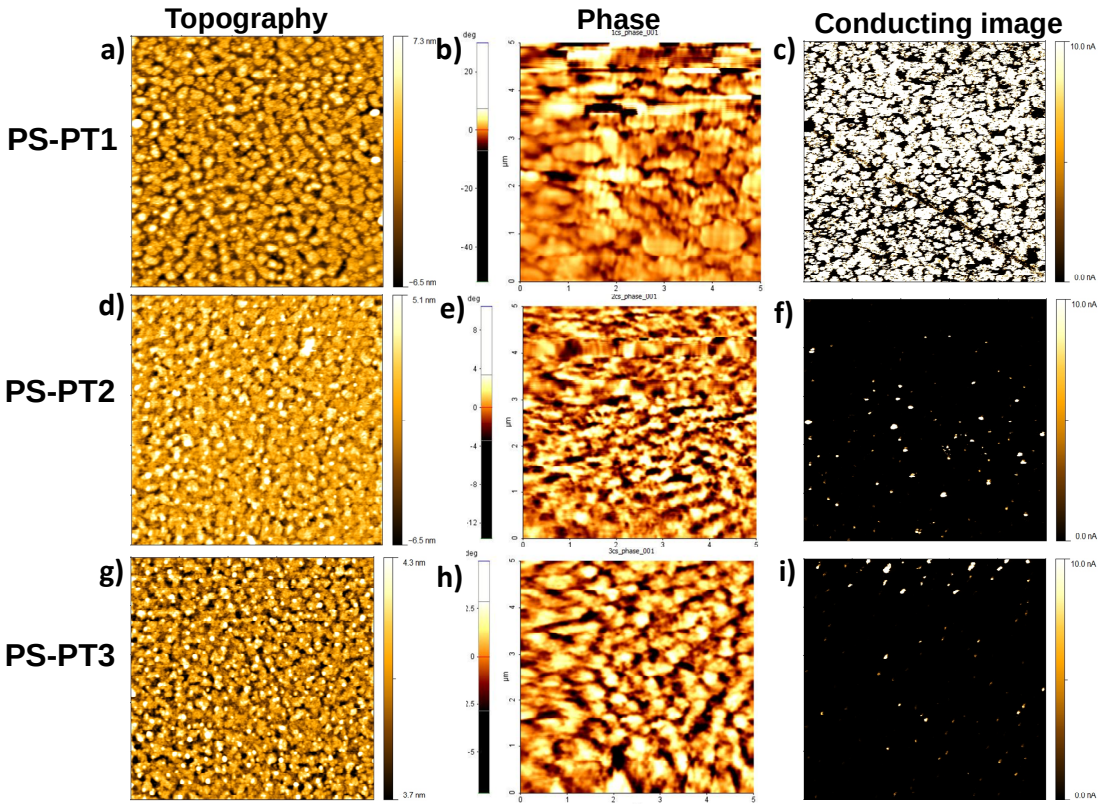

Figure 96. AFM images of three different diblock films spin coated from chloroform on ITO glass. a), d), g): topography images; b), e), h): phase images; c), f), i): conducting images.

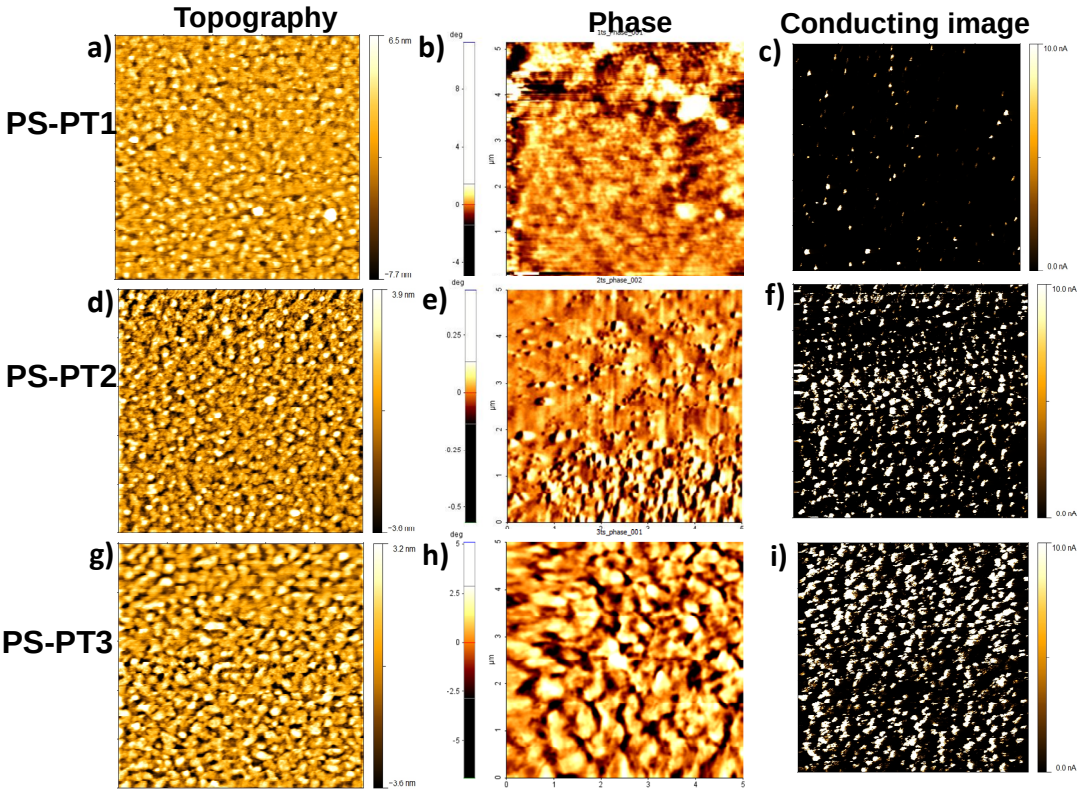

Figure 97. AFM images of three different diblock films spin coated from toluene on ITO glass. a), d), g): topography images; b), e), h): phase images; c), f), i): conducting images.

Similarly the three different hybrid diblock copolymers PS-Mo-PTs were spin coated on ITO glasses from chloroform and toluene solvents. Then the films were annealed at lower temperature compared to the diblocks at around 120° C for 6 h as the hybrid diblocks start degrading around 150° C evident from the TGA studies. The topography and conducting images before and after annealing for all three different size hybrid diblock films of PS-Mo-PT1, PS-Mo-PT2 and PS-Mo-PT3 obtained from spin-

coating from chloroform solvent are shown in Figure 98, 99 and 100, respectively. The topography images for all three hybrid films before annealing are featureless and similar to the diblock PS-PT films. An insignificant amount of change in topography can be observed for these films after thermally annealed. On the other hand the conductivity of these films has improved after thermal annealing as evident from the conducting images. Though the conductive regions are not very high in PS-Mo-PT1 films but they are much more pronounced in PS-Mo-PT2 films whereas for PS-Mo-PT3 films almost the entire film is covered with white conductive regions as shown in Figure 100.

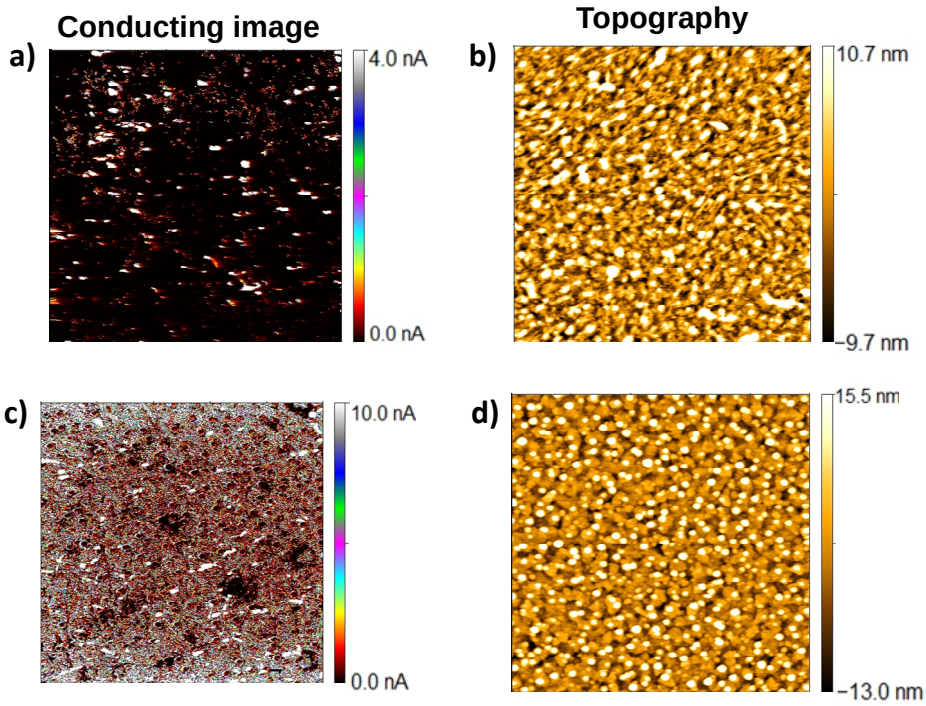

Figure 98. AFM images of hybrid diblock PS-Mo-PT1 films spin coated from chloroform on ITO glass. a), b): before annealing; c), d): after annealing

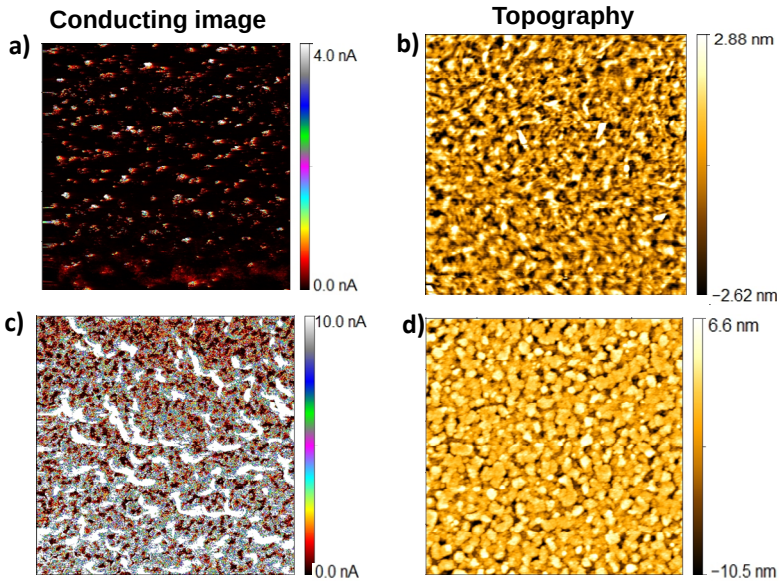

Figure 99. AFM images of hybrid diblock PS-Mo-PT2 films spin coated from chloroform on ITO glass. a), b): before annealing; c), d): after annealing

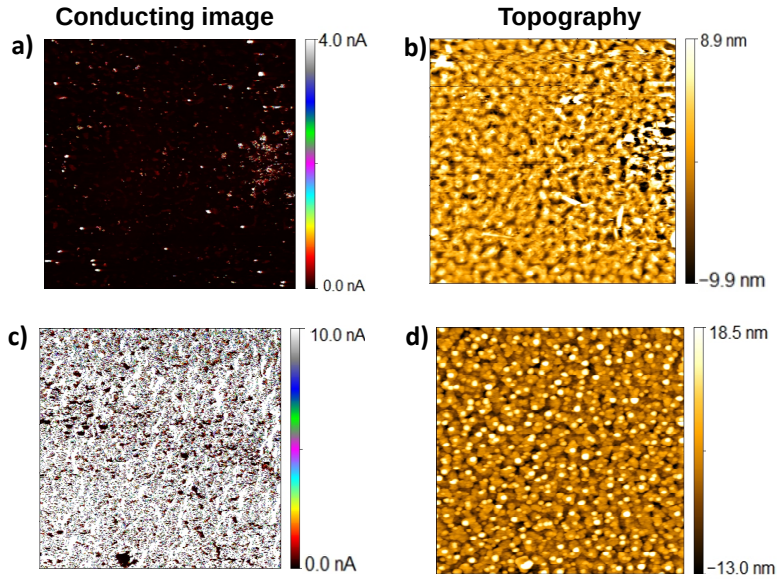

Figure 100. AFM images of hybrid diblock PS-Mo-PT3 films spin coated from chloroform on ITO glass. a), b): before annealing; c), d): after annealing

The topography and conducting images, before and after annealing, of the three hybrid diblock films, spin coated from toluene are illustrated in Figure 101, 102 and 103 for PS-Mo-PT1, PS-Mo-PT2 and PS-Mo-PT3 hybrid diblocks, respectively. Likewise, the topography images for all three hybrids remain unchanged after thermal annealing. The conductivity increase after annealing as can be seen from the conducting images. Though the conductive regions are distributed all over the hybrid films in all three hybrids, highest conductivity is observed in the PS-Mo-PT1 film.

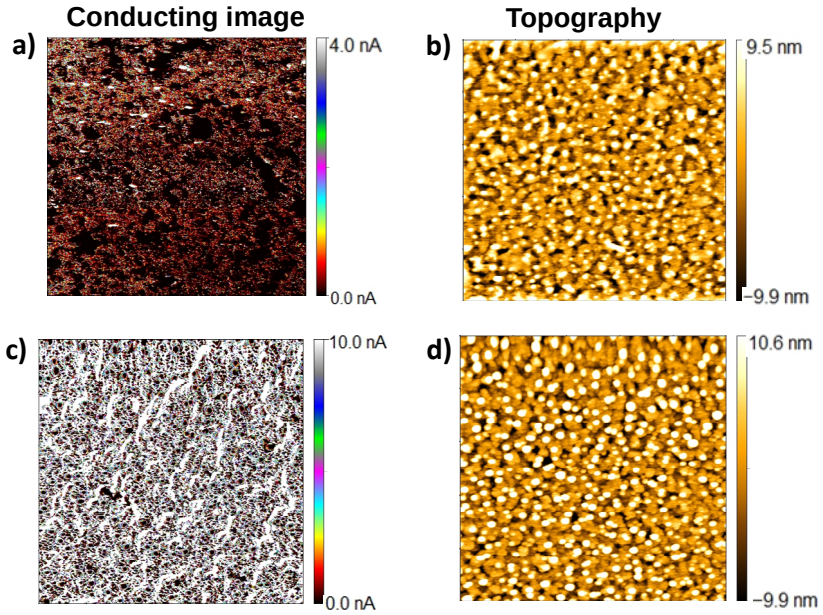

Figure 101. AFM images of hybrid diblock PS-Mo-PT1 films spin coated from toluene on ITO glass. a), b): before annealing; c), d): after annealing

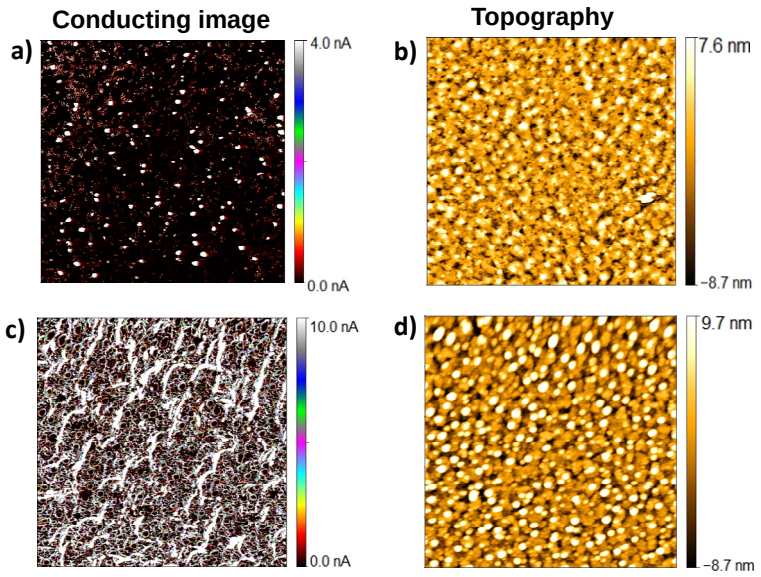

Figure 102. AFM images of hybrid diblock PS-Mo-PT2 films spin coated from toluene on ITO glass. a), b): before annealing; c), d): after annealing

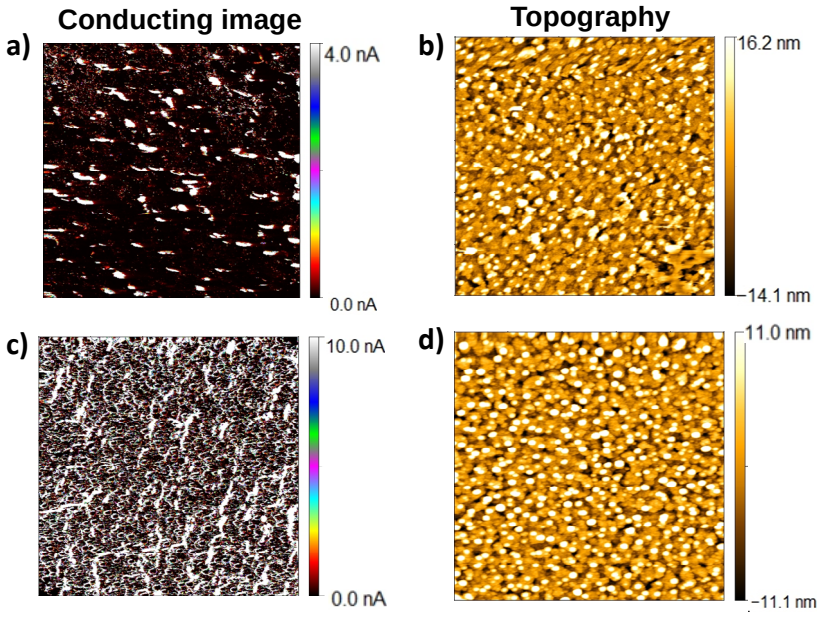

Figure 103. AFM images of hybrid diblock PS-Mo-PT3 films spin coated from toluene on ITO glass. a), b): before annealing; c), d): after annealing

5.3.8. Photovoltaic Study

The photovoltaic devices for all three hybrid diblock copolymers were prepared into a cell structure of Glass/ITO/ZnO (seed layer, 150-160 nm)/ZnO nanords (~400 nm)/PS-Mo-PT(**1–3**)/Au (150 nm). A 150-160 nm thick ZnO seed layer was deposited onto the ITO substrate by sputtering. On the seed layer ZnO nanorod arrays were grown by hydrothermal reaction in an aqueous precursor solution of $Zn(NO_3)_2.6H_2O$ (0.05 M) and hexamethylenetetramine (0.05 M) heated at 90°C as explained in the experimental section.[177] The ZnO nanorods, after heating to 80°C, were immersed into the chloroform solutions of hybrid diblock copolymer (5mg/mL) and dried. The active layer was made by spin coating of the chloroform solution of hybrid diblock copolymer (20 mg/mL) onto the pre-treated ZnO nanorod arrays. The spin coated films on the ZnO nanorods were annealed at 120°C in air for 10 min, followed by deposition of Au contact via thermal evaporation in high vacuum.

A general working principle of solar cell is based on the mechanism of the donor-acceptor bulk heterojunction devices (BHJ). The donor material (P3HT) after harvesting incoming sunlight through ITO/ZnO side generates excitons. These generated excitons diffuse to the donor-acceptor interface to dissociate into free charge carriers. Separated holes transport within donor material through hopping to the anode, whereas the separated electrons transport within the acceptor material to the cathode. Initially solar cells were prepared in absence of ZnO from these hybrid diblock copolymers. Negligible efficiency of those solar devices prompted the

fabrication of solar cells with ZnO nanorods. ZnO materials are excellent electron acceptors. They are environmental friendly, indefinitely stable and can be synthesized inexpensively into different shapes and sized using various methods. Although efficient charge separation is achieved in BHJ devices, they usually suffer from discontinuous charge transport pathways. Sometimes there is a possibility of the trapping of charges in some isolated phases leading to recombination loss. These problems can be overcome with a structuring of a nanostructured acceptor by improving electron transport through it. These nanorods are well defined robust charge carrier pathways with high carrier mobility. By controlling the dimension of the vertically aligned nanostructures, polymers are also allowed to align themselves in a way to improve interchain coupling leading to better exciton diffusion and charge transport. This makes donor material to penetrate in between the scaffold of ZnO nanorods. The ZnO nanorods anchored to the conducting substrate not only provide a direct pathway for electron transport to the back contact but also increase polymer/ZnO interfacial area, which in turn improve the overall cell performance.[178]

The transmittance spectra of the ZnO seed layer and ZnO nanorods on the ZnO seed layer in the UV-visible region are shown in Figure 104. High transparency (77-100%) was observed for the sputtered ZnO seed layer in the range of 385 nm to 1100 nm. The growth of ZnO nanorods on the seed layer significantly decreased the transparency of the whole film down to 40-72% at 525 to 1100 nm and down to 0-32% at 380-485 nm.

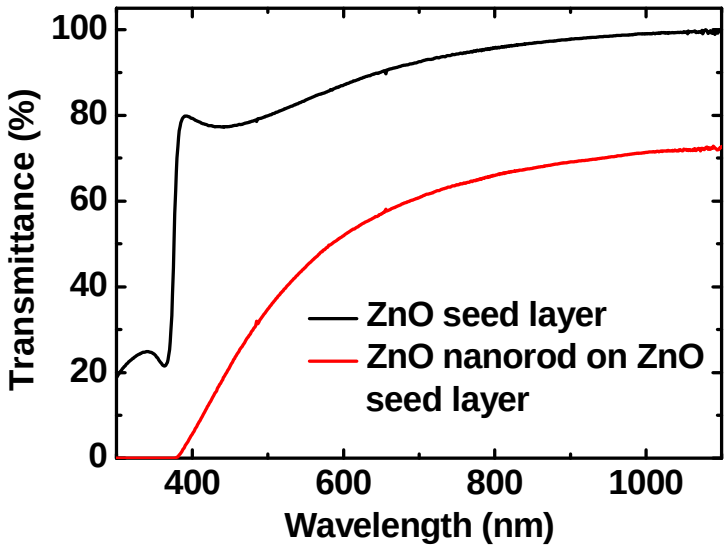

Figure 104. Transmittance of the ZnO seed layer on ITO glass and ZnO nanorods on ZnO seed layer

The AFM topography images of the ZnO seed layer and ZnO nanorods are shown in Figure 105. It can be observed from Figure 105a that the ZnO nanoparticles deposited by sputtering with average particle size of ~25 nm are connected closely and form an irregular ZnO seed layer. The uniformly vertical alignment of the ZnO nanorods on this sputtered ZnO seed layer can clearly be seen in Figure 105b. The nanorod formation was further supported by the SEM images as shown in Figure 106. The average length of the nanorods is evaluated to be ~400 nm. The arrays consist of nanorods with diameter of ~160 nm and inter-distance of several tens to a few hundreds of nanometers.

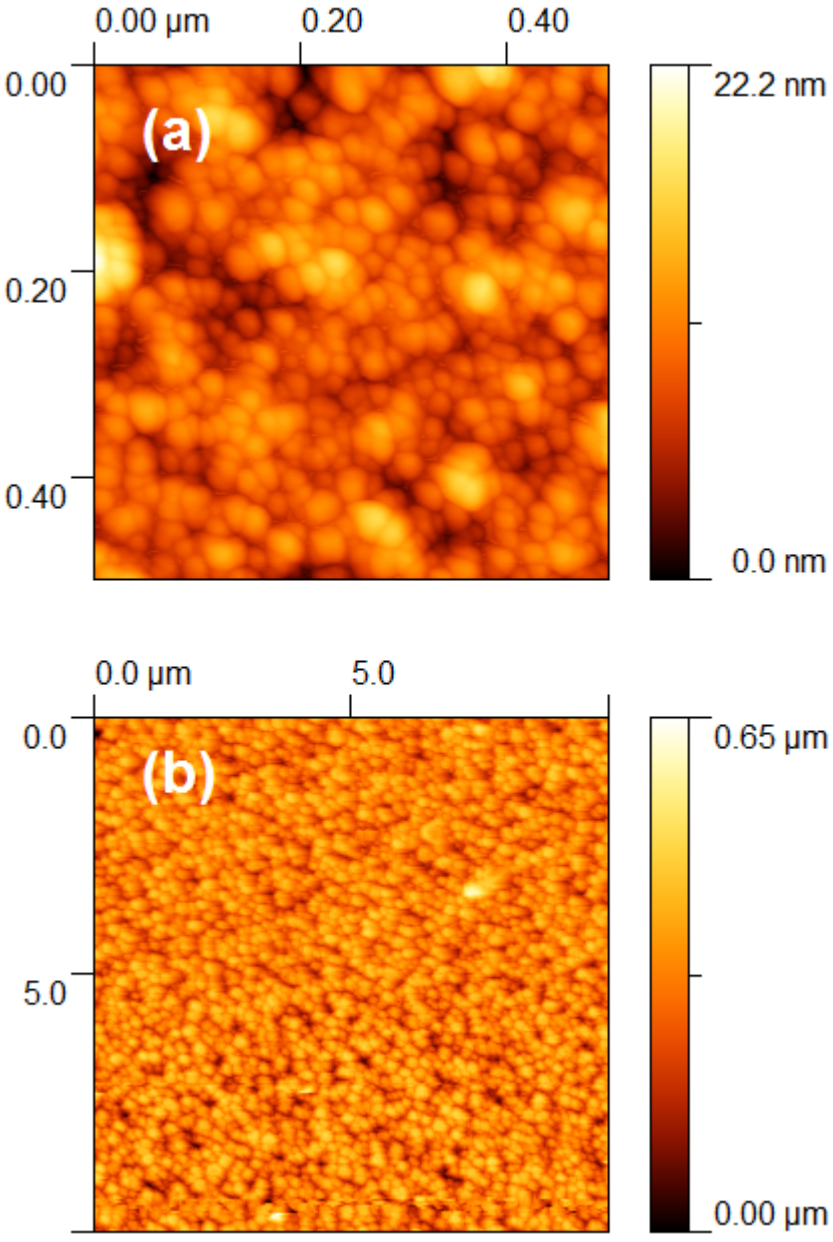

Figure 105. AFM topography images of the films of (a) ZnO seed layer, and (b) ZnO nanorods

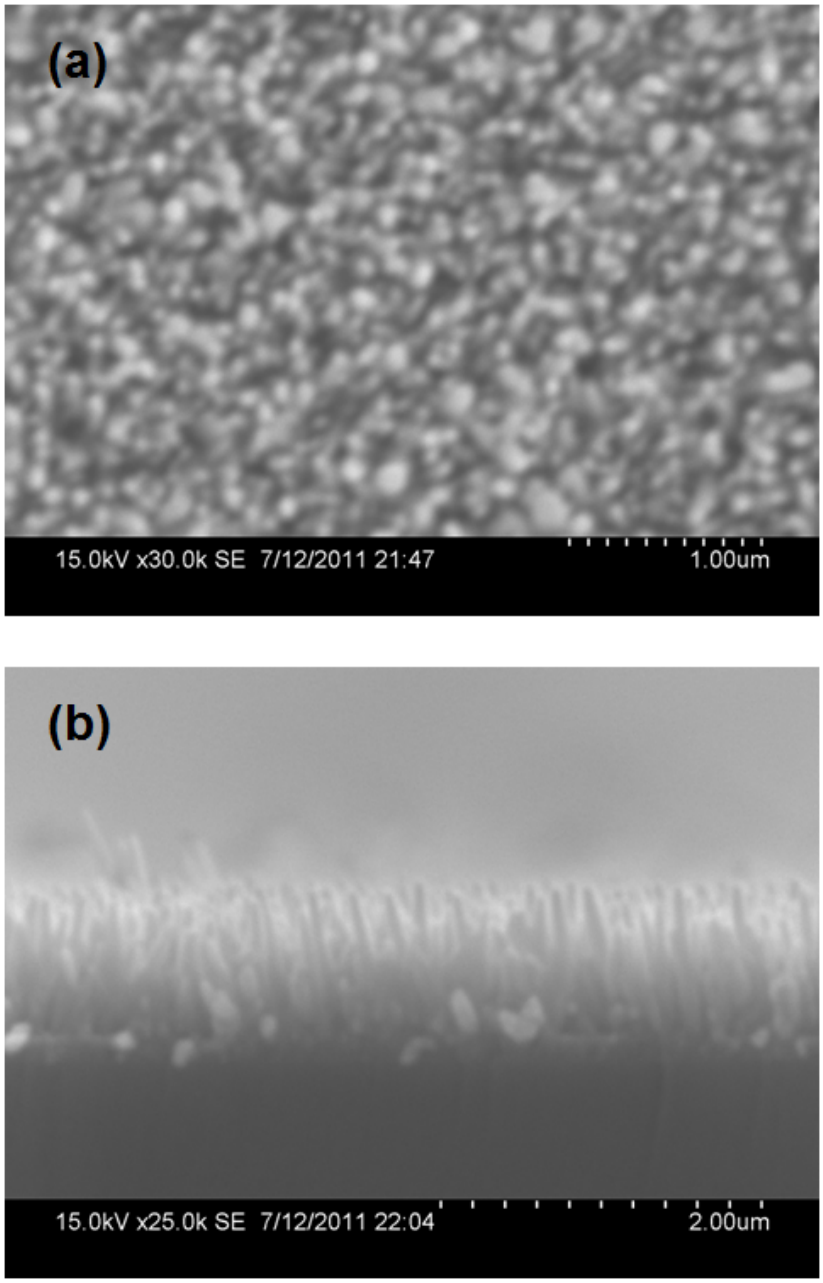

Figure 106. SEM images of the ZnO nanorods grown on ZnO seed layer, a) surface and b) cross-section

The current density-voltage (J-V) curves of all the three hybrid diblock copolymers were measured with a solar simulator with an AM1.5 filter at an intensity of ~100 mW/cm^{-2} and plotted in Figure 107. The short-circuit current densities (J_{sc}), the open-circuit voltages (V_{oc}), the fill factors (FF) and the power conversion efficiencies (η) for all three devices are summarized in Table 8.

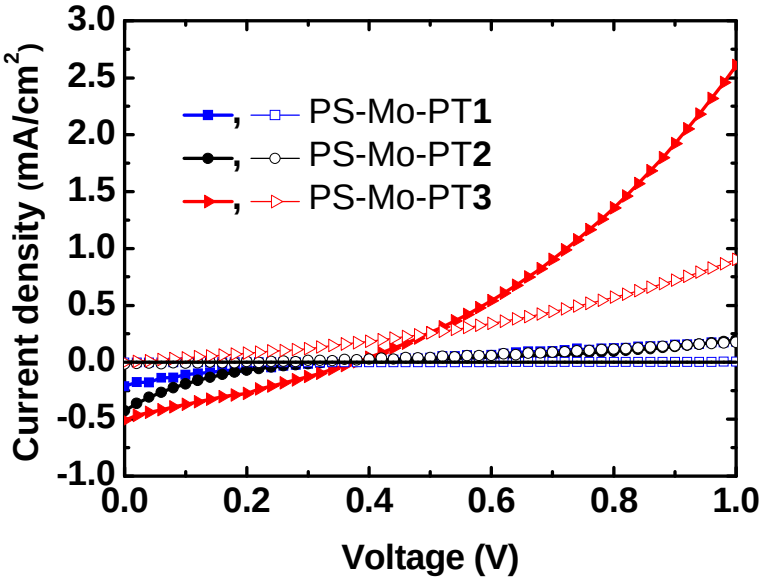

Figure 107. Current density–voltage curves (empty: dark; filled: illuminated) for the cell structures of Glass/ITO/ZnO (seed layer, 150-160 nm)/ZnO nanords (~400 nm)/PS-Mo-PT(**1**–**3**)/Au (150 nm), under 1-sun AM 1.5G illumination.

Table 8. Parameters of solar cells made by diblock copolymers PS-Mo-PT(**1–3**) with cell structures of Glass/ITO/ZnO (seed layer, 150-160 nm)/ZnO nanords (~400 nm)/PS-Mo-PT(**1–3**)/Au (150 nm), under 1-sun AM 1.5G illumination.

active material	cell area (cm^2)	V_{OC} (V)	J_{SC} (mA/cm^2)	FF	η (%)
PS-Mo-PT**1**	0.36	0.34	0.21	0.17	0.012
PS-Mo-PT**2**	0.36	0.36	0.43	0.12	0.019
PS-Mo-PT**3**	0.36	0.38	0.51	0.28	0.055

The efficiencies of all three hybrid diblock copolymers based devices are not very encouraging. The one probable reason might be the inefficient charge transfer rather than inefficient charge transport pathways. However, the device based on PS-Mo-PT3 exhibited the highest efficiency due to the increased current density and fill factor (FF). Cells with higher fill factor have a low series resistance and less dissipation of current produced by light to internal losses. Increased current in higher molecular weight films might be due to the higher charge carrier mobility because in high molecular weight films longer chains connect the ordered domains (where several chains are locally aligned) to provide a pathway for charge transport between crystalline domains.[139h] In addition, the charge carriers can travel farther along longer chains before they have to hop to another chains, and as longer chains give charge carriers more opportunities for hopping to

neighboring chains. This net reduction on hopping events can result in increased mobility.

5.4. Conclusions

Three varying molecular size regioregular PT based POM-containing hybrid diblock copolymers through post-polymerization approach were synthesized. The absolute molecular weights of all the three different PT blocks were determined by MALDI-TOF measurements. Click chemistry was used to couple the rigid P3HT blocks with the flexible PS blocks. GPC measurements have confirmed the formation of the diblock copolymers with narrow molecular weight distributions. The POM cluster attachments were carried out in nitrobenzene solvent. The cluster attachments to all the diblock copolymers were confirmed by GPC using light scattering detector, IR, and optical spectroscopy. The PT blocks and the corresponding diblock copolymers exhibited sharp melting temperatures in DSC thermograms which increased with increasing molecular weight of the PT blocks. The hybrid diblock copolymers showed two absorption bands in both chloroform and toluene solutions, one at 450 nm due to π-π^* transitions of the PT backbone and the other at 350 nm attributed to the ligand-to-metal charge transfer transition of functionalized Mo6 clusters. The absorption peak of the three hybrid diblock copolymer films exhibited broader absorption peaks with distinct bathochromic shift which indicates a regular ordered arrangement of the backbone chains. Though the fluorescence quantum yields of any of the PT blocks, diblock

copolymers and hybrid diblocks in both chloroform and toluene solvents were not very high, little fluorescence quenching observed for the hybrid diblock copolymers in solutions. The conductive AFM images of the three diblock copolymer films spin coated from chloroform showed opposite trends than those of films spin coated from toluene. Highest conductive regions were observed for the lowest molecular size diblock in case of spin coated film from chloroform whereas for toluene it was the highest molecular size diblock. The fluorescence dynamic studies of the three hybrid diblock copolymers revealed that the charge transfers were not very efficient in solution which resulted in poor photovoltaic device efficiencies.

5.5. Experimental Section

Materials. Tetrahydrofuran (THF) was purified by distillation over sodium pellets and benzophenone. CuBr was purified by washing consecutively with glacial acetic acid, absolute ethanol and ethyl ether, and then dried under vacuum. N, N, N´, N´, N´-pentamethyldiethylenetriamine (PMDETA, 99%) was distilled in vacuo before use. All other chemicals were purchased either from Aldrich or Acros and were used as received unless otherwise stated. PS-N3 coil block was synthesized in two steps according to our previously published method.[98] Compound 14 was prepared by bromination with NBS according to literature procedure.[154a]

Instrumentation. All reactions were conducted under the protection of nitrogen. The ^{1}H and ^{13}C NMR were collected on a Varian INOVA 400 MHz FTNMR

spectrometer. All samples were referenced to the deuterated solvents. GPC measurements were performed at 30°C on a Tosoh Ecosec HLC 8320GPC system equipped with a differential refractometer, UV detector, and styragel column with THF as the eluent. PSS (polymer standards service) WinGPC Unity version 7.5.0 system equipped with light scattering detector coupled to the Tosoh Ecosec system was used for analysis. The calibration curve was determined by the use of five polystyrene standards from 8000 to 90,000. FT-IR spectra were obtained from IR Affinity-1 FTIR-8400S instrument (Shimadzu Co.) using the attenuated total reflection (ATR) method (ZnSe crystal). UV-Vis absorption spectra were measured on a Hewlett-Packard 8452A diode array spectrophotometer, and photoluminescence were measured using a Shimadzu RF-5301PC spectrofluorophotometer. Fluorescence quantum yields for solution were determined using quinine sulfate in 1N H_2SO_4 (φ_{fl} ~0.55) as the standard. Thermal analysis was performed on Perkin Elmer DSC 8000 and on Shimadzu TGA-60 at the heating rate of 10°C/min. A Voyager DE Pro (Perceptive Biosystems/ABI) MALDI-TOF mass spectrometer was used for mass measurement, operating in both linear and reflector mode. Dithranol (1, 8-dihydroxyanthrone) was used as the matrix in all the measurements except for the highest molecular weight P3AT. In this case terthiophene was the matrix of choice. A solution of highest molecular weight P3AT (5mg/mL) in THF and a solution of terthiophene matrix (75mg/mL) in THF were mixed in a ratio of 1:10. A current sensing AFM (CSAFM) produced by Molecular Imaging Corporation was used for the AFM study. The measurements were done on contact mode. The voltage was usually set at 0.5 V and the intensity of the laser was 1mW at 670 nm.

Sample Preparation for AFM on ITO glass. The ITO glass was cleaned by sonication in detergent followed by water, acetone and isopropanol and subsequently dried in an oven overnight. One mg of each of the polymer samples was dissolved separately in 1mL of chloroform and toluene solution inside a glovebox. The hybrid DCPs were heated at 50° C to get them dissolve in toluene. The solutions were filtered through 0.45 μm PTFE filter prior to spin coating on ITO glasses at spin rates of 500 rpm. All the films were dried in a vacuum oven overnight. The diblock copolymers were thermally annealed at 170° C for 6 h and the hybrid diblocks were annealed at 120 °C for 6 h.

Femtosecond time-resolved fluorescence measurements. Time-resolved fluorescence measurements for PS-Mo-PT(**1–3**) in solution were carried out by using a femtosecond fluorescence upconversion (FFU) technique [1–2]. The solutions were prepared with anhydrous, deoxygenated $CHCl_3$ at a concentration of ~0.48 mg/mL for PS-Mo-PT**1**, ~0.53 mg/mL for PS-Mo-PT**2**, and ~0.54 mg/mL for PS-Mo-PT**3**. The FFU system used in this work is a FOG 100 system (CDP, Russia) with a mode-locked Ti:sapphire laser (Tsunami, Spectra Physics) light source pumped by a 10-W CW Nd:YVO_4 laser (Millennia, Spectra-Physics). Briefly, the samples were excited by the second harmonic light (400 nm) generated by doubling a fundamental light at wavelength of ~800 nm from the mode-locked Ti-sapphire laser with a pulse width of ~57 fs and a pulse repetition rate of 86 MHz, through a β-barium borate nonlinear crystal. The output spectrum of the laser radiation was monitored with a spectrum analyzer (Ocean Optics), to ensure pure mode-locking regime of the femtosecond

laser. The polarization of the excitation beam for anisotropy measurements was controlled by a Berek's plate. The sample was rotated to avoid possible photo-degradation and other accumulative effects. The fluorescence emitted from the sample was collected with an achromatic lens and then directed onto another β-barium borate nonlinear crystal. The fundamental light passed through a motorized optical delay line and then mixed with the sample emission in the nonlinear crystal to generate a sum frequency light. The sum frequency light was dispersed by a monochromator and detected via a photomultiplier tube (Hamamatsu R1527P). The instrument response function (IRF) was estimated to be ~255 fs (full-width at half maximum, FWHM). Fluorescence anisotropy (γ) can be given by the equation:

$$\gamma = (F_{par} - G \cdot F_{per}) / (F_{par +} 2G \cdot F_{per}), \quad (1)$$

where F_{par} and F_{per} are the fluorescence intensity for the parallel and perpendicular polarization, respectively; G factor was calibrated by measuring the polarized fluorescence decay of perylene in toluene, which gives equal polarized fluorescence intensity after a complete rotation diffusion in tens of picoseconds.

The fluorescence data were fitted with a multi-exponential decay/rise model, in which the fluorescence (or anisotropy) signal $F(t)$ can be theoretically expressed by convolution of the IRF $r(t)$ with a molecule-response function $f(\tau)$,

$$F(t) = \int_0^\infty r(t-\tau) f(\tau) d\tau \quad (2)$$

where $r(t)$ is a Gaussian function with laser pulse width and $f(\tau)$is given by:

$$f(\tau) = \sum_i A_i \exp\left(-\frac{\tau}{\tau_i}\right) \quad (3)$$

where the factor *A* represents the relative weights (or amplitudes) of the corresponding components, whose sign can distinguish rising or decay process; τ is the rising or decay time constant.

Photovoltaic device fabrication and characterization. Indium tin oxide (ITO) pre-coated glass with a sheet resistance of 8–12 Ω/square was purchased from Delta Technologies. The ITO glass was cut into one inch by one inch pieces, and the ITO was patterned into 1.4 cm wide and 1 inch long rectangle in the middle by etching with aqua regia vapour. The ITO glass substrates were then cleaned in an ultrasonic bath sequentially by hot detergent, hot deionized (DI) water, toluene, acetone, and isopropyl alcohol (IPA), each for 15 minutes, and then dried in nitrogen stream. A 150-160 nm thick ZnO seed layer was deposited onto the ITO substrate by sputtering. ZnO nanorod arrays were grown on the ZnO seed layer by hydrothermal reaction in an aqueous precursor solution of $Zn(NO_3)_2 \cdot 6H_2O$ (0.05 M) and hexamethylenetetramine (0.05 M) heated at 90°C and stirred at 500 rotations per minute (RPM) for 2 h.[177] The ZnO nanorods were rinsed with DI water and IPA and dried in nitrogen stream. Solutions of PS-Mo-PT(**1–3**) for solar cell device fabrication were prepared by dissolving the diblock copolymer in $CHCl_3$ at 5 mg/mL and 20 mg/mL followed by ultrasonication for 20 s. Right before use, the solutions were filtered to remove the undissolved large particles. The substrates with ZnO nanorods were heated to 80°C, immediately immersed into the 5 mg/mL diblock copolymer

solution for 5 min, taken out and dried with N_2 blowing. Then the 20 mg/mL diblock copolymer solution was spin coated on the above films at 600-800 rpm for 40 s. The films were annealed at 120°C in air for 10 min. Subsequently, a 150 nm thick Au contact was deposited on the top of the diblock copolymer film by thermal evaporation in high vacuum (< 5×10^{-6} mbar). The active area of 0.36 cm^2 of the devices was defined by the area of deposited Au electrode through shadow mask.

Current-voltage characteristics were measured using an Agilent 4155C semiconductor parameter analyzer. Devices were illuminated with an Oriel Xenon Arc Lamp Solar Simulator with an AM1.5 filter at an intensity of ~100 mW/cm^2 (1-sun air mass 1.5 global illumination), which was calibrated with a Hamamatsu mono-crystalline Si cell standardized by National Renewable Energy Laboratory (NREL). Short circuit current density (J_{SC}), open circuit voltage (V_{OC}), and fill factor (FF) were obtained from the *J*–*V* curves. The conversion efficiency was calculated by $\eta = J_{SC}V_{OC}FF/P_{in}$, where P_{in} is the incident power density; and FF is given by $J_{max}V_{max}/J_{SC}V_{OC}$, where $J_{max}V_{max}$ is the maximum output power density of solar cell.

Synthesis of HT-PATs by GRIM. PT1. 2, 5-dibromo-3-hexylthiophene (3.00 g, 9.19 mmol) (14) was dissolved in 10 mL freshly distilled THF and stirred under nitrogen protection. Then tert-butylmagnesium chloride (1.0M solution in THF) (9.51 mL, 9.19 mmol) was added to it through a pump-purged syringe and stirred the solution for 2 h at room temperature. The reaction mixture was then diluted with 100 mL of THF followed by addition of Ni(dppp)Cl_2 (0.095 g, 0.190 mmol, 2.10 mol %) and the red colored solution was stirred for 30 min at room temperature. After that the resulting polymer was

capped at one end of the chain with one shot addition of ethynylmagnesium bromide (0.5 M solution in THF) (9.19 mL, 4.60 mmol) and the solution was stirred for additional 15 min at room temperature. The reaction was quenched with 300 mL of methanol. Soxhlet extractions were performed with methanol (to remove monomer), followed by hexanes (to remove catalyst and oligomers) and finally chloroform. The chloroform fraction was concentrated and dried under vacuum to afford 1.2 g (78% yield) dark violet polymer. ^{1}H NMR (400 MHz, $CDCl_3$, 25° C): δ 6.96 (br), 3.51 (br), 2.78 (br), 1.69 (br), 1.42 (br), 1.33 (br), 0.89 (br). ^{13}C NMR ($CDCl_3$, 400 MHz): δ 139.88, 133.68, 130.47, 128.59, 31.71, 30.52, 29.47, 29.28, 22.67, 14.15. Anal. Calcd. For $C_{252}H_{351}S_{25}Br$: C, 71.01; H, 8.30. Found: C, 70.35; H, 8.26. GPC: M_n=6634, PDI=1.10. MALDI MS: M_n=4230, PDI=1.04.

PT2. The exact same procedure as for PT1 was adopted except that the Ni(dppp)Cl_2 catalyst (0.083 g, 0.156 mmol) loading was decreased to 1.70 mol%. The resulting dark violet colored polymer was obtained in 80% yield (1.24 g). ^{1}H NMR (400 MHz, $CDCl_3$, 25° C): δ 6.96 (br), 3.51 (br), 2.78 (br), 1.69 (br), 1.42 (br), 1.33 (br), 0.89 (br). ^{13}C NMR ($CDCl_3$, 400 MHz): δ 139.88, 133.68, 130.47, 128.59, 31.71, 30.52, 29.47, 29.28, 22.67, 14.15. Anal. Calcd. For $C_{372}H_{519}S_{37}Br$: C, 71.39; H, 8.36. Found: C, 71.10; H, 8.11. GPC: M_n=8810, PDI=1.2. MALDI MS: M_n=6244, PDI=1.05.

PT3. The exact same procedure as for PT1 was adopted except that the Ni(dppp)Cl_2 catalyst (0.035 g, 0.06 mmol) loading was further decreased to 0.70 mol%. The resulting dark violet colored polymer was obtained in 72% yield (1.10 g). ^{1}H NMR (400 MHz, $CDCl_3$, 25° C): δ 6.96 (br), 3.51 (br), 2.78 (br), 1.69 (br), 1.42 (br), 1.33 (br), 0.89 (br). ^{13}C NMR ($CDCl_3$, 400 MHz): δ 139.88, 133.68, 130.47, 128.59, 31.69, 30.51,

29.46, 29.26, 22.66, 14.13. Anal. Calcd. For $C_{842}H_{1177}S_{84}Br$: C, 71.85; H, 8.43. Found: C, 70.04; H, 8.20. GPC: M_n=16150, PDI=1.2. MALDI MS: M_n=14019, PDI=1.01.

Representative synthetic procedure of PS-PT by click chemistry. PS-PT1. PS-N3 (0.22 g, 0.05 mmol) and CuBr (0.007 g, 0.05 mmol) were charged to a two-neck flask. The flask was then evacuated and backfilled with nitrogen three times. PMDETA (10.5 μL, 0.05 mmol) and freshly distilled THF (5 mL) were added to the above solution. To the resulting yellow colored homogenous solution was added dropwise a THF solution of PT1 (0.1 g, 0.025mmol in 5 mL THF).The resulting red solution was stirred at 60°C for 48h. The reaction mixture was then filtered through neutral alumina to remove the copper catalyst. The solution was concentrated and precipitated into methanol (100 mL). The crude red solid was collected by vacuum filtration and washed with acetone to remove excess PS-N3. The red solid polymer was dried under vacuum at 50°C. (0.150 g, 75%). ^{1}H NMR (400 MHz, $CDCl_3$, 25° C): δ 7.80 (br), 7.71 (br), 6.96 (br), 6.70 (br), 2.78 (br), 2.05 (br), 1.67 (br), 1.42 (br), 1.33 (br), 0.89 (br). ^{13}C NMR ($CDCl_3$, 400 MHz): δ 139.87, 133.66, 130.45, 128.58, 123.45, 31.69, 30.50, 29.46, 29.26, 22.65, 14.13. Anal. Calcd. For $C_{580}H_{628}S_{25}N_{21}O_{38}Br$: C, 74.24; H, 6.75; N, 3.13. Found: C, 71.01; H, 7.25; N, 1.98. GPC: M_n=8396, PDI=1.3.

PS-PT2. Red solid polymer yielded (0.120 g, 83%). ^{1}H NMR (400 MHz, $CDCl_3$, 25° C): δ 7.80 (br), 7.71 (br), 6.96 (br), 6.70 (br), 2.78 (br), 2.05 (br), 1.67 (br), 1.42 (br), 1.33 (br), 0.89 (br). ^{13}C NMR ($CDCl_3$, 400 MHz): δ 139.87, 133.66, 130.45, 128.58, 123.45, 31.69, 30.50, 29.46, 29.26, 22.65, 14.13. Anal. Calcd. For $C_{700}H_{796}S_{37}N_{21}O_{38}Br$: C, 73.88; H, 7.05; N, 2.59. Found: C, 71.49; H, 7.30; N, 1.26. GPC: M_n=10550, PDI=1.3.

PS-PT3. Red solid polymer obtained (0.100 g, 77%). ^{1}H NMR (400 MHz, $CDCl_3$, 25° C): δ 7.80 (br), 7.71 (br), 6.96 (br), 6.70 (br), 2.78 (br), 2.05 (br), 1.67 (br), 1.42 (br), 1.33 (br), 0.89 (br). ^{13}C NMR ($CDCl_3$, 400 MHz): δ 139.87, 133.66, 130.45, 128.58, 123.45, 31.69, 30.50, 29.46, 29.26, 22.65, 14.13. Anal. Calcd. For $C_{1170}H_{1454}S_{84}N_{21}O_{38}Br$: C, 73.21; H, 7.64; N, 1.53. Found: C, 70.20; H, 7.56; N, 1.01. GPC: M_n=18798, PDI=1.3.

Representative synthetic procedure for deprotection of phthalimide group. PS2-PT1. PS-PT1 diblock copolymer (0.050 g) was dissolved in freshly distilled THF in a two neck flask. Then excess of hydrazine monohydrate was added to the red solution with constant stirring and the reaction mixture was refluxed for overnight under nitrogen protection. The resulting solution was cooled to room temperature and the reddish white precipitate was filtered off. The red colored filtrate was stripped off the solvent and precipitated from methanol to yield a dark violet colored powder. (0.040 g). ^{1}H NMR (400 MHz, $CDCl_3$, 25° C): δ 6.96 (br), 6.29 (br), 2.78 (br), 2.03 (br), 1.67 (br), 1.42 (br), 1.33 (br), 0.89 (br).

PS2-PT2. Dark violet colored solid obtained. (0.065 g). ^{1}H NMR (400 MHz, $CDCl_3$, 25° C): δ 6.96 (br), 6.29 (br), 2.78 (br), 2.03 (br), 1.67 (br), 1.42 (br), 1.33 (br), 0.89 (br).

PS2-PT3. Dark violet colored solid obtained. (0.030 g). ^{1}H NMR (400 MHz, $CDCl_3$, 25° C): δ 6.96 (br), 6.29 (br), 2.78 (br), 2.03 (br), 1.67 (br), 1.42 (br), 1.33 (br), 0.89 (br).

General synthetic procedure for hybrid DCP. PS-Mo_6-PT1. In a two-neck flask were added deprotected DCP (0.030 g) and DCC (0.17 g, 0.824

mmol). The flask was degassed and backfilled with nitrogen. Then hexamolybdate cluster $[Mo_6O_{19}]^{2-}$. $2N(C_4H_9)_4^+$ (1.00 g, 0.733 mmol) dissolved in nitrobenzene was added to the reaction vessel and the reaction mixture was stirred at 125° C for 5 h. The reaction mixture turned to brownish red color. The resulting solution was cooled to room temperature. Dark violet solid precipitated out which was filtered and washed thoroughly with chloroform to get rid of byproduct urea. The chloroform filtrate was stripped off the solvent and the resulting solid was washed with hot acetonitrile to get rid of any remaining free cluster. The hybrid DCP thus formed is brown solid. (0.10 g). ^{1}H NMR (400 MHz, $CDCl_3$, 25° C): δ 6.96 (br), 4.03 (br), 3.45 (br), 3.30 (br), 2.78 (br), 2.16 (br), 1.91 (br), 1.66 (br), 1.57 (br), 1.35 (br), 1.07 (br), 0.97 (br). Molybdenum content: 33.45%

PS-Mo_6-PT2. Brown solid powder formed. (0.12 g). ^{1}H NMR (400 MHz, $CDCl_3$, 25° C): δ 6.96 (br), 4.03 (br), 3.45 (br), 3.30 (br), 2.78 (br), 2.16 (br), 1.91 (br), 1.66 (br), 1.57 (br), 1.35 (br), 1.07 (br), 0.97 (br). Molybdenum content: 29.13%

PS-Mo_6-PT3. Brown solid powder obtained. (0.15 g). ^{1}H NMR (400 MHz, $CDCl_3$, 25° C): δ 6.96 (br), 4.03 (br), 3.45 (br), 3.30 (br), 2.78 (br), 2.16 (br), 1.91 (br), 1.66 (br), 1.57 (br), 1.35 (br), 1.07 (br), 0.97 (br). Molybdenum content: 6.29%

REFERENCES

1. a) Whitesides, G. M.; Grzybowski, B. *Science* **200**2, *295*, 2418. b) Hamley, I. W. The Physics of Block Copolymers; Oxford University Press, Inc.: New York, 1998. c) Hadjichristidis, N.; Pitsikalis, M.; Iatrou, H. *Adv. Polym. Sci*. **200**5, *189*, 1.
2. Krausch, G.; Magerle, R. *Adv. Mater*. **2002**, *14*, 1579.
3. a) Fredrickson, G. H.; Bates, F. S. *Annual Rev. Mater. Sci*. **1996**, *26*, 501. b) Floudas, G.; Vazaiou, B.; Schipper, F.; Ulrich, R.; Wiesner, U.; Iatrou, H.; Hadjichristidis, N. *Macromolecules* **2001**, *34*, 2947. c) Khandpur, A. K.; Foerster, S.; Bates, F. S.; Hamley, I. W.; Ryan, A. J.; Bras, W.; Almdal, K.; Mortensen, K. *Macromolecules* **1995**, *28*, 8796. d) Matsen, M. W.; Bates, F. S. *Macromolecules* **1996**, *29*, 1091. e) Simon, P. F. W.; Ulrich, R.; Spiess, H. W.; Wiesner, U. *Chem. Mater*. **2001**, *13*, 3464. f) Choucair, A.; Eisenberg, A. *Eur. Phys. J. E*. **2003**, *10*, 37. g) Stewart, S.; Liu, G. *Angew. Chem. Int. Ed*. **2009**, *39*, 340. h) Jain, S.; Bates, F. S. *Science* **2003**, *300*, 460. i) Li, Z.; Kesselman, E.; Talmon, Y.; Hillmyer, M. A.; Lodge, T. P. *Science* **2004**, *306*, 98. j) Pochan, D. J.; Chen, Z. Y.; Cui, H. G.; Hales, K.; Qi, K.; Wooley, K. L. *Science* **2004**, *306*, 94. k) Spatz, J. P.; Moessmer, S.; Moller, M. *Angew. Chem. Int. Ed. Engl*. **1996**, *35*, 1510.
4. Klok, H-A.; Lecommandoux, S. *Adv. Mater*. **2001**, *13*, 1217.

5. Segalman, R. A. *Mater. Sci. Eng*. **2005**, *R 48*, 191.

6. a) Li, C. Y.; Tenneti, K. K.; Zhang, H.; Wan, X.; Chen, E.; Zhou, Q.; Carlos, A.; Igos, S.; Hsiao, B. S. *Macromolecules* **2004**, *37*, 2854. b) Chochos, C. L.; Tsolakis, P. K.; Gregoriou, V. G.; Kallitsis, J. K. *Macromolecules* **2004**, *37*, 2502. c) Tu, Y.; Wan, X.; Zhang, H.; Fan, X.; Chen, X.; Zhou, Q.; Chau, K. *Macromolecules* **2003**, *36*, 6565.

7. Sary, N.; Mezzenga, R.; Brochon, C.; Hadziioannou, G.; Ruokolainen, J. *Macromolecules* **2007**, *40*, 3277.

8. Olsen, B. D.; Segalman, R. A. *Mater. Sci. Eng*. **2008**, *R 62*, 37.

9. a) Mao, G.; Ober, C. K. *Handbook of Liquid Crystals* b) Demus, D.; Goodby, J.; Gray, G. W.; Spiess, H. W.; Vill, V.; Eds.; Wiley-VCH: Weinheim, 1998, Vol. 3, pp 66.

10. Olsen, B. D.; Segalman, R. A. *Macromolecules* **2006**, *39*, 7078.

11. Hoeben, F. J. M.; Jonkheijm, P.; Meijer, E. W.; Schenning, A. P. H. *Chem. Rev*. **2005**, *105*, 1491.

12. a) Gallot, B. *Prog. Polym. Sci*. **1996**, *21*, 1035. b) Teneti, K. K.; Chen, X.; Li, C. Y.; Tu, Y.; Wan, X.; Zhou, Q-F.; Sics, I.; Hsiao, B. S. *J. Am. Chem. Soc*. **2005**, *127*, 15481.

13. a) Skotheim, T. A.; Ed. *Handbook of Conducting Polymers*; Marcel Dekker, Inc.: New York, 1986; Vols. 1 and 2. b) Skotheim, T. A.; Ed. *Electroresponsive Molecular and Polymeric Systems*; Marcel Dekker, Inc.: New York, 1991: Vol. 2. c) Kiess, H. G.; Ed. *Conjugated Conducting*

Polymers: Springer Series in Solid State Science: Springer-Verlag: Berlin, 1992: p 102.

14. a) Tew, G. N.; Pralle, M. U.; Stupp, S. I. *Angew. Chem. Int. Ed*. **2000**, *39*, 517. b) Tew, G. N.; Pralle, M. U.; Stupp, S. I. *J. Am. Chem. Soc*. **1999**, *121*, 9852. c) Schneider, A.; Zanna, J.; Yamada, M.; Findelmann, H.; Thomann, R. *Macromolecules* **2000**, *33*, 649.
15. Shah, M.; Ganesan, V. *Macromolecules* **2010**, *43*, 543.
16. a) Pope, M. T. Heteropoly and Isopoly Oxometalates: Springer-Verlag: New York, NY, 1983. b) Pope, M. T.; Muller, A. *Angew. Chem. Int. Ed. Engl*. **1991**, *30*, 34. c) Polyoxometalates: From Platonic Solids to Anti-Retroviral Activity: Pope, M. T.; Muller, A.; Eds.; Kluwer Academic Publishers: Dordrecht, The Netherlands, 1994, p. 113. d) Cotton, F. A.; Wilkinson, G.; Murillo, C. A.; Bochman, M. Advanced Inorganic Chemistry; John Wiley & Sons. Inc.: New York, NY, 1999. e) Hill, C. L.; Guest Editor; *Chem. Rev*. **1998**, *98*, 1. f) Long, D-L.; Burkholder, E.; Cronin, L. *Chem. Soc. Rev*. **2007**, *36*, 105.
17. Katsoulis, D. E. *Chem. Rev*. **1998**, *98*, 359.
18. a) Rhule, J. T.; Hill, C. L.; Judd, D. A. *Chem. Rev*. **1998**, *98*, 327. b) Gouzerh, P.; Proust, A. *Chem. Rev*. **1998**, *98*, 77.
19. Jeannin, Y. P. *Chem. Rev*. **1998**, *98*, 51.
20. Hubbard, D. J.; Johnston, A. R.; Casalongue, H. S.; Sarjeant, A. N.; Norquist, A. J. *Inorg. Chem*. **2008**, *47*, 8518.

21. Strong, J. B.; Yap, G. P. A.; Ostrander, R.; Liable-Sands, L. M.; Rheingold, A. L.; Thouvenot, R.; Gouzerh, P.; Matta, E. A. *J. Am. Chem. Soc*. **2000**, *122*, 639.

22. Li, J.; *J. Clust. Sci*. **2002**, *13*, 137.

23. Hirsch, A. *Synthesis* **1995**, 895.

24. Bridgeman, A. J.; Cavigliasso, G. *Inorg. Chem*. **2002**, *41*, 1761.

25. a) Peng, Z. *Angew. Chem. Int. Ed*. **2004**, *43*, 930. b) Li, Q.; Wu, P.; Wei, Y.; Xia, Y.; Wang, Y.; Guo, H. *Z. Anorg. Allg. Chem.* **2005**, *631*, 773. c) Kang, J.; Bubin, X.; Peng, Z.; Zhu, X.; Wei, Y.; Powell, D. R. *Angew. Chem. Int. Ed*. **2005**, *44*, 6902. d) Li, Q.; Wei, Y.; Guo, H.; Zhan, C-G. *Inorg. Chim. Acta* **2008**, *361*, 2305.

26. a) Gouzerh, P.; Jeannin, Y.; Proust, A.; Robert, F. *Angew. Chem*. **1989**, *101*, 1377; *Angew. Chem. Int. Ed. Engl*. **1989**, *28*, 1363. b) Proust, A.; Thouvenot, R.; Robert, F.; Gouzerh, P. *Inorg. Chem*. **1993**, *32*, 5299.

27. Bank, S.; Liu, S.; Shaikh, S. N.; Sun, X.; Zubieta, J.; Ellis, P. D. *Inorg. Chem*. **1988**, *27*, 3535.

28. Proust, A.; Thouvenot, R.; Herson, P. *J. Chem. Soc. Dalton Trans*. **1999**, 51.

29. Kwen, H.; Young, Jr. V. G.; Matta, E. A. *Angew. Chem*. **1999**, *111*, 1215; *Angew. Chem. Int. Ed*. **1999**, *38*, 1145.

30. Du, Y.; Rheingold, A. L.; Matta, E. A. *J. Am. Chem. Soc*. **1992**, *114*, 346.

31. Proust, A.; Thouvenot, R.; Chaussade, M.; Robert, F.; Gouzerh, P. *Inorg. Chim. Acta* **1994**, *224*, 81.

32. Stark, J. L.; Young, Jr. V. G.; Matta, E. A. *Angew. Chem*. **1995**, *107*, 2751; *Angew. Chem. Int. Ed. Engl*. **1995**, *34*, 2547.

33. Stark, J. L.; Rheingold, A. L.; Matta, E. A. *J. Chem. Soc. Chem. Commun*. **1995**, 1165.

34. Clegg, W.; Errington, R. J.; Fraser, K.; Holmes, S. A.; Schafer, A. *J. Chem. Soc. Chem. Commun*. **1995**, 455.

35. Wei, Y.; Xu, B.; Barnes, C. L.; Peng, Z. *J. Am. Chem. Soc*. **2001**, *123*, 4083.

36. Roesner, R. A.; McGrath, S. C.; Brockman, J. T.; Moll, J. D.; West, D. X.; Swearingen, J. K.; Castineiras, A. *Inorg. Chim. Acta* **2003**, *342*, 37.

37. a) Ribot, F.; Banse, F.; Sanchez, C.; Lahcini, M.; Jousseaume, B. *J. Sol-Gel Sci. Technol*. **1997**, *8*, 529. b) Foerster, S.; Antonietti, M. *Adv. Mater*. **1998**, *10*, 195. c) Watson, K. J.; Zhu, J.; Nguyen, S. T.; Mirkin, C. A. *J. Am. Chem. Soc*. **1999**, *121*, 462. d) Okumura, A.; Tsutsumi, K.; Hashimoto, T. *Polym. J*. **2000**, *32*, 520. e) Pyun, J.; Matyjaszewski, K.; Kowalewski, T.; Savin, D.; Patterson, G.; Kickelbick, G.; Huesing, N. J. Am. Chem. Soc. 2001, 123, 9445. f) Matsuura, Y.; Matsukawa, K.; Kawabata, R.; Higashi, N.; Niwa, M.; Inoue, H. *Polymer* **2002**, *43*, 1549. g) Gratt, J. A.; Cohen, R. E. *J. Appl. Polym. Sci*. **2004**, *88*, 177. h) Koh, K.; Ohno, K.; Tsujii, Y.; Fukuda, T. *Angew. Chem. Int. Ed*. **2003**, *42*,

4194. i) Laruelle, G.; Parvole, J.; Francois, J.; Billon, L. *Polymer* **2004**, *45*, 5013. j) Ro, H. W.; Kim, K. J.; Theato, P.; Gidley, D. W.; Yoon, D. Y. *Macromolecules* **2005**, *38*, 1031. k) Chen, Y.; Du, J.; Xiong, M.; Zhang, K.; Zhu, H. *Macromol. Rapid Commun*. **2006**, *27*, 741. l) Stone, D. A.; Allcock, H. A. *Macromolecules* **2006**, *39*, 4935. m) Zhou, J.; Wang, L.; Dong, X.; Chen, T.; Yang, Q.; Chen. C.; Chen, X. *Nanotechnology* **2006**, *17*, 2745. n) Zhang, L.; Abbenhuis, H. C. L.; Yang, Q.; Wang, Y. M.; Magusin, P. C. C. M.; Mezari, B.; VanSanten, R. A.; Li, C. *Angew. Chem. Int. Ed.* **2007**, *46*, 5003. o) Masuda, T.; Yamamoto, S.; Moriya, O.; Kashio, M.; Sugizaki, T. *Polym. J*. **2008**, *40*, 126. p) Hirai, T.; Leolukman, M.; Hayakawa, T.; Kakimoto, M.; Gopalan, P. *Macromolecules* **2008**, *41*, 4558. q) Liao, C. C.; Wu, H. Y.; Saikia, D.; Pan, Y. C.; Chen, Y. K.; Fey, G. T. K.; Kao, H. M. *Macromolecule*s **2008**, *41*, 8956. r) Zhang, K.; Gao, L.; Chen, Y. *Macromolecules* **2008**, *41*, 1800. s) Zhang, W.; Zhuang, X.; Li, X.; Lin, Y.; Bai, J.; Chen, Y. *React. Funct. Polym*. **2009**, *69*, 124. t) Monge, S.; Zhang, X.; Giani, O.; Robin, J. J. *React. Funct. Polym*. **2009**, *69*, 380.

38. a) Manners, I. *Chem. Commun*. **1999**, 857. b) Manners, I. *Science* **2001**, *294*, 1664. c) Wang, X.; Winnik, M. A.; Manners, I. *Macromolecules* **2005**, *38*, 1928.

39. a) Hou, S.; Man, K. Y. K.; Chan, W. K. *Langmuir* **2003**, *19*, 2485. b) Cheng, K. W.; Chan, W. K. *Langmuir* **2005**, *21*, 5247.

40. Gohy, J. F.; Lohmeijer, B. G. G.; Varshney, S. K.; Schubert, U. S. *Macromolecules* **2002**, *35*, 7427.

41. Lammertink, R. G. H.; Hempenius, M. A.; Thomas, E. L.; Vancso, G. J. *J. Polym. Sci. Part B: Polym. Phys*. **1999**, *37*, 1009.

42. a) Shimidzu, T.; Ohtani, A.; Aiba, M.; Honda, K. *J. Am. Chem. Soc., Faraday Trans*. **1988**, *84*, 3941. b) Bidan, G.; Genies, E. M.; Lapkowski, M. *J. Chem. Soc., Chem. Commun*. **1988**, 533. c) Fabre, B.; Bidan, G.; Laplowski, M. *J. Chem. Soc. Chem., Chen. Commun*. **1994**, 1509. d) Gomez-Romero, P.; Lira-Cantu, M. *Adv. Mater*. **1997**, *9*, 144. e) Otero, T. F.; Cheng, S. A.; Huerta, C. F. *J. Phys. Chem. B* **2000**, *104*, 10522. f) Otero, T.F.; Cheng, S. A.; Alonso, D.; Huerta, F. *J. Phys. Chem. B*. **2000**, *104*, 10528. g) Cheng, S. A.; Otero, T. F.; Coronado, E.; Gomez-Garcia, C. J.; Martinez-Ferrero, E.; Gimenez-Saiz, C. *J. Phys. Chem. B* **2002**, *106*, 7585.

43. Liu, S.; Kurth, D. G.; Bredenkotter, B.; Volkmer, D. *J. Am. Chem. Soc*. **2002**, *124*, 12279.

44. Judeinstein, P. *Chem. Mater*. **1992**, *4*, 4.

45. Mayer, C. R.; Thouvenot, R.; Lalot, T. *Chem. Mater*. **2000**, *12*, 257.

46. a) Schroden, R. C.; Blanford, C. F.; Melde, B. J.; Johnson, B. J. S.; Stein, A. *Chem. Mater*. *2001*, **13**, 1074. b) Johnson, B. J. S.; Stein, A. *Inorg. Chem*. **2001**, *40*, 801.

47. Moore, A. R.; Kwen, H.; Beatty, A. M.; Matta, E. A. *Chem. Commun*. **2000**, *18*, 1793.

48. Favette, S.; Hasenknopf, B.; Vaissermann, J.; Gouzerh, P.; Roux, C. *Chem. Commun*. **2003**, *21*, 2664.

49. Schubert, U. *Chem. Mater*. **2001**, *13*, 3487.

50. Sanchez, C.; de A. A. Soler-Illia, G. J.; Ribot, F.; Lalot, T.; Mayer, C.R.; Cabuil, V. *Chem. Mater*. **2001**, *13*, 3061.

51. Reinoso, S.; Vitoria, P.; Felices, L. S.; Lezama, L.; Gutierrez-Zorrilla, J. M. *Chem.-Eur. J*. **2005**, *11*, 1538.

52. Zhu, Y.; Xiao, Z.; Ge, N.; Wang, N.; Wei, Y.; Wang, Y. *Cryst. Growth Des*. **2006**, *6*, 1620.

53. Szreder, T.; Wishart, J. F.; Dietz, M. L. *J. Phys. Chem. B* **2007**, *111*, 4685.

54. Poulos, A. S.; Constantin, D.; Davidson, P.; Imperor, M.; Pansu, B.; Panine, P.; Nicole, L.; Sanchez, C. *Langmuir* **2008**, *24*, 6285.

55. Zhang, J.; Song, Y. F.; Cronin, L.; Liu, T. *J. Am. Chem. Soc*. **2008**, *130*, 14408.

56. Cao, R. G.; Liu, S. X.; Liu, Y.; Tang, Q. Wang, L.; Xie, L. H.; Su, Z. M. *J. Solid State Chem*. **2009**, *182*, 49.

57. a) Zhu, L.; Zhu, Y.; Meng, X.; Hao, J.; Li, Q.; Wei, Y.; Lin, Y. *Chem.-Eur. J*. **2008**, *14*, 10923. b) Zhu, Y.; Wang, L.; Hao, J.; Xiao, Z.; Wei, Y.; Wang, Y. *Cryst. Growth Des*. **2009**, *9*, 3509. c) Zhu, Y.; Wang, L.; Hao,

J.; Yin, P.; Zhang, J.; Li, Q.; Zhu, L.; Wei, Y. *Chem.-Eur. J.* **2009**, *15*, 3076.

58. Compain, J. D.; Mialane, P.; Dolbecq, A.; Marrot, J.; Proust, A.; Nakatani, K.; Yu, P.; Secheresse, F. S. *Inorg. Chem*. **2009**, *48*, 6222.

59. Tian, A. X.; Ying, J.; Peng, J.; Sha, J. Q.; Su, Z. M.; Pang, H. J.; Zhang, P.P.; Chen, Y.; Zhu, M.; Shen, Y. *Cryst. Growth Des*. **2010**, *10*, 1104.

60. Wang, Y.; Li, W.; Wu, L. *Langmuir* **2009**, *25*, 13194.

61. a) Adamczyk,, L.; Kulesza, P. J.; Miecznikowski, K.; Palys, B.; Chojak, M. Krawczyk, D. *J. Electrochem. Soc*. **2005**, *152*, E98. b) Chen, H.; Xie, L.; Lu, H.; Yang, Y. *J. Mater. Chem*. **2007**, *17*, 1258. c) Han, Y.; Xiao, Y.; Zhang, Z.; Liu, B.; Zheng, P.; He, S.; Wang, W. *Macromolecules* **2009**, *42*, 6543. d) Qi, W.; Wu, L. *Polym. Int*. **2009**, *58*, 1217. e) Kulak, A.; Kokorin, A.; Kulak, T.; Meissner, D. *Proc. Est. Acad. Sci*. **2009**, *58*, 12. f) Schaming, D.; Allain, C.; Farha, R.; Goldmann, M.; Lobstein, S.; Giraudeau, A.; Hasenknopf, B.; Ruhlmann, L. *Langmuir* **2010**, *26*, 5101.

62. a) Lu, M.; Xie, B.; Kang, J. H.; Chen, T.; Yang, Y.; Peng, Z. *Chem. Mater*. **2005**, *17*, 402. b) Xu, B.; Lu, M.; Kang, J.; Wang, G.; Brown, J.; Peng, Z. *Chem. Mater*. **2005**, *17*, 2841.

63. Chun, S. B.; Mather, P. T. *Mater. Res. Soc. Symposium Proc*. **2001**, 661.

64. a) Hayakawa, T.; Seino, M.; Goseki, R.; Hirai, T.; Kikuchi, R.; Kakimoto, M.; Tokita, M.; Yokohama, H.; Horiuchi, S. *Polym. J*. **2006**, *38*, 567. b)

Hirai, T.; Leolukman, M.; Jin, S.; Goseki, R.; Ishida, Y.; Kakimoto, M.; Hayakawa, T.; Ree, M.; Gopalan, P. *Macromolecules* **2009**, *4*2, 8835.

65. a) Cohen, S.; Martien, A.; Hofs, B.; Voets, I. K.; De Keizer, A. *Curr. Opinion in Colloid & Interface Sci*. **2005**, *10*, 30. b) Katsampas, I.; Tsitsiliannis, C. *Macromolecules* **2005**, *38*, 1307. c) Bromberg, L. *Handbook of Polyelectrolytes and their Applications* **2002**, *3*, 23. d) Foerster, S.; Abetz, V.; Mueller, A. H. E. *Advances in Polymer Science* **2004**, *166*, 173. e) Zhang, L.; Barlow, R. J.; Eisenberg, A. *Macromolecules* **1995**, *28*, 6055. f) Guenoun, P.; Muller, F.; Delsanti, M.; Auvray, L.; Chen, Y.; Mayes, J. W.; Tirrell, M. *Phys. Rev. Lett*. **1998**, *81*, 3872. g) Cui, H.; Chen, Z.; Wooley, K. L.; Pochan, D. J. *Macromolecules* **2006**, *39*, 6599.

66. a) Weaver, J. W. M.; Armes, S. P.; Liu, S. *Macromolecules* **2003**, *36*, 9994. b) Solomatin, S. V.; Bronich, T. K.; Eisenberg, A.; Kabanov, V. A.; Kabanov, A. V. *Langmuir* **2004**, *20*, 2066. c) Berret, J. F.; Vigolo, B.; Eng, R.; Herve, P.; Grillo, I.; Yang, L. *Macromolecules* **2004**, *3*7, 4922. d) Pergushov, D. V.; Remizova, E. V.; Gradzielski, M.; Lindner, P.; Feldthusen, J.; Zezin. A. B. *Polymer* **2004**, *4*5, 367.

67. a) Lindner, S. M.; Thelakkat, M. *Macromolecules* **2004**, *37*, 8832. b) Lindner, S. M.; Huettner, S.; Chiche, A.; Thelakkat, M.; Krausch, G. Angew. Chem. Int. Ed. Engl. **2006**, *45*, 3364.

68. Moad, G.; Solomon, D. H. *The Chemistry of Free-Radical Polymerization*;

Pergamon: Oxford, 1995.

69. Webster, O. W. *Science* **1991**, *251*, 887

70. a) Szwarc, M. *Nature* **1956**, *178*, 1168. b) Penczek, S.; Kubisa, P.; Szymanski, R. *Makromol. Chem. Rapid Commun*. **1991**, *12*, 77. c) Quirk, R.P.; Lee, B. *Polym. Int*. **1992**, *27*, 359. d) Matyjaszewski, K. *Macromolecules* **1993**, *26*, 1787.

71. Szwarc, M.; *Carbanions, Living Polymers and Electron Transfer Processes*; Wiley: NewYork, 1968**.**

72. Matyjaszewski, K.; Sawamoto, M. *Cationic Polymerizations: Mechanisms, Synthesis, and Applications*; Marcel Dekker: NewYork, 1996, pp 265-380.

73. a) Matyjaszewski, K.; Gaynor, S.; Greszta, D.; Mardare, T.; Shigemoto, T. *Macromol. Symp*. **1995**, *98*, 73. b) Colombani, D. *Prog. Polym. Sci*. **1997**, *98*, 73. c) Matyjaszewski, K. *In Controlled Radical Polymerization*; Matyjaszewski, K.; Ed.; ACS Symp. 685: American Chemical Society: Washington, DC, 1998; p 258. d) Matyjaszewski, K.; Davis, T. P.; Eds. *Handbook of Radical Polymerization*; Wiley-Interscience: Hoboken, NJ, 2002. e) Matyjaszewski, K.; Ed. *Advances in controlled/Living Radical Polymerization*; ACS Symp. Ser. 854; American Chemical Society: Washington, DC, 2003. f) Matyjaszewski, K. *Chem. Eur. J*. **1999**, *5*, 3095 g) Patten, T. E.; Matyjaszewski, K. *Acc. Chem. Res*. **1999**, *32*, 895.

74. Braunecker, W. A.; Matyjaszewski, K. *Prog. Polym. Sci*. **2007**, *32*, 93-146.

75. a) Wang, J. S.; Matyjaszewski, K. *J. Am. Chem. Soc*. **1995**, *117*, 5614. b) Kato, M.; Kamigaito, M.; Sawamoto, M.; Higashimura, T. *Macromolecules* **1995**, *28*, 1721. c) Percec, V.; Barboiu, B. *Macromolecules* **1995**, *28*, 7970. d) Patten T. E.; Matyjaszewski, K. *Adv. Mater*. **1998**, *10*, 901. e) Coessens, V.; Pintauer, T.; Matyjaszewski, K. *Prog. Polym. Sci*. **2001**, *26*, 337. f) Davis, K. A.; Matyjaszewski, K. *Adv. Polym. Sci*. **2002**, *159*, 2-166. g) Patten, T. E.; Xia, J.; Abernathy, T.; Matyjaszewski, K. *Science* **1996**, *272*, 866.

76. Xia, J.; Matyjaszewski, K. *Macromolecules* **1997**, *30*, 7697.

77. Matyjaszewski, K.; Xia, J. *Chem. Rev*. **2001**, *101*, 2921.

78. a) Fischer, H. *Chem. Rev*. **2001**, *101*, 3581. b) Fukuda, T.; Goto, A.; Ohno, K. *Macromol Rapid Commun*. **2000**, *21*, 151.

79. Matyjaszewski, K. *J. Phys. Org. Chem*. **1995**, *8*, 197.

80. a) Matyjaszewski, K.; *J. Macromol. Sci., Pure Appl. Chem*. **1997**, *A34*, 1785. b) Goto, A.; Fukuda, T. *Macromol. Rapid Commun*. **1999**, *20*, 633.

81. Matyjaszewski, K.; Patten, T. E.; Xia, J. *J. Am. Chem. Soc*.**1997**, *119*, 674.

82. a) Pintauer, T.; Qiu, J.; Kickelbick, G.; Matyjaszewski, K. *Inorg. Chem*. **2001**, *40*, 2818. b) Pintauer, T.; Zhou, P.; Matyjaszewski, K. *J. Am. Chem. Soc*. **2002**, *124*, 8196.

83. Qiu, J.; Matyjaszewski, K. *Macromolecules* **1997**, *30*, 5643.

84. Huang, X.; Wirth, M. J. *Macromolecules* **1999**, *32*, 1694.

85. Matyjaszewski, K.; Jo, S.; Paik, H.; Gaynor, S. G. *Macromolecules* **1997**, *30*, 6398.

86. Wang, J. S.; Matyjaszewski, K. *Macromolecules* **1995**, *28*, 7901.

87. Wang, J. S.; Matyjaszewski, K. *Macromolecules* **1995,** *28***,** 7572.

88. Xia, J.; Zhang, X.; Matyjaszewski, K. *ACS Symp. Ser*. **2000**, *760*, 207.

89. Matyjaszewski, K.; Wei, M.; Xia, J.; McDermott, N. E. *Macromolecules* **1997**, *30*, 8161.

90. Qiu, J.; Matyjaszewski, K.; Thouin, L.; Amatore, C. *Macromol. Chem. Phys*. **2000**, *201*, 1625.

91. a) Davis, K. A.; Paik, H-j.; Matyjaszewski, K. *Macromolecules*, **1999**, *32*, 1767. b) Gaynor, S. G.; Qiu, J.; Matyjaszewski, K. *Macromolecules* **1998**, *31*, 5951. c) Woodworth, B. E.; Metzner, Z.; Matyjaszewski, K. *Macromolecules* **1998**, *31*, 7999. d) Bernhardt, P. V.; *J. Am. Chem. Soc*. **1997**, *119*, 771.

92. Matyjaszewski, K.; Shipp, D. A.; Wang, J. L.; Grimaud, T.; Patten, T. E. *Macromolecules* **1998**, *31*, 6836.

93. a) Coessens, V.; Matyjaszewski, K. *J. Macromol. Sci., Pure Appl. Chem*. **1999**, *A36*, 653. b) Coessens, V.; Matyjaszewski, K. *J. Macromol. Sci., Pure Appl. Chem*. **1999**, *A36*, 811.

94. a) Matyjaszewski, K. *Macromolecules* **1998**, *31*, 4710. b) Lutz, J. F.; Matyjaszewski, K. *J. Polym. Sci., Part A: Polym. Chem*. **2005**, *43*, 897.

95. a) Fuente, J. L. de la; Fernandez-Sanz M.; Fernandez-Garcia, M.; Madruga, E. L. *Macromol. Chem. Phys*. **2001**, *202*, 2565. b) Davis, K. A.; Matyjaszewski, K. *Macromolecules* **2000**, *33*, 4039.

96. Kosynkin, D. V.; Tour, J. M. *Org. Lett*. **2001**, *3*, 991.

97. Gibson, M. S.; Bradshaw, R. W. *Angew. Chem. Int. Ed. Eng*. **1968**, *7*, 920.

98. Chakraborty, S.; Keightley, A.; Dusevich, V.; Wang, Y.; Peng, Z. *Chem. Mater*. **2010**, *22*, 3995.

99. a) van der Maarel, J. R. C.; Groenewegen, W.; Egelhaaf, S. U.; Laap, A. *Langmuir* **2000**, *16*, 7510. b) Groenewegen, W.; Laap, A.; Egelhaaf, S. U.; van der Maarel, J. R. C. *Macromolecules* **2000**, *33*, 4080. c) Dingenouts, N.; Patel, M.; Rosenfeldt, S.; Pontoni, D.; Narayanan, T.; Ballauff, M. *Macromolecules* **2004**, *37*, 8152.

100. Xia, J.; Zhang, X.; Matyjaszewski, K. *Macromolecules* **1999**, *32*, 3531.

101. a) Khan, M. N. *J. Org. Chem*. **1996**, *61*, 8063. b) Meuer, S.; Zentel, R. *Macromol. Chem. Phys*. **2008**, *209*, 158.

102. a) Uegaki, H.; Kotami, Y.; Kamigaito, M.; Sawamoto, M. *Macromolecules* **1997**, *30*, 2249. b) Huang, C. F.; Kuo, S. W.; Chen, J. K.; Chang, F. C. *J. Polym. Res*. **2005**, *12*, 449.

103. Vidts, K. R. M.; Prez, F. E. D. *Eur. Polym. J*. **2006**, *42*, 43.

104. Tsarevsky, N. V.; Braunecker, W. A.; Brooks, S. J.; Matyjaszewski, K. *Macromolecules* **2006**, *39*, 6817.

105. a) Ciampolini, M.; Nardi, N. *Inorg. Chem*. **1966**, *5*, 41. b) Feng, L.; Hu, J.; Liu, Z.; Zhao, F.; Liu, G. *Polymer* **2007**, *48*, 3616.

106. a) Wu, K. H.; Wang, Y. R.; Hwu, W. H. *Polym.Degrad. Stabil*. **2003**, *79*, 195. b) Fu, Y.; Chen, H.; Qiu, D.; Wang, Z.; Zhang, X. *Langmuir* **2002**, *18*, 4989.

107. Li, Q.; Wu, P.; Wei, Y.; Wang, Y.; Wang, P.; Guo, H. *Inorg. Chem. Commun*. **2004**, *7*, 524.

108. Gunes, S.; Neugebauer, H.; Sariciftci, N. S. *Chem. Rev*. 2007, 107, 1324.

109. Tang, C.W. *Appl. Phys. Lett*. 1986, 48, 183.

110. Winder, C.; Sariciftci, N.S. *J. Mater. Chem*. 2004, 14, 1077.

111. a) Yu, G.; Gao, J.; Hummelen, J. C.; Wudl, F.; Heeger, A. J. *Science*, **1995**, *270*, 1789. b) Brabec, C. J.; Sariciftci, N. S.; Hummelen, J. C. *Adv. Funct. Mater*. **2001**, *11*, 15. c) Chidichimo, G.; Filippelli, L. *Int. J. Photoenergy*. **2010**, *123534*, 1.

112. Caokley, K. M.; Mcgehee, M. D. *Chem. Mater*. **2004**, *16*, 4533.

113. Sivula, k.; Ball, Z. T.; Watanabe, N.; Frechet, J. M. J. *Adv. Mater*. **2006**, *18*, 206.

114. a) Lodge, T. P.; Muthukumar, M. *J. Phys. Chem*. **1996**, *100*, 13275 b) Stupp, S. I.; LeBonheur, V.; Walker, K.; Li, L. S.; Huggins, K. E.; Keser, M.; Amstutz, A. *Science*, **1997**, *276*, 384.

115. a) Helfand, E.; Wasserman, Z. R. *In Developments in Block Copolymers-1*; Goodman, I.; Ed.; Applied Science Publishers: New York, 1982;

Chapter 4. b) Bates, F. S.; Fredrickson, G. H. *Annu. Rev. Phys. Chem*. **1990**, *41*, 525. c) Bates, F. S. *Science* **1991**, *251*, 898. d) Stalmach, U.; de Boer, B.; Videlot, C.; van Hutten, P. F.; Hadziioannou, G. J. *Am. Chem. Soc*. **2000**, *122*, 5464.

116. Leclere, P.; Parente, V.; Bredas, J. L.; Francois, B.; Lazzaroni, R. *Chem. Mater*. **1998**, *10*, 4010.

117. a) Sary, N.; Rubatat, L, Brochon, C.; Hadziioannou, G.; Rukokolainen, J.; Mezzenga, R. *Macromolecules* **2007**, *40*, 6990. b) Sary, N.; Mezzenga, R. Brochon, C.; Hadziioannou, G.; Rukokolainen, J. *Macromolecules* **2007**, *40*, 3277.

118. a) De Boer, B.; Stalmach, U.; van Hutten, P. F.; Melzer, C.; Krasnikov, V. V.; Hadziioannou, G. *Polymer* **2001**, *42*, 9097. b) Van der V.; Marleen, H.; De Boer, B.; Stalmach, U.; Van de Wetering, K. I.; Hadziioannou, G. *Macromolecules* **2004**, *37*, 3673. c) Segalman, R. A.; Brochon, C.; Hadziioannou, G.; Sun, S-S.; Sariciftci, N. S.; Eds.; Taylor & Francis: London, 2005; pp. 403.

119. a) Li, W. J.; Wang, H. B.; Yu, L. P.; Morkved, T. L.; Jaeger, H. M. *Macromolecules* **1999**, *32*, 3034. b) Olsen, B. D.; Segalman, R. A. *Macromolecules* **2005**, *38*, 10127.

120. a) Marsitzky, D.; Brand, T.; Geerts, Y.; Klapper, M.; Mullen, K. *Macromol. Rapid Commun*. **1998**, *19*, 385. b) Francke, V.; Rader, H. J.; Geerts, Y.; Mullen, K. *Macromol. Rapid Commun*. **1998**, *19*, 275. c)

Hempenius, M. A.; Langeveld-Voss, B. M. W.; van Haare, J.; Janssen, R. A. J.; Sheiko, S.S.; Spatz, J. P.; Moller, M.; Meijer, E. W. *J. Am. Chem. Soc*. **1998**, *120*, 2798. d) Kukula, H.; Ziener, U.; Schops, M.; Godt, A. *Macromolecules* **1998**, *31*, 5160. e) Wang, H. B.; Wang, H. H.; Urban, V. S.; Littrell, K. C.; Thivagarajan, P.; Yu, L. P. *J. Am. Chem. Soc*. **2000**, *122*, 6855.

121. a) Moliton, A.; Hiorns, R. C. *Polymer International* **2004**, *53*, 1397. b) Coakley, K. M.; McGehee, M. D. *Chem. Mater*. **2004**, *16*, 4533. c) Nguyen, T. P.; Destruel, P. *Handbook of Luminescence, Display Materials, and Devices* **2003**, *1*, 1.

122. a) Kolb, H. C.; Finn, M. G.; Sharpless, K. B. *Angew. Chem. Int. Ed*. **2001**, *40*, 2004. b) Binder, W. H.; Sachsenhofer, R. *Macromol. Rapid Commmun*. **2007**, *28*, 15. c) Meldal, M.; Tomoe, C. W. *Chem. Rev*. **2008**, *108*, 2952. d) Brase, G.; Gil, C.; Knepper, K.; Zimmermann, V. *Angew. Chem. Int. Ed.* **2005**, *44*, 5188.

123. a) Huisgen, R.; Szeimies, G.; Mobius, L. *Chem. Ber*. **1967**, *100*, 2494. b) Gothelf, K. A. Jorgensen, *Chem. Rev. 1998, 98,* 863. d) Padwa, A. *1,3-Dipolar Cycloaddition Chemistry* , Wiley: New York 1984.

124. Boren, B. C.; Narayan, S.; Rasmussen, L. K.; Zhang, L.; Zhao, H.; Lin, Z.; Jia, G.; Fokin, V. V. *J. Am. Chem. Soc*. **2008**, *130*, 8923.

125. a) Laurent, B. A.; Grayson, S. M. *J. Am. Chem. Soc*. **2006**, *128*, 4238. b) Parrish, B.; Breitenkamp, R. B.; Emrick, T. *J. Am. Chem. Soc*. **2005**, *127*,

7404. c) Joralemon, M.; O'Reilly, R. K.; Hawker, C. J.; Wooley, K. L. *J. Am. Chem. Soc*. **2005**, *127*, 16892. d) Sumerlin, B. S.; Tsarevsky, N. V.; Louche, G.; Lee, R. Y.; Matyjaszewski, K. *Macromolecules* **2005**, *38*, 7540. e) Golas, P. L.; Tsarevsky, N. V.; Matyjaszewski, K. *Macromol. Rapid Commun*. **2008**, *29*, 1167. f) Droumaguet, B. L.; Velonia, K. *Macromol. Rapid Commun*. **2008**, *29*, 1073.

126. a) Coessens, V.; Pintauer, T.; Matyjaszewski, K. *Prog. Polym. Sci*. **2001**, *26*, 337. b) Matyjaszewski, K.; Nakgawa, Y.; Gaynor, S. G. *Macromol. Rapid. Commun.* **1997**, *18*, 1057. c) Lutz, J-F.; Borner, H. G.; Weichenhan, K. *Macromol. Rapid. Commun*. **2005**, *26*, 514.

127. Maddux, T.; Li, W.; Yu, L. *J. Am. Chem. Soc*. **1997**, *119*, 844.

128. Kretzschmann, H.; Meier, J. *Tetrahedron Lett*. **1991**, *32*, 5059.

129. Wilson, A. A.; Dannals, R. F.; Ravert, H. T.; Frost, J. J.; Wagner, H. N. *J. Med. Chem*. **1989**, *32*, 1057.

130. Xiao, J.; Li, J.; Li, C.; Huang, C.; Li, Y.; Cui, S.; Wang, S.; Liu, H. *Tetrahedron Lett*. **2008**, *49*, 2656.

131. a) Lee, M.; Cho, B-K.; Zin, W-C. *Chem. Rev*. **2001**, *101*, 3869. b) Jenekhe, S. A.; Chen. X. L. *Science* **1999**, *283*, 372. c) Lin, C. L.; Tung, P. H.; Chang, F. C. *Polymer* **2005**, *46*, 9304.

132. Rayleigh, L. *Nature*, **1911**, *86*, 416. b) Stenzel, M. H.; Kowollik- Barner, C.; Davis, T. P. *J. Polym. Sci. Part A: Polym. Chem*. **2006**, *44*, 2363. c) Bunz, U. H. F. *Adv. Mater*. **2006**, *18*, 973. d) Widawski, G.; Rawiso, M.;

Francois, B. *Nature* **1994**, *369*, 387. e) Srinivasarao, M.; Collings, D.; Philips, A.; Patel, S. *Science* **2001**, *292*, 79.

133. a) Scurlock, R. D.; Wang, B.; Ogliby, P.R.; Sheats, J. R.; Clough, R. L. *J. Am. Chem. Soc.* **1995**, *117*, 10194. b) Genlick, G. H.; Warman, J. M. *Chem. Phys. Lett*. **1997**, *277*, 361. c) Neugebauer, H.; Brabec, C.; Hummelen, J. C.; Sariciftci, N. S. *Sol. Energy Mater. Sol. Cells* **2000**, *61*, 35. d) Moet, D. J. D.; Koster, L. J. A.; Boer, B de; Blom, P. W. M. *Chem. Mater*. **2007**, *19*, 5856.

134. a) Bao, Z.; Dodabalapur, A.; Lovinger, A. *J. Appl. Phys. Lett*. **1996**, *69*, 4108. b) Katz, H. E.; Bao, Z. *J. Phys. Chem. B* **2000**, *104*, 671. c) Hugger, S.; Thomann, R.; Heinzel, T.; Thurn-Albrecht, T. *Colloid Polym. Sci*. **2004**, *282*, 932.

135. a) Yamamoto, T.; Komarudin, D.; Arai, M.; Lee, B.; Suganuma, H.; Asakawa, N.; Inoue, Y.; Kubota, K.; Sasaki, S.; Fukuda, T.; Matsuda, H. *J. Am. Chem. Soc*. **1998**, *120*, 2047.

136. Bao, Z.; Feng, Y.; Dodabalapur, A.; Raju, V. R.; Lovinger, A. J. *Chem. Mater*. **1997**, *9*, 1299.

137. Masubuchi, S.; Kazama, S. *Synth. Met*. **1995**, *74*, 151.

138. a) Bao, Z.; Dodabalapur, A.; Lovinger, A. J. *Appl. Phys. Lett*. **1996**, *69*, 4108. b) Kim, Y.; Cook, S.; Tuladhar, S. M.; Choulis, S.A.; Nelson, J.; Durrant, J.R.; Bradley, D. D.C.; Giles, M.; Mcculloch, I.; Ha, C-S.; Ree, M. *Nature Mater*. **2006**, *5*, 197.

139. a) Liu, J.; Sheina, E.; Kowalewski, T.; McCullough, R. D. *Angew. Chem. Int. Ed.* **2002**, *41*, 329. b) Kline, R. J.; McGehee, M. D.; Kadnikova, E. K.; Liu, J.; Frechet, J. M. J.; Toney, M. F. *Macromolecules* **2005**, *38*, 3312. c) Yang, H.; Shin, T. J.; Yang, L.; Cho, K.; Ryu, C. Y.; Bao, Z. *Adv. Funct. Mater*. **2005**, *15*, 671. d) Kim, D. H.; Park, Y. D.; Jang, Y.; Yang, H.; Kim, Y. H.; Han, J. I.; Moon, D. G.; Park, S.; Chang, T.; Chang, C.; Joo, M.; Ryu, C. Y.; Cho, K. *Adv. Funct. Mater*. **2005**, *1*5, 77. e) Zhang, R.; Li, B.; Iovu, M. C.; Jeffries-El, M.; Sauve, G.; Cooper, J.; Jia, S.; Tristram-Nagle, S.; Smilgies, D. M.; Lambeth, D. N.; McCullough, R. D.; Kowalewski, T. *J. Am. Chem. Soc*. **2006**, *128*, 3480. f) Yang, H.; Shin, T. J.; Bao, Z.; Ryu, C. Y. *J. Polym. Sci., Part B: Polym. Phys.***2007**, *45*, 1303. g) Paudinger, F.; Rittberger, R. S.; Sariciftci, N. S. *Adv. Funct. Mater*. **2003**, *13*, 1. h) Kline, R. J.; McGehee, M. D.; Kadnikova, E. K.; Liu, J.; Frechet, J. M. J. *Adv. Mater*. **2003**, *15*, 1519.

140. a) Jen, K-Y.; Miller, G. G.; Elsenbaumer, R.L. *J. Chem. Soc. Chem. Commun*. **1986**, 1346. b) Elsenbaumer, R. L.; Jen, K-Y.; Oboodi, R. *Synth. Met*. **1986**, *15*, 169.

141. a) Ruiz, J.P.; Gieselman, M. B.; Nayak, K.; Marynick, D.S.; Reynold, J. R. *Synth. Met*. **1989**, *28*, C481. b) Swager, T. M.; Marsella, M. J.; Bicknell, L.K.; Zhou, Q. *Polym. Prepr*. **1994**, *35*, 206. c) Marsella, M.; Carroll, P. J.; Swager, T. M. *J. Am. Chem. Soc*. **1994**, *116*, 9347. d) Bouman, M. M.; Meijer, E. W. *Polym. Prepr*. **1994**, *35*, 309. e) Ikenoue, Y.; Votani, N.;

Patil, A. O.; Wudl, F.; Heeger, A. J. *Synth. Met*. **1989**, *30*, 305. f) Patil, A.O.; Ikenoue, Y.; Wudl, F.; Heeger, A. J. *J. Am. Chem. Soc*. **1987**, *109*, 1858. g) McCullough, R. D.; Williams, S.P. *J. Am. Chem. Soc*. **1993**, *115*, 11608.

142. a) Sato, M.; Morii, H. *Macromolecules* **1991**, *24*, 1196. b) Sato, M.; Morii, H. *Polym. Commun*. **1991**, *32*, 436. c) Barbarella, G.; Bongini, A.; Zambianchi, M. *Macromolecules* **1994**, *27*, 3039.

143. a) Elsenbaumer, R. L.; Jen, K-Y.; Miller, G. G.; Eckhardt, H.; Shacklette, L. W.; Jow, R. *Electronic Properties of Conjugated Polymers*; Kuzmany, H.; Mehring, M.; Roth, S.; Eds.; *Springer Ser. Solid State. Sci*. **1987**, *76*, 400. b) Souto, Maior, R. M.; Hinkelmann, K.; Eckert, H.; Wudl, F. *Macromolecules* **1990**, *23*, 1268. c) Roncali, J. *Chem. Rev*. **1992**, *92*, 711. d) Roncali, J.; Carreau, R.; Yassar, A.; Marque, P.; Garnier, F.; Lemaire, M. *J. Phys. Chem*. **1987**, *91*, 6706. e) Tour, J. M.; Wu, R.; Schumm, J. S. *J. Am. Chem. Soc*. **1991**, *113*, 7064. f) Wei, Y.; Chan, C-C.; Tian, J.; Jang, G-W.; Hsueh, K. F. *Chem. Mater*. **1991**, *3*, 888. g) Mao, H.; Holdcroft, S. *Macromolecules* **1992**, *25*, 554.

144. a) Sato, M.; Tanaka, S.; Kaeriyama, K. *J. Chem. Soc. Chem. Commun*. **1986**, 873. b) Lemaire, M.; Roncali, J.; Garnier, F.; Garreau, R.; Hannecart, E. French Patent 86.04744, April 4, 1986. c) Kaeriyama, K.; Sato, M.; Tanaka, S. *Synth. Met*. **1987**, *18*, 233.

145. a) Yoshino, K.; Nakajima, S.; Onoda, M.; Sugimoto, R. *Synth. Met*. **1989**, *28*, C349. b) Osterholm, J. E.; Laakso, J.; Nyholm, P.; Isotalo, H.; Stubb, H.; Inganas, O.; Salaneck, W. R. *Synth. Met*. **1989**, *28*, C435.

146. a) Yamamoto, T.; Morita, A.; Miyazaki, Y.; Maruyama, T.; Wakayama, H.; Zhou, Z-h.; Nakamura, Y.; Kanbara, T.; Sasaki, S.; Kubota, K. *Macromolecules* **1992**, *25*, 1214.

147. a) McCullough, R. D.; Lowe, R. D. *J. Chem. Soc. Chem. Commun*. **1992**, 70. b) McCullough, R. D.; Lowe, R. D.; Jayaraman, M.; Anderson, D. L. *J. Org. Chem*. **1993**, *58*, 904. c) McCullough, R. D.; Lowe, R. D.; Jayaraman, M.; Ewbank, P. C.; Anderson, D. L.; Tristram-Nagle, S. *Synth. Met*. **1993**, *55*, 1198. d) McCullough, R. D.; Tristram-Nagle, S.; Williams, S. P.; Lowe, R. D.; Jayaraman, M. *J. Am. Chem. Soc*. **1993**, *115*, 4910. e) McCullough, R. D.; Williams, S. P.; Tristram-Nagle, S.; Jayaraman, M.; Ewbank, P. C.; Miller, L. *Synth. Met*. **1995**, *67*, 279.

148. a) Taylor, E. C.; Vogel, D. D. *J. Org. Chem*. **1985**, *50*, 1002. b) Slocum, D. W.; Gierer, P. L.; *J. Org. Chem*. **1976**, *41*, 3668. c) Slocum, D. W.; Gierer, P. L. *J. Chem. Soc. Chem. Commun*. **1977**, 305.

149. Kumada, M. *Pure Appl. Chem*. **1980**, *52*, 669.

150. a) Chen, T-A.; Rieke, R. D. *J. Am. Chem. Soc*. **1992**, *114*, 10087. b) Chen, T-A.; Rieke, R. D. *Synth. Met*. **1993**, *60*, 175. c) Chen, T-A.; O'Brien, R. A.; Rieke, R. D. *Macromolecules* **1993**, *26*, 3462. d) Chen, T-A.; Wu, X.;

Rieke, R. D. *J. Am. Chem. Soc*. **1995**, *117*, 233. e) Wu, X.; Chen, T-A.; Rieke, R. D. *Macromolecules* **1996**, *29*, 7671.

151. Negeshi, E. *Organometallics in Organic Synthesis*; Wiley & Sons: New York, 1980; Vol. 1.

152. a) Stille, J. K. *Angew. Chem. Int. Ed. Engl.* **1986**, *25*, 508. b) Iraqi, A.; Barker, G. W. *J. Mater. Chem*. **1998**, *8*, 25. c) McCullough, R. D.; Ewbank, P. C.; Loewe, R. S. *J. Am. Chem. Soc*. **1997**, *119*, 633.

153. a) Miyaura, N.; Ishiyama, T.; Sasaki, H.; Ishikawa, M.; Satoh, M.; Suzuki, A. *J. Am. Chem. Soc.* **1989**, *111*, 314. b) Guillerez, S.; Bidan, G. *Synth. Met*. **1998**, *93*, 123.

154. a) Loewe, R. S.; Khersonsky, S. K.; McCullough, R. D. *Adv. Mater*. **1999**, *11*, 250. b) Loewe, R. S.; McCullough, R. D. *Polym. Prepr*. **1999**, *40*, 852. c) Loewe, R. S.; Ewbank, P. C.; Liu, J.; Zhai, L.; McCullough, R. D. *Macromolecules* **2001**, *34*, 4324.

155. a) Odian, G. *Principles of Polymerization*, 3rd ed.; Wiley: New York, 1991. b) Yokoyama, A.; Miyakoshi, R.; Yokozawa, T. *Macromolecules* **2004**, *37*, 1169.

156. a) Sheina, E. E.; Liu, J.; Iovu, M. C.; Laird, D. W.; McCullough, R. D. *Macromolecules* **2004**, *37*, 3526. b) Iovu, M. C.; Sheina, E. E.; Gil, R. R.; McCullough, R. D. *Macromolecules* **2005**, *38*, 8649.

157. a) Benn, R.; Mynnot, R.; Topalovic, I.; Scott, F. *Organometallics*, **1989**, *8*, 2290. b) Scott, F.; Kruger, C.; Betz, P. *J. Organomet. Chem*. **1990**, *387*,

113. c) Browning, J.; Green, M.; Penfold, B. R.; Spencer, J. L.; Stone, F. G. A. *J. Chem. Soc. Chem. Commun*. **1973**, 31.

158. a) McCullough, R. D. *Adv. Mater*. **1998**, *10*, 93. b) Zhai. L.; Pilston, R. L.; Zaiger, K. L.; Stokes, K. K.; McCullough, R. D. *Macromolecules* **2003**, *36*, 61. c) Benanti, T. L.; Kalaydjian, A.; Venkataraman, D. *Macromolecules* **2008**, *41*, 8312.

159. a) Liu, J.; McCullough, R. D. *Macromolecules* **2002**, *35*, 8. b) Langeveld-Voss, B. M. W.; Janssen, R. A. J.; Spiering, A. J. H.; van Dongen, J. L. J.; Vonk, E. C.; Claessens, H. A. *Chem. Commun*. **2000**, *2000*, 81. b) Jayakannan, M.; van Dongen, J. L. J.; Janssen, R. A. *Macromolecules* **2001**, *34*, 8.

160. a) Jeffries-El, M.; Sauve, G.; McCullough, R. D. *Adv. Mater*. **2004**, *16*, 1017. b) Jeffries-El, M.; Sauve, G.; McCullough, R. D. *Macromolecules* **2005**, *38*, 10346.

161. a) Tamao, K.; Sumitani, K.; Kiso, Y.; Zembayashi, M.; Fujioka, A.; Kodama, S.-I.; Nakajima, I.; Minato, A.; Kumada, M. *Bull. Chem. Soc. Jpn.* **1976**, *49*, 1958. b) Crabtree, R. H. *The Organometallic Chemistry of the Transition Metals*, 3rd ed.; John Wiley & Sons, New York 2001. c) Tolman, C. A.; Seidel, W. C.; Gosser, L. W. *Organometallics* **1983**, *2*, 1391.

162. Urien, M.; Erothu, H.; Cloutet, E.; Hiorns, R. C.; Vignau, L.; Cramail, H. *Macromolecules* **2008**, *41*, 7033.

163. a) Rader, H. J.; Spickermann, J.; Kreyenschmidt, M.; Mullen, K. *Macromol. Chem. Phys*. **1996**, *197*, 3285. b) Liu, J.; Loewe, R. S.; McCullough, R. D. *Macromolecules* **1999**, *32*, 5777.

164. Miyakoshi, R.; Yokoyama, A.; Yokozawa, T. *Macromol. Rapid Commun*. **2004**, *25*, 1663.

165. a) Sperling, L. H. *Introduction to Physical Polymer Science*, 3rd ed.; John Wiley & Sons: New York, 2001. b) Zen, A.; Saphiannikova, M.; Neher, D.; Grenzer, J.; Grigorian, S.; Piersch, U.; Asawapirom, U.; Janietz, S.; Scherf, U.; Lieberwirth, I.; Wegner, G. *Macromolecules* **2006**, *39*, 2162.

166. Malik, S.; Nandi, A. K. *J. Polym. Sci., Part B* **2002**, *40*, 2073.

167. a) Swinnen, A.; Zhao, J.; van Assche, G.; Vanderzande, D.; D'Olieslaeger, M.; Manca, J. V.; Van Mele, B. *Proc. SPIE* **2007**, *6656*, 665619. b) Kuila, B. K.; Nandi, A. K. *Macromolecules* **2004**, *37*, 8577. c) Kuila, B. K.; Nandi, A. K. *J. Phys. Chem. B* **2006**, *110*, 1621. d) Zhao, Y.; Yuan, G.; Roche, P.; Leclerc, M. *Polymer* **1995**, *36*, 2211. e) Hugger, S.; Thomann, R.; Heinzel, T.; Thurn-Albrecht, T. *Colloid Polym. Sci*. **2004**, *282*, 932. f) Kim, J. Y.; Frisbie, C. D. *J. Phys. Chem. C* **2008**, *112*, 17726.

168. a) Xie, Y.; Li, Y.; Xiao, L.; Qiao, Q.; Dhakal, R.; Zhang, Z.; Gong, Q.; Galipeau, D.; Yan, X. *J. Phys. Chem. C* **2010**, *114*, 14590. b) Clark, J.; Silva, C.; Friend, R. H.; Spano, F. C. *Phys. Rev. Lett*. **2007**, *98*, 206406. c) Tretiak, S.; Saxena, A.; Martin, R. L.; Bishop, A. R. *Phys. Rev. Lett*. **2002**, *89*, 097402.

169. Xu, B.; Holdcroft, S. *Macromolecules* **1993**, *26*, 4457.

170. a) Samuel, I. D.; Rumble, G.; Friend, R. H. *In Primary Photoexcitations in Conjugated Polymers: Molecular Excitation versus Semiconductor Band Model*; Sariciftci, N. S., Ed.; World Scientific Publishing Co.: Singapore, 1997. b) Gill, R. E.; Malliaras, G. G.; Wildeman, J.; Hadziioannou, G. *Adv. Mater*. **1994**, *6*, 132. c) Greenham, N. C.; Samuel, I. D. W.; Hayes, G. R.; Phillips, R. T.; Kessener, Y. A. R. R.; Moratti, S. C.; Holmes, A. B.; Friend, R. H. *Chem. Phys. Lett*. **1995**, *241*, 89. d) Chen, F.; Mehta, B.; Takiff, L.; McCullough, R. D. *J. Mater. Chem*. **1996**, *6*, 1763. e) Osterbacka, R.; An, C. P.; Jiang, X. M.; Vardeny, Z. V. *Science*, **2000**, *287*, 839.

171. a) Saadeh, H.; Goodson, T., III; Yu, L. *Macromolecules* **1997**, *30*, 4608. b) Perepichka, I. F.; Perepichka, D. F.; Meng, H.; Wudl, F. *Adv. Mater*. **2005**, *17*, 2281.

172. Cook, S.; Furube, A.; Katoh, R. *Energy Environ. Sci*. **2008**, *1*, 294.

173. a) Li, J.; Yan, M.; Xie, Y.; Qiao, Q. *Energy Environ. Sci*. **2011**, *4*, 4276. b) Beenken, W. J. D.; Pullerits, T. *J. Phys. Chem. B*. **2004**, *108*, 6164.

174. a) Scheblykin, I. G.; Yartsev, A.; Pullerits, T.; Gulbinas, V.; Sundstrom, V. *J. Phys. Chem. B* **2007**, *111*, 6303. b) Westenhoff, S.; Daniel, C.; Friend, R. H.; Silva, C.; Sundstrom, V.; Yartsev, A. *J. Chem. Phys*. **2005**, *122*, 094903.

175. Nakamura, T.; Araki, Y.; Ito, O.; Takimiya, K.; Otsubo, T. *J. Phys. Chem. A* **2008**, *112*, 1125.

176. a) Kobayashi, T.; Yoshizawa, M.; Stamm, U.; Taiji, M.; Hasegawa, M. *J. Opt. Soc. Am. B* **1990**, *7*, 1558. b) Grage, M. M. L.; Zaushitsyn, Y.; Yartsev, A.; Chachisvilis, M.; Sundstrom, V.; Pullerits, T. *Phys. Rev. B* **2003**, *67*, 205207. c) Yang, X.; Dykstra, T. E.; Scholes, G. D. *Phys. Rev. B* **2005**, *71*, 045203.

177. a) Lee, Y.; Zhang, Y.; Ng, S. L. G.; Kartawidjaja, F. C.; Wang, J. *J. Am. Ceram. Soc.* **2009**, *92*, 1940. b) Li, Q.; Bian, J.; Sun, J.; Wang, J.; Luo, Y.; Sun, K.; Yu, D. *Appl. Surf. Sci*. **2010**, *256*, 1698.

178. a) Greene, L. E.; Law, M.; Yuhas, B. D.; Yang, P. *J. Phys. Chem. C* **2007**, *111*, 18451. b) Lee, T-H.; Sue, H-J.; Cheng, X. Nanotechnology 2011, 22, 285401. c) Beek, W. J. E.; Wienk, M. M.; Janssen, R. A. J. Adv. Mater. 2004, 16, 1009.

VITA

Sanjiban Chakraborty was born on September 18, 1978 in Calcutta (now Kolkata), India, where he attended elementary and high schools. His interest in chemistry began to grow during the initial days of high school. Sanjiban was accepted to the department of Chemistry at University of Calcutta, India from where he majored in chemistry. He received his bachelor's degree in 2000. His inclination towards the field of applied chemistry prompted him to pursue the engineering career. He got admitted to the department of Polymer Science and Technology at the same university. During this time he had worked at the Product Application and Research Centre (PARC) in Reliance Industries Limited (RIL), Mumbai, India as a R&D trainee for two months. Sanjiban received his B.Tech (Bachelor of Technology) degree in polymer science and technology in the year 2003. In an aspiration of receiving higher education, Sanjiban joined the chemistry department of UMKC for his Ph.D. study in the fall semester of 2005.

During his Ph.D study in Prof. Zhonghua Peng's group, Sanjiban had been devoted in the research area of Organic/Inorganic Hybrids, mainly Polyoxometalate containing diblock copolymers. He was initiated as a member of "The Honor Society of Phi Kappa Phi" in 2008. He received Graduate Student Travel Award for two consecutive years (2010 and 2011). The doctoral study presented him with the opportunity to showcase his work at various national meetings. The list of publications which he had co-authored and the list of presentations at various conferences are given below.

Publications

- Synthesis and optical properties of triphenylene-based dendritic donor perylene diimide acceptor systems. Bagui, Mahuya; Dutta, Tanmoy; **Chakraborty, Sanjiban**; Melinger, Joseph S.; Zhong, Haizhen; Keightley, Andrew; Peng, Zhonghua. *Journal of Physical Chemistry A* **2011**, *115*, 1579.

- Synthesis and optical properties of a rod-coil diblock copolymer with polyoxometalate clusters covalently attached to the coil block, **Chakraborty, Sanjiban**; Keightley, Andrew; Dusevich, Vladimir; Wang, Yong; Peng, Zhonghua. *Chemistry of Materials*, **2010**, *22*, 3995.

- Syntheses and optical properties of triphenylene-containing conjugated polymers**.** Chou, Ching-En; Wang, Degang; Bagui, Mahuya; Hsu, Jeffrey; **Chakraborty, Sanjiban**; Peng, Zhonghua. *Journal of Luminescence*, **2010**, *130*, 986.

- Synthesis and optical properties of triphenylene-based conjugated dendrons**.** Bagui, Mahuya; Melinger, Joseph S.; **Chakraborty, Sanjiban**; Keightley, J. Andrew; Peng, Zhonghua. *Tetrahedron* **2009**, *65*, 1247.

- Synthesis of AB2-functionalized triphenylene derivatives. Kang, Jeonghee; Wang, Degang; Mahuya, Bagui; **Chakraborty, Sanjiban**; Peng, Zhonghua. *Letters in Organic Chemistry* **2006**, *3*, 674.
- Synthesis and morphological studies of thiophene based diblock copolymer with polyoxometalate clusters attached to the coil block. **Chakraborty, Sanjiban**; Da-Ming, Zhu; Yan, XingZhong; Peng, Zhonghua. *Manuscript prepared.*

Posters and Presentations

- **Chakraborty, Sanjiban**; Kwon, Osung; Zhu, Da-Ming; Peng, Zhonghua. 'Synthesis and thin film morphological studies of rod-coil diblock copolymers with polyoxometalate clusters tethered to the flexible block'. Poster, **242nd ACS National Meeting, Denver, CO, United States, August 28-September 1, 2011.**

- **Chakraborty, Sanjiban**; Kwon, Osung; Zhu, Da-Ming; Peng, Zhonghua. 'Synthesis and thin film morphological studies of rod-coil diblock copolymers with polyoxometalate clusters tethered to the flexible block'. Poster, **45th Midwest Regional Meeting of the American Chemical Society, Wichita, KS, United States, October 27-30, 2010.**

- **Chakraborty, Sanjiban**; Peng, Zhonghua. Synthesis and optical studies of rod-coil diblock copolymers with polyoxometalate clusters tethered to the flexible block. Poster, **Materials Research Society (MRS) Spring Meeting, San Francisco, CA, United States, April 5-9, 2010.**

- **Chakraborty, Sanjiban**; Peng, Zhonghua. Synthesis and optical properties of a rod-coil diblock copolymer with polyoxometalate clusters covalently attached to the coil block. Poster, **239th ACS National Meeting, San Francisco, CA, United States, March 21-25, 2010.**

- **Chakraborty, Sanjiban;** Peng, Zhonghua. Synthesis and Optoelectronic Study of Donor-Acceptor Type Rod Coil Diblock Copolymer with Polyoxometalate Cluster Covalently Attached to the Coil Block. Presentation, **44th Midwest Regional Meeting of the American Chemical Society, Iowa City, IA, United States, October 21-24, 2009.**